Cardiff University
School Of Chemistry

Development of New Ligand Frameworks and Complexes for Applications in Imaging

Thesis submitted for the degree of Doctor of Philosophy

by:

Timothy John Smith

Supervisors: Prof. P. G. Edwards & Dr. A. J. Amoroso; **September 2013**

DECLARATION

This work has not previously been accepted in substance for any degree and is not concurrently submitted in candidature for any degree.

Signed…… (candidate) Date……

STATEMENT 1

This thesis is being submitted in partial fulfilment of the requirements for the degree of Doctor of Philosophy.

Signed…… (candidate) Date……

STATEMENT 2

This thesis is the result of my own independent work/investigation, except where otherwise stated. Other sources are acknowledged by explicit references.

Signed…… (candidate) Date……

STATEMENT 3

I hereby give consent for my thesis, if accepted, to be available for photocopying and for interlibrary loan, and for the title and summary to be made available to outside organisations.

Signed…… (candidate) Date……

Acknowledgements

Firstly I want to dedicate this work to Flora, a wonderful girlfriend whom without I can honestly say, I could not have got through this. We've had many awesome times since meeting as undergraduates and you truly are my rock and best friend! Thanks for being strong through the tough times and being there during the good. I look forward to our future together and let the good times keep rolling. Thanks dude!

Secondly I would like to thank Angelo and Pete for giving me the opportunity of this PhD studentship and for their support throughout.

Most importantly I want to thank my loving family who have supported and believed in me all my life and have got me to where I am today. I hope you will read this thesis fully and appreciate what I've been doing all this time. ☺

I would also like to spare a thank you for Mike Coogan who always had time for me and has given me much support, encouragement and wildlife joy over the last few years. Cheers Mike.

Lastly but by no means least I like to raise a pint to all my great friends from department. Kate and Shaun for the lunch time chin wags and long live the great camping holidays. Brendan and Tom for the extensive antics and laughs in the lab and finally Woody and Hallett for their dedication to Thursday nights and attempts to wind me up at the pub!..only joking. Cheers guys!

Summary

A detailed investigation into the transition metal complexes of various chelating nitrogen donor ligands, form the basis of this thesis. *Chapter* 1 discusses the synthesis and co-ordination of a xylyl bridged bis-tacn ligand, which has been shown to form sandwich type structures. *Chapters* 2 and 3 discuss the synthesis and co-ordination behaviour of two novel tripodal tris-(pyridyl-pyrazolyl) ligand frameworks, **L2** and **L3**. The ligand **L2**, forms stable mononuclear compounds which display predominantly trigonal prismatic geometries for a series of transition metals, with only a few exceptions (Cr(III), Re(I) and In(III)). For **L1**, the relationship between octahedral and trigonal prismatic character has been investigated, with varied *d*-electron configurations of the metal centre. Continuous shape mapping analysis (CShM) has been employed to assist in the quantification of their geometric distortions. For **L3**, a similar investigation has been discussed, where the potentially hexadentate ligand was found to form a series of five co-ordinate transition metal complexes, with predominately square pyramidal geometries. *Chapter* 4 investigates the co-ordination chemistry of a tetradentate bis-(pyrazolyl)bipyridine ligand with various di-cationic transition metals, forming distorted octahedral geometries, often involving co-ordination of the perchlorate counter ions. In *Chapter* 5, the synthesis of a novel tripodal bis-quinoline ligand, **L5**, has been introduced along with a detailed discussion of its co-ordination behaviour with a variety of transition metals, where the Cu(II) complex forms a trimeric structure involving co-ordination of a capping perchlorate counter-anion. The addition of a *para*-substituted phenyl-bromide group, as the third tripodal 'arm', gives this molecule potential for further functionalisation through coupling reactions. *Chapter* 6 investigates the co-ordination properties of Cu(II) and Re(I) with a similar bis-quinoline tripodal ligand, which contains a lipophilic butyl appendage. A series of luminescence experiments were performed for the Re(I) complex in order to determine its photophysical properties with varying levels of acid.

Abbreviations

Å	Angstroms
Ar	Aromatic
ATSE	Diacetyl-bis(N4-ethylthiosemicarbazone)
ATSM	Diacetyl-bis(N4-methylthiosemicarbazone)
β^+/ β^-	Positron/electron radiation
β	Nephelauxetic parameter
B	Racah parameter
br	Broad
Bu	Butyl
BuLi	Butyllithium
bipy	Bipyridine
ca.	Circa
$CDCl_3$	Deuterated chloroform
CD_3CN	Deuterated acetonitrile
cm	Centimetre
cm^{-1}	Wavenumber
δ	NMR chemical shift
DOTA	1,4,7,10-tetraazacyclododecane-1,4,7,10-tetraacetic acid
Δ	Crystal field splitting
d	Doublet
DCM	Dichlormethane
dd	Doublet of doublets
DMF	N,N'-dimethylformamide
DMSO	Dimethylsulphoxide
ε	Extinction coefficient
Ed	Edition
e.g.	*Exempli gratia* (for example)
eq	Equivalents
ES-MS	Electrospray mass spectrometry

Et. al.	*Et alii* (and others)
g	gramme
Glc	Glucose
^{1}H	Proton
h	Hour
HOMO	Highest occupied molecular orbital
HRMS	High resolution mass spectrometry
Hz	Hertz
IR	Infrared spectroscopy
J	Coupling constant
KBr	Potassium bromide
kJ	Kilojoule
λ	Wavelength
λ_{max}	Wavelength of maximum absorption or emission
L	Ligand
LFSE	Ligand field stabilization energy
LUMO	Lowest occupied molecular orbital
m	Multiplet
M	Metal
MLCT	Metal-to-ligand-charge-transfer
Me	Methyl
MeCN	Acetonitrile
mg	Milligram
MHz	Megahertz
Mr	Molecular weight
min	Minutes
ml	Millilitre
mol	Mole
mmol	Millimoles
MRI	Magnetic resonance imaging
m/z	Mass/charge ratio
NIR	Near infrared

nm	Nanometre
NMR	Nuclear magnetic resonance
NOTA	1,4,7-triazacyclononane-1,4,7-triacetic acid
o	Ortho
Oh	Octahedral
ORTEP	Oak-ridge thermal ellipsoid plot
^{o}C	Degrees Celcius
^{o}	Degrees (angular)
p	Para
PET	Positron emission tomograghy
Ph	Phenyl
ppm	Parts per million
Phen	Phenanthroline
py	Pyridine
R	Alkyl or aryl group
rt	Room temperature
s	Singlet
SP	Square pyramidal
t	Triplet
$t_{1/2}$	half-life
tacn	1,4,7-triazacyclononane
TBM	tris(2,2-bipyrid-6-yl)methanol
TBP	Trigonal bipyramidal
t-Bu	Tert-Butyl
TETA	1,4,8,11-tetraazacyclotetradecane-1,4,8,11-tetraacetic acid
TE2A	4,11-bis(carboxymethyl)-1,4,8,11-tetraazabicyclo[6.6.2]hexadecane
terpy	Terpyridine
THF	Tetrahydrofuran
TP	Trigonal prismatic
UV	Ultraviolet
Vis	Visible
ϕ	Bailar twist angle

Contents

Chapter 3: A Tripodal Pyridyl Diphenyl-Pyrazole Framework and its Co-ordination Complexes with Various Transition Metals

Chapter 4: Bipodal Bis-pyridyl dimethylpyrazole Framework and Co-ordination with Various Transition Metals

Chapter 5: Tripodal Bis-quinoline Bromo-benzyl Framework and Co-ordination with Various Transition Metals

Chapter 1:

Ortho-Xylene Linked Bis-tacn Ligand Framework and Co-ordination with Transition Metals

1.0 Abstract

This chapter discusses further investigations into the co-ordination behaviour of mononuclear sandwich complexes of the ligand 1,2-bis(1,4,7-triazacyclonon-1-ylmethyl)benzene (**L1**). To date only Cu(II), Ni(II) and Zn(II) complexes of this system have been structurally investigated. Herein five novel sandwich type complexes using the metals Co(II), Fe(II), Ga(III), Cd(II) and Hg(II) with **L1** have been isolated and characterized by techniques including IR, Mass spectrometry and ^{1}H-NMR spectroscopy. The complexes **1.2** and **1.4** (Fe(II) and Cd(II)) were also structurally characterised by single crystal X-ray diffraction, in which they were confirmed to form the desired hexa-coordinate sandwich structures with two tacn rings. The Fe(II) complex gave a highly twisted conformation with a geometry intermediate between octahedral and trigonal prismatic (Bailar angle = 30.37°), whereas the Cd(II) structure was better described as a distorted trigonal prism (Bailar angle = 23.64°).

1.1 Introduction

In the field of medicine there is huge demand for patient diagnosis techniques, and these can come in a number of different forms. Techniques such as Computed Tomography (CT), Magnetic Resonance Imaging (MRI), Positron Emission Tomography (PET) and Single Photon Emission Computed Tomography (SPECT) are some more modern procedures used for *in vivo* diagnosis. Having the ability to image the inside of a body non-invasively gives medics a large advantage in determining the correct treatment. It is widely known that drugs administered for these techniques are rarely ideal candidates, so continuous research and development on these systems is vital. One great advantage with PET over more established imaging techniques is its sensitivity in detection of the substrate.[1-2] This makes PET a great technique for drug discovery as only picomoles (~10^{-12}) of substrate are required for testing, and therefore cause minimal effect on the subject. However larger amounts are needed for effective therapeutic doses (≥ 10^{-9} moles).[3]

PET imaging is the main focus behind the aims and design of this project. PET relies on the detection of a pair of gamma rays at 180 degrees to each other, appearing from the same point within the body. These are created by radioactive positron emitting isotopes that undergo an annihilation reaction with a surrounding electron and thus give off gamma radiation. This essential feature of PET means that only some element isotopes can be used for this type of

imaging, such as ^{52}Fe, $^{62/63}Zn$, $^{64/67}Cu$, ^{68}Ga and ^{99m}Tc (as well as some non-metal isotopes e.g. ^{18}F, ^{11}C, ^{13}N and ^{15}O), shown in table 1.[2,4-5] Besides ^{18}F, the organic radio-isotopes are rarely practical, as their half lives are short and once produced they tend to require longer, more complicated reactions in order to create the active drug, compared with traditional coordination chemistry where complexing the "hot" metal is generally quicker and less complicated.

Table 1: Showing the various common radioisotopes in Nuclear Medicine Imaging.

Isotope	Half-life ($t_{1/2}$)	Bio-relevant oxidation states
$^{64, 67}Cu$	13, 61 h	Cu^{+} and Cu^{2+}
$^{62, 63}Zn$	9.3 hr, 38.5min	Zn^{2+}
^{52}Fe	8.3 h	Fe^{2+} and Fe^{3+}
^{55}Co	17.5 h	Co^{+}, Co^{2+} and Co^{3+}
^{99m}Tc	6 h	Tc^{+} and Tc^{5+}
$^{66, 67, 68}Ga$	10, 78, 1 h	Ga^{3+}
$^{186, 188}Re$	90, 17 h	Re^{+} and Re^{5+}
$^{86, 90}Y$	15, 64 h	Y^{3+}
^{111}In	67 h	In^{3+}
^{89}Zr	78 h	Zr^{4+}
^{117}Lu	160 h	Lu^{3+}
$^{111,123}I$, ^{15}O, ^{13}N, ^{18}F, ^{11}C	2.5 days, 13 h, 2 min, 10 min, 109.8 min, 20.4 min	-

Using transition metal, lanthanide or actinide complexes, as potential imaging agents in PET creates problems, as the majority of heavy metals are toxic and in later reactions will also be radioactive, so careful consideration needs to be taken before administering such elements. The best way around this danger is to create complexes with high stability. To achieve this complexes must be; (i) Kinetically stable so as not to decompose in the body and release free metal ions causing toxicity (ii) They must also be thermodynamically stable so that the metal ions do not exchange with biogenic ligands or ions causing negative effects to the organism.[6] The half lives of these positron emitters can vary greatly but are typically in the range of a few minutes to hours, which leaves little time between creating and administering the tracer.[5] As a result it is usually required that the isotopes are made nearby and that synthesis of the drugs is quick and uncomplicated.

Using large polydentate ligands with specifically positioned donor groups, such as nitrogen, oxygen, phosphorus and/or sulphur, it is possible to create complexes of high stability (EDTA for example).[7] Another example is [$^{64}Cu^{II}$ATSM] which is a compound that has for some time proven useful in PET imaging (Sch. 1). The ligand in this complex contains both nitrogen and sulphur donors fixed within a fairly rigid structure, which provides a high affinity for Cu^{II} upon complexation.[2,8] The reason for its success is due to the drugs hypoxia selectivity.[8] Hypoxia is a pathological condition where oxygen concentration in tissue becomes very low (typically ≤10%). This condition is associated with many illnesses such as heart disease, strokes and various cancers. This selectivity allows PET imaging to identify areas of hypoxia and thus can improve patient prognosis. Furthermore, due to the unique radioactive properties of ^{64}Cu (emitting both β^+ and β^- radiation), the compound has potential to double up as a radiotherapy drug, as trials have shown increased survival rates among tumour bearing rodents.[9]

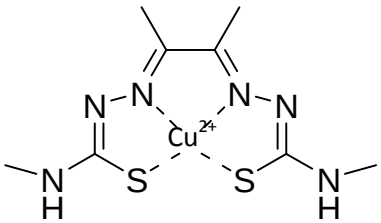

Scheme 1: [$^{64}Cu^{II}$ATSM]

Targeted agents are a newer development in the search for useful PET probes, using specific functionalities (such as pendent sugars, lipids or proteins) to target certain tissues within the body. This is not only to improve imaging but also to decrease damage to healthy tissue, which in turn allows for smaller doses to be used. The ^{64}Cu complex in scheme 1 has more recently been modified with the addition of a glucose pendent (Sch. 2), which is known as [Cu^{II}ATSE/A-Glc].[10] *In vivo* studies have found the complex to exhibit increased tumour selectivity (in hepatic cells) with greatly improved contrast in the PET image. [10-11]

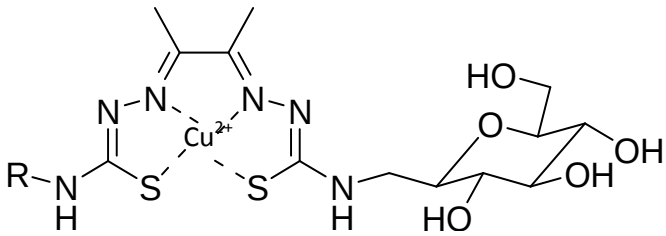

Scheme 2: [$^{64}Cu^{II}$ATSE/A-Glc]

Macrocycles are a branch of polydentate ligands that often have strong and specific binding to metals, generally due to their rigid structures and fixed donor group positions. Macrocyclic chemistry is a well studied area with many examples of such ligands being known, such as crown ethers, porphyrins and cyclophanes to name a few.[12-14] Another group called azamacrocycles, similar to crown ethers, are based around nitrogen donor groups.[15] Some of these compounds have already shown great potential in medical imaging, for example TETA and DOTA (Sch. 3).[16-17] The aza-macrocycle TETA (a derivative of cyclam) possesses a symmetrical ring containing 14 atoms, 4 of which are nitrogen, and appending from each nitrogen is an acetate group. These pendent groups provide flexible oxygen donors which increase ligand donor ability, but also provide polar contacts that improve solubility in media such as water.

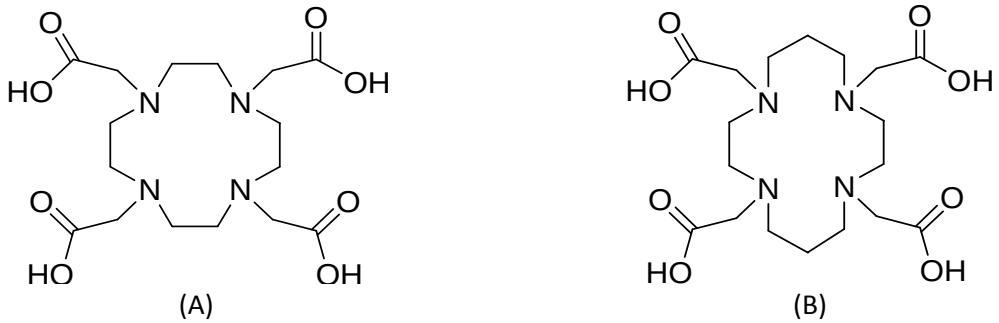

Scheme 3: (A) = DOTA. (B) = TETA

This compound has been successfully labelled with ^{64}Cu *via* co-ordination with the four nitrogens and has also shown significant uptake by cells. However, the stability of this complex *in vivo* needs to be improved. More recently it was found that cross bridged cyclam and derivatives showed major increases in complex stability under biological conditions.[18] This property was utilized in the complex ^{64}CuCB-TE2A (Sch. 4) which has shown significantly lower transchelation *in vivo* to ceruloplasmin (a major copper carrying protein in blood) and thus is an improved imaging agent compared to TETA.[18-19]

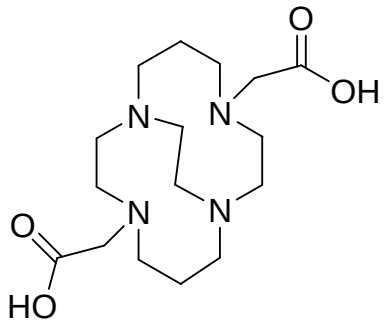

Scheme 4: ^{64}CuCB-TE2A

This success has put similar aza-macrocycles at the centre of much research for potential imaging tracers. To date, research has concentrated on the synthesis and potential applications of aza-macrocycles such as cyclen, cyclam or larger macrocycles, however there is another structure known as 1,4,7-triazacyclononane (tacn) which also draws attention for imaging applications. tacn is a small aza-macrocycle which consists of only three nitrogen donors each linked by an ethyl group to form a ring. This size of ring is ideal for strong coordination to first row transition metals.[20] There is literature precedent for period 3 metal complexes with tacn, very few of which are being presented as potential PET tracers.[20-22] One example that has been tested is a compound called NOTA (Sch. 5) with the metal Gallium(III).[23] This has shown to have the criteria of high thermodynamic and kinetic stability even within biological conditions, with a binding constant of log K_{st} = 30.98, further suggesting the potential for tacn based compounds in PET.[23]

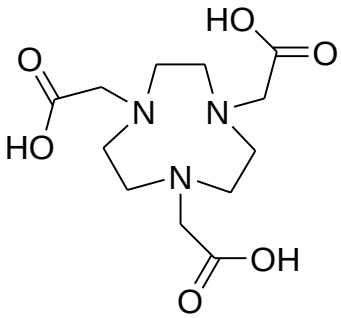

Scheme 5: The ligand NOTA.

In light of the great potential macrocycles have shown, in forming stable metal complexes, and the literature precedence indicating their future in PET imaging, it is in this chapter that further investigations into tacn based complexes is carried out. As tacn is only a tridentate ligand and the majority of transition metals can form hexa-coordinate structures, it is of interest to develop novel bis-tacn linked ligand frameworks with the ability to bind a single metal ion, with the intention that these will form strong kinetically and thermodynamically stable complexes.

1.2 Results and discussion

1.21 Ligand synthesis

The starting material 1,4,7-triazacyclononane (tacn) was prepared prior to ligand synthesis on a large scale using published methods.[24] This involved a six step process of tosylate protections of ethane-1,2-diol and diethylene triamine, cyclisation of these two protected products, deprotection of the newly formed 9-membered ring and finally neutralisation of the trihydrobromide salt to release the free tacn ligand.

The tacn ring was then functionalised by refluxing it with N,N'-dimethylformamide dimethyl acetal producing Triaza-tricyclo[5.2.1.0]decane (**S1**) which has been previously described (Sch. 6).[25] This was dried, to remove any methanol from the reaction product and was placed into a kugervohr distillator under vacuum at 130°C. Pure **S1** was obtained as colourless oil. Compound **S1** has a central CH moiety that allows one of the amine functions of the tacn, to be reacted readily with an alkyl-halide.

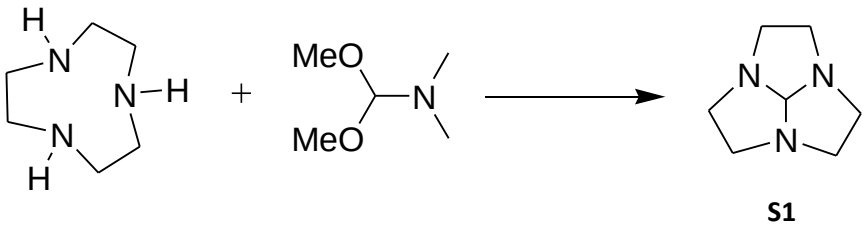

Scheme 6: Synthesis of Triaza-tricyclo[5.2.1.0]decane (**S1**)

Triaza-tricyclo[5.2.1.0]decane (**S1**) and 1,2-dibromoxylene were dissolved separately in acetonitrile and were mixed together slowly under a nitrogen environment. The dibromide salt of the Di-Triaza-tricyclo[5.2.1.0]decane Xylyl product precipitated immediately, and was isolated as a white hygroscopic solid. The salt was refluxed in water to liberate the central CH function of each Triaza-tricyclo[5.2.1.0]decane, creating one formyl group on each tacn ring. The addition of NaOH to the refluxing mixture was required to remove the formyl groups, creating the desired linked tacn product 1,2-bis(1,4,7-triazacyclonon-1-ylmethyl)benzene (**L1**) (Sch. 7).[26] The pure product was isolated by extraction into chloroform followed by evaporation to dryness, giving **L1** as a white solid, yield 83%.

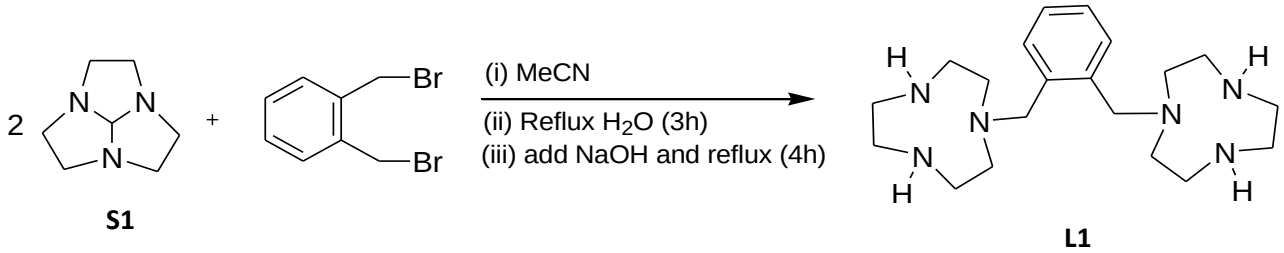

Scheme 7: Synthesis of **L1** (1,2-bis(1,4,7-triazacyclonon-1-ylmethyl)benzene) from **S1** and α,α-dibromo-*o*-xylene.

1.22 Synthesis of complexes

Previous complexations of **L1** with transition metals have been achieved in the literature using typically a 2:1 metal:ligand ratio.[27-29] The purpose for this research was to develop sandwich type complexes using only a 1:1 ratio of the *bis*-tacn framework. Three examples using Cu(II), Ni(II) and Zn(II) have already shown this ligand can form such structures.[26,29-30] These were created by placing the ligand HCl salt in aqueous conditions and mixing it with the appropriate metal halide. The general procedure for the following complexes were made using the free ligand in various organic solvents (typically 0.2mmol, in acetonitrile) followed by the addition of 1eq of the required metal salt (using large couterions such as perchlorate and hexafluorophosphate), producing the complex as a precipitate. Solubility of these compounds was only achieved in water and sparingly in DMSO making analysis difficult in most cases.

Attempts at creating sandwich complexes, see scheme 8, of this ligand with new metals were investigated with little success. Since there is literature precedent for the synthesis of the Cu^{2+}, Zn^{2+} and Ni^{2+} complexes by single-crystal X-ray diffraction, experiments were attempted following similar procedures with other transition metals such as Fe^{2+}, Fe^{3+}, Cd^{2+}, Co^{2+}, Cr^{2+}, Cr^{3+}, Hg^{2+}, Ru^{3+}, Mn^{2+}, Mn^{3+}, V^{3+}, Ga^{3+} and even Eu^{3+}, Gd^{3+} and La^{3+}. The reactions were attempted using the chloride, nitrate and perchlorate precursors of the metals.

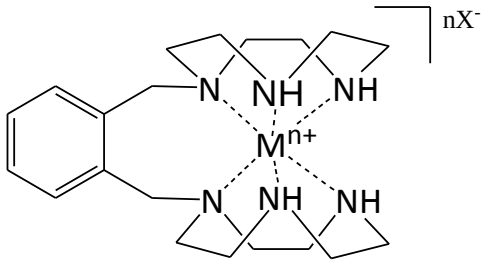

Scheme 8: Desired sandwich arrangement of complexes with **L1**. M = Fe(II), Co(II), Cd(II), Hg(II) and Ga(III).

Various solvents such as ethanol, methanol, acetonitrile and THF were used in attempts to isolate complexes. The chloride counterions were exchanged using $AgPF_6$ and $AgBF_4$ in further attempts at complexation to reduce ligand competition, however this investigation showed only a few encouraging results. 1:1 metal:ligand complexes using Co^{2+}, Fe^{2+}, Cd^{2+}, Hg^{2+} and Ga^{3+} were confirmed by mass spectrometry and ^{1}H-NMR spectroscopy, with Gallium being the most exciting due to its potential use in PET imaging applications.

1.23 NMR spectroscopy

The free ligand **L1** can be identified by three main regions in its ^{1}H NMR spectrum. A pair of doublets are present at approximately 7.2ppm and 7.5ppm, corresponding to the phenyl group of the xylyl bridge. These are generally quite sharp peaks because of the rigidity of the aromatic ring. The second region corresponds to the two CH_2 linkers connecting to the tacn moieties which produce a strong singlet at around 4.0 ppm. The third region shows two multiplets between 2.5-2.7ppm, which are attributed to the flexible CH_2 groups within the tacn macrocycle. Using these regions it is possible to compare and contrast the ^{1}H-NMR spectra of the complexes which were isolated. However, it must be noted that solubility of these complexes was poor and generally required the use of polar solvents (DMSO), and making suitably concentrated samples was still difficult. As a result, no discernible peaks could be observed in the ^{13}C-NMR spectra of the complexes.

The ^{1}H-NMR spectrum of the Fe(II) complex (**1.2**) was found to display significant broadening of the peaks for all three regions highlighted above, where peak multiplicities could not be distinguished, which may be due to the electronic nature of d^6 Iron. However, the fact that a spectrum was obtained between 0-10ppm may provide some evidence of a low spin metal centre in this complex. The two aromatic peaks within the ^{1}H NMR spectrum are seen to have moved only slightly with respect to the ligand, with the more up-field doublet shifting most significantly from 7.25 ppm to 7.30 ppm. The most noticeable change in the spectrum came from the macrocyclic CH_2 groups which appeared to be split into three distinct broad signals which were shifted down-field by between 0.1-0.3 ppm.

The Ga(III) complex (**1.3**) showed the poorest solubility of all of the isolated complexes. However, a very weak spectrum of the sample was obtained from MeOD. From the ^{1}H-NMR spectrum, it was possible to identify the three key regions discussed for the ligand, which

confirmed the presence of the complex, however, in the gallium spectrum, these signals were significantly broadened even though Ga(III) is diamagnetic. For example, the macrocyclic CH_2 region displayed an extremely broad undefined peak spreading from 2.5-2.9ppm, which integrated to the correct number of protons (24H). Concurrently the two aromatic signals were also broadened to the extent where they appeared to merge, but again integrated to the correct number of equivalent protons (4H). One potential reason for this extreme broadening may be attributed to the two natural isotopes of gallium (^{69}Ga and ^{71}Ga with 60% and 39% abundances respectively) which both have nuclear spins of 3/2, and thus, would give rise to a larger amount of peaks per proton signal.

Compound **1.4** is the Cd(II) complex, which is also diamagnetic, and showed a much more defined signal set compared to the Ga(III) complex. The first identifying feature for the complex in this spectrum was the two aromatic doublets, both of which had shifted down-field by 0.2ppm compared with the ligand. Secondly, the macrocyclic CH_2 signals were also seen to have shifted down-field by between 0.05 - 0.3 ppm, with significant broadening. The most interesting feature of this spectrum comes from the bridging CH_2 groups, which had split significantly into two distinct doublets at 3.65ppm and 4.45 ppm. This large splitting is attributed to the magnetic inequivalence enforced on protons of each CH_2. This can be better appreciated when looking at the crystal structure of **1.4**, where it is seen that the rigidity of the sandwich formation causes the aromatic ring to bend to one side of the structure, creating a unique environment for each proton.

The spectrum obtained for complex **1.5** (Hg(II)) showed a similar result to that of Cd(II). Again the two aromatic doublets are seen to have shifted down-field by 0.2 ppm, with the large splitting of the bridging CH_2 singlet into two discrete doublets also being observed (3.65 ppm and 4.4ppm). One interesting feature in the Hg(II) ^1H NMR spectrum is the appearance of two broad macrocyclic NH singlets at 3.75 ppm and 4.05 ppm, which are attributed to the rigid conformation of the tacn rings, enforced by co-ordination to the metal centre.

1.24 X-Ray Crystallography data

All single crystal data was collected at 150K on a Bruker/Nonius Kappa CCD diffractometer using graphite monochromated Mo-Kα radiation (λ = 0.71703 Å). It was possible to isolate products, suitable for crystallographic studies, for only two of the novel complexes discussed above, **1.2** and **1.4**. Both data sets reveal that the complexes attain the desired sandwich type structure that was anticipated, with their relevant crystal parameters and details of data collection presented in Table 2.

Table 2: Crystallographic data for complexes **1.2** and **1.4**

Compound	Fe(II) 1, 2-Di(triazacyclononane)xylene (**1.2**)	Cd(II) 1, 2-Di(triazacyclononane)xylene (**1.4**)
Chemical formula	$[FeC_{20}H_{36}N_6][2Cl]$	$[CdC_{20}H_{36}N_6][2ClO_4].CH_3CN$
Mr, g/mol	487.05	712.90
Crystal system	Monoclinic	Monoclinic
Space Group	$P2_1/c$	$P2_1/n$
T (k)	150	150
a, Å	13.6991 (3)	9.1653 (4)
b, Å	10.8148 (3)	9.4467 (4)
c, Å	18.1020 (5)	32.8614 (16)
α, deg	90.00	90.00
β, deg	109.198 (2)	95.096 (2)
γ, deg	90.00	90.00
V, $Å^3$	2532.72 (11)	2834.0 (2)
Z	4	4
D_c g/cm^3	1.399	1.671
μ(Mo K α), mm^{-1}	0.833	1.018
Observed Reflections	5775	4316
Reflections collected	10587	6008
R_{int}	0.0415	0.0354
R_I [I>2σ(I)]	0.0447	0.0460
wR_2 (all data)	0.1139	0.1117

Crystal structure of $[Fe(C_{20}H_{36}N_6)][Cl]_2$ (**1.2**)

Small pale orange crystals suitable for crystallographic studies were grown *via* vapour diffusion of petroleum ether (40/60) into a concentrated ethanol solution of the complex. The data reveal that the compound forms a 1:1 metal:ligand ratio as intended, creating the sandwich type structure, with the molecule crystallising in the monoclinic space group $P2_1/c$ (Fig. 1). The asymmetric unit consists of one complex, two chloride counterions and one ethanol solvent molecule, and the symmetry of the complex is best described as C_1. The metal centre is six co-ordinate with a geometry resembling a twisted octahedron. The Fe(II) centre lies between both tacn moieties with all six available nitrogen donors involved in co-ordination.

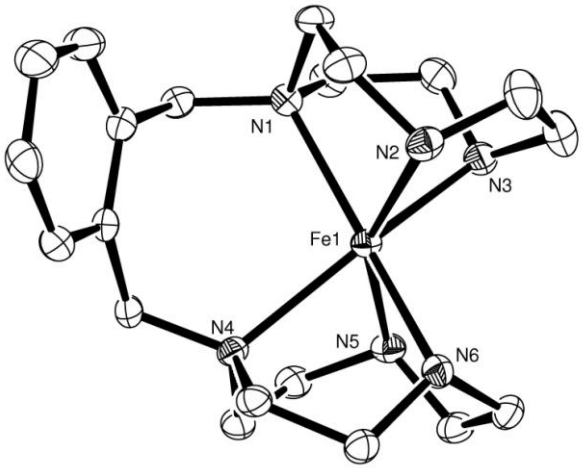

Figure 1: ORTEP Perspective view of the asymmetric unit for $[Fe(\mathbf{L1})][Cl]_2$ with atom labelling. Displacement ellipsoids are shown at 50% probability with H atoms and two chloride counter ions having been excluded for clarity.

The six Fe-N bond lengths were found to be a mean distance of 2.246 (2) Å. These lengths were compared to the simple Fe(II) bis-tacn complex ($[Fe(tacn)_2][Cl]_2$) which was found to have significantly shorter bond lengths (average Fe-N bond = 2.03(1) Å). For comparison, these values were also compared with the analogous Fe(III) complex ($[Fe(tacn)_2][Cl]_3$) which was found, on average, to have even shorter bonds (average Fe-N bond = 1.99(1) Å).[31] The longer bonds associated with **1.2** are owed to the constraints imposed by the xylyl bridge, where the free ligand has a preposition for trigonal prismatic geometries and the Fe(II) has a preference for octahedral. As a result, the Fe(II) centre of **1.2** gave a distorted geometry approximately half way between octahedral and trigonal prismatic, represented by the Bailar twist angle, ϕ, of 30.37° (see Fig. 2). This is expected to cause poorer orbital overlap compared to an ideal

octahedral, as seen in the two $Fe(tacn)_2$ examples, and therefore requires longer bonds in order to gain some stability.

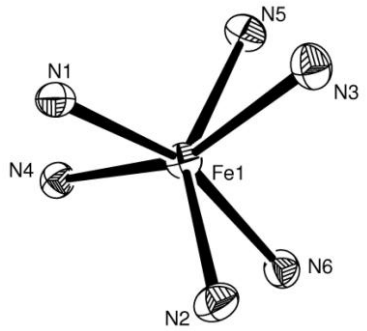

Figure 2: A view of the core geometry, looking from above, of [Fe(**L1**)][Cl]$_2$ showing the extent of bailar twisting. Where N1 to N3 lie within the top plane and N4 to N6 lying in the lower plane. Displacement ellipsoids given at a 50% probability.

In addition, the length of the linker chain may also have played a role in restricting the two tacn moieties from coming closer together in a sandwich formation. This is made evident when looking at the Fe-N1 and Fe-N4 bond lengths (Table 3) which are both noticeably longer than the other co-ordinative bonds. This is a feature also present in the analogous Zn(II) complex ([Zn(**L1**)][ClO_4]$_2$), where the Zn-N1 and Zn-N4 bonds are, on average, slightly longer that those not connected to the xylyl linker group (2.220(4) Å compared to 2.190(4) Å).[30] This effect can also be noted between intra-ring N_{cis}-Fe-N_{cis} 'bite' angles, where N1-Fe-N4 presents an angle of 100.85(7)° compared to N2-Fe-N6 and N3-Fe-N5 which gave angles of *ca*. 85°, confirming that the xylyl linker does have an effect on the two tacn rings, preventing them from co-ordinating in a perfectly parallel conformation.

Table 3: Selected bond Distances (Å) and Angles (deg) for complex **1.2**			
Bond	Length (Å)	Bond	Length (Å)
Fe1-N1	2.2746 (19)	Fe1-N4	2.3196 (19)
Fe1-N2	2.215 (2)	Fe1-N5	2.2372 (19)
Fe1-N3	2.225 (2)	Fe1-N6	2.2048 (19)
Bonds	Angle (°)	Bonds	Angle (°)
N1-Fe1-N2	78.21 (2)	N2- Fe1-N6	87.08 (7)
N1-Fe1 –N3	78.35 (7)	N3- Fe1-N4	157.43 (7)
N1- Fe1-N4	100.85 (7)	N3- Fe1-N5	83.97 (7)
N1- Fe1-N5	119.36 (7)	N3- Fe1-N6	109.19 (7)
N1- Fe1-N6	161.85 (7)	N4- Fe1-N5	76.77 (7)
N2- Fe1-N3	78.12 (8)	N4- Fe1-N6	78.56 (7)
N2- Fe1-N4	124.09 (7)	N5- Fe1-N6	78.40 (7)
N2- Fe1-N5	151.80 (7)		

Crystal structure of $[Cd(C_{20}H_{36}N_6)][ClO_4]_2$ (**1.4**)

Colourless crystals of the complex [Cd(**L1**)][ClO_4]$_2$, suitable for X-ray crystallography, were achieved by vapour diffusion of diethyl ether into a concentrated acetonitrile solution of **1.4**. The data collected showed that the compound crystallised in the monoclinic space group $P2_1/n$ with the asymmetric unit containing one complex, two perchlorate counter ions and one acetonitrile solvent molecule. The Cd(II) centre was seen to co-ordinate with all six available nitrogen donors in the desired sandwich conformation, see figure 3, where the molecular symmetry of the compound is best described as C_1, analogous to that of complex **1.2.**

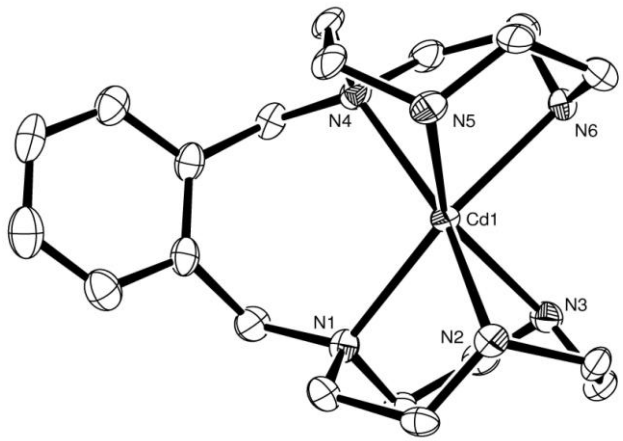

Figure 3: ORTEP Perspective view of the asymmetric unit for [Cd(**L1**)][ClO_4]$_2$ with atom labelling. Displacement ellipsoids are shown at 50% probability with H atoms and two perchlorate counterions being excluded for clarity.

In this complex, the metal centre geometry is best described as a distorted trigonal prism which gave an approximate Bailar twist angle of 23.64°, seen clearly in figure 4. As the Cd(II) ion is d^{10} and has no stereoelectronic preferences in geometry, so the observed twist angle may suggest that the ligand has a favoured twisted conformation and not a preposition for an ideal trigonal prism as first thought. This is interesting as the analogous Zn(II) complex (Zn(**L1**)][ClO_4]$_2$) was found to form a geometry much closer to octahedral.[30] This could be owed to the ionic size of Cd(II) (95 pm) compared to Zn(II) (74 pm) which would push the two macrocyclic rings further apart. This is significant as it was suggested by Thöm *et. al*. that repulsive van der Waals forces between the two rings may be what is favouring a staggered conformation (octahedral).[32] Thus, if the two macrocycles were held further apart, by a larger ion, it is reasonable to assume that these forces would be reduced, and therefore decrease the octahedral tendency of the complex.

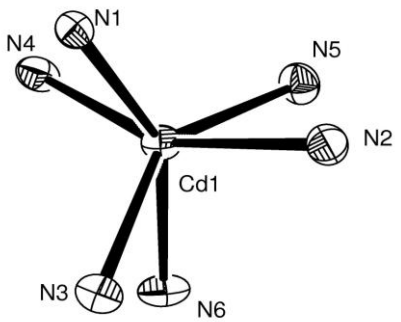

Figure 4: A view of the core geometry of [Cd(**L1**)][(ClO_4)$_2$], looking from above, showing the extent of bailar twisting, where N1 to N3 lie within the top plane and N4 to N6 lie in the lower plane. Displacement ellipsoids are given at a 50% probability.

As expected, the Cd-N bond lengths are longer than those seen in the Fe(II) example, giving a bond range of 2.340(4) to 2.402(4) Å. These were compared to the Cd(II) *bis*-tacn complex [Cd(tacn)$_2$][ClO_4]$_2$, which was found to have comparable bond lengths of between 2.351(3) and 2.382(3)Å.[33] In an identical fashion to complex **1.2**, the Cd-N1 and Cd-N4 bonds were observed to be slightly longer than those to the other nitrogen donors (noting however, the lengths of Cd-N3 and Cd-N5 fall within the error margin of bonds to N1 and N4), and is also reflected in the N_{cis}-Cd-N_{cis} 'bite' angle (N1-Cd-N4 = 100.92(14) compared to the other two equivalent angles *ca*. 88°), see table 4, and is again owed to the restricting nature of the bridging xylyl group.

Table 4: Selected bond Distances (Å) and Angles (deg) for complex **1.4**			
Bond	Length (Å)	Bond	Length (Å)
Cd1-N1	2.402 (4)	Cd1-N4	2.396 (4)
Cd1-N2	2.345 (4)	Cd1-N5	2.375 (4)
Cd1-N3	2.385 (4)	Cd1-N6	2.340 (4)
Bonds	Angle (°)	Bonds	Angle (°)
N1-Cd1-N2	75.74 (14)	N2- Cd1-N6	116.10 (15)
N1-Cd1-N3	74.97 (14)	N3- Cd1-N4	125.06 (14)
N1- Cd1-N4	100.92 (14)	N3- Cd1-N5	147.91 (15)
N1- Cd1-N5	129.59 (15)	N3- Cd1-N6	86.14 (15)
N1- Cd1-N6	154.52 (14)	N4- Cd1-N5	75.37 (14)
N2- Cd1-N3	74.98 (14)	N4- Cd1-N6	75.93 (15)
N2- Cd1-N4	158.66 (15)	N5- Cd1-N6	74.71 (15)
N2- Cd1-N5	90.41 (14)		

In light of these findings, attempts were made at creating novel 3-carbon spaced bis-tacn ligands, with the intention of producing a better template for sandwich complexes, with less geometric strain from the linker group. However, all successive reaction attempts using shorter spacer groups such as dichloroacetone and 3-chloro-2-chloromethylpropene proved unsuccessful.

1.3 Conclusion

This chapter has described the formation of five novel complexes using the metals Co(II), Fe(II), Ga(III), Cd(II) and Hg(II) with the ligand 1,2-bis(1,4,7-triazacyclonon-1-ylmethyl)benzene (**L1**). All complexes were synthesised in a 1:1 metal:ligand ratio in order to form the desired sandwich type conformation between the two macrocyclic rings. In all cases, the mononuclear species was confirmed by mass spectrometry, with adequate ^{1}H-NMR data collected for the Fe(II), Ga(III), Cd(II) and Hg(II) complexes. Observation of peak shifting and broadening of the proton peaks in these spectra provided sufficient evidence that these compounds existed in solution, however, insufficient multiplicities and peak definition for the Fe(II) and Ga(III) complexes meant confirmation of the intended sandwich type structure, in solution, was not possible. Single crystal X-ray diffraction data was collected successfully for the Fe(II) and Cd(II) complexes, both confirming the formation of the desired mononuclear sandwich structure. In both examples the metal centres were hexa-coordinate with distorted geometries. In the case of Fe(II) the geometry was found to be equal between octahedral and trigonal prismatic, where as the Cd(II) structure was best described as a distorted trigonal prism, giving approximate Bailar twist values of 30.37 and 23.62° respectively (Table 5). The larger Bailar angle was attributed to the stereoelectronic preference of Fe(II) for octahedral geometries.

Table 5: showing the bailar twist angle of complexes **1.2** and **1.4**.

Complex	Torsion angle between N1-N4 (°)	Torsion angle between N2-N6 (°)	Torsion angle between N3-N5 (°)	Average (°)
1.2	30.03	30.44	30.67	30.37
1.4	23.80	23.28	23.85	23.64

In both complexes, the M-N1 and M-N4 bond lengths were found to be longer than those of the other N-donors within the complex, highlighting that the xylyl bridge group is involved in distorting the co-ordination sphere. This is also supported by the angle N1-M-N4 in both compounds being larger (ca. 100°) than their equivalent angles from N2-M-N5 and N3-M-N6 (ca. 84-90°), suggesting that the 4-carbon spaced xylyl bridge is not ideal and may possibly be too long to give the most stable binding conformation.

1.4 Experimental

Triaza-tricyclo[5.2.1.0]decane (**S1**):

A mixture of tacn (4.8g, 0.037mol) and N,N'-dimethylformamide dimethyl acetal (4.7g, 5.24ml, 0.039mol) was prepared and heated at reflux for 5 h. Once allowed to cool the mixture was evaporated for 1 h. The oil residue was then placed on a kugervohr distillator under vacuum at 130°C. The trapping flask was cooled with a dry ice/acetone mixture. The product was a colourless oil. Yield 3.83g (0.03mol, 80.3%). ^{1}H-NMR (D_2O, 250 MHz): δ_H = 4.95(1H, s, CH), 2.99(6H_{eq}, m, CH_{eq}), 2.72(6H_{ax}, m, CH_{ax}). ^{13}C-NMR (D_2O, 62.5MHz): δ_C = 51.9(CH_2), 115.5(CH).

1, 2-Di(triazacyclononane)Xylene (**L1**):

A solution of Triaza-tricyclo[5.2.1.0]decane (1.11g, 7.98 mmol) in acetonitrile (40ml) was made and stirred under a nitrogen atmosphere. A solution of α, α-dibromo xylene (1.05g, 3.99 x 10^{-3} moles) in acetonitrile (20ml) was added dropwise to the solution *via* a cannula over 1 h. The white precipitate produced was filtered off and dissolved in distilled water (25ml). This mixture was then refluxed, with stirring, for 3 h. NaOH pellets (1.45g, 0.036 mol) were added slowly over 1 h straight into the reaction mixture. Once the base had been added the reaction was refluxed for a further 3 h. The mixture was allowed to cool to RT and the product was extracted with Chloroform (3x40ml). The chloroform layers were combined and dried over $MgSO_4$. After filtering the slightly yellow solution was evaporated to dryness giving a yellow oil product. A yellow powder could be obtained if the product was dissolved in DCM and then evaporated. Yield 1.19g (3.32 mmol, 83%). ^{1}H-NMR ($CDCl_3$, 250 MHz): δ_H = 7.26(2H, m, CH), 7.13(2H, m, CH), 3.81(4H, s, CH_2), 2.67(12H_{eq}, m, CH_{eq}(tacn)), 2.54(12H_{ax}, m, CH_{ax}(tacn)), 2.21(4H, s, NH). ^{13}C-NMR ($CDCl_3$, 100.6 MHz): δ_C = 40.2, 46.6, 53.1, 59.3, 126.9, 130.1, 138.5.

Co(II) 1, 2-Di(triazacyclononane)xylene, [$CoC_{20}H_{36}N_6$][2PF_6] (**1.1**):

A solution of 1, 2-Di[triazacyclononane]Xylene (75.6mg, 0.21mmol) in ethanol (5ml) was made and stirred under N_2. To this a bright blue solution of $Co(PF_6)_2$ (74mg, 0.21mmol) in ethanol was added drop wise over 15 minutes. After 45 minutes the product precipitated as a pale pink powder. Yield 0.035g (0.05mmol, 23%). (ES-MS) *m/z* calcd. 564.1975 ; exp. 564.1844 $[CoC_{20}H_{34}N_6(PF_6)]^+$ (50%) FT-IR (KBr/cm^{-1}) ν = 3446br+m, 3231m, 1653m, 1495m, 1457m, 1252br+s, 1167s, 1104w, 1066w, 1029s, 983w. UV-Vis 340.5nm (498.8), 543.5nm (86.1)

Fe(II) 1, 2-Di(triazacyclononane)xylene, $[FeC_{20}H_{36}N_6][2Cl]$ (**1.2**):

A solution of 1, 2-Di[triazacyclononane]xylene (57.6mg, 0.16mmol) in ethanol (5ml) was made and stirred under N_2. To this a yellow solution of $FeCl_2$ (20.3mg, 0.16mmol) in ethanol was added drop wise over 15 minutes. The cloudy orange solution was filtered through celite to give a clear orange solution, then the volume was reduced slightly under vacuum. Vapour diffusion recrystalisation was setup using the ethanol complex solution and petroleum ether generating pale orange crystals. Yield 0.037g (0.077mmol, 48%). ^{1}H-NMR (DMSO, 250 MHz): δ_H = 7.43(2H, d, J=4.5Hz CH), 7.31(2H, d, J=4.5Hz, CH), 3.86(4H, d, J=11Hz, CH_2), 3.63(2H, s, NH), 3.42(6H, m, CH_2), 3.31(2H, s, NH), 2.94(6H, br+s, CH_2), 2.78(6H, br+s, CH_2), 2.65(6H, br+s, CH_2). ^{13}C-NMR data could not acquired due to insufficient solubility of the complex in deuterated solvents. (ES-MS) *m/z* calcd. 515.1836 ; exp. 515.1835 $[FeC_{20}H_{34}N_6(ClO_4)]^+$ (20%). FT-IR (KBr/cm^{-1}) ν = 3434br+s, 2962m, 2916m, 2845m, 1635m, 1491m, 1456m, 1363w, 1261s, 1103s, 1019s, 863w, 802s. UV-Vis 359nm (827.8), 379nm (692.8), 468.5nm (184.8), 499.6nm (168.9), 690nm (39.8)

Ga(III) 1, 2-Di(triazacyclononane)xylene, $[GaC_{20}H_{36}N_6][3Cl]$ (**1.3**):

A solution of gallium(III)chloride (80mg, 0.45mmol) was dissolved in dry acetonitrile (2ml) and added slowly to a second acetonitrile solution containing **L1** (164mg, 0.45mmol). Upon addition a white precipitate immediately formed and the mixture was continued to stir for a further 3 h. The precipitate was filtered *in vacuo* washed with diethyl ether (5ml) and dried under N_2. The solid was only sparingly soluble in methanol making analysis difficult. Yield 74mg (0.14mmol, 31%). ^{1}H-NMR (MeOD, 400 MHz): δ_H = 7.44(2H, m, CH), 7.31(2H, m, CH), 3.90(2H, s, CH_2), 2.73(24H, m, CH_2). ^{13}C-NMR data could not acquired due to insufficient solubility of the complex in deuterated solvents. HRMS (ES-MS) *m/z* calcd. 427.2101 ; exp. 427.2109 $[GaC_{20}H_{34}N_6]^+$ (100%). FT-IR (KBr/cm^{-1}) ν = 3405br+s, 3255s, 2925s, 2854s, 2364w, 1653m, 1457m, 1360m, 1284w, 1261w, 1102m, 1014m, 906w, 783w.

Cd(II) 1, 2-Di(triazacyclononane)xylene, $[CdC_{20}H_{36}N_6][2ClO_4]$ (**1.4**):

A solution of Cadmium(II) perchlorate (50mg, 0.12mmol) was dissolved in acetonitrile (3ml) and added slowly to a solution of **L1** (43mg, 0.12mmol) also in acetonitrile (4ml) resulting in a suspension. The mixture was stirred overnight and filtered through celite. The colourless filtrate was then reduced giving the product as an off-white solid. Purification was achieved by vapour diffusion of diethyl ether into an acetonitrile solution of the complex over a week yielding

colourless crystals 21mg (0.03mmol, 26%). ^{1}H-NMR (DMSO, 400 MHz): δ_H = 7.59(2H, m, CH), 7.43(2H, m, CH), 4.47(2H, d, J=12Hz, CH_2), 3.79(2H, s, NH), 3.65(2H, d, J=12Hz, CH_2), 3.42(2H, s, NH), 2.90(10H, m, CH_2), 2.69(14H, br+m, CH_2). ^{13}C-NMR data could not acquired due to insufficient solubility of the complex in deuterated solvents. HRMS (ES-MS) *m/z* calcd. 569.1517; exp. 569.1535 $[CdC_{20}H_{36}N_6][ClO_4]$ (25%), calcd. 471.1954 ; exp. 471.1992 $[CdC_{20}H_{35}N_6]^+$ (10%).

Hg(II) 1, 2-Di(triazacyclononane)xylene, $[HgC_{20}H_{36}N_6][2Cl]$ (**1.5**):

A solution of Mercury(II)chloride (50.5mg, 0.19mmol) was dissolved in acetonitrile (3ml) and added slowly to a solution of **L1** (67mg, 0.19mmol) in acetonitrile (4ml). Upon addition, a white precipitate immediately formed. The mixture was stirred for 3 h before filtering. The complex was collected as a white solid yielding 61mg (0.1mmol, 52%). ^{1}H-NMR (DMSO, 400 MHz): δ_H = 7.54(2H, m, CH), 7.37(2H, m, CH), 4.40(2H, d, J=12Hz, CH_2), 4.05(2H, s, NH), 3.72(2H, s, NH), 3.63(2H, d, J=12Hz, CH_2), 3.18(2H, m, CH_2), 2.94(8H, br+m, CH_2), 2.63(16H, m, CH_2).). ^{13}C-NMR data could not acquired due to insufficient solubility of the complex in deuterated solvents. HRMS (ES-MS) *m/z* calcd. 593.2358; exp. 593.2366 $[HgC_{20}H_{36}N_6Cl]^+$ (26%).

1.5 References

1. Smith. S. V, *J Phys Conf Ser*, 185, **2009**, 012044.
2. Wadas. T. J, Wong. E. H, Weisman. G. R, Anderson. C. J, *Chem. Rev*, 110, **2010**, 2858-2902.
3. Kitson. S. L, Cuccurullo. V, Ciarmiello. A, Salvo. D, Mansi. L, *Current Radiopharmaceuticals*, 2*,* **2009**, 224-253.
4. Miller. P. W, *J Chem Technol Biotechnol*, 84, **2009**, 309-315.
5. Anderson. C. J, Welch. M. J, *Chem. Rev*, 99, **1999**, 2219-2234.
6. M. I. M. Prata, A. C. Santos, C. F. G. C. Geraldes, J. J. P. de Lima, *Nucl Med Biol*, 26, **1999**, 707-710.
7. Furia. T. E, Sequestrants in Foods, Chapter 6, CRC handbook of food additives, **2006**.
8. Vavere. A. L, Lewis. J. S, *Dalton Trans*, **2007**, 4893-4902.
9. Lewis. J. S, *PNAS*, 98.3, **2000**, 1206-1211.
10. Bayly. S. R, King. R. C, Honess. D. J, Barnard. P. J, Betts. H. M, Holland. J. P, Hueting R, Bonnitcha. P. D, Dilworth. J. R, Aigbirhio. F. I, Christlieb. M, *J Nucl Med*, 49, **2008**, 1862-1868.
11. Betts. H. M, Barnard. P. J, Bayly. S. R, Dilworth. J. R, Gee. A. D, Holland. J. P, *Angew. Chem. Int. Ed*, 47, **2008**, 8416-8419.
12. A. V. Tsukanov, A. D. Dubonosov, V. A. Bren, V. I. Minkin, *Chemistry of Hetrocyclic compounds*, 44, **2008**, 8, 899-923.
13. C. M. Drain, A. Varotto, I. Radivojevic, *Chem Rev,* 109, **2009**, 1630-1658.
14. Yamato. T, Fujita. K, Okuyama**.** K, Tsuzuki. H, *New J Chem,* 24, **2000**, 221-228.
15. Chartres. J .D, Lindoy. L. F, Meehan. G. V, *Coord Chem Rev,*116-117 *,* **2001**, 249-286.
16. Bartholoma. M. D, Louie. A. S, Valliant. J. F, Zubieta. J, *Chem. Rev*, 110, **2010**, 2903-2920.
17. Bass. L. A, Wang. M, Welch. M. J, Anderson. C. J, *Bioconjugate. Chem*, 11, **2000**, 527-532.
18. Boswell. C. A, Sun. X, Niu. W, Weisman. G. R, Wong. E. H, Rheingold. A. L, Anderson. C. J, *J. Med. Chem,* 47, **2004**, 1465-1474.
19. Lewis. E. A, Boyle. R. W, Archibald. S. J, *Chem. Commun*, **2004,** 2212-2213.
20. Yang. R, Zompa. L. J, *Inorg. Chem*, 15, **1976**, 7, 1499-1502.
21. Okamoto. M. S, Barefield. E. K, *Inorg. Chim. Acta*, 17, **1976**, 91-96.
22. Hage. R, Gunnewegh. E. A, Niel. J, Tjan. F. S. B, Weyhermtiller. T, Wieghardt. K, *Inorg. Chim. Acta*, 268, **1998**, 43-48.
23. Prata. M. I. M, Santos. A. C, Geraldes. C. F. G. C, de Lima. J. J. P*, Nucl. Med. Biol,* 26, **1999**, 707-710.
24. (a) J. Richman, T. Atkins, J. Am. Chem. Soc., 21, 1980, 3635. (b) D. Parker, in D. Parker (Ed.), Macrocycles Synthesis, Oxford University Press, Oxford, 1996.
25. X. Zhang, W-Y. Hsieh, T. N. Margulis, L. J. ZompaInorg. *Inorg. Chem*. **1995**, 34, 2883-2888.

26. B. Graham, G. D. Fallon, M. T. W. Hearn, D. C. R. Hockless, G. Lazarev, L. Spiccia, *Inorg. Chem*., **1997**, 36, 6366-6373.
27. F. H. Fry, L. Spiccia, P. Jensen, B. Moubaraki, K. S. Murray, E. R. T. Teikink, *Inorg. Chem*., 42, **2003**, 18, 5594.
28. M. J. Belousoff, B. Graham, L. Spiccia, *Eur. J. Inorg. Chem*., **2008**, 4133-4139.
29. B. DasGupta, C. Katz, T. Israel, M. Watson, L. J. Zompa, *Inorg Chim Acta*, 292, **1999**, 172-181.
30. F. H. Fry, G. D. Fallon, L. Spiccia, *Inorg Chim Acta*, 346, **2003**, 57-66.
31. J. A. Boeyens, A. G. S. Forbes, R. D. Handcock, K. Wieghardt*., Inorg. Chem*., **1985**, 24, 2926-2931.
32. V. J. Thom, J. C. A. Boeyens, G. J. McDougall, R. D. Hancock, *J. Am. Chem. Soc*., **1984**, 106, 3198-3207.
33. H. Strasdeit, A-K. Duhme, M. Weber, S. Pohl, *Acta. Cryst*. **1992,** C48, 437-440.

Chapter 2:

Tripodal Pyridyl Dimethyl-pyrazole Framework with Preferences for Trigonal Prismatic Coordination Geometries

2.0 Abstract

A tripodal ligand (**L2**) has been developed consisting of a methanol centre appended with three pyridyl-dimethylpyrazole moieties providing a potentially trigonal prismatic hexa-dentate chelate. This ligand has been complexed with a variety of di and tri-cationic transition metals and main group metals to investigate its coordination chemistry and electronic properties. Most metals form discrete monomeric complexes with hexa-imine co-ordination. X-ray crystal structures have been obtained for several complexes and structural properties have been rationalised and contrasted using geometric calculations, such as SHAPE and Bailar twist angles. Multi-nuclear NMR spectroscopy, FTIR spectroscopy, HR mass spectrometry, UV-Vis spectroscopy and CHN micro-analyses have also been obtained giving a full analysis of their composition and structure.

2.1 Introduction

<u>The Bailar Twist</u>

The Bailar twist is a concept adopted by inorganic chemists as a conventional means of representing the structural interconversion of octahedral and trigonal prismatic coordination geometries. As the name suggests, John Bailar in 1958 first published the observations that hexa coordinate tris-chelate molecular complexes showed racemisation without the dissociation of any ligand(s), suggesting that the mechanism must involve the formation of a trigonal prismatic intermediate.[1] This theory is long accepted and is best visualised in Fig. 1 where two parallel triangles (one above the metal centre and one below) twist about the C_3 axis. The Bailar twist angle (φ) is defined by the mean torsion angle between *cis* vertices on separate trigonal planes. Therefore φ = 0° represents a perfect trigonal prism (eclipsed conformation) and rotating a single plane by 60° produces a perfect octahedral geometry (φ = 60°).

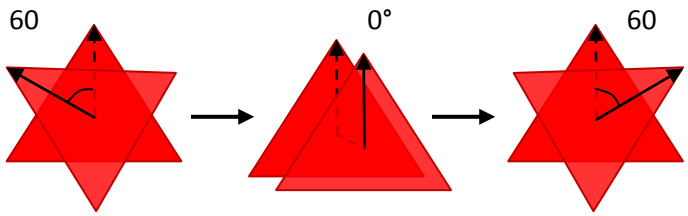

Figure 1: The Bailar twist interconversions between octahedral and trigonal prismatic geometries.

Trigonal Prismatic vs Octahedral Coordination Geometries

In six coordinate complexes there are two distinct geometries, trigonal prismatic and octahedral. All complexes of this coordination number, which accounts for the majority of observed structures, can be defined as O_h, TP or somewhere between the two. For the most part, octahedral is the more favoured geometry and can be justified through certain ligand conditions. Maximising intra-ligand bonding interactions (a), minimising all non-bonded contacts (b) and maximising metal-ligand orbital overlap (c).[2] In an octahedral scenario internuclear donor atom distances have been maximised. This repulsive force has a larger effect among TP geometries as the eclipsed donor atoms only have a separation $\sqrt{2/3}$ the value of O_h, therefore increasing the amount of non-bonded contacts and going against condition (b). This symptom could be resolved by (i) lengthening the metal-ligand bonds but would consequently reduce its stability in reference to condition (c) or (ii) by trigonal elongation, however this would again cause conflict with condition (b). This clearly indicates why octahedral complexes are generally more favoured and reveals that a rigid ligand framework is needed to help enforce a TP arrangement.

Another factor to consider is the stereoelectronic preferences of different metal cations as this can also influence the geometry of a complex. The amount of influence is determined by comparison of Ligand Field Stabilisation Energies (LFSE) between O_h and TP geometries. A calculation was used to determine the different LFSE levels of a complex as a function of the twist angle, φ , provided that the polar angle, $\cos^{-1}\sqrt{1/3}$, remains constant*. See equation (1).[2-4]

$$V_{LF} = 14eq\sqrt{\pi}\{-Y_4^0 - \sqrt{\frac{5}{14}}[(1-e^{-i3\alpha})Y_4^3 - (1-e^{i3\alpha})Y_4^{-3}]\}(r^4/R^5 9) \qquad (1)$$

e =electronic charge, r =radius, q = effective charge, R = metal to ligand distance and Y_l^m are spherical harmonics.[2-4]

* The polar angle is defined as the angle between the C_3 axis and the nearest donor atom. This value is shown to differ very little over a range of octahedral complexes[3] and so is assumed constant in these calculations.

So when φ = 0° (i.e. TP geometry) the orbital energy levels are calculated to be:

$$E(e'') \equiv E(d_{xz}, d_{yz}) = 8/3\ D_q \quad (2)$$
$$E(e') \equiv E(d_{x^2-y^2}, d_{xy}) = -2/3\ D_q \quad (3)$$
$$E(a_1') \equiv E(d_{z^2}) = -4\ D_q \quad (4)$$

Determined from equation 1 the *d*-orbital energy span for an octahedron and trigonal prism are (30/3) and (20/3), respectively.[2] Figure 2 shows that for most six co-ordinate complexes the LFSE for a TP will be less stable than that of an O_h geometry. Comparisons of various d^n metal electronic arrangements show that d^0, d^1, low spin d^2, high spin d^5, high spin d^6 and d^{10} are exceptions to this energetically favourable conformation and show no preference for either octahedral or trigonal prismatic geometry (fig. 3).

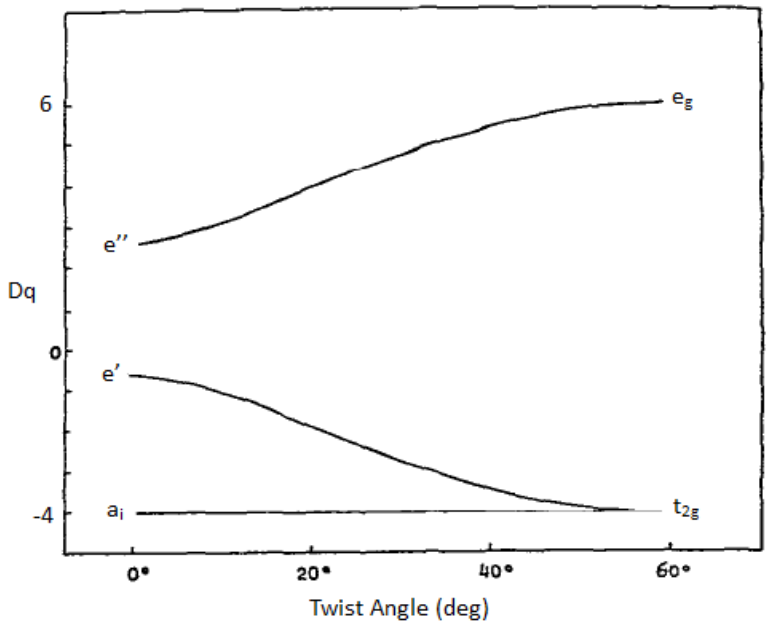

Figure 2: A diagram showing the energy change in *d*-orbitals as a function of Bailar twist angle from TP (0°) to O_h (60°).[2]

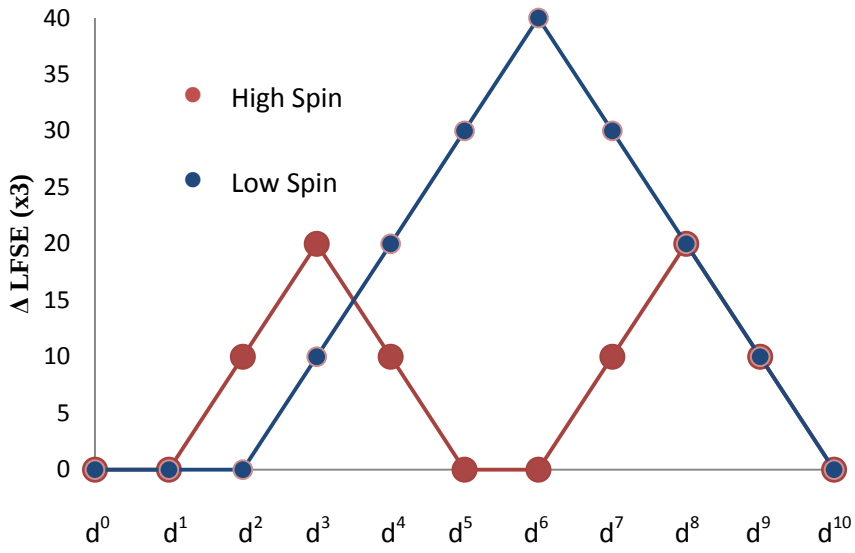

Figure 3: Graph showing the difference in LFSE between the two geometries at various *d*-orbital occupation numbers. Where ΔLFSE = LFSE(O_h) – LFSE(TP).[2]

More advanced calculations incorporating important electronic repulsion effects between the *d*-orbitals were also performed. These repulsive energies were confirmed to further stabilise an octahedral geometry in the cases of d^8 and low spin d^6 systems.[2] Contrary to this the octahedral geometry of a high spin d^7 system was found to be significantly destabilised by this effect. In an example of high spin Co^{II} it was seen that the octahedral arrangement was only 5Kcal/mole more stable than the TP geometry, therefore giving virtually no octahedral preference.[2]

Continuous Shape Mapping (CShM)

Identifying shape/symmetry of a hexa-coordinate complex is not simply a decision of octahedral or trigonal prismatic geometries. In fact perfect symmetry is rarely attainable in reality so it is more sensible to consider it as a scale running from one extreme to the another[5] and this approach is not only constrained to hexa-coordinate geometries.[5-11] A study of this was developed by Alvarez and co-workers where a co-ordination geometry is analysed with reference to an idealised polyhedron.[9]

The program SHAPE was developed to assist in the calculation of *distance* of a particular molecular structure from a stated ideal polyhedron, allowing insight into the geometry and any distortions despite the mode of binding. Firstly the Cartesian coordinates of the investigated polyhedron (with N vertices) are considered, Q_k (where k = 1,2,3…N). This is also done for an

ideal polyhedron with the same number of vertices giving coordinates P_k (where k = 1,2,3…N). From this, the two sets of coordinates are compared and the distances between each of their vertices are calculated. This approach is repeated until a set of P_k coordinates are found that best minimises these comparable distances, with accordance to equation 5.

$$S = \min \frac{\sum_{k=1}^{N} |Q_k - P_k|^2}{\sum_{K=1}^{N} |Q_k - Q_0|^2} . 100 \qquad (5)$$

Where S is the 'shape' measure of the investigated structure and Q_0 is the coordinative vector for the centre of mass of the investigated structure.

Shape values, S, range from 0-100 where 0 = perfect symmetry. So in translation, if the vertices of a structure lie in close proximity to those of an ideal polyhedron, then a near zero shape measurement is achieved and conversely the larger the value of S, the less similar the investigated and ideal structures are.

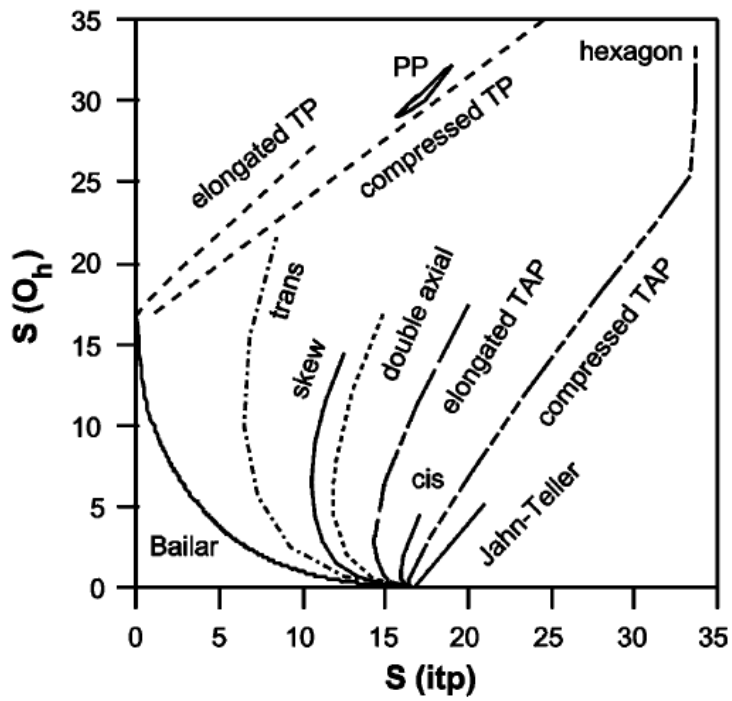

Figure 4: Scatterplot of the octahedral and trigonal prismatic shape measures of a model ML_6 complex for several distortion modes.[9]

Alvarez *et. al.* produced the scatterplot (or shape map) shown in Figure 4 from which the S (Octahedral) and S (Trigonal prism) values of various interconversions and distortions are plotted against each other, with the Bailar twist being shown as one of these distortions.[9]

The ideal Bailar interconversion pathway shown as the solid line in the bottom left corner of figure 4 can be represented by the equation 6:

$$arcsin\frac{\sqrt{S(Oct)}}{10} + arcsin\frac{\sqrt{S(TP)}}{10} = \theta_{Oct,TP} \qquad (6)$$

Where $\theta_{Oct,TP}$ is a constant (24.149) for this particular pair of polyhedra, representing the symmetry angle.[8]

In most cases a structure will not lie directly on the path of minimal distortion as seen above. In this event the deviation can be measured by following equation 7:

$$\Delta(TP, Oct) = \frac{1}{\theta_{Oct,TP}}\left[arcsin\frac{\sqrt{S(Oct)}}{10} + arcsin\frac{\sqrt{S(TP)}}{10}\right] - 1 \qquad (7)$$

<u>Review of trigonal prismatic compounds</u>

It was long thought that six coordinate complexes in their ground state would inevitably have octahedral stereochemistry despite the ligand framework. For the most part, this assumption is true and shows that trigonal prismatic (TP) geometries are comparatively rare and interesting. The first ever TP stereochemistry was reported in 1923 for the extended lattice structure of MoS_2 and WS_{2-} minerals.[12] However it was not until Ibers and Eisenburg in 1965 that the first ever discrete TP complex was identified *via* single crystal X-ray diffraction. They characterised a dithiolato complex, Re-tris(cis-1,2-diphenylethene-1,2-dithiolato), which was shown to have a near perfect TP geometry and an overall molecular symmetry of C_3. [13-15] This led to more investigation of dithiolate transition metal complexes, such as $Mo(S_2C_2H_2)_3$ and the first row transition metal complex $V[S_2C_2(C_6H_5)_2]_3$, which also exhibited a TP or near TP geometry, along with some chromium and tungsten examples, which finally established TP coordination geometries within the field of chemistry.[16-18] This was further investigated with the analogous complexes of $[M\{S_2C_2(CN)_2\}]^{2-}$ (M= V, Mo and Fe)[19-21] and found that a two electron reduction caused their geometry to change (twist) away from TP, along the three fold axis, towards a more octahedral position. This prompted the use of Bailar's twist analogy as it was now

understood that O_h, TP and all intermediate stereochemistries could be related through the degree of twist (α).

In 1970 Wentworth *et. al.*[3,22,23] were also investigating TP co-ordination environments. They created a series of mononuclear first row transition metal complexes (Zn^{II}, Mn^{II}, Co^{II}, Fe^{II} and Ni^{II}) with the Schiff base ligand *cis,cis*-1,3,5-tris(pyridine-2-carboaldimino)cyclohexane ($(py)_3$tach (Fig. 5). Space filling molecular modelling calculations of this ligand revealed that the N-donor groups can adopt the vertices of an ideal TP geometry. Studies into the Zn^{II} complex of $(py)_3$tach, *via* X-ray diffraction, found that the co-ordination did indeed remain largely undeviated from a TP geometry, which is owed to the lack of stereoelectronic preference in d^{10} metal ions. Continued studies using powder X-ray diffraction revealed that the Mn^{II} and Co^{II} complexes have essentially indistinguishable diffraction patterns from that gained by the analogus zinc complex, allowing Wentworth to conclude that these complexes also maintain a TP geometry in the solid state. Unfortunately the Fe^{II} and Ni^{II} complexes displayed substantially different diffraction patterns to the three previous metals discussed, suggesting that they both adopt non-TP geometries. Electronic absorption spectra supported the conclusions drawn from the diffraction data of the two complexes, which provided strong evidence for octahedral or near-octahedral co-ordination environments in both examples. Later investigations, by single crystal X-ray diffraction, revealed the complex $[Ni^{II}(py)_3tach]^{2+}$ did indeed have a non-TP geometry and gave a Bailar twist angle of 32°.[23] In conclusion it was realised that, while the ligand had a conformational preference for TP structures, the co-ordination of strongly octahedral favouring metals, such as low-spin d^6 and d^8 (Fe^{II} and Ni^{II} respectively) can greatly influence the final geometry, twisting away from an ideal TP conformation. Whilst the Co^{II} (high spin d^7) ion does have some preference for octahedral geometries, the difference in ligand-field stabilisation energies is substantially lower and therefore not sufficient to influence the preferred ligand conformation in $[Co^{II}(py)_3tach]^{2+}$.

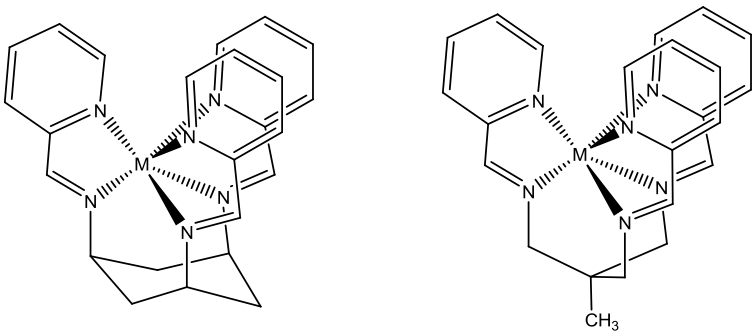

Figure 5: Various metal complexes of the ligand $(py)_3$tach (left) and $(py)_3$tame (right) that have revealed predominately trigonal prismatic co-ordination. (ref 3 + 24)

Fleischer *et. al.* investigated a very similar ligand 1,1',1''-tris(pyridine-2-carboxaldiminomethyl)ethane ($(py)_3$tame) (Fig. 5).[24] In this example the free ligand was also able to adopt a TP configuration, owed to the sp^3 hybridised bridge head carbon creating the ideal angles between pendent arms. The structural rigidity of this ligand is however, lowered compared with that of $(py)_3$tach, and consequently its corresponding Zn^{II} complex revealed a large Bailar twist angle of 28° showing a geometry virtually equal between O_h and TP. A similar situation was revealed in the analogous Mn^{II}, Co^{II} and Ni^{II} complexes where it was proposed that they exhibit very similar geometries. It is unsurprising then that the Fe^{II} complex (low spin d^6) of $(py)_3$tame presented a much larger Bailar twist angle, *ca.* 43°, which is attributed to its strong octahedral preferences along with a less rigid ligand framework.

Larger coordinating systems that are linked together from both ends of the structure have been reported by Raymond *et. al*. They prepared two macrobicyclc tris(catecholate) ligands bicappedTRENCAM (BCT) and bicappedTPTCAM (BCTPT), see Figure 6.[25] Using single crystal X-ray diffraction the Ti^{IV}, V^{IV} and Fe^{III} complexes of BCT reveal a pseudo-TP co-ordination in all cases, where their observed Bailar twist angles are only 8.1°, 11.2° and 10.4° respectively. This is in contrast to the analogous Al^{III} and Ga^{III} complexes, which were found to be more accurately described as pseudo-O_h in geometry, with Bailar twist angles of 40.3° and 34.2° respectively. Spectroscopic evidence, suggested that the TP geometries, of the d-block metal complexes, were stabilised by π-bonding through better orbital overlap. Unfortunately these d-orbitals are filled in the case of Ga^{III}, and are too high in energy for Al^{III}, and therefore have geometries decided largely on repulsive forces.

BCTPT is a slightly larger ligand framework where each capping arm has been extended by one CH_2 unit, see Figure 6. In this case, only the Fe^{III} complex was investigated and was found to have a large Bailar twist angle of 39.5°, indicative of a pseudo-O_h geometry.[25] It is evident therefore, that the addition of extra CH_2 spacer groups in BCTPT, lead to a reduction in the ligand framework rigidity and consequently steric interactions now have less influence on the resulting conformation.

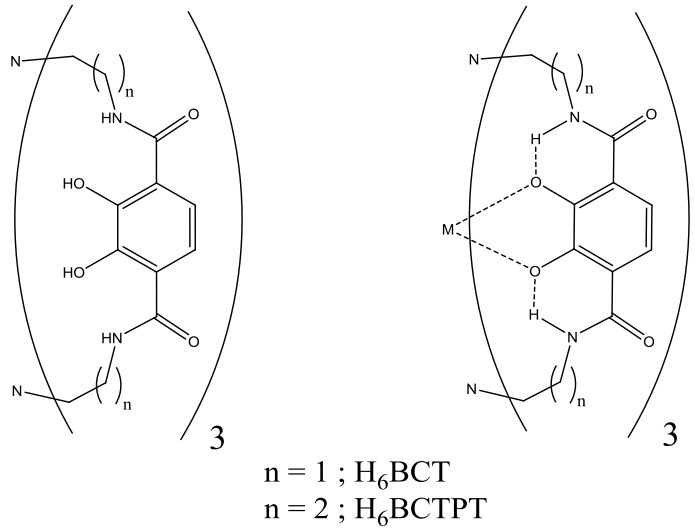

Figure 6: Examples of ligands H_6BCT and H_6BCTPT (left) and their co-ordination mode observed with various transition metal ions, M= Ti^{IV}, V^{IV}, Fe^{III}, Al^{III} and Ga^{III} (right).[25]

Ward and McCleverty *et. al*. have more recently discussed the hexadentate podand ligand tris[3-(2-pyridyl)pyrazol-1-yl]hydroborate (Tp^{py}), (Fig. 7).[26-28,42] This ligand is constructed of three, fairly rigid, bidentate units which are similar in construction to bipyridine. All three pyridyl-pyrazolyl units are tethered at one end by an anionic hydroborate group, where the free ligand naturally adopts a TP conformation. Simple molecular modelling studies added that significant ligand strain would incur from the formation of an octahedral species in a monomeric complex and therefore should encourage TP geometries. However, complexes of Tp^{py} with Zn^{II} and Mn^{II} were isolated and revealed that they actually form tetrameric $[M_4L_4]^{4+}$ O_h complexes. Each ligand binds to three metals, one via each pendent arm, and facially cap one triangular plane of the tetrahedral metal cluster. Conversely to this, the Co^{II} complex was found to produce the desired monomeric TP species, $[Co(Tp^{py})][PF_6]$. Initially the resulted geometries seem contrary to predictions that would be made from simple LSFE theory, where it would be assumed that high-spin d^7 (Co^{II}) metal ions would favour an octahedral environment and that

the Zn^{II} and Mn^{II} ions, with no stereoelectronic preferences (d^{10}), would be predicted to co-ordinate in the unrestrained TP fashion. When also considering the electronic repulsive engeries, due to the occupied metal d-orbitals, as discussed previously (Page 27), the behaviour of the Co^{II} complex can be justified. Incorporation of these electronic effects, in the case of high spin d^7, shows that a TP geometry is only ~5Kcal less stable than its octahedral analogue, and when presented with a rigid TP ligand, like Tp^{py}, it becomes the favoured geometry. It is also evident from various spectroscopic data that the three separate structures were maintained in solution, with no interconversion between tetrameric and monomeric species, demonstrating their stability. In conclusion it was proposed that the different binding modes observed were driven by the stereoelectronic preferences of the metal ion used.

A more recent study by Amoroso *et. al.* into the ligand tris(2,2'-bipyrid-6-yl)methanol, (TBM, see Fig. 7), described the rigid hexadentate tripodal system as having a pre-position for pseudo-TP geometries, and was successfully complexed with several first row transition metals (Mn^{II}→Zn^{II}) as well as Cd^{II}.[30,31] All of these complexes were found to produce descrete monomeric hexdentate structures, where all of the geometries were described as pseudo-TP, and reported Bailar twist angles of ≤25.1°. Unlike Tp^{py}, TBM is a neutral ligand and therefore the formation of tetramers is considered less favourable due to greater electrostatic repulsions involved in clustering. It is also claimed that having no 5-membered rings within the donor system makes the ligand more sterically suited for chelating to a single metal ion. The steric constraints of TBM prevent the formation of octahedral geometries and as a result there is poorer overlap between the six homoleptic donors. This results in the ligand field being considered weaker, generally giving high-spin complexes, which in the case of Fe^{II} reduces the octahedral preference of the metal ion. The Co^{II}, Ni^{II} and Cu^{II} complexes, which do have strong O_h preferences, show the largest trigonal twist angles towards O_h geometry (16.8°, 25.1° and 17° respectively). In contrast, as expected, the metal ions Mn^{II}, Zn^{II} and Cd^{II} all produced the smallest twist angles (≤15.5°), again owed to their lack of stereoelectronic preference. It was also noted that ionic radius had some influence over the resulting core geometry, where larger ions were found to produce the smallest twist angles, and hence have more TP character. As a result these larger metal ions showed significant deviation from the ideal TP shape which has been attributed to the divergent (truncated) nature of the ligand arms which become splayed as the ion becomes larger.

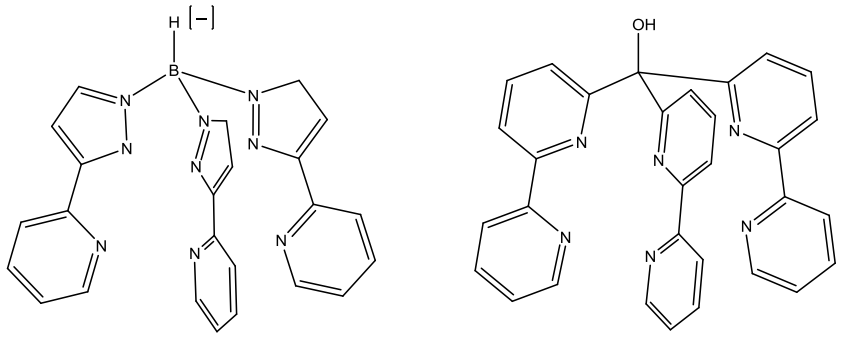

Figure 7: Example of previous ligands with a rigid TP donor arrangement. Left; tris[3-(2-pyridyl)pyrazol-1-yl]hydroborate (Tp^{py}),[26] right; tris(2,2-bipyrid-6-yl)methanol (TBM).[30,31]

In light of the difficulties found in chapter 1, concerning poor complex productivity, challenging analysis and lengthy unpractical syntheses, with no success in synthesising novel bis-tacn chelates, it was of interest to instead focus on developing novel tripodal-based systems, again with an N_6 donor set that could form stable complexes with a variey of metals. The incorporation of a 1-carbon bridge-head group instead of the 4-carbon linker in **L1** is intended to reduce conformational restraints in the complexes produced, in turn increasing the binding affinity.

The work reported in this chapter discusses the synthesis and coordination chemistry of a semi-rigid hexadentate tripodal ligand, tris(2-(3,5-dimethylpyrazole)pyridine)methanol (**L2**, Fig. 8) with a series of p-block and transition metal ions. This ligand shows a preposition for TP geometry and we aim to use different d-electronic configurations and different metal ion radii to examine the relationship between the octahedral and trigonal prismatic characters of these compounds. This will be investigated in both the solid and solution state, and will also show how the incorporation of a substituted 5-membered pyrazole moiety can change this relationship compared to complexes of TBM (Fig. 7).

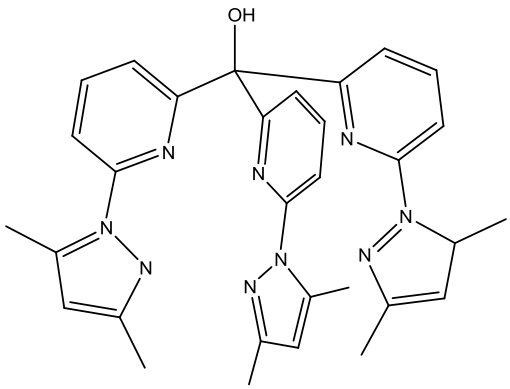

Figure 8: Ligand framework of Tris(6-(2,4-dimethylpyrazol-1-yl)pyrid-2-yl)methanol (**L2**)

2.2 Results and Discussion

2.21 Ligand Synthesis

The bis(2-(6-bromopyridyl))ketone (**S1**) starting material was synthesised by a modification of the literature method described by B. C. Gibb *et. al.*[29] in which the reaction mixture was left for 12h, to slowly reach ambient temperature. Purification of the ketone also followed a modified procedure, involving column chromatography using a 30/70 hexane/dichloromethane solvent system, used to separate the desired bis(2-(6-bromopyridyl)ketone from the 2,6-dibromo bipyridine (**S4**) which is formed as a side product from the homo-coupling of the lithio-pyridine precursor (Sch. 1). This gave the desired product in a yield of 60-70%, comparable to that achieved in the literature method (67%).

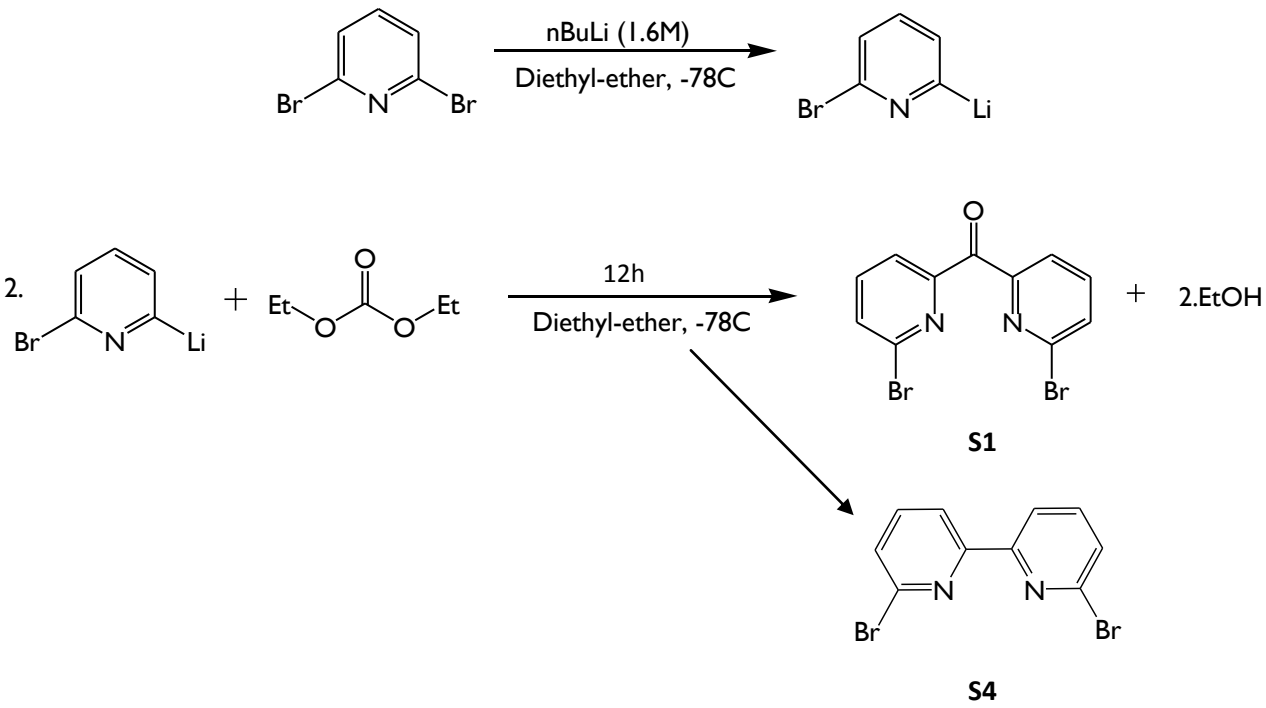

Scheme 1: Synthesis of Bis(2-(6-bromopyridyl)ketone (**S1**) including minor side product 2,6-dibromo bipyridine (**S4**).

The compound, tris(6-bromopyridin-2-yl)methanol (**S2**), was synthesised in accordance with literature methods.[29] However, purification was achieved using the same amended purification method applied to the bis(2-(6-bromopyridyl)ketone (**S1**).

The pre-formed bis(2-(6-bromopyridyl)ketone (**S1**) was added to 1.1 equivalents of the reactive organolithium pyridyl reagent to form the tripodal scaffold **S2** (Sch. 2). The pure compound was then isolated by silica column chromatography (hexane/DCM, 30/70).

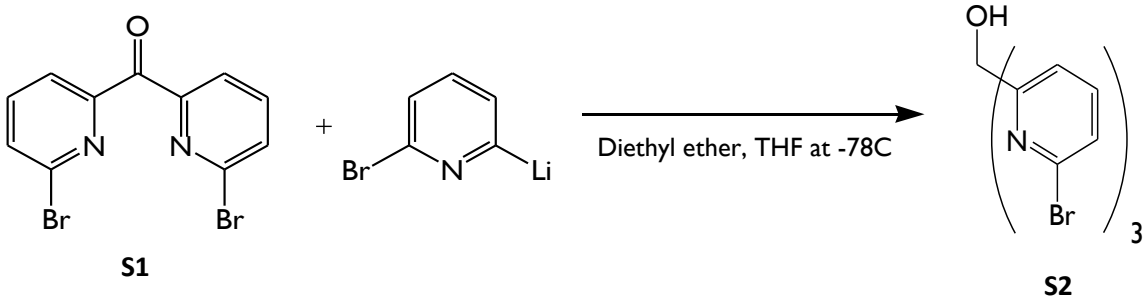

Scheme 2: Synthesis of Tris(6-bromopyridin-2-yl)methanol (**S2**)

This tripodal framework has already been employed as a building block for many different chelating products, showing its usefulness in the development of novel ligands.[30-34] Due to the enhanced reactivity of the bromide on the C-N π-bond of each pyridyl unit, it was possible to directly displace the halide by treatment with hydrazine hydrate as a solvent and refluxing for approximately 14 h. Producing the tris(hydrazino)-tripodal species (**S3**, Sch 3). A small amount of solid precipitated upon cooling (mono and bis substituted impurities), and could be removed by filtration to give a pure hydrazine tripod solution. The filtrate was reduced to a sticky glass-like solid *in vacuo* with gentle heating. The yellow solid was then triturated with cold ethanol (dry) until a paler, powdery solid was achieved, often requiring sonication. The pale solid was filtered off in a N_2 atmosphere as the product was found to be highly hygroscopic, which can be expected for a compound containing three pendent hydrazino functionalities. The desired product was isolated in high purity and was confirmed by ^{1}H- and ^{13}C-NMR spectroscopy, which showed that the three aromatic CH signals had shifted upfield, and HR-Mass Spectrometry which displayed the correct molecular ion signal at 353.17 m/z corresponding to **S3**.

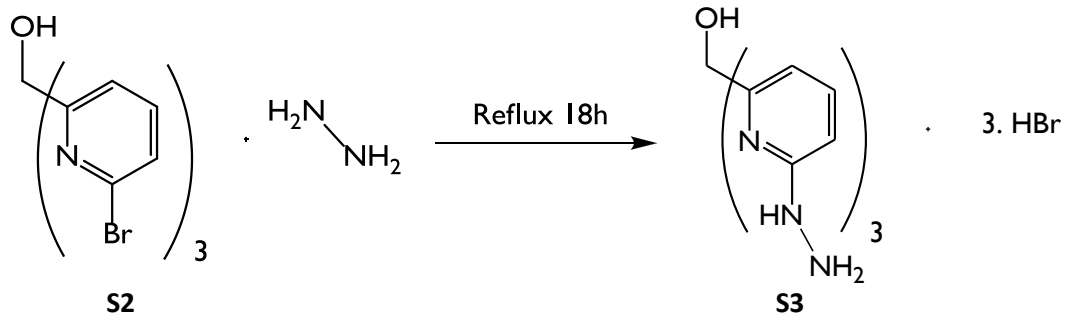

Scheme 3: Synthesis of the intermediate tris(6-hydrazinopyridin-2-yl)methanol (**S3**)

The new product tris(6-hydrazinopyridin-2-yl)methanol (**S3**) was then condensed with 4 equivalents of 2,4-pentanedione in an ethanol/methanol (2:1) solvent by heating, for a further 14h. The solvent was removed *in vacuo* to give a crude yellow oil which contained the tris(dimethyl-pyrazole) heterocyclic ligand (**L2**), summarised in Scheme 4, as a major constituent. This mixture was washed with diethyl ether and the washings were combined, and evaporated to give the pure product in more than 60% yield, confirmed by NMR spectroscopy with further evidence from mass spectrometry.

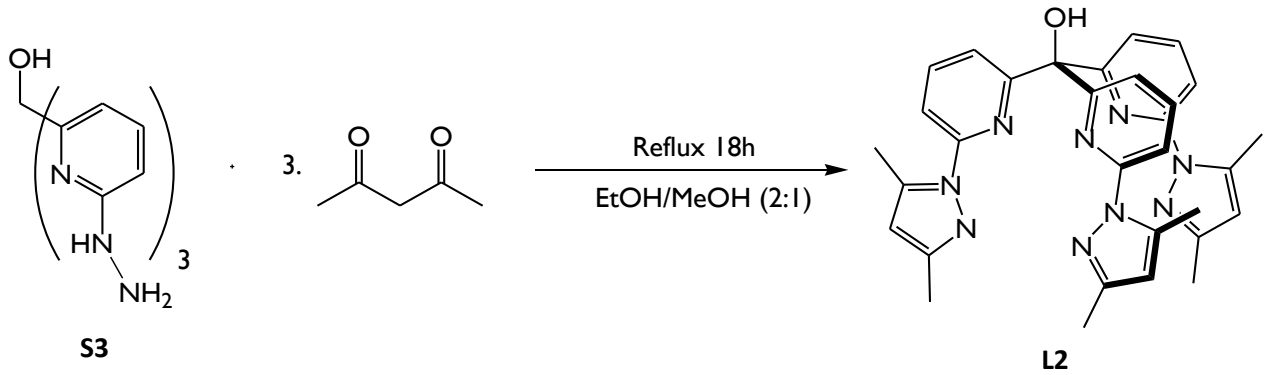

Scheme 4: Synthetic route to Tris(6-(3,5-dimethylpyrazol-1-yl)pyrid-2-yl)methanol (**L2**).

2.22 Synthesis of Complexes

This ligand (**L2**) can be treated with a series of transition metal perchlorates, chlorides or hexafluorophosphates by simply stirring a solution of the ligand in chloroform/acetonitrile (typically 0.1mmol in 3 ml) and subsequently adding a solution of the metal salt dissolved in MeCN or THF (typically 1-2 ml). A vivid colour change is usually observed during the formation of all of the complexes except for the Zn(II), Cd(II) and Hg(II) analogues which is typical as d^{10} systems are renowned for giving white/colourless solids and solutions. All of the complex solutions **2.1 - 2.12** (see table 1) were filtered through celite and must be precipitated from acetonitrile with diethyl ether to give the pure complexes.

Table 1: Showing complex label with the corresponding metal ion used

Complex label	Ion used
2.1	Cr(III)
2.2	Mn(II)
2.3	Fe(III)
2.4	Fe(II)
2.5	Co(II)
2.6	Ni(II)
2.7	Cu(II)
2.8	Zn(II)
2.9	In(III)
2.10	Cd(II)
2.11	Hg(II)
2.12	Re(I)

All of the complexes were prepared in a 1:1 (metal : Ligand) ratio, with exception of complex **2.12** (3:1) as $Re(CO)_5Br$ is well known for its co-ordination to bidentate imines such as bipy *via* the loss of two CO groups. The complex solutions were stirred for 24h to ensure equilibrium was reached before attempting isolation however, colour changes generally occurred within seconds. Most complexes could be crystallised from varying organic solvents by vapour diffusion giving samples suitable for X-ray crystallographic studies.

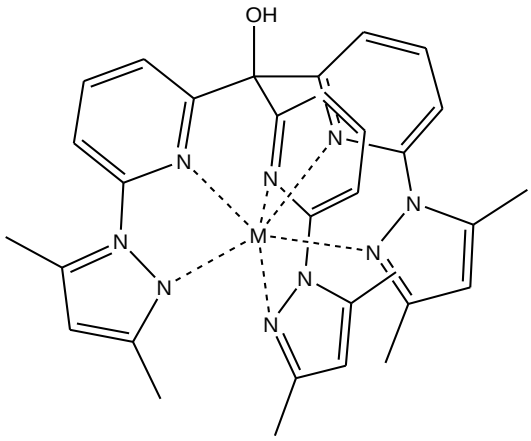

M = Zn(II),Cu(II), Ni(II), Co(II), Fe(II), Fe(III), Mn(II), Cd(II), Hg(II),

Figure 9: Schematic diagram showing the general co-ordinating arrangement of the various transition metal ions.

Spectroscopic Properties of Complexes

2.23 Vibrational spectroscopy

The IR spectra of **L2** and all complexes were collected using KBr discs and the data displayed in tables 2 and 3. The pyridine ring vibrations of complexes **2.1**-**2.12**, typically 1600cm^{-1} to 1425cm^{-1}, are seen to have shifted compared to the free ligand **L2**. These shifts are indicative of the pyridine nitrogens coordinating to the metal centre. The π(C-H) vibrations, attributed to the rocking modes of the pyridyl C-H bonds, are also seen to shift for the same reason and in both cases the number of absorption peaks observed falls to 3. Less peaks suggest that complexation has led to a more symmetrical and rigid structure therefore providing fewer modes of vibration. In all the spectra a broad band between 3250 – 3500cm^{-1} can be seen and could be attributed to the tertiary alcohol groups however, water contaminating the KBr is more likely. A very strong and broad band near 1100cm^{-1} and a strong sharp vibration near 622cm^{-1} correspond to the perchlorate counter ions and is exhibited in the spectra for all of the complexes reported. The presence of only 2 bands is evidence that the counter ions are non co-ordinating.[35] This evidence of pyridine complexation and un-coordinated perchlorate counter ions agrees with that found in the x-ray diffraction data. Two very strong bands (2021cm^{-1} and 1894cm^{-1}) are seen in the spectra for compound **2.12** due to co-ordinated carbonyl groups and fall within the typical range of terminally bound CO *ca*. 2150-1850cm^{-1}, which correlates with the x-ray data (Page. 80).[36]

Table 2: Showing characteristic vibrational modes of **L2** and complexes					
compound	Aromatic ν(C-H)	ν (O-H)	ν (C=N) and (C=C)	π(C-H)	ν (Cl-O)
L2	3128.46(m), 3109.17(m), 3095.19(m)	3439.9 (m)	1594.64(s), 1575.1(s),1563.5(s) &1455.99(br+s), 1378.85(s)	823.94(s), 811.89(s), 794.53(s), 779.10(s)	n/a
2.1	3096.15(br+s)	3383.28 (br+s)	1607.03(s), 1577.49(br+s) and 1453.1(br+s)	813.81(s), 781.99(s), 748.25(m)	---
2.2	3135.69(m), 3109.87(m)	3346.85 (br+s)	1603.52(s), 1587.58(s), 1564.95(s) and 1467.56(br+s), 1428.34(s)	808.03(s), 777.17(m), 749.21(s)	1096.33(br+s), 621.93(s)
2.3	3130.14(m), 3095.01(m)	3399.89 (br+s)	1606.41(s), 1578.21(s), 1562.78(s) and 1470.7(br+s), 1425.62(s)	811.16(br+s) , 780.07(m), 752.34(m)	1109.35(br+s), 622.56(s)
2.4	3126.04(m), 3098.41(m)	3299.61 (br+m)	1603.52(s), 1587.38(s), 1561.09(s) and 1473.35(br+s), 1420.65(s)	808.99(s), 776.21(m), 747.28(s)	1094.4(br+s), 621.93(s)
2.5	3125.08(m), 3103.39(m)	3285.14 (br+m)	1604.48(s), 1589.06(s), 1563.5(s) and 1474.8(br+s), 1417.91(s)	803.21(s), 776.69(m), 747.76(s)	1109.83(br+s), 623.38(s)
2.6	3126.1(m), 3103.87(m)	3393.75 (br+s)	1604.48(s), 1590.5(s), 1563.99(s) and 1475.28(br+s), 1421.25(s),	805.14(s), 776.21(m), 748.25(s),	1105.98(br+s), 623.86(s)
2.7	3135.78(m), 3114.47(m)	3451.96 (br+s)	1608.34(s), 1583.27(s), 1567.09(s) and 1465.63(br+s), 1431.31(s),	808.99(s), 781.99(m), 750.17(m)	1088.62(br+s), 623.86(s)
2.8	3126.04(m), 3102.52(m)	3302.5 (br+s)	1603.52(s), 1589.91(s), 1562.06(s) and 1473.35(br+s), 1421.13	806.10(s), 777.17(m), 748.25(s)	1106.94(br+s), 622.89(s)
2.9	3132.31(m), 3101.46(m)	3381.10 (br+m)	1595.2(s), 1578.93(br+s) and 1475.01(s), 1453.1(br+s)	811.89(s), 781.99(s), 744.87(m)	---

Table 3: Characteristic vibrational modes for complexes **2.10**-**2.12**					
compound	Aromatic ν(C-H)	ν (O-H)	ν (C=N) and (C=C)	π(C-H)	ν (Cl-O) or (M-C) and (CΞO)
2.10	3130.38(m), 3102.20(m)	3334.32 (br+s)	1601.59(s), 1591.25(s), 1565.43(s) and 1466.12(br+s), 1432.85(s)	808.02(s), 778.62(m), 745.84(s)	1091.51(br+s), 622.41(s)
2.11	3129.42(m), 3101.2(m)	3342.03 (br+s)	1599.18(s), 1589.20(s), 1563.02(s) and 1465.63(br+s), 1430.92(s)	809.47(s), 781.99(m), 746.80(s)	1089.58(br+s), 622.41(s)
2.12	3093.19(w), 3038.85(w)	3360.35 (br+m)	1603.52(s), 1585.46(m), 1563.02(s) and 1453.58(s), 1420.8(s)	805.62(m), 737.16(m)	2021.03(s), 1894.24(br+s)

2.24 ^{1}H NMR and ^{13}C NMR spectroscopy

The d^{10} nature of group 12 metals inherently means they are diamagnetic and therefore it was possible to perform NMR experiments on these compounds to help confirm their coordination modes. The ^{1}H and ^{13}C NMR spectrum of **L2**, **2.8**, **2.10** and **2.11** were measured in $CDCl_3$ or CD_3CN solutions and were measured at ambient temperature. ^{1}H NMR spectra from the ligand and complexes were very characteristic, with only three aromatic protons to consider, two methyl singlets, a lone proton from the back bone of the pyrazole function and the apical hydroxyl proton. This simplicity is a consequence of the three fold symmetry (C_{3v}) adopted by the ligand and most importantly the complexes.

The three aromatic proton resonance frequencies for all the complexes were shifted downfield, by at least 0.2 ppm (Figs. 10 - 15) with respect to the free ligand **L2**. There are still only three aromatic proton environments present in their respective spectra indicating that some form of 3-fold symmetrical complexation has occurred. Zn^{2+} is a relatively small transition metal ion making it a reasonably hard Lewis acidic ion. This Lewis acidity causes an inductive effect upon coordination of the Zn^{2+} ion with the ligand and gives rise to significant shifts in resonance frequency. The same effect is present in both the Cd and Hg complexes. Interestingly, noting that these latter metals are considered "softer", the ^{1}H-NMR data also suggests that the negative inductive effect is greater in both **2.10** and **2.11**, relative to the Zn complex. Heavier transition metals are known to form stronger bonds to softer donors as there is generally better overlap between metal and donor orbitals, therefore allowing more charge transfer. This could account for the large shift observed in the ^{1}H-NMR spectra of **2.10** and **2.11**.

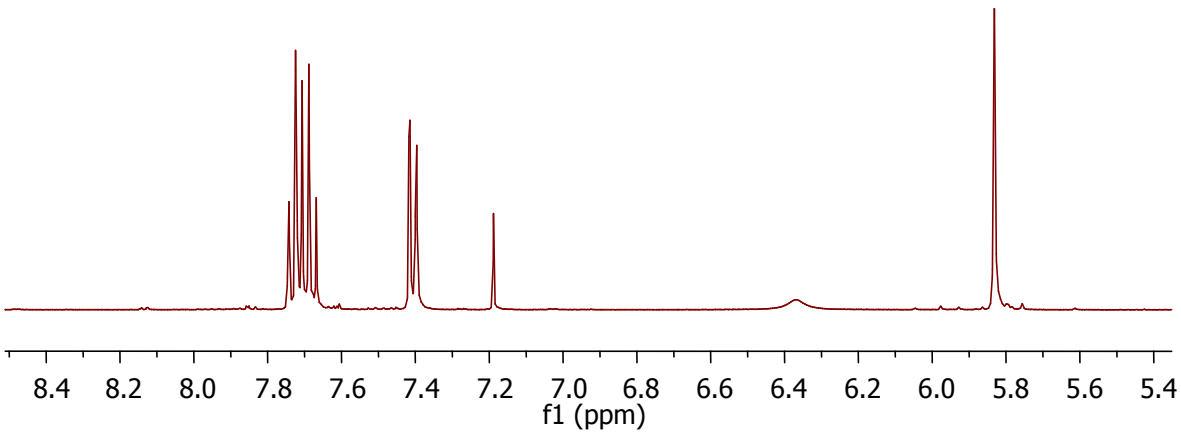

Figure 10: ^{1}H NMR of the parent Ligand **L2** in CD_3CN.

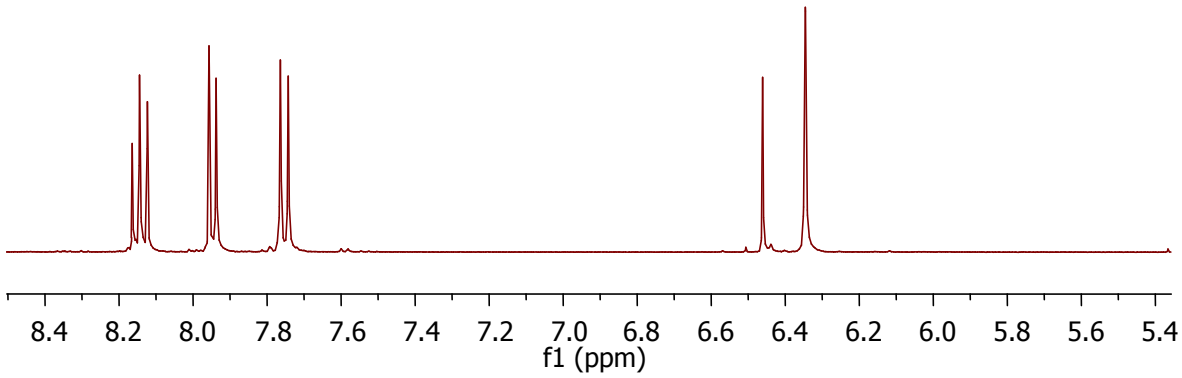

Figure 11: ^{1}H NMR of the Zn^{II} complex **2.8** in CD_3CN.

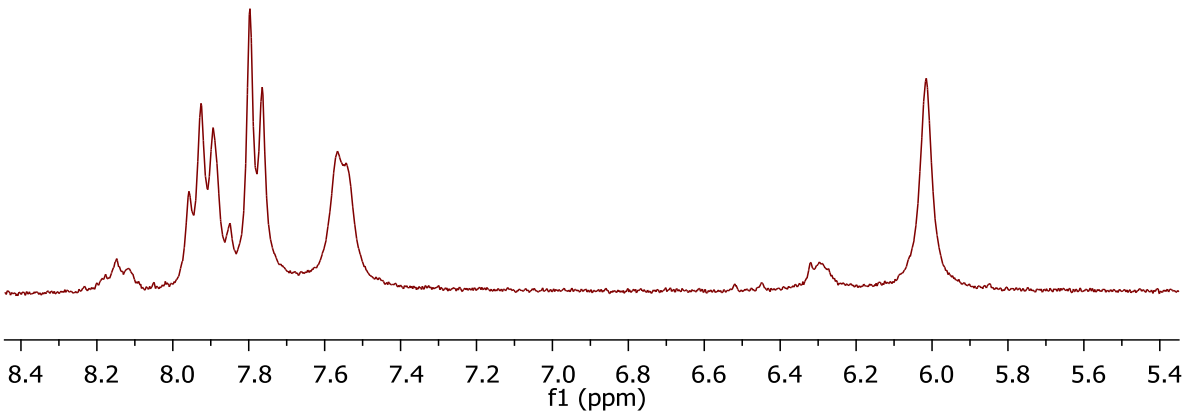

Figure 12: ^{1}H NMR of the In^{III} complex **2.9** in CD_3CN.

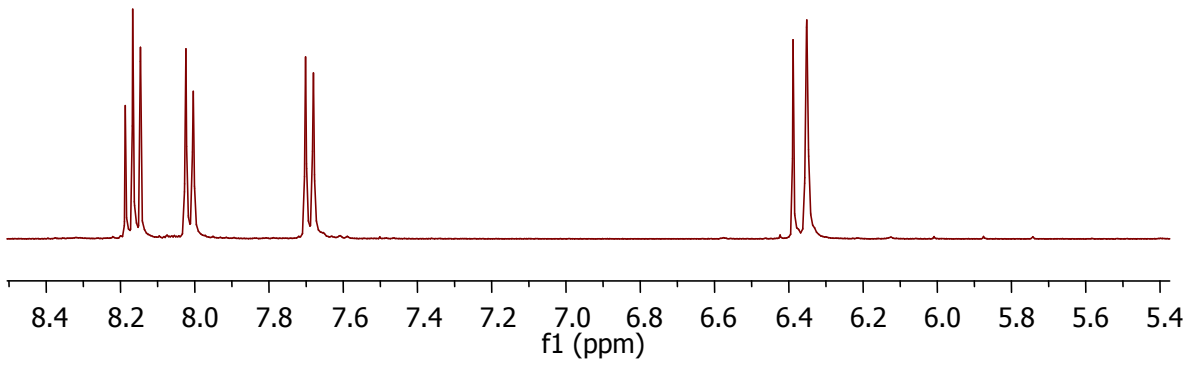

Figure 13: ^{1}H NMR of the Cd^{II} complex **2.10** in CD_3CN.

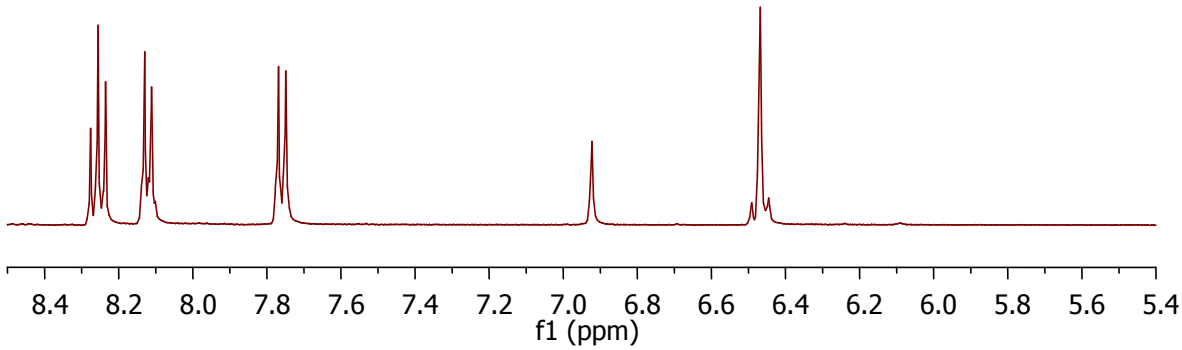

Figure 14: ^{1}H NMR of the Hg^{II} complex **2.11** in CD_3CN.

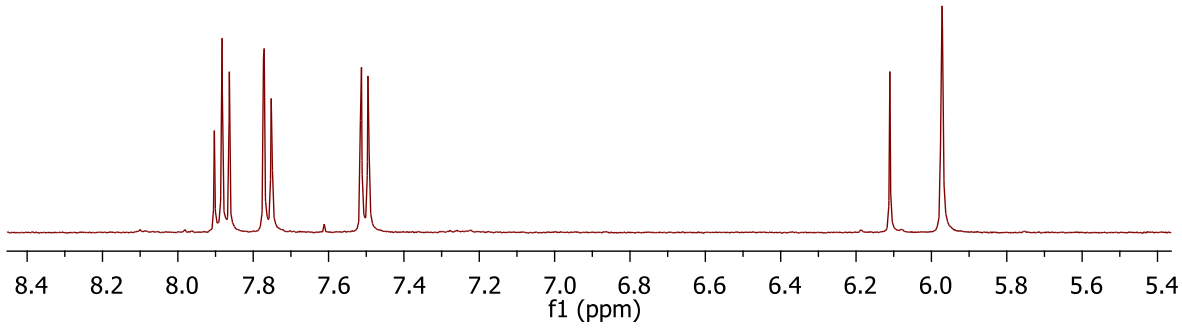

Figure15: ^{1}H-NMR of the tris-Rhenium complex **2.12** in CD_3CN.

2.25 Electronic Absorption Spectra: UV/Vis

The electronic absorption spectra of **L2** and complexes **2.1**-**2.7** and **2.12** have been measured and the data is displayed in Table 4. All of the compounds were analysed from an acetonitrile solution in a 1cm quartz cuvette at various concentrations ranging from $9.9x10^{-3}$ to $3.2x10^{-6}$ mol dm^{-3}. The electronic absorption spectra for all complexes of **L2** possess two intense peaks between 254nm and 293nm, these are attributed to the intra-ligand π-π* transitions characteristic of bipyridine like molecules.

Table 4: Electronic absorption spectral assignments

compound	π-π* transitions / λ (nm)	MCLT λ (nm)	d-d transitions / λ (nm)	Dq	B (cm^{-1})	B^b
L2	259.3(43,668), 287.3(41,797)	–	–	-	-	-
2.1 (Cr3+)	254.5(31,873), 289.9(23,904)	hidden	452.3(170), 619.3(130),	1612	576	0.56
2.2 (Mn2+)	254.2(36,797), 293.5(37,879)	~350 (weak shoulder)(1082)	Not observed	-	-	-
2.3 (Fe3+)	260.8(32,228), 288.2(34,183)	~350 (shoulder)(1984)	Not observed	-	-	-
2.4 (Fe2+)	254.9(104,972), 284.2(91,160)	~300 (shoulder)(22,000)	559.8(96), 609.2(86),	-	-	-
2.5 (Co2+)	254.7(33,099), 290.3(29,577)	~305 (shoulder)(17,000)	491.0(30), 631.0(17), 1073.6(17)	1367	581	0.519
2.6 (Ni2+)	256.4(39,371), 289.2(30,709)	~300 (shoulder)(20,000)	558.1(26), 818.2(21), 963.7(35)	1333	629	0.58
2.7 (Cu2+)	258.8(40,396), 287.5(37,923)	Hidden	705.2(106)	1403	-	-
2.12 (Re1+)	261.0(59,215), 285.2(62,010)	~300 (shoulder)	-	-	-	-

*figure in brackets represents molar absorption coefficients ε ($M^{-1}cm^{-1}$).

Compound 2.1: The Chromium(III) complex **2.1** presents two observable bands in the visible region of the spectrum, one at 16155 cm^{-1} (v_1) and the other at 22123 cm^{-1} (v_2), see figure 16. As expected from the crystallographic data and the kinetic inertness of Cr(III), the complex is known to possess, a strong octahedral geometry (Page. 54). From this the solution geometry is also assumed octahedral and therefore the transitions can be assigned as $^4T_{2g}(F) \leftarrow {}^4A_{2g}$ and

$^4T_{1g}(F) \leftarrow {}^4A_{2g}$ in increasing energy, where $v_2/v_1 = 1.37$. Using a d^3 Tanabe-Sugano diagram for an octahedral complex it is possible to approximate *Dq* and the Racah inter-electronic repulsion parameter *B*, which calculate as 1612 cm^{-1} and 576 cm^{-1} respectively (Δ/B = 28). The nephelauxetic ratio, β = 0.56 (assuming free ion $[Cr^{III}]$, B = 1030cm^{-1}) and again shows a great deal of covalency within the bonds to the metal centre.[37]

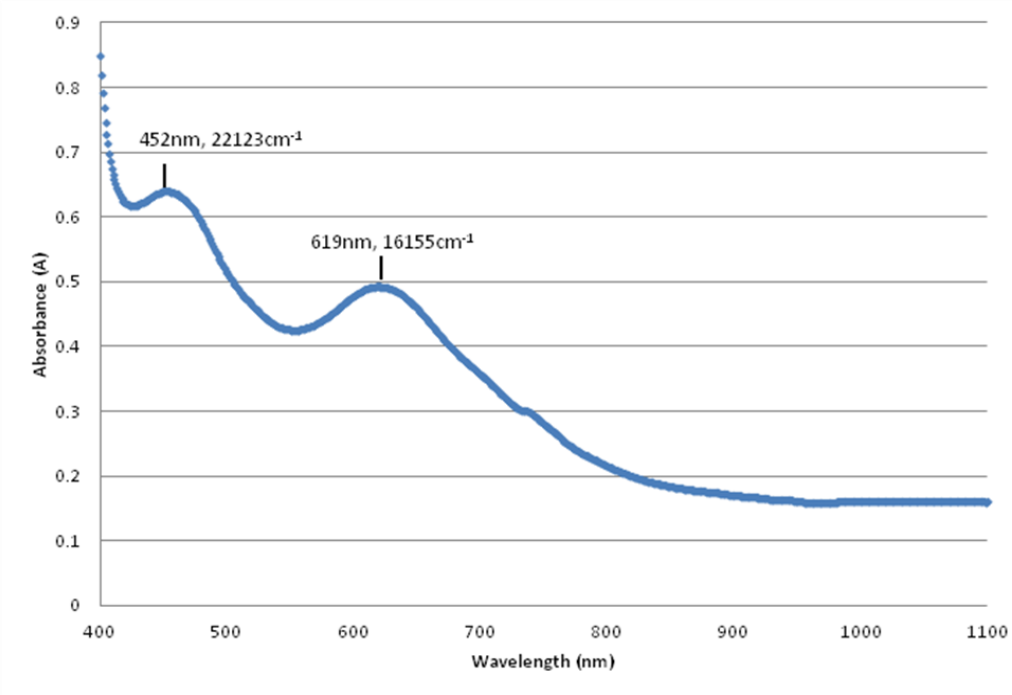

Figure 16: Visible region of the electronic aborption spectrum for **2.1** $[Cr^{III}(\mathbf{L2})]^{3+}$

<u>Compound 2.2:</u> The manganese(II) complex **2.2** reveals no d-d transition peaks even in a concentrated solution. The molar extinction coefficient for octahedral Mn^{2+} complexes are typically in the range of 10^{-2} – 10^{-1} $dm^3mol^{-1}cm^{-1}$ and it is not surprising that these spin forbidden transitions are not seen. To observe these particular transitions a sample with concentrations of ≥10M (with 1cm path length) would be required and unfortunately concentrations of this magnitude were not possible due to the low solubility of the complex. It should also be noted that at higher concentrations even a weak tail from high energy organic absorptions can be enough to obscure these weak transitions from the spectrum.

Compound 2.3: The Iron(III) complex **2.3,** which is d^5 in nature, is known to be HS and shows no observable d-d transitions. Unlike manganese(II), which is also d^5, Iron(III) has an extra positive charge giving it a greater ability to polarize coordinated ligands. As a result this allows the metal centre to produce intense charge transfer absorptions at much lower energies than Mn^{II} tailing into the visible region, which explains the orange colour of this complex. As a consequence of this CT the relatively weak d-d transitions are therefore obscured from view (Fig. 17).

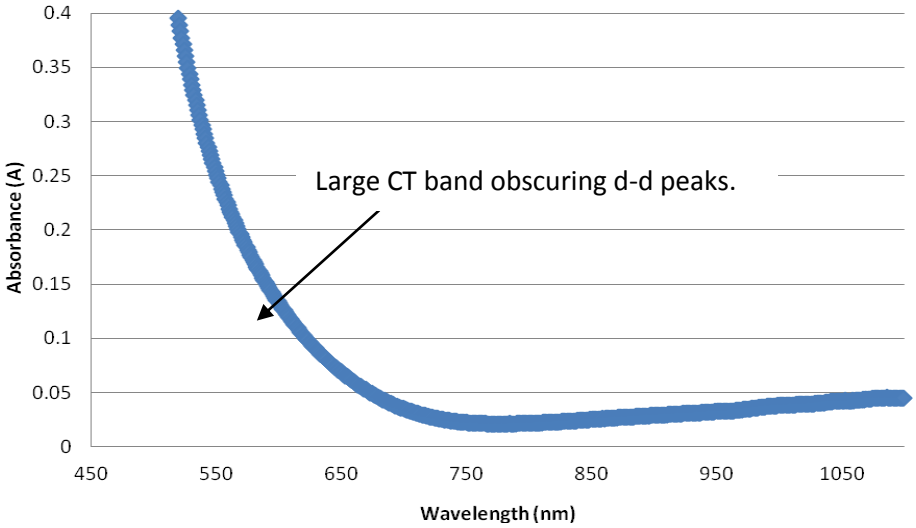

Figure 17: Electronic absorption spectra of the visible region for the Fe(III) complex **2.3**, showing how the CT band overwhelms other weak transitions as far as 750nm.

Compound 2.4: The Iron(II) complex **2.4** presents two d-d transition bands, one at 17862 cm^{-1} and a shoulder at 16415 cm^{-1}(Fig. 18), which is comparable to the analogous tris(2,2'-bipyrid-2-yl)methanol complex $[Fe^{II}(TBM)]^{2+}$, which has peaks at 20120 cm^{-1} and 17953 cm^{-1}.[30+32] The complex **2.4** is also known to be high spin from the magnetic moment studies, μ = 4.45 BM (Page 83). In the instance of octahedral high spin Fe^{2+} there is only one spin-allowed transition ($(t_{2g})^4(e_g)^2 \rightarrow (t_{2g})^3(e_g)^3$, *i.e.* $^5E_g \leftarrow {}^5T_{2g}$). However, the existence of two bands in the visible region have been suggested to be part of the ^5E_g state splitting to remove degeneracy of the asymmetrically filled T_{2g} subset. This is a feature noted for octahedral $Fe^{2+}(bipy)_3$ type compounds giving peaks at 20367 cm^{-1} and 19120 cm^{-1}.[38] However, with this compound both absorption peaks of **2.4** are significantly red shifted in comparison to octahedral $[Fe(bipy)_3]^{2+}$. Wentworth *et. al.* also made similar observations of shifting with the complex $[Fe^{II}((py)_3tach)]^{2+}$, cis,cis-1,3,5-tris(pyridine-2-carboxaldimino)cyclohexane ($(py)_3tach$), a ligand that exhibits a

coordination environment similar to **L2** that sterically prefers trigonal prismatic geometries.[3] The shifting and relatively high molar extinction coefficients of **2.4**, $[Fe^{II}((py)_3tach)]^{2+}$ and $[Fe^{II}(TBM)]^{2+}$ suggest some twist from the ideal geometry and provide evidence that the complexes may retain a predominantly trigonal prismatic geometry even in solution, which is also supported by crystallographic data (Page 60). It is to be noted that this is not conclusive evidence as similar behaviour has been recorded in the octahedral complex $[Fe^{(II)}(o\text{-phenanthroline})_3]^{2+}$.[39]

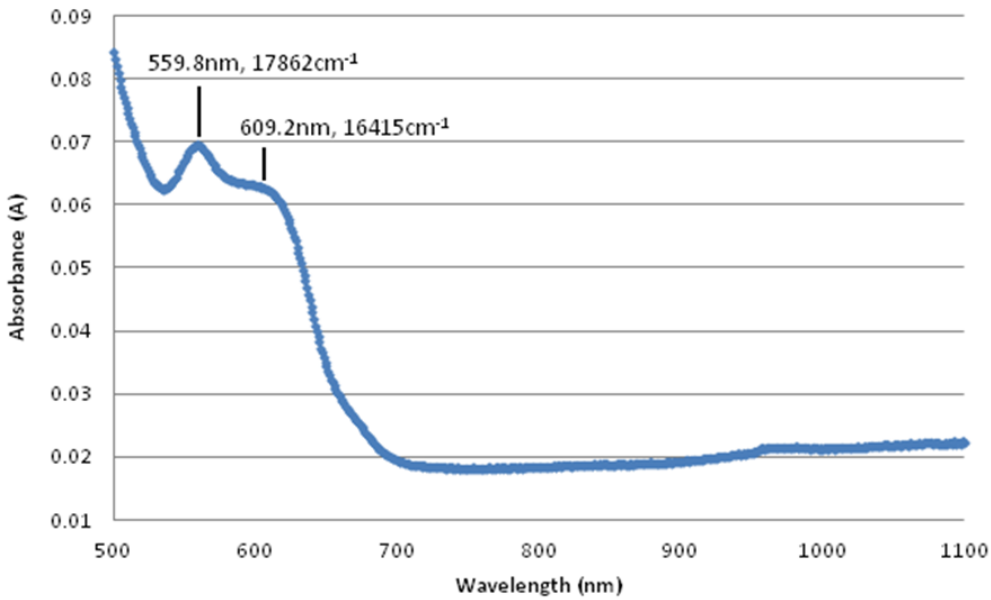

Figure 18: Visible region of the electronic aborption spectrum for **2.4** $[Fe^{II}(L2)]^{2+}$ performed in CH_3CN, with relative peak energies labelled.

<u>Compound 2.5:</u> The absorption bands for the Co^{II} compound **2.5** (Fig. 19), which has been assumed trigonal prismatic, based on single crystal X-ray diffraction (Page. 62) data, was assigned using the appropriate d^7 Tanabe-Sugano diagram (Fig. 20). The visible region of the spectrum consists of three observable peaks, a broad low energy band at 9319 cm^{-1} attributed to a combination of the spin allowed transitions $^4A_2'$, $^4A_2''$+ $^4A_1''$, $^4E''(F)\leftarrow{}^4E'$, the second band seen at 15848 cm^{-1} is labelled as the transition $^4E''(P)\leftarrow{}^4E'(F)$ and finally the third band occurring at 20368 cm^{-1} is therefore assigned as the $^4A_2'(P)\leftarrow{}^4E'(F)$ transition. Note: in the analogous tripodal bipy complex ($[Co^{II}(TBM)]^{2+}$) this third band is obscured by a large metal to ligand charge transfer (MLCT) peak.[30,32]

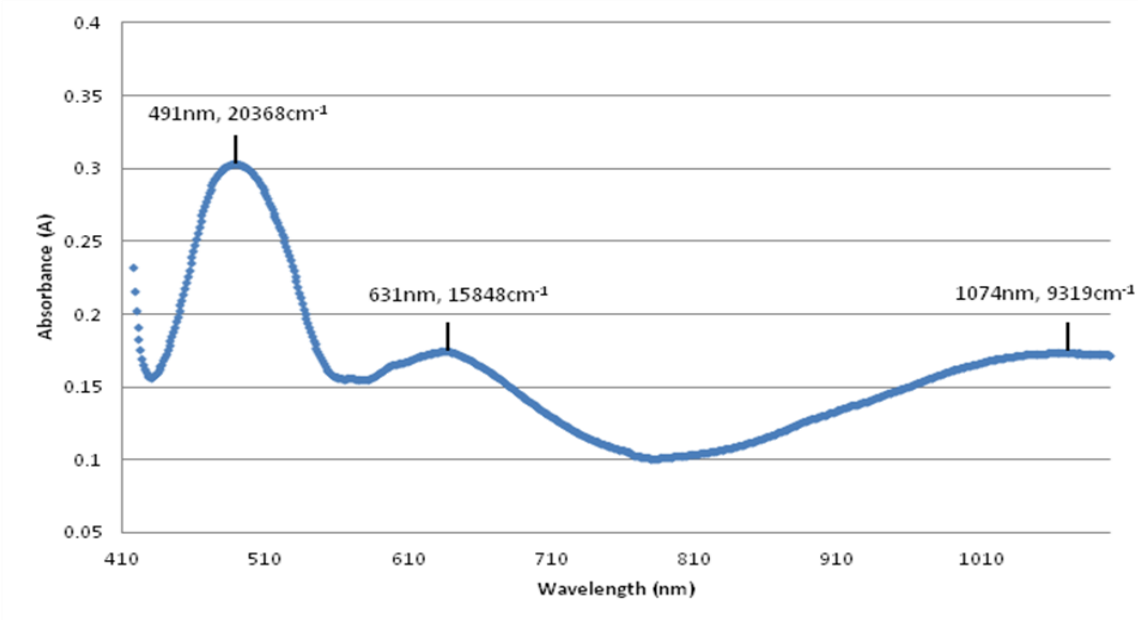

Figure 19: Visible region of the electronic aborption spectrum for **2.5** $[Co^{II}(\mathbf{L2})]^{2+}$ performed in CH_3CN, with relative peak energies labelled.

Using Figure 20 it is possible to approximate *Dq* and the Racah Parameter, *B,* for a trigonal prismatic d^7 metal. taking the transition at 9319 cm^{-1} as the midpoint of the lower manifold, *Dq* and *B* were calculated as 1366 cm^{-1} and 581 cm^{-1} respectively (*Dq/B* = 2.35). The nephlauxetic ratio, β = 0.519 (assuming free ion $[Co^{II}]$, *B* =1120 cm^{-1}),[37] shows the metal centre to have a significant degree of covalency within bonding. It is also possible to calculate the two ligand field splitting parameters $\Delta_1 = \Delta_2 = 3\frac{1}{3}Dq$ = 4552 cm^{-1}, (this is still assuming a perfect trigonal prism), which is comparable to the $[Co^{II}(TBM)]^{2+}$ complex with a value of 5070 cm^{-1}.[30,32] Although crystal data suggests otherwise, these measurements are in solution so the same complex was also treated as though octahedral in geometry. This gives 9319 cm^{-1} as the $^4T_{2g}(F) \leftarrow {}^4T_{1g}$ transition and 15848 cm^{-1} as $^4T_{1g}(P) \leftarrow {}^4T_{1g}$ transition. On this basis *Dq* was found to be 932 cm^{-1} and *B* equal to 424 cm^{-1}. These values are significantly lower than that found for the octahedral complex $[Co(bipy)_3][Cl]_2$ (Dq = 1112 cm^{-1} and B = 794 cm^{-1}) which is expected by twisting the geometry away from octahedral towards TP.[57] In conclusion the Dq value from the TP scenario of **2.5** is in better agreement with Dq of $[Co^{II}(bipy)_3]^{2+}$ (1366 cm^{-1} *vs* 1267 cm^{-1}) and therefore supports the presence of a more TP like geometry in solution.

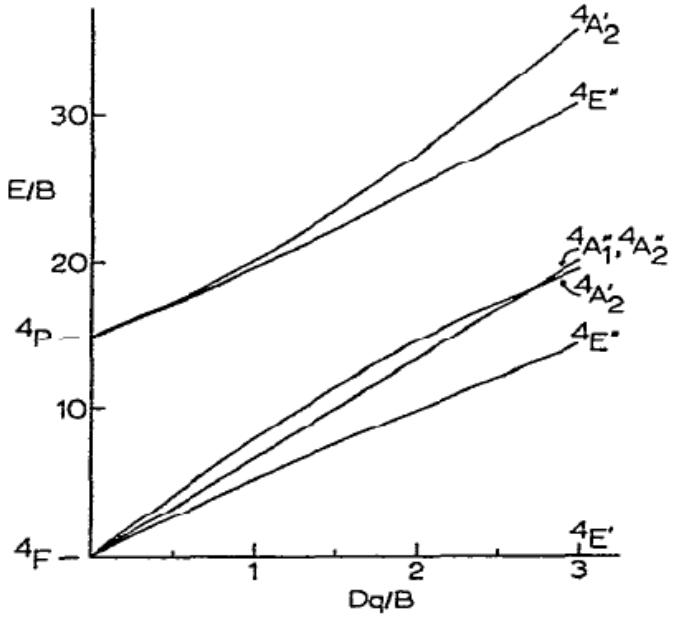

Figure 20: Energy level diagram for a d^7 trigonal prismatic complex.[3]

<u>Compound 2.6</u>: There are three clear d-d transitions present in the visible region for complex **2.6.** Firstly due to the nature of Ni^{II}, (which generally show a stronger preference for O_h than TP), it is assumed that the metal centre is octahedral allowing the following transitions to be assigned: $^3T_{2g}\leftarrow{}^3A_{2g}$, $^3T_{1g}(F)\leftarrow{}^3A_{2g}$, $^3T_{1g}(P)\leftarrow{}^3A_{2g}$ which appear at 10377, 12223 and 17917 cm^{-1} respectively (Fig. 21). Using this information and the appropriate d^8 Octahedral Tanabe-Sugano diagram *Dq* was found to be 1037 cm^{-1} and *B* to be <208 cm^{-1}. This is a very low *B* value which is much lower than typical values ($[Ni(bipy)_3]Cl_2.7H_2O$, *B* = 672 cm^{-1} and $[Ni(2\text{-}(2\text{-pyridyl})imidazole)_2](NO_3)_2.2H_2O$, *B* = 747 cm^{-1})[57] and so this does not support the presence of an octahedral centre in solution and was calculated by the v_2/v_1 ratio of 1.18 only fitting at the extreme end of the T-S diagram (*Dq*/*B* >50). The complex was then modelled to a trigonal prismatic geometry allowing the bands to be assigned alternatively to the spin-forbidden $^1E'\leftarrow{}^3A_2'$ and two spin-allowed $^3E'\leftarrow{}^3A_2'$, $^3E''(P)+{}^3A_2'(P)\leftarrow{}^3A_2'$ in increasing energy (Fig. 22), in this case the spectroscopic parameters become *Dq* = 1333 cm^{-1} and *B* = 629 cm^{-1} (*Dq/B* = 2.12). Using this data the third band ($^3E''(P)+{}^3A_2'(P)\leftarrow{}^3A_2'$) is predicted to appear at 16792 cm^{-1} which is close however slightly lower than the observed 17917 cm^{-1}. The ligand field splitting parameters are $\Delta_1 = \Delta_2 = 4444$ cm^{-1}, assuming a perfect TP geometry. Alternatively the two low energy observable bands could be assigned in reverse instead ascribing $^3E'\leftarrow{}^3A_2'$ as the lowest

energy transition, this then gives *Dq* as 1103 cm^{-1} and *B* as 721 cm^{-1}(*Dq/B* = 1.53) with the third band predicted to occur at 16574 cm^{-1}.

On the basis of d-orbital splitting of a trigonal prism (Fig. 2 in intro), the ligand field splitting parameters are proposed; $\Delta_1 \equiv E(d_{x2-y2}, d_{xy}) - E(d_{z2})$ and $\Delta_2 \equiv E(d_{xz}, d_{yz}) - E(d_{x2-y2}, d_{xy})$ therefore in this instance, assuming a perfect trigonal prism, $\Delta_1 = \Delta_2 = 3\frac{1}{3}Dq$ = 3673cm^{-1}. Both predictions of v_3 do not fit perfectly with the observed data, however the first TP scenario gave a

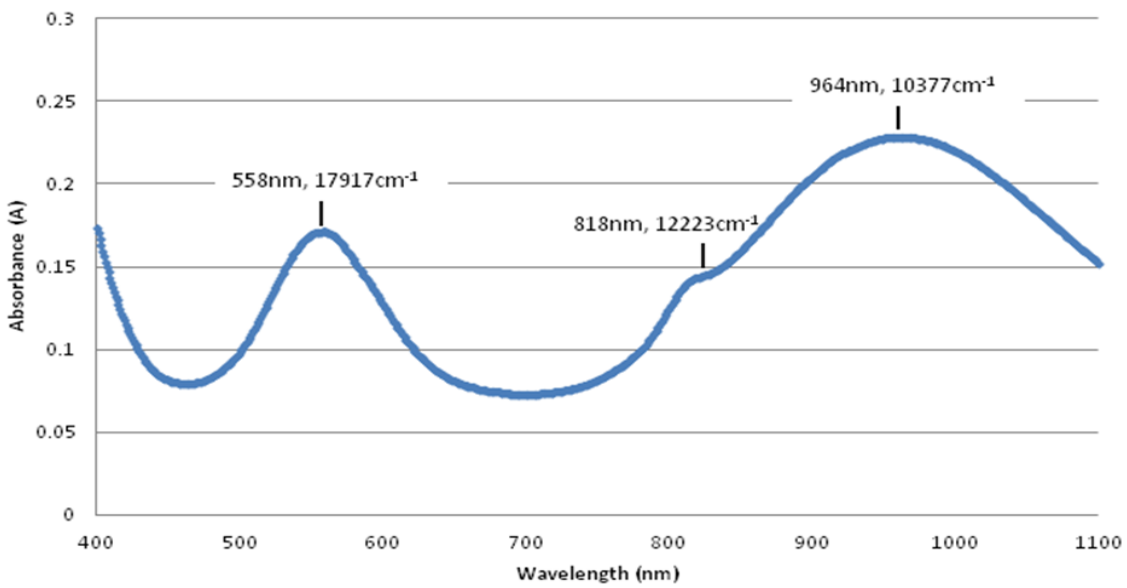

Figure 21: Visible region of the electronic aborption spectrum for **2.6** $[Ni^{II}(L2)]^{2+}$ performed in CH_3CN, with relative peak energies labelled.

closer result and is therefore believed to be a better fit. These calculated values correlate well against the known complex $[Ni^{II}(TBM)]^{2+}$ which has similar geometry giving *Dq* as 1,323cm^{-1} and *B* as 630cm^{-1}.[30,32] It must be noted that the similarities in the two TP sets of calculated values makes it impossible to unequivocally assign the UV-Vis transitions for this complex.

Overall this encourages the conclusion that the Ni^{II} complex retains some TP character in solution. However, the inaccuracy of the predicted v_3 band perhaps suggests the true structure is intermediate of TP and O_h and that neither model accurately fits the compound. This would also be consistent with crystallographic data which shows the complex possesses a large twist away from an ideal TP (Bailar twist of 31.74°) (Page. 64). Therefore, whilst the energy level

diagram provides a satisfactory ordering of the terms involved, the spectroscopic parameters calculated should therefore be treated tentatively. Note that in the TP scenario there are also two remaining spin-allowed transitions $^1E''\leftarrow{}^3A_2'$ and $^3A_1'',^3A_2''\leftarrow{}^3A_2'$ which occur at too low energy (between 3,000 and 5,000 cm^{-1}) and many weak spin-forbidden transitions that were unobservable within the range of the spectrum.

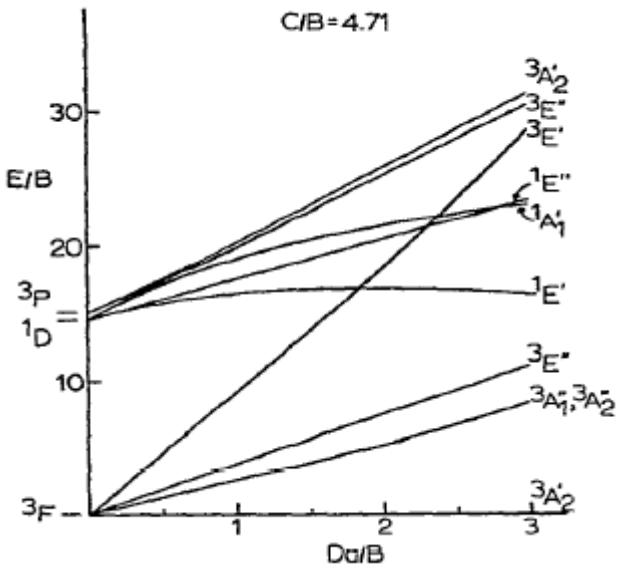

Figure 22: Energy level diagram for a d^8 trigonal prismatic complex.[3]

<u>Compound 2.7:</u> The copper(II) complex **2.7** presents only one broad asymmetric band in the visible region situated at 14184 cm^{-1} (Fig. 23) and is considered a combination of two spin allowed transitions; $^2E'\leftarrow{}^2E''$ and $^2A_1'\leftarrow{}^2E''$. The d-d peak maxima of $[Cu(bipy)_3]^{2+}$ (octahedral) is seen at 14814 cm^{-1} (675nm) which is slightly higher energy than found for **2.7**. This could be expected considering the geometry is distorted away from octahedral, because twisting would decrease the ligand field strength and hence increase λ_{max}. This distortion is supported by the X-ray data for **2.7,** where the bailar twist angle was calculated to be 25.70°, suggesting that the complex possibly retains a twisted conformation in solution. It must be noted that a Jahn-Teller distortion is also present in the complex that hasn't been taken into consideration for these calculations. This would also further complicate the electronic spectrum.[40]

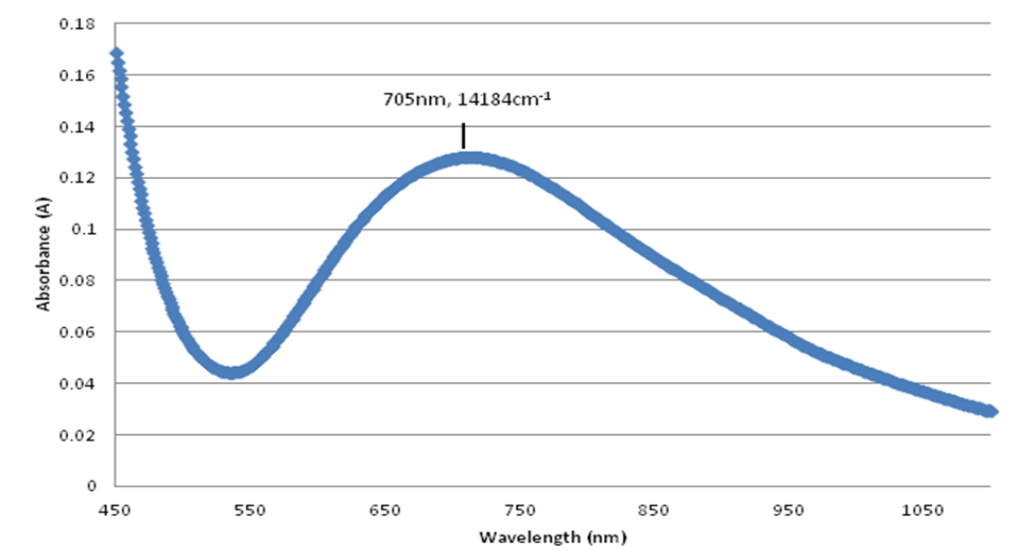

Figure 23: Visible region of the electronic aborption spectrum for **2.7** $[Cu^{II}(L2)]^{2+}$ performed in CH_3CN, with relative peak energies labelled.

<u>Compound 2.12:</u> The spectra for complex **2.12** shows two strong bands at 38314cm^{-1} and 35087cm^{-1} which occur from the π→π* transitions of the ligand, there is also the presence of a slight shoulder occurring at approximately 33333cm^{-1} (300nm) which is attributed to the MLCT transition in the complex. Rhenium(I) is a low spin d^6 metal involved in a strong CT transition and as a result has no observable d-d transitions in the spectra.

2.26 Crystallographic Data

Details of crystal parameters and data collection are shown in Tables 1A and 1B of appendix (page 102). All the complexes of **L2** have been shown to form 6-coordinate metal species in the solid state. This is as expected for the metals used and the coordinating donor groups available. The three pyridyl nitrogens as well as the three equivalent nitrogens from the appended pyrazole rings are involved in coordination in most cases with exception to **2.1**, **2.9** and **2.12**. These two donor groups each have a lone pair of donating electrons which together have the ability to point in a similar direction, in an analogous fashion to a bipyridine, towards the centre of the tripod cavity. This type of complexation has been demonstrated previously using similar ligand frameworks[28,31,41] e.g. tris(2,2'-bipyrid-2-yl)methanol (TBM) a tripod with three appending bipy groups. By changing the appending six membered rings (pyridines) in TBM for five membered ones (dimethyl-pyrazole) comparisons can be made to identify any binding relationships between the two analogues to investigate whether the ambidentate nature of the ligand favours coordination of more electron rich first row transition metals. The presence of the apical hydroxyl group in the ligand provides a seventh potential co-ordinating donor, the oxygen being a harder donor than both the pyridine and pyrazole and has shown to be involved in co-ordination for complexes **2.1** and **2.9**. The last complex **2.12** was synthesised in a 3:1 metal:ligand ratio due to Re(I) having a well known affinity for α,α'-diimines and resulted in a 3:1 complex with each metal binding to one ligand arm.

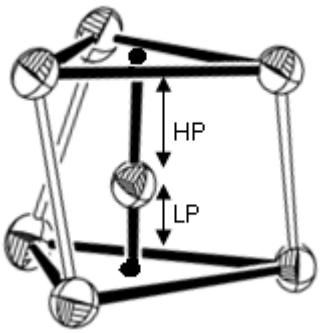

Figure 24: shows the respective distances of metal ion from the higher (HP) and lower (LP) planes in the effective trigonal prism, giving a representation on the position of a metal within the ligand cavitiy.

In complexes **2.2**-**2.8** and **2.10** the metal occupies the central cavity created by the ligand arms with all six nitrogens donating. The position of the donors in these compounds can be thought to form the vertices of a trigonal prism around the metal centre, shown in Figure 24, where the metal sits within the central space. The higher plane (triangular face) is made from connecting the pyridine vertices together whilst the lower plane is resulted from the connected pyrazoles. In most cases the higher and lower planes are not identical in size, generally with the lower plane being larger. This breaks down the ideal trigonal prism and forms a more truncated type of geometry (B) seen in Figure 25, which is used to help explain some of the crystallographic data. In addition, the bailar twist parameter can be measured using the centroid function in ORTEP, the two triangular planes can be aligned and an angle of "torsion" can therefore be calculated.

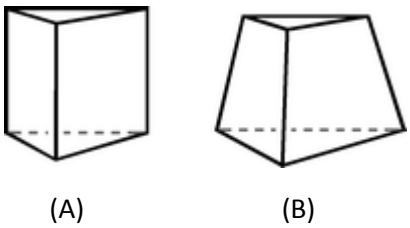

Figure 25: The difference in coordination geometry between a trigonal prism (**A**) and a truncated trigonal prism (**B**).[24]

Crystal Structure of [Cr(L2)Cl_3] (2.1)

Dull dark green rhombic crystals suitable for crystallographic data collection were obtained for the complex [Cr^{III}(L2)Cl_3] (Fig. 26). This was carried out using diethyl ether and a concentrated complex solution in acetonitrile *via* the method of vapour diffusion. The complex crystallised in a triclinic P-1 space group with the asymmetric unit consisting of two virtually identical tricationic complexes surrounded by six acetonitrile solvent molecules. The solvent and second complex having been omitted for clarity and selected bond lengths and angles shown in Table 7. The Cr^{III} centre has a distorted octahedral geometry with the six coordination sites taken by three chlorides (three coordinating counter ions from the $CrCl_3.THF_3$ starting material), two nitrogens (one pyridyl and one pyrazoyl, coming from the same ligand arm) and one oxygen (from the apical tertiary alcohol group). This structure is clearly different to other complexations of **L2**, predominately due to the chromium being of the higher oxidation state 3+

and preferring octahedral geometry. As a result, the Cr^{III} centre is of a "harder" nature than the 2+ metals and therefore seeks harder donors. Cl^- and O are much harder donors than N so it is

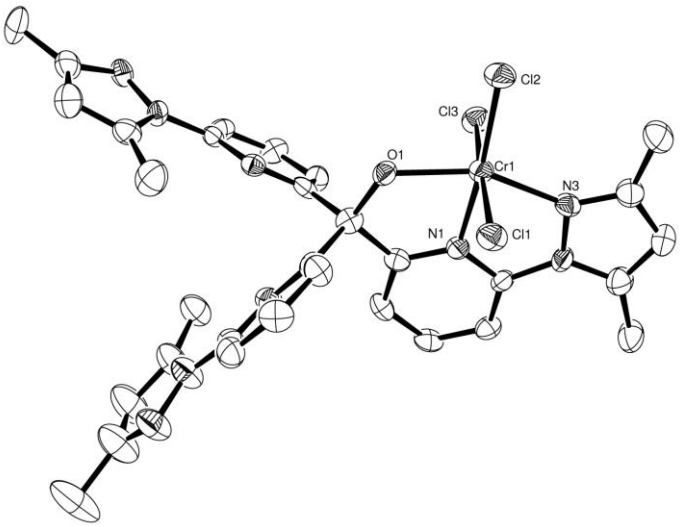

Figure 26: ORTEP Perspective view of the asymmetric unit for $[Cr^{III}(\mathbf{L2})][(Cl)_3]$ with atom labelling. Displacement ellipsoids are shown at 50% probability with H atoms excluded for clarity.

expected that the Cr^{III} avoids a hexamine coordination within the cavity of the three ligand arms, as Cr^{III} is kinetically inert it is expected that the solid state structure is the same as in solution. Also of note, the donating oxygen is assumed to be neutral (i.e. still bound to its affiliated hydrogen) as this would otherwise unbalance the overall charge of the complex. There are 6 bonds of two different bond lengths associated with the Cr^{III} centre which are seen in both complexes present in the unit cell. 3 from the chlorides (mean bond lengths Cr1 2.316 (2) Å and Cr2 2.319 (2) Å) which are more electrostatic in character and are slightly longer than expected bond lengths from literature 2.2746 (7) Å.[44] The other 3 bonds from the ligand, two N-donors from a ligand arm and one apical OH (mean bond lengths Cr1 = 2.002 Å and Cr2 = 2.020 Å) are more covalent in character and match closely with literature of Cr^{III} bound to a pyridyl-pyrazole unit (2.040 (2) Å- 2.0948 (19) Å).[44] Both the *fac* [58,59] and *mer*[60,61] arrangements of Cr(III) complexes are reported in the literature with the *fac* conformer considered more thermodynamically stable, theoretically.[62] However, it is the disposition of the donor atoms in **L2** that causes preference for the observed *mer* arrangement, also it is likely that the *fac* conformer would be much more constrained sterically and therefore less favourable in this example.

This *mer* arrangement causes a slight deviation from an ideal octahedron as the donors associated with the ligand are restricted in their movement.[27] As mentioned previous the

geometry of the metal centre is predominately octahedral, this is represented by SHAPE analysis for Cr1 and Cr2, including trigonal prismatic values for comparison. For octahedral Cr1 $S(O_h)$ = 1.74299 and Cr2 $S(O_h)$= 1.98164 and for trigonal prismatic Cr1 S(TP) = 13.34801 and Cr2 S(TP) = 12.68524. The overall molecular symmetry of the system is C_1 as there are no symmetry operations to account for.

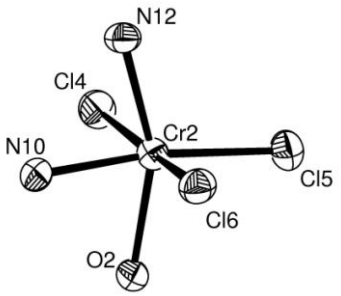

Figure 27: A view of the slightly distorted octahedral core geometry for $[Cr^{III}(\mathbf{L2})][(Cl)_3]$ with atom labelling. Displacement ellipsoids are shown at 50% probability.

Table 7: Selected bond Distances (Å) and Angles (°) for **2.1**			
Bond	Length (Å)	Bond	Length (Å)
Cr1-N1	2.002 (5)	Cr2 - N10	1.989 (6)
Cr1-N3	2.042 (6)	Cr2 –N12	2.032 (6)
Cr1-O1	2.022 (5)	Cr2 –O2	2.039 (5)
Cr1-Cl2	2.329 (2)	Cr2 –Cl4	2.330 (2)
Cr1-Cl2	2.285 (2)	Cr2 –Cl5	2.296 (2)
Cr1-Cl3	2.335 (2)	Cr2 –Cl6	2.332 (2)
Bonds	Angle (°)	Bonds	Angle (°)
N1- Cr1 -N3	78.0 (2)	N10- Cr2 –N12	78.6 (3)
N1- Cr1 –O1	78.3 (2)	N10- Cr2 –O2	77.4 (2)
N1- Cr1 –Cl2	88.70 (18)	N10- Cr2 –Cl4	89.14 (17)
N1- Cr1 –Cl2	174.99 (18)	N10- Cr2 –Cl5	171.95 (19)
N1- Cr1 –Cl3	85.89 (18)	N10- Cr2 –Cl6	85.12 (17)
N3- Cr1 –O1	156.0 (2)	N12- Cr2 –O2	155.9 (2)
N3- Cr1 –Cl2	86.87 (18)	N12- Cr2 –Cl4	87.10 (18)
N3- Cr1 –Cl2	106.73 (16)	N12- Cr2 –Cl5	108.82 (18)
N3- Cr1 –Cl3	88.20 (18)	N12- Cr2 –Cl6	84.79 (18)
O1- Cr1 –Cl2	88.93 (16)	O2- Cr2 –Cl4	90.99 (15)
O1- Cr1 –Cl2	97.13 (14)	O2- Cr2 –Cl5	95.24 (16)
O1- Cr1 –Cl3	93.77 (16)	O2- Cr2 –Cl6	94.69 (15)
CL2- Cr1 –Cl2	93.23 (8)	Cl4- Cr2 –Cl5	94.31 (8)
CL2- Cr1 –Cl3	173.34 (8)	Cl4- Cr2 –Cl6	170.86 (9)
Cl2- Cr1 –Cl3	92.48 (8)	Cl5- Cr2 –Cl6	92.30 (8)

Crystal Structure of $[Mn(L2)][ClO_4]_2$ (2.2)

The compound $[Mn^{II}(\mathbf{L2})][(ClO_4)_2]$ was crystallised by slow vapour diffusion of Petroleum ether into a concentrated acetonitrile solution of the complex, yielding pale orange crystals suitable for X-ray crystallography. The structure formed in a monoclinic $P2_1/c$ space group with two analogous monomeric complexes per asymmetric unit. In both cases the Mn^{II} centre is hexa-coordinate with all six nitrogen donors involved in bonding, three from pyridines and three from the pyrazoles (Fig. 28). The two complexes within the asymmetric unit follow a C_3 like molecular symmetry with both the coordination centres in the solid state being close to a trigonal prismatic geometry.

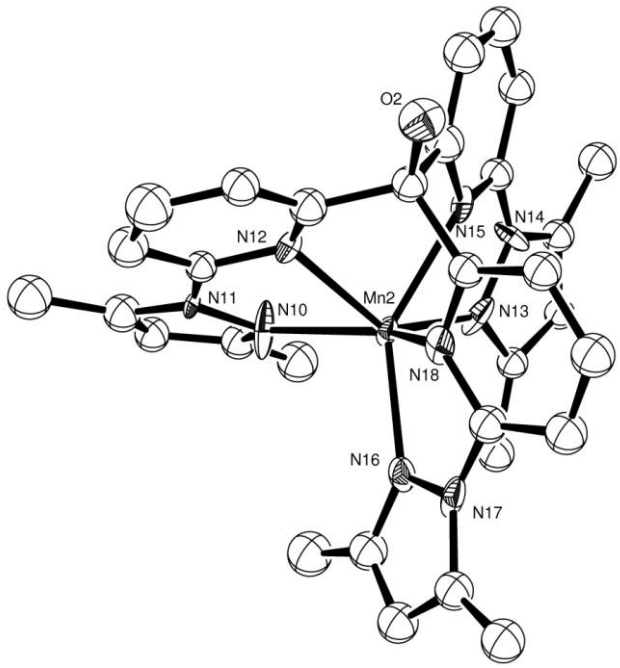

Figure 28: ORTEP Perspective view of the asymmetric unit for $[Mn^{II}(\mathbf{L2})][(ClO_4)_2]$ with atom labelling. Displacement ellipsoids are shown at 50% probability with H atoms and two perchlorate counterions have been excluded for clarity. Only one of two crystallographically independent complexes is shown, the other is very similar.

The co-ordinating bond lengths range from 2.211(9) Å to 2.264(9) Å and are within the range set by the analogous tris-Bipy compound $(Mn(TBM))^{2+}$, octahedral $(Mn(bipy)_3)^{2+}$ complex and octahedral $(Mn(py\text{-}pyz)_3)^{2+}$ complex 2.207(9) Å to 2.294(4) Å.[30,45,47] The Mn^{II} centres reveal small Bailar twist angles (mean angle of twist for Mn1 = 8.95° and Mn2 = 13.07°) however, in the case of Manganese the angles are very small, about half the size of that produced by the next smallest ion in the series (Fe^{III}, **2.4**). As Van Gorkum *et. al.* discussed, in the solid state this favoured geometry is attributed to crystal packing effects as the respective octahedral and

trigonal prism geometries share almost identical calculated energies and therefore no driving force in preferring either geometry.[46]

SHAPE analysis further supports the Mn^{II} geometry to be more trigonal prismatic in character than octahedral (Mn2 = 2.60031 and 11.37773 respectively) and (Mn1 = 1.98014 and 13.08827 respectively), which is backed up by the very low Bailar twist angle. It should be noted that Mn^{II} has a relatively large ionic radii which could be pushing the ligand arms further apart. This is thought to reduce any Me-Me interactions and accounts for the smaller effect on the Bailar twist and increased TP character.

Table 8: Selected bond Distances (Å) and Angles (°) for **2.2**

Bond	Length (Å)	Bond	Length (Å)
Mn1-N1	2.231 (10)	Mn2-N10	2.211 (9)
Mn1-N3	2.249 (11)	Mn2-N12	2.262 (9)
Mn1-N4	2.243 (11)	Mn2-N13	2.240 (10)
Mn1-N6	2.244 (11)	Mn2-N15	2.257 (10)
Mn1-N7	2.232 (10)	Mn2-N16	2.219 (9)
Mn1-N9	2.246 (11)	Mn2-N18	2.264 (9)
Bonds	**Angle (°)**	**Bonds**	**Angle (°)**
N1- Mn1-N3	71.3 (4)	N10- Mn2 –N12	71.0 (4)
N1- Mn1 -N4	99.0 (4)	N10- Mn2 –N13	101.2 (4)
N1- Mn1 -N6	137.0 (4)	N10- Mn2 –N15	119.8 (4)
N1- Mn1 -N7	99.5 (4)	N10- Mn2 –N16	101.5 (4)
N1- Mn1 -N9	124.2 (4)	N10- Mn2 –N18	139.0 (4)
N3- Mn1 -N4	122.9 (4)	N12- Mn2 –N13	138.6 (4)
N3- Mn1 -N6	79.6 (4)	N12- Mn2 -N15	78.1 (3)
N3- Mn1 -N7	135.9 (4)	N12- Mn2 –N16	120.0 (4)
N3- Mn1 -N9	78.4 (4)	N12- Mn2 –N18	77.9 (3)
N4- Mn1 -N6	71.1 (4)	N13- Mn2 –N15	71.0 (3)
N4- Mn1 -N7	100.9 (4)	N13- Mn2 –N16	101.3 (4)
N4- Mn1 -N9	136.7 (4)	N13- Mn2 –N18	119.8 (3)
N6- Mn1 -N7	123.3 (4)	N15- Mn2 –N16	138.7 (3)
N6- Mn1 -N9	77.8 (4)	N15- Mn2 –N18	77.6 (3)
N7- Mn1 -N9	72.0 (4)	N16- Mn2 –N18	71.6 (3)

Crystal Structure of $[Fe(L2)][ClO_4]_3$ (2.3)

The complex $[Fe(\mathbf{L2})][ClO_4]_3$ gave dark orange crystals suitable for crystallographic data collection. These were obtained by vapour diffusion of petrol ether (40/60) into a concentrated acetonitrile solution of **L2**. The structure crystallised in the trigonal space group R-3 with the asymmetric unit containing only 1/3 of the entire complex including one perchlorate counterion, giving the whole compound a molecular symmetry of C_3. The Fe(III) centre exists in a distorted TP geometry co-ordinating to all six possible nitrogen donors with a Bailar twist angle of ϕ = 21.28°(Fig. 29). The mean Fe-N bond lengths for **2.3** (2.160 (7) Å)) compare very closely to that of **2.4** (2.156 (4) Å) with the bond lengths to the different N-donors in **2.3** (Fe-pyrazoyl and Fe-pyridyl) being virtually identical, see Table 9. Reports of Fe(III) and Fe(II) bipy complexes observed Fe-N bonds of similar lengths, that also do not vary much depending on charge, where the Fe(III) complex typically gave a Fe-N length of 2.188 (2) Å and the Fe(II) gave 2.19 (3) Å.[63,64] This similarity in Fe-donor bond lengths is less occurrant in other complexes and is thought to be due to Irons particular ionic radii, as smaller metals are observed to fit higher up within the ligand cavity shortening the M-pyridyl bonds and conversely for larger ions. For this complex the metal centre is assigned as being predominately trigonal prismatic in character based upon the calculated SHAPE data (S(TP) = 3.761 and $S(O_h)$ = 7.876) which shares similarities with the Fe(II) complex **2.4** (Fe(II) ϕ = 23.04° which gives S(TP) = 4.164 and $S(O_h)$ = 7.256).

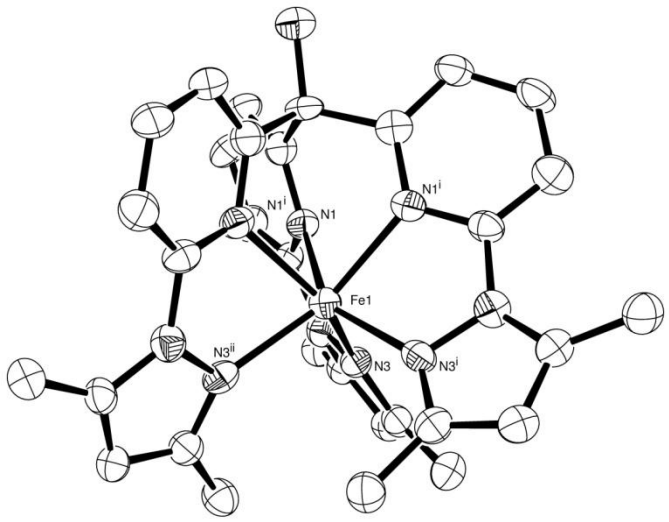

Figure 29: ORTEP Perspective view of the complex $[Fe^{III}(\mathbf{L2})][(ClO_4)_3]$ with atom labelling. Noting that the asymmetric unit is one third of the complex viewed above. Displacement ellipsoids are shown at 50% probability with all perchlorate counterions excluded for clarity.

Table 9: Selected bond Distances (Å) and Angles (°) for complex **2.3**			
Bond	Length (Å)	Bond	Length (Å)
Fe1-N1	2.161 (6)	Fe1-N3	2.159 (7)
Fe1-N1^{i}	2.161 (6)	Fe1-N3^{i}	2.159 (7)
Fe1-N1^{ii}	2.161 (6)	Fe1-N3^{ii}	2.159 (7)
Bonds	Angle (°)	Bonds	Angle (°)
N1- Fe1 –N1^{i}	81.55 (3)	N3- Fe1 -N3^{ii}	99.30 (2)
N1- Fe1 –N1^{ii}	81.55(3)	N1^{i}- Fe1 –N^{ii}	81.55 (3)
N1- Fe1 –N3	72.16 (2)	N1^{i}- Fe1-N3^{i}	72.16 (2)
N1- Fe1 –N3^{i}	146.07 (2)	N1^{i}- Fe1 –N3^{ii}	146.07 (2)
N1- Fe1 –N3^{ii}	114.37 (2)	N3^{i}- Fe1-N1^{ii}	114.37 (2)
N3- Fe1 –N1^{i}	114.37 (2)	N3^{i}- Fe1 –N3^{ii}	99.30 (2)
N3- Fe1 –N1^{ii}	146.07 (2)	N1^{ii}- Fe1 –N3^{ii}	72.16 (2)
N3- Fe1-N3^{i}	99.30 (2)		

Crystal Stucture of [Fe(L2)][ClO_4]$_2$ (2.4)

Crystals suitable for X-ray crystallographic studies of the complex [Fe^{II}(**L2**)][(ClO_4)$_2$] were obtained by the method of vapour diffusion. A concentrated acetonitrile solution of the complex was prepared allowing slow diffusion of diethyl ether, yielding light orange crystals. The Fe^{II} cation conforms with most the other examples and crystallises in the monoclinic space group P2$_1$/c and contains one complex in the asymmetric unit (Fig. 30). The Fe^{II} lies within the ligand cavity with all six potential nitrogen donors involved in co-ordination. The Fe-N bonds for the different N-donors are similar in length (mean bond lengths for Fe-pyridyl 2.155(4) Å and Fe-pyrzolyl 2.157(4) Å) which is also very similar to complex **2.3**. These bond lengths also compared very well with the Fe(II) complex of 6-(3, 5-dimethyl-1H-pyrazol-1-yl)picolinic acid (DPPA) where the Fe-N bonds range from 2.109(3) Å to 2.212(3) Å.[48] The mean Bailar twist angle, ϕ, for this Iron complex is 23.04°. The angle is even smaller than that calculated for Zn^{II}, which has no preference, this is possibly attributed to the electronic arrangement in the metal centre. Van Gorkum *et. al.* has attributed the solid state trigonal prismatic structure of similar HS Mn^{II} complexes to be due to crystal packing influences, as DFT calculations show only minor differences in the calculated energies between the trigonal prismatic and octahedral geometries they observed.[46]

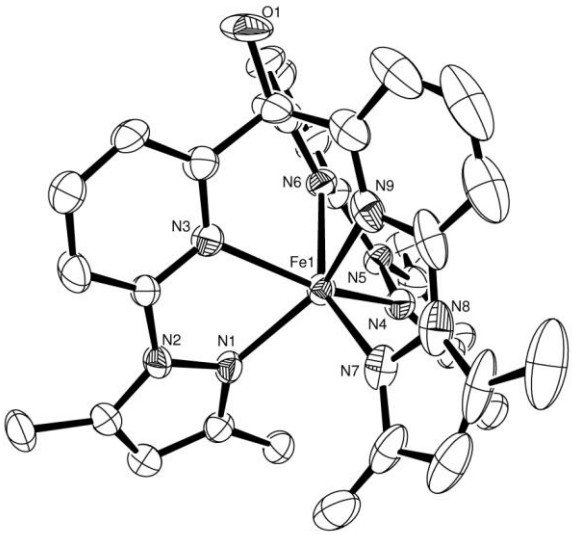

Figure 30: ORTEP Perspective view of the asymmetric unit for $[Fe^{II}(\mathbf{L2})][(ClO_4)_2]$ with atom labelling. Displacement ellipsoids are shown at 50% probability with H atoms and two perchlorate counterions have been excluded for clarity.

However, it is known that the effective ionic radius of Fe(II) (78 pm) is relatively large when compared to other first row transition metals, Co(II)→Zn(II) (≤ 74.5 pm). This property is also thought to reduce the Bailar angle, ϕ, due to lowered steric interactions between the terminal methyl groups and therefore electronics may not be the only contributing factor. SHAPE analysis reveals the Fe^{II} geometry to be more trigonal prismatic in character (S(TP) = 4.16386) than octahedral ($S(O_h)$ = 7.25608) which is backed up by the relatively low Bailar twist angle.

Table 10: Selected bond Distances (Å) and Angles (°) for complex **2.4**

Bond	Length (Å)	Bond	Length (Å)
Fe1-N1	2.148 (4)	Fe1-N6	2.171 (4)
Fe1-N3	2.155 (4)	Fe1-N7	2.156 (4)
Fe1-N4	2.172 (4)	Fe1-N9	2.139 (4)
Bonds	**Angle (°)**	**Bonds**	**Angle (°)**
N1- Fe1 -N3	72.30 (15)	N3- Fe1 -N9	81.38 (16)
N1- Fe1 -N4	98.90 (15)	N4- Fe1 -N6	71.72 (14)
N1- Fe1 -N6	111.45 (15)	N4- Fe1-N7	99.64 (16)
N1- Fe1 -N7	99.12 (16)	N4- Fe1 -N9	114.04 (15)
N1- Fe1 -N9	146.89 (15)	N6- Fe1-N7	149.06 (17)
N3- Fe1 -N4	146.44 (16)	N6- Fe1 -N9	83.28 (17)
N3- Fe1 -N6	81.40 (14)	N7- Fe1 -N9	73.13 (18)
N3- Fe1-N7	113.60 (16)		

Crystal Structure of $[Co(L2)][ClO_4]_2$ (2.5)

The complex $[Co^{II}(\mathbf{L2})][(ClO_4)_2]$ formed bluish grey coloured rhombic crystals, grown by the vapour diffusion of diethyl ether into a concentrated acetonitrile solution of the complex. The compound crystallises in the monoclinic space group $P2_1/c$ and contains only one complex per asymmetric unit, again the overall molecular symmetry very close to C_3. The Co^{II} centre exists in a distorted trigonal prismatic (TP) environment where all six available amines (three pyridyl (N1, N4 and N7) and three pyrazolyl (N3, N6 and N9)) are involved in coordination (Fig. 31). The Co-N bonds to the pyridines are shorter (mean bond length 2.105(3) Å) than the Co-N bond lengths to the pyrazoles (mean bond length 2.131(3) Å). This is contrary to what was observed by the analogous Zinc complex, despite the two metals being similar in size. It is considered that the octahedral twisting favoured by Co(II) is also reducing any terminal methyl interactions which in turn may allow the ligand arms to slightly pull in towards the cavity, giving the deviated bond lengths observed. The coordinative bond lengths range from 2.095 (4) Å to 2.150 (3) Å which are again slightly smaller but, however, do fit in the same range to those from the tris-bipy equivalent $[Co(TBM)]^{2+}$ (range 2.111 (3) Å to 2.200 (3) Å)[31] and also fit well with the Co(II) complex of 4-(trimethylammonio)benzenethiolate) with 2,6-bis(pyrazol-3-yl)pyridine, $[Co(Tab)(bdmppy)Cl]^{+}$, giving a Co-N bond range of 2.0699(19) Å to 2.1460(19) Å.[49]

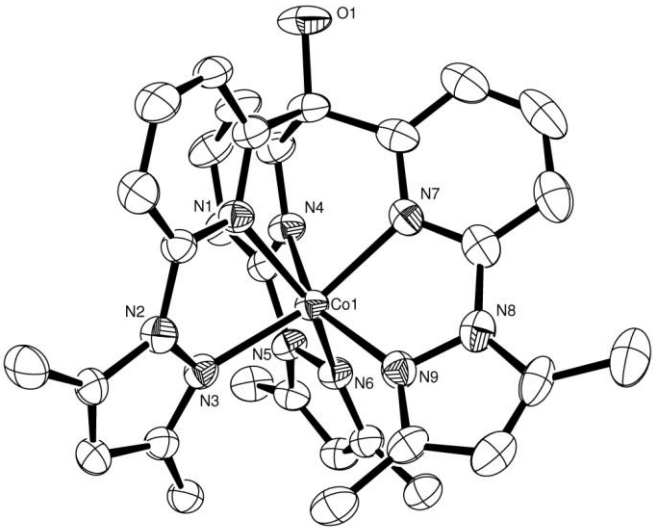

Figure 31: ORTEP Perspective view of the asymmetric unit for $[Co^{II}(\mathbf{L2})][(ClO_4)_2]$ with atom labelling. Displacement ellipsoids are shown at 50% probability with H atoms and two perchlorate counterions have been excluded for clarity.

The mean Bailar twist angle, ϕ, for this Cobalt complex is 25.90°. This is slightly larger than that observed for the zinc compound (**2.8**), the electronic nature of high spin Co^{II} (d^7) could explain this as there is, although small, some preference towards an octahedral arrangement which maybe increasing the twist. SHAPE analysis correlates with the twist angle showing that the Co retains mostly TP character as expected, however it is approaching octahedral geometry (**2.5** $S(O_h)$ = 6.17696 and S(TP) = 4.48966).

There are two notable groups of angles, three between the Co^{II} and pyridines (e.g. N1-Co-N7 ≈ 83°) and three similar angles between the pyrazoles (e.g. N3-Co-N9 ≈ 97°)(Fig. 32). These angles show that a truncated distortion (Fig. 15) occurs on the Co^{II} complex centre. It can be seen that the degree of truncation is reduced compared with **2.8** (The N···N distances of the bottom triangular face of **2.5** are slightly smaller than that measured in **2.8**, therefore a lower degree of truncation), this is proposed to be due to the Co^{II} co-ordinating higher up in the ligands cavity.

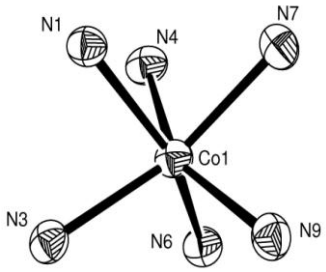

Figure 32: View of complex core showing only the co-ordinating atoms. Displacement ellipsoids are shown at 50% probability.

Table 11: Selected bond Distances (Å) and Angles (°) for complex **2.5**			
Bond	Length (Å)	Bond	Length (Å)
Co1-N1	2.102 (3)	Co1-N6	2.150 (3)
Co1-N3	2.129 (3)	Co1-N7	2.095 (4)
Co1-N4	2.118 (3)	Co1-N9	2.116 (4)
Bonds	Angle (°)	Bonds	Angle (°)
N1- Co1 -N3	74.06 (13)	N3- Co1 -N9	98.06 (13)
N1- Co1 -N4	82.64 (12)	N4- Co1-N6	73.08 (12)
N1- Co1 -N6	149.28 (14)	N4- Co1-N7	83.98 (14)
N1- Co1 -N7	82.66 (13)	N4- Co1-N9	151.34 (14)
N1- Co1 -N9	112.63 (13)	N6- Co1-N7	112.45 (13)
N3- Co1 -N4	109.70 (14)	N6- Co1-N9	97.45 (13)
N3- Co1-N6	96.42 (13)	N7- Co1-N9	74.65 (14)
N3- Co1-N7	150.79 (12)		

Crystal Structure of $[Ni(L2)][ClO_4]_2$ (2.6)

The compound $[Ni^{II}(\mathbf{L2})][(ClO_4)_2]$ was crystalised by slow vapour diffusion of diethyl ether into a concentrated acetonitrile solution of the complex. The compound crystallised in a monoclinic $P2_1/c$ space group yielding intense purple rhombic crystals suitable for data collection. As seen in previous examples, the asymmetric unit contains one dicationic complex with two perchlorate counter-anions with all six nitrogen moieties coordinated. The complex framework again possesses a C_3 like symmetry with the internal geometry greatly twisted from the ideal trigonal prismatic (Fig. 33). The Ni-N bond lengths for this structure are similar to those of Zn^{II} and Co^{II} (**2.8** and **2.5**) with the bond lengths to the pyrazoles (mean bond length 2.105 (3) Å) being slightly longer than those to the pyridines (mean bond length 2.049 (3) Å). Again this reveals a slight truncation in the geometry of the Ni^{II} centre, this however is reduced due to the high amount of twisting present in the complex structure (Fig. 34). These bonds also compare well with a known Ni(II) complex bearing a 2-pyrazolyl substituted 1,10-phenanthroline ligand giving Ni-N bond lengths ranging from 1.981(3)Å to 2.225(3) Å).[50]

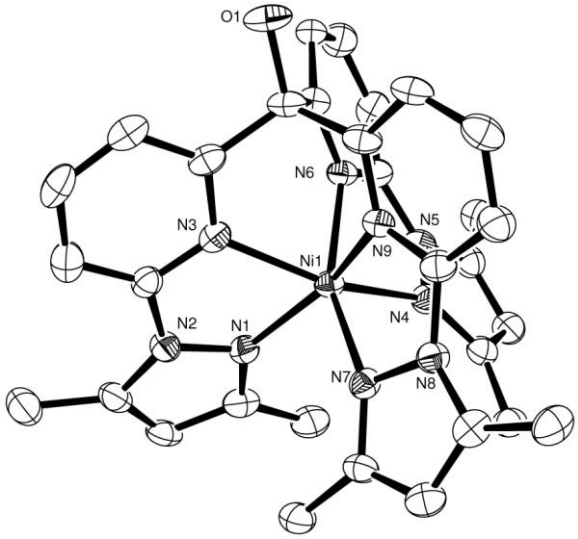

Figure 33: ORTEP Perspective view of the asymmetric unit for $[Ni^{II}(\mathbf{L2})][(ClO_4)_2]$ with atom labelling. Displacement ellipsoids are shown at 50% probability with H atoms and two perchlorate counterions have been excluded for clarity.

The mean Bailar twist angle, ϕ, for the Ni^{II} complex is 31.74°, this is the largest twist observed for this series of compounds, being owed to the d^8 metal ions strong preference for octahedral geometry. In fact from SHAPE analysis studies it can be seen the Ni^{II} centre possesses more octahedral character (4.34233) than trigonal prismatic (6.16218), although neither are close enough to accurately describe the geometry of the coordination sphere, which is backed up by the ϕ angle being higher than 30°. This property of having more octahedral character is only unique to Ni^{II} in the series of 2+ metals.

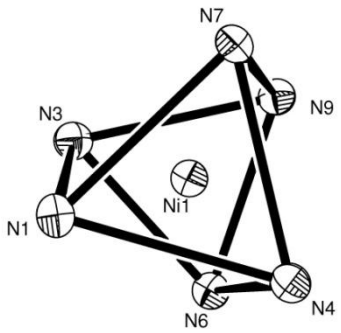

Figure 34: A view of the core geometry, looking from below, of $[Ni^{II}(\mathbf{L2})][(ClO_4)_2]$ showing the extent of bailar twisting. Co-ordinating bonds have been removed and replaced with lines to represent the distorted trigonal prismatic geometry. Displacement ellipsoids given at a 50% probability.

Table 12: Selected bond Distances (Å) and Angles (°) for complex **2.6**			
Bond	Length (Å)	Bond	Length (Å)
Ni1-N1	2.091 (3)	Ni1-N6	2.041 (3)
Ni1-N3	2.049 (3)	Ni1-N7	2.118 (3)
Ni1-N4	2.105 (3)	Ni1-N9	2.057 (3)
Bonds	Angle (°)	Bonds	Angle (°)
N1-Ni1-N3	75.79 (14)	N3- Ni1-N9	85.80 (13)
N1-Ni1 -N4	96.39 (13)	N4- Ni1-N6	75.40 (14)
N1- Ni1-N6	107.13 (14)	N4- Ni1-N7	96.13 (13)
N1- Ni1-N7	97.50 (14)	N4- Ni1-N9	106.14 (13)
N1- Ni1-N9	156.76 (13)	N6- Ni1-N7	154.60 (14)
N3- Ni1-N4	154.72 (14)	N6- Ni1-N9	84.47 (13)
N3- Ni1-N6	83.91 (14)	N7- Ni1-N9	74.83 (13)
N3- Ni1-N7	108.62 (13)		

Crystal Structure of $[Cu(L2)][ClO_4]_2$ (2.7)

Dark green rhombic crystals were grown by vapour diffusion of petroleum ether 40/60 into a concentrated acetonitrile solution of the complex. This allowed collection of a suitable crystallographic data set for the compound $[Cu^{II}(\mathbf{L2})][(ClO_4)_2]$ (Fig. 35). This molecule crystallises in the monoclinic space group $P2_1/c$ with one complex and two perchlorate counter ions per asymmetric unit. The molecular symmetry of this complex still closely relates to C_3, however deviates more from the ideal symmetry than previous complexes (**2.4** and **2.8**). Cu^{II} being d^9 has a strong natural affinity towards distorted octahedral and trigonal pyramidal geometries, which includes influences such as the Jahn Tellar effect (often a stretching of the dz^2 axis). These properties have caused one of the ligand arms (N1 and N3) to be kept at a further distance from the Cu^{II} centre, which is clearly interpreted by the bond lengths of Cu1-N1 (2.264(2) Å and Cu1-N3 (2.367(2) Å) in Table 13. The four remaining Cu-N bonds range from 2.009(2) Å to 2.059(2) Å and compare well with the pyridyl-pyrazole co-ordination of $[Cu(bdmpp)-(N_3)]^+$ which gives a Cu-N bond range of 2.021(4) Å - 2.096(4) Å.[51] The two longer bonds are clearly indicative of a Jahn-Teller distortion but of an unusual type, unlike the well-known distortion from octrahedral Cu^{II} ions, where the two longer bonds are mutually *trans* as expected.

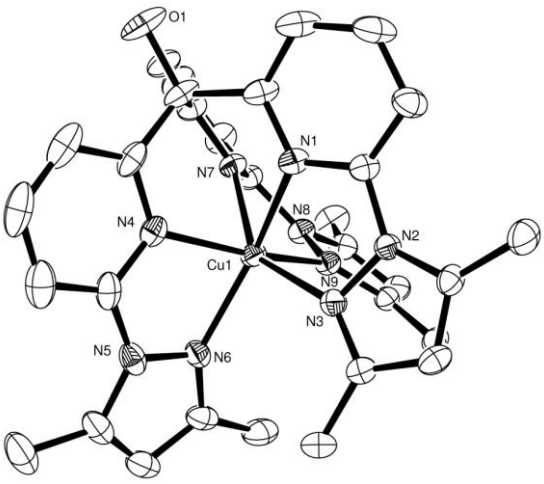

Figure 35: ORTEP Perspective view of the asymmetric unit for $[Cu^{II}(\mathbf{L2})][(ClO_4)_2]$ with atom labelling. Displacement ellipsoids are shown at 50% probability with H atoms and two perchlorate counterions have been excluded for clarity.

This rare trigonal prismatic Jahn-Teller distortion is also observed in the analogous system $[Cu(TBM)]^{2+}$, where the three ligand arms are 2,2-bipyridines giving elongated Cu-N bond lengths of 2.349(3) and 2.859(4) Å, and contains a mutually *cis* distortion represented schematically in Figure 37.[31] In addition it is noted that the two elongated bonds are of different lengths to each other by ~0.1Å. This non-degenerate *cis* distortion has been attributed to a second order Jahn-Teller effect in which the d_{yz} and p_z hybridize giving further stabilisation.[40] This more unsymmetrical structure, not due to Bailar twisting, in turn pushes the Cu^{II} geometry further from a trigonal prismatic configuration. However SHAPE analysis reveals the metal centre to still retain a prodominently trigonal prismatic character (O_h = 6.44979 and TP = 4.75765).

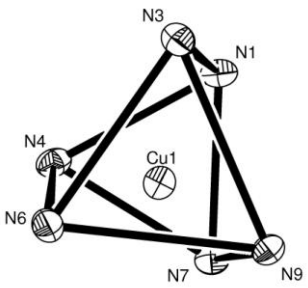

Figure 36: A view from below the Copper centre illustrating the ligand framework twisting and unsymmetrical alignment of one ligand arm (N1 and N3).

From Figure 36, it is just possible to see the Cu^{II} centre lying further from the ligand arm containing the pyridine (N1) and the pyrazole (N3). It must be noted from this reduced symmetry a lowering of accuracy in the calculation for the degree of twist in the ligand arms (as the centroids on each triangular plane no longer line up with the Cu^{II} centre). However, the mean Bailar twist angle, ϕ, for this complex was calculated to be 25.70°.

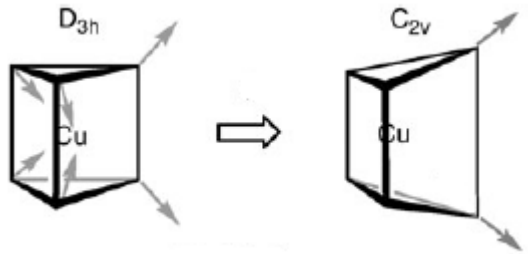

Figure 37: Diagram of the unusual Jahn Teller effect on TP structures showing the cis elongation of two bonds also resulting in a change to the symmetry order from D_{3h} to C_{2v}.

Table 13: Selected bond Distances (Å) and Angles (°) for complex **2.7**

Bond	Length (Å)	Bond	Length (Å)
Cu1-N1	2.264 (2)	Cu1-N6	2.053 (2)
Cu1-N3	2.367 (2)	Cu1-N7	2.059 (2)
Cu1-N4	2.009 (2)	Cu1-N9	2.019(2)
Bonds	**Angle (°)**	**Bonds**	**Angle (°)**
N1-Cu1-N3	67.06 (8)	N3- Cu1-N9	96.37 (8)
N1-Cu1 -N4	81.26 (9)	N4- Cu1-N6	78.28 (9)
N1- Cu1-N6	146.78 (9)	N4- Cu1-N7	86.10 (9)
N1- Cu1-N7	81.24 (8)	N4- Cu1-N9	158.70 (9)
N1- Cu1-N9	107.29 (8)	N6- Cu1-N7	122.74 (9)
N3- Cu1-N4	104.93 (8)	N6- Cu1-N9	101.13 (9)
N3- Cu1-N6	93.34 (8)	N7- Cu1-N9	76.29 (8)
N3- Cu1-N7	143.86 (9)		

Crystal Structure of $[Zn(L2)][ClO_4]_2$ (2.8)

Crystals suitable for X-ray crystallographic studies of the complex $[Zn^{II}(\mathbf{L2})][(ClO_4)_2]$ were obtained through vapour diffusion of diethyl ether into a concentrated acetonitrile solution of the complex, yielding colourless needle-like crystals. The complex crystallised in a $P2_1/c$ space group with the asymmetric unit containing one dicationic complex and two perchlorate counter-anions. The d^{10} Zn^{II} ion has no stereochemical preference and typically the geometry follows the most stable conformation allowed by the ligand. The overall molecular symmetry of the structure is most closely described as C_3 with the molecular structure of the zinc complex shown in Figure 38, with selected bond lengths and angles shown in Table 14.

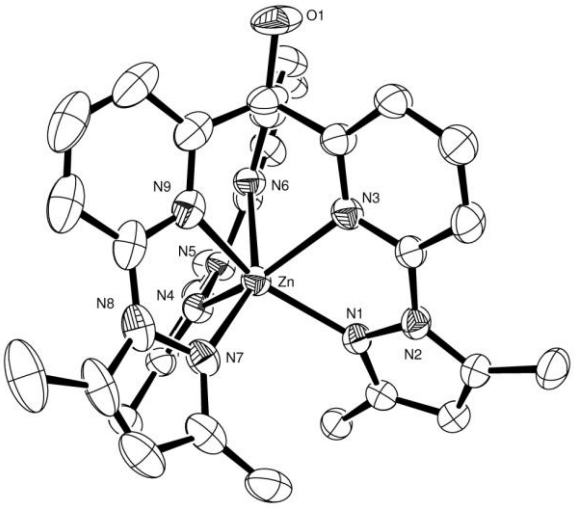

Figure 38: ORTEP Perspective view of the asymmetric unit for $[Zn^{II}(\mathbf{L2})][(ClO_4)_2]$ with atom labelling. Displacement ellipsoids are shown at 50% probability with H atoms and two perchlorate counterions have been excluded for clarity.

The geometry of the zinc centre is best described as a distorted trigonal prism *via* six donating nitrogen moieties (Fig. 39). Three coordinating pyridyl functions make up the upper trianglular plane of the prism (N3, N6 and N9) whilst three donating pyrazole moieties construct the triangular base of the prism (N1, N4 and N7), Figure 39, also schematically shown in Figure 24. From Table 14 it can be noted that the Zn-N bond lengths from the pyrazoles (2.112-2.143 (3) Å) are significantly shorter than those from the coordinating pyridine nitrogens (2.164-2.192 (3) Å), which shows a distortion from the ideal trigonal prismatic shape. However, both bond types fit well within the Zn-N bond range of the complex $[Zn(DPPA)]^{2+}$ (2.077 (3) – 2.219 (3) Å).[52] This difference in bond length can be related with two different types of N-Zn-N angles in the

complex, 3 from the pyridines (e.g. N3-Zn-N9, ≈ 81°) and three from the pyrazoles (e.g. N1-Zn-N7, ≈ 100°). Furthermore the N···N distances between each pyridyl unit (mean distance 2.816 Å) is significantly longer than the N···N distances between a pyridine and pyrazole of the same ligand arm (mean distance 2.558 Å), thus indicating a vertical compression relative to an ideal trigonal prism.

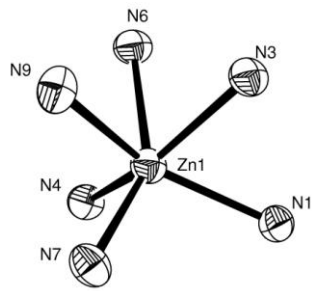

Figure 39: View of complex core showing only the co-ordinating atoms.
Displacement ellipsoids are shown at 50% probability.

Interestingly the N···N distances for the pyrazole triangular plane are much larger than that of the pyridine plane (mean distance 3.254 Å). This, along with the compression evidence indicates a significant degree of truncation in the coordination geometry of the complex, most aptly due to the divergent nature of the three arms from the apical methanol bridge and the steric interaction of the three terminal methyl groups. Interestingly the coordinative bond lengths of 2.112 (3) Å to 2.192 (3) Å for this compound are slightly smaller than that of the analogous tris-bipy ($Zn(TBM)^{2+}$) compound which gives bond lengths of 2.140 (3) Å to 2.211 (3) Å.[31] This is possibly to allow more orbital overlap due to the pyrazole component having a slightly different angle of donation than the equivalent bipy complex.

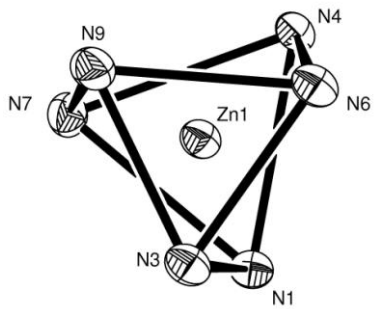

Figure 40: A view of the core geometry, looking from above*, of $[Zn^{II}(\mathbf{L2})][(ClO_4)_2]$ showing the extent of bailar twisting. Co-ordinating bonds have been removed and replaced with lines to represent the distorted trigonal prismatic geometry. Displacement ellipsoids given at a 50% probability. *the top of the molecule has been defined as the apical alcohol moiety.

In Figure 40, it can be seen that the two triangular faces of the zinc coordination geometry are not in line with one another, unlike that for an ideal trigonal prism. The mean bailar twist angle, ϕ, for this complex is 24.49°, this is significantly larger than analogous tris-bipy based zinc complex ($Zn(TBM)^{2+}$), where ϕ = 15.5°.[31] One reason for this increased torsion angle could be due to the three terminal methyl groups, which sterically cause the pyrazole groups to twist off the same plane as the pyridines. This twist angle is similar to that calculated for **2.5** (Co(II)) and consequently has similar SHAPE values ($S(O_h)$ = 6.74518 and S(TP) = 4.39971) showing that the Zn(II) geometry is between the two ideals but retains more TP character. If a twist angle of 30° was observed then the expected SHAPE values would be virually identical to each other. Overall this shows that ligand sterics and crystal packing forces must be playing some role in the metal centre's geometry.

Table 14: Selected bond Distances (Å) and Angles (°) for **2.8**

Bond	Length (Å)	Bond	Length (Å)
Zn1-N1	2.112 (3)	Zn1-N6	2.192 (3)
Zn1-N3	2.167 (3)	Zn1-N7	2.118 (3)
Zn1-N4	2.143 (3)	Zn1-N9	2.164 (3)
Bonds	**Angle (°)**	**Bonds**	**Angle (°)**
N1-Zn1-N3	73.25 (10)	N3-Zn1-N9	80.10 (11)
N1-Zn1-N4	99.46 (11)	N4-Zn1-N6	72.02 (10)
N1-Zn1-N6	110.33 (11)	N4-Zn1-N7	100.35 (11)
N1-Zn1-N7	100.08 (11)	N4-Zn1-N9	112.67 (11)
N1-Zn1-N9	147.85 (11)	N6-Zn1-N7	149.40 (12)
N3-Zn1-N4	146.77 (11)	N6-Zn1-N9	81.82 (11)
N3-Zn1-N6	80.17 (10)	N7-Zn1-N9	73.86 (12)
N3-Zn1-N7	112.80 (11)		

Crystal Structure of $[In(III)_2(L2)]$ (2.9)

Colourless crystals suitable for crystallographic studies were collected for the complex $[(In)_2(\mathbf{L2})Cl_5.H_2O]$. The crystals were obtained through vapour diffusion of diethyl ether into a 1:1 metal:ligand complex solution in acetonitrile. The complex crystallised in the orthorhombic space group Pccn with only one dimetallic complex per asymmetric unit. The resulting structure contains two Indium(III) centres for each ligand molecule with both metals adopting a hexa co-ordinated arrangement with near octahedral geometry shown in Scheme 5, which is confirmed by SHAPE analysis O_h = 4.27002 and TP = 9.30133. The two In(III) centres are not identical with In1 co-ordinating to one ligand arm (N1 and N3), a bridging oxygen (O1) and three chloride counter ions (Cl2, Cl2 and $Cl5^i$) whilst In2 is bound to another ligand arm (N4 and N6), the same bridging oxygen (O1), a water molecule (O2) and two chloride counter ions. Indium (III) is a d^{10} metal ion and has no stereochemical preference however the 3+ charge of Indium makes it a Lewis acidic (hard) ion, more so than the 2+ transition metals previous. As a result the metal centres have a preferred co-ordination with oxygen (harder donor) rather than nitrogen. The overall molecular symmetry of the complex is C_1 as no symmetry operations could be identified (Fig. 41).

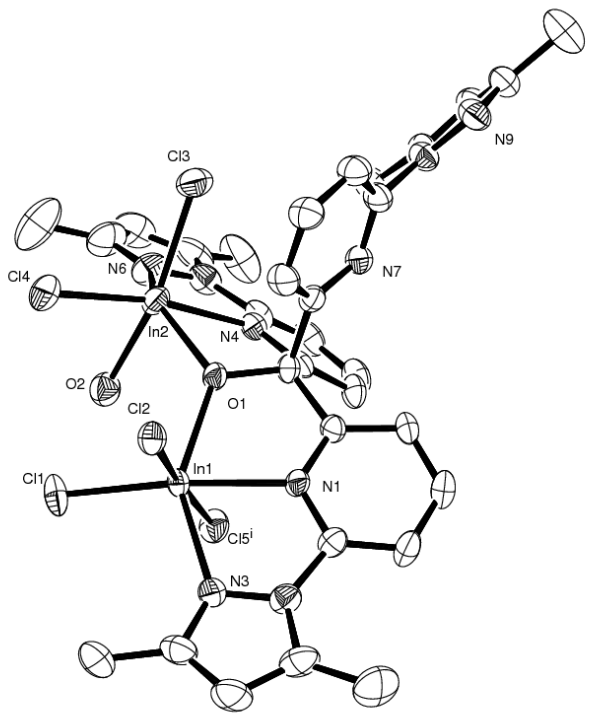

Figure 41: ORTEP Perspective view of the asymmetric unit for $[2In^{III}(\mathbf{L2})][(Cl)_5.H_2O]$ with atom labelling. Displacement ellipsoids are shown at 50% probability with H atoms excluded for clarity.

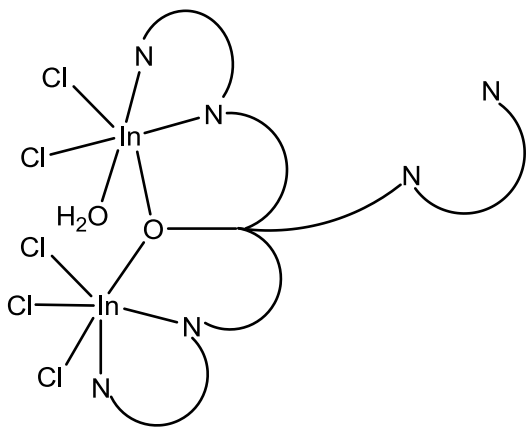

Scheme 5: More clearly showing the bonding mode of complex **2.9**. Only co-ordinating atoms are identified.

The average In-Cl bond length for **2.9** is 2.435 (12) Å whilst the In-O bonds from bridging OH measure on average 2.209(3) Å. The four In-N bonds have a mean bond length of 2.273 (4) Å) and are of comparable length to the In-(pyridine-pyrazole) bonds of the complex [In_2Cl_4(py-pyr)$_2$(dmf)$_2$] which range from 2.223 (2) – 2.289 (2) Å.[53] The In-Cl and In-O bonds of **2.9** are also comparable to the same known complex (2.4520 (7) Å and 2.230(2) Å respectively).[53] The mean bite angle to the ligand arms is 70.12° (13) which is slightly smaller than previous complexes but the angle does correlate when compared to metals of similar ionic radii (e.g. Cd(II) = 69.57°)(Page 87, Table 22).

Table 15: Selected bond Distances (Å) and Angles (°) for **2.9**			
Bond	Length (Å)	Bond	Length (Å)
In1-N1	2.230 (3)	In2 – N4	2.271 (3)
In1-N3	2.305 (4)	In2 –N6	2.286 (4)
In1-O1	2.206 (3)	In2 –O1	2.212 (3)
In1-Cl2	2.4086 (11)	In2 –O2	2.247 (3)
In1-Cl2	2.4447 (10)	In2 –Cl3	2.4242 (13)
In1-Cl5^{i}	2.4974 (11)	In2 –Cl4	2.3992 (12)
Bonds	Angle (°)	Bonds	Angle (°)
N1- In1 -N3	70.80 (12)	N4- In2 –N6	69.44 (14)
N1- In1 –O1	74.65 (11)	N4- In2 –O1	72.57 (11)
N1- In1 –Cl2	170.50 (9)	N4- In2 –O2	89.37 (12)
N1- In1 –Cl2	93.08 (9)	N4- In2 –Cl3	93.00 (9)
N1- In1 –Cl5^{i}	81.79 (9)	N4- In2 –Cl4	170.44 (9)
N3- In1 –O1	145.26 (11)	N6- In2 –O1	138.92 (13)
N3- In1 –Cl2	106.85 (9)	N6- In2 –O2	76.08 (15)
N3- In1 –Cl2	86.84 (10)	N6- In2 –Cl3	88.29 (12)
N3- In1 –Cl5^{i}	90.67 (10)	N6- In2 –Cl4	113.81 (12)
O1- In1 –Cl2	107.83 (8)	O1- In2 –O2	88.60 (12)
O1- In1 –Cl2	91.52 (8)	O1- In2 –Cl3	108.89 (8)
O1- In1 –Cl5^{i}	87.93 (8)	O1- In2 –Cl4	101.47 (8)
CL2- In1 –Cl2	96.00 (4)	O2- In2 –Cl3	162.25 (9)
CL2- In1 –Cl5^{i}	89.09 (4)	O2- In2 –Cl4	82.94 (10)
Cl2- In1 –Cl5^{i}	174.80 (4)	Cl3- In2 –Cl4	96.05 (5)

Crystal Structure of [Cd(L2)][ClO_4]$_2$(2.10)

Large colourless crystals of the complex [Cd^{II}(**L2**)][(ClO_4)$_2$] were grown by vapour diffusion, using a concentrated acetonitrile solution of the complex and diethyl ether. The crystals suitable for data collection showed three separate molecular complexes in the asymmetric unit with the compound crystallising in the monoclinic space group Cc. All three complexes are monomeric and dicationic with a total of six perchlorate counterions to balance the charge. In each case the Cd^{II} centre is co-ordinated via the three pyridyl N-donors and three pyrazoyl N-donors from the same ligand, Figure 42, again the overall molecular symmetry of each complex is approximately C_3. The mean Bailar twist angles for Cd1, Cd2 and Cd3 are 12.15° 11.76° and 11.48° respectively. The degree of twist for the Cd^{II} complexes has greatly reduced in comparison to the Zn^{II} (mean Bailar twist angle 24.49°) analogue, this suggests that metal ionic

radii does have an effect on the overall geometry, where larger ions spread the ligand arms out further and reduce methyl interactions therefore requiring less twist away from the ideal TP. These small Bailar angles also correlate with the calculated SHAPE data of the three cadmium centres which reveal them to all have a predominantly TP character (Cd1: O_h = 11.88583 and TP = 2.28015, Cd2: O_h = 11.97864 and TP = 2.60559, Cd3: O_h = 12.05130 and TP = 2.94208).

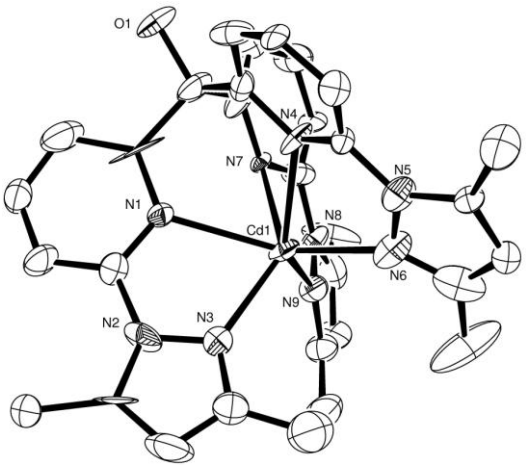

Figure 42: ORTEP Perspective view of the asymmetric unit for $[Cd^{II}(\mathbf{L2})][(ClO_4)_2]$ with atom labelling. Displacement ellipsoids are shown at 50% probability with H atoms and two perchlorate counterions have been excluded for clarity. Only one of three crystallographically independent complex units is shown, the other two being analogous to this one.

With a larger metal centre the donating ligand arms are therefore not pulled in as greatly towards the molecular cavity, which in turn reduces steric intra-molecular interactions between the appending methyl groups. Lowering methyl interactions then allows the Cd^{II} complexes, in the solid state, to form the more natural trigonal prismatic geometry presented by the ligand framework. This is backed up by the longer Cd-N bonds, (bond lengths range 2.253 (12) -2.428 (7) Å), compared with Zn^{II}, (which only range 2.112 (3)-2.192 (3) Å). The Cd-N bond lengths do however compare with Cd(II) complexes containing only one pyridyl-pyrazole unit, (bonds ranging 2.294 (18) – 2.389 (5).[54] The presence of some slightly longer bonds in **2.10** may be an effect of positioning three pyridyl-pyrazole units, as opposed to only one, around the metal centre. From Table 16 it is seen that the three Cd centres all coordinate closer to the pyrazole donors, namely due to the large size of Cd^{II} stopping the ion from fitting higher up within the ligand cavity. For each cadmium centre the effective trigonal prism shape formed again shows an apparent vertical compression even though the N···N distances between pyridine-pyrazoles of the same ligand arms average 2.646 Å and stay fairly fixed across the whole series of

complexes (Tab. 22). Whilst the average N···N distances between pyridines in the upper plane and N···N distances of the pyrazoles in the lower plane are 3.006 Å and 3.549 Å respectively which reflects image (b) from Figure 25. This also confirms that truncation is also present in the complexes of larger metal ion as the lower plane is approximately 0.54 Å bigger than the upper plane. This also shows that the degree of truncation may slightly be influenced by the size of the co-ordinating ion, as this difference in upper and lower plane lengths is 0.44 Å in the Zn(II) example (**2.8**) compared with 0.54Å for Cd(II).

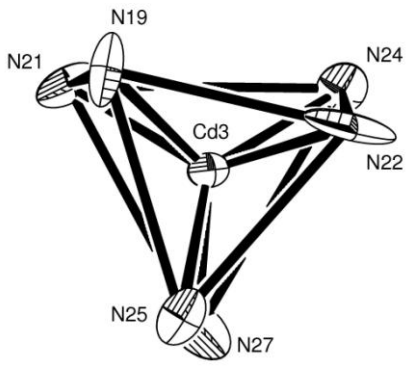

Figure 43: A view of the core geometry, looking from below, of $[Cd^{II}(\mathbf{L2})][(ClO_4)_2]$ showing the extent of bailar twisting. Solid lines have been added to represent the distorted trigonal prism geometry. Displacement ellipsoids given at a 50% probability.

Table 16 demonstrates how all the cadmium complexes bond in a similar fashion with the pyridine donors providing longer bonds. However, it can be noted that there is a significant amount of variation between the individual complexes especially between Cd1 and Cd3.

Table 16: Average bond length comparison between different Cd-N donor types.

	Mean bond length to pyridines, Å	Mean bond length to pyrazoles, Å
Cd1	2.402 (10)	2.261 (15)
Cd2	2.347 (10)	2.289 (10)
Cd3	2.332 (10)	2.303 (10)
	(all longer)	

Table 17: Selected bond Distances (Å) and Angles (°) for **2.10**					
Bond	Length (Å)	Bond	Length (Å)	Bond	Length (Å)
Cd1-N1	2.397 (10)	Cd2-N10	2.336 (10)	Cd3-N19	2.328 (10)
Cd1-N3	2.255 (15)	Cd2-N12	2.288 (10)	Cd3-N21	2.317 (10)
Cd1-N4	2.381 (10)	Cd2-N13	2.341 (10)	Cd3-N22	2.308 (12)
Cd1-N6	2.253 (12)	Cd2-N15	2.275 (11)	Cd3-N24	2.290 (11)
Cd1-N7	2.428 (7)	Cd2-N16	2.365 (10)	Cd3-N25	2.331 (9)
Cd1-N9	2.275 (8)	Cd2-N18	2.304 (10)	Cd3-N27	2.303 (10)
Bonds	Angle (°)	Bonds	Angle (°)	Bonds	Angle (°)
N1- Cd1 -N3	68.04 (4)	N10- Cd2 –N12	69.8 (4)	N19- Cd3 -N21	69.7 (4)
N1- Cd1 -N4	76.3 (4)	N10- Cd2 –N13	79.9 (4)	N19- Cd3 -N22	80.8 (5)
N1- Cd1 -N6	137.0 (4)	N10- Cd2–N15	120.2 (5)	N19- Cd3 -N24	119.5 (5)
N1- Cd1 -N7	76.0 (3)	N10- Cd2 –N16	80.2 (4)	N19- Cd3 -N25	83.1 (4)
N1- Cd1 -N9	119.2 (4)	N10- Cd2 –N18	137.7 (4)	N19- Cd3 -N27	138.7 (5)
N3- Cd1 -N4	117.7 (5)	N12- Cd2–N13	138.1 (4)	N21- Cd3 -N22	137.8 (5)
N3- Cd1 -N6	105.1 (5)	N12- Cd2 -N15	100.5 (4)	N21- Cd3 -N24	98.1 (5)
N3- Cd1 -N7	135.1 (4)	N12- Cd2–N16	122.1 (5)	N21- Cd3 -N25	121.7 (5)
N3- Cd1 -N9	105.9 (5)	N12- Cd2 –N18	103.0 (5)	N21- Cd3 -N27	98.6 (5)
N4- Cd1 -N6	70.1 (4)	N13- Cd2 –N15	70.2 (4)	N22- Cd3 -N24	70.6 (4)
N4- Cd1 -N7	76.7 (3)	N13- Cd2 –N16	78.4 (4)	N22- Cd3 -N25	82.1 (4)
N4- Cd1 -N9	136.2 (4)	N13- Cd2 –N18	118.9 (5)	N22- Cd3 -N27	123.2 (6)
N6- Cd1 -N7	119.6 (5)	N15- Cd2–N16	137.4 (5)	N24- Cd3 -N25	139.7 (4)
N6- Cd1 -N9	103.6 (5)	N15- Cd2 –N18	102.1 (5)	N24- Cd3 -N27	101.1 (5)
N7- Cd1 -N9	69.3 (3)	N16- Cd2 –N18	68.6 (4)	N25- Cd3 -N27	69.5 (4)

Crystal Structure of $[Hg(L2)][ClO_4]_2$ (2.11)

X-ray crystallographic data were collected from colourless crystals of the compound $[Hg^{II}(\mathbf{L2})][(ClO_4)_2]$. These were grown by vapour diffusion using a concentrated acetonitrile solution of complex and diethyl ether/petroleum ether (50:50). The complex was found to be monoclinic in the space group Cc and contain two unique complexes in the asymmetric unit. Both dicationic complexes are monomeric, each with two corresponding perchlorate counterions. As expected the two Hg^{II} metal centres each occupy a ligand cavity where all available N-donors are involved in co-ordination (Fig. 44).

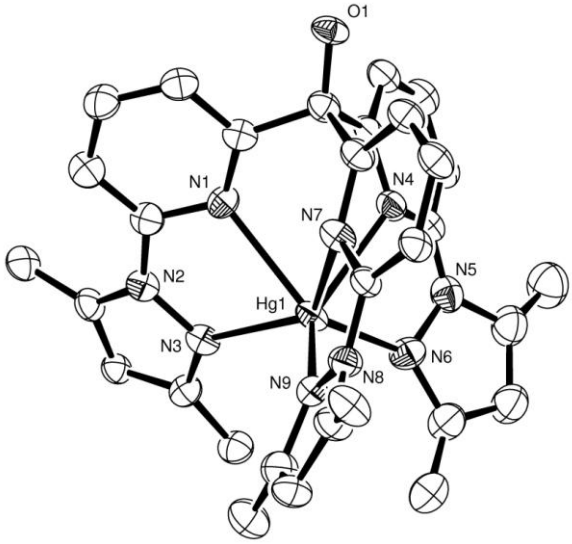

Figure 44: ORTEP Perspective view of half the asymmetric unit for [Hg^{II}(**L2**)][$(ClO_4)_2$] with atom labelling. Displacement ellipsoids are shown at 50% probability with H atoms and two perchlorate counterions have been excluded for clarity. Only one of two crystallographically independent complex units is shown, the other being analogous to this one.

The Hg···N bond lengths range from 2.234(9)-2.504(12) Å, which are only slightly longer than those observed for the analogous cadmium complex (**2.10**). However the Hg-N bond lengths in a complex with 2,6-bis(3,4,5-trimethyl-*N*-pyrazolyl)pyridine (btmpp) match only with the longer Hg-pyridyl bonds, ranging from 2.428(5) Å to 2.532(5) Å.[55] The Hg-pyridyl bonds (mean bond length Hg1 = 2.483Å and Hg1a = 2.495Å) are significantly longer than those to the pyrazoles (Hg1 = 2.258 Å and Hg1a = 2.257 Å), a common feature for larger metal ions complexing with **L2**. As seen in previous examples the average N···N distances between the pyridines on the upper plane are much smaller than those between pyrazoles in the lower plane (2.977 Å and 3.650 Å respectively) with a difference of 0.67Å. This again reveals the truncating nature of these complexes and shows that the degree of truncation can be in part related to the size of the co-ordinating ion, with the amount truncation shown by Hg(II) > Cd(II) > Zn(II) (0.67 Å - 0.54 Å – 0.44 Å respectively) and can be owed to the large ionic radius of Hg(II) (Fig. 45).

The mean Bailar twist angle ,φ, for Hg1 and Hg1a are 8.36° and 1.69°, respectively. Unusually one of the complexes (Hg1) retains a much larger Bailar angle relative to the other (Hg1a), albeit that the overall amount of twist in both cases are the smallest throughout the whole series of complexes. The small Bailar twist angle can again be attributed to the large ionic radii of the metal centre, where Hg^{II} > Cd^{II} > Zn^{II}. This even larger metal centre pushes the ligand arms outward and therefore reducing to a minimum any steric interactions, between terminal

methyls, that may favour a twisted conformation. This is supported by SHAPE analysis of the two centres where it can be clearly seen the complexes possess mainly trigonal prismatic character compared with octahedral (Hg1: O_h = 14.11439 and TP = 3.03287, Hg1a: O_h = 17.31997 and TP = 2.62163). However it must be noted that even though there is a high amount of TP character present, the geometry still deviates up to 40% from the ideal Bailar path of interconversion (Tab. 23). This amount of distortion is attributed to the truncation of the co-ordination sphere, due to the ligand arms being tethered at one end, and the large ionic radii of Hg(II) which results in different bond lengths to pyridyl and pyrazoyl donors, causing the metal ion to sit low within the ligand cavity (Fig. 45).

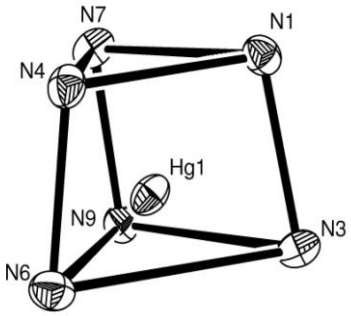

Figure 45: TP representation of complex core with co-ordinating bonds removed. Showing how the Hg^{2+} ion sits low in the co-ordinating cavity and slight truncation of overall geometry. Displacement ellipsoids are shown at 50% probability.

Table 18: Selected bond Distances (Å) and Angles (°) for **2.11**			
Bond	Length (Å)	Bond	Length (Å)
Hg1-N1	2.497 (9)	Hg1A - N1A	2.504 (12)
Hg1-N3	2.266 (9)	Hg1A –N3A	2.266 (11)
Hg 1-N4	2.468 (8)	Hg1A –N4A	2.480 (11)
Hg 1-N6	2.275 (8)	Hg1A –N6A	2.267 (10)
Hg 1-N7	2.484 (8)	Hg1A –N7A	2.501 (11)
Hg 1-N9	2.234 (9)	Hg1A –N9A	2.237 (12)
Bonds	Angle (°)	Bonds	Angle (°)
N1- Hg1 -N3	66.5 (3)	N1A- Hg1A -N3A	66.9 (4)
N1- Hg1 -N4	73.6 (3)	N1A- Hg1A -N4A	73.2 (5)
N1- Hg1 -N6	130.6 (3)	N1A- Hg1A -N6A	124.5 (7)
N1- Hg1 -N7	74.2 (3)	N1A- Hg1A -N7A	72.9 (4)
N1- Hg1 -N9	118.8 (3)	N1A- Hg1A -N9A	126.1 (6)
N3- Hg1 -N4	118.6 (4)	N3A- Hg1A -N4A	125.8 (6)
N3- Hg1 -N6	105.5 (4)	N3A- Hg1A -N6A	106.6 (7)
N3- Hg1 -N7	131.3 (3)	N3A- Hg1A -N7A	124.2 (6)
N3- Hg1 -N9	108.3 (3)	N3A- Hg1A -N9A	108.3 (6)
N4- Hg1 -N6	68.9 (2)	N4A- Hg1A -N6A	68.3 (4)
N4- Hg1 -N7	73.6 (3)	N4A- Hg1A -N7A	73.4 (5)
N4- Hg1 -N9	131.8 (3)	N4A- Hg1A -N9A	124.8 (6)
N6- Hg1 -N7	122.0 (4)	N6A- Hg1A -N7A	128.1 (6)
N6- Hg1 -N9	110.0 (4)	N6A- Hg1A -N9A	108.7 (7)
N7- Hg1 -N9	67.1 (3)	N7A- Hg1A -N9A	67.5 (4)

Crystal Structure of $[(Re(CO)_3Br)_3(L2)]$ (2.12)

A concentrated $CHCl_3$ solution of the complex $[(Re(CO)_3Br)_3(\mathbf{L2})]$ yielded yellow rhombic crystals suitable for X-ray crystallographic studies. The complex crystallised in the triclininc P-1 space group with one neutral complex and two chloroform molecules per asymmetric unit. Viewing Fig. 47 it can be seen within the complex there are three rhenium metal centres of identical nature each co-ordinate with one pyrazole-pyridine arm, three carbonyls and one bromide counter ion. All the Re(I) centres are strongly octahedral in geometry, as expected by low spin d^6 Re(I), and the overall molecular symmetry of the complex is close to C_3, shown in Figure 46.

The mean Re-C and Re-Br bond lengths observed for **2.12** are 1.86(6) Å and 2.624(7) Å respectively. Re-N bond lengths range from 2.09(2) Å - 2.34(2) Å, however the Re-pyridine bond lengths (2.34(2) Å) are longer on average than the Re-pyrazole bonds (2.15(3) Å). This is

possibly due to the presence of a carbonyl *cis* to the co-ordinating pyridine. This CO group appears to be interacting sterically with its neighbouring pyridine ring (through space) causing the CO to be non-linear, seen in Figure 46. It is this interaction that is thought to prevent the Re centre from co-ordinating closer to the pyridine and hence the longer Re-pyridine bonds. Albeit the different bond lengths compare well with the known Re(I) 2,6-bis[1-methyl-5-(thiophen-2-yl)-pyrazol-3-yl)pyridine complex which has Re-N bonds ranging 2.135(5) - 2.259(4) Å, Re-Br length of 2.6222(6) Å and Re-C bond lengths ranging from 1.895(6) to 1.917(6) Å.[56]

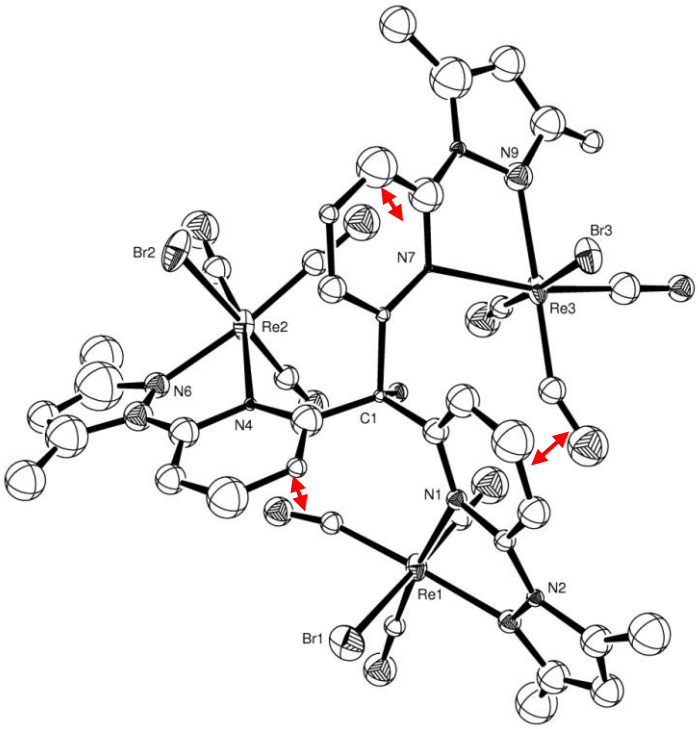

Figure 46: ORTEP Perspective view of the asymmetric unit for $[(Re(CO)_3Br)_3(\mathbf{L2})]$ with atom labelling. The red arrows represent the steric interaction between carbonyls and their neighbouring pyridine ring causing a bend. Displacement ellipsoids are shown at 50% probability with H atoms and two chloroform solvent molecules having been excluded for clarity.

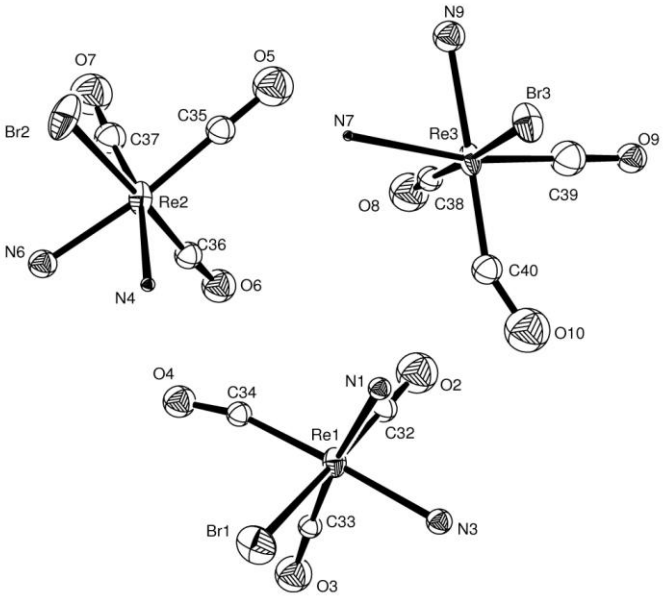

Figure 47: View of the three Rhenium cores showing only the co-ordinating atoms. Displacement ellipsoids are shown at 50% probability.

Table 19: Selected bond Distances (Å) and Angles (°) for **2.12**

Bond	Length (Å)	Bond	Length (Å)	Bond	Length (Å)
Re1-N1	2.33 (2)	Re2-N4	2.34 (2)	Re3-N7	2.34 (2)
Re1-N3	2.15 (2)	Re2-N6	2.09 (3)	Re3-N9	2.22 (2)
Re1-C32	1.79 (6)	Re2-C35	1.87 (6)	Re3-C38	1.87 (6)
Re1-C33	1.79 (5)	Re2-C36	1.76 (4)	Re3-C39	1.91 (7)
Re1-C34	1.95 (6)	Re2-C37	1.80 (7)	Re3-C40	1.97 (6)
Re1-Br1	2.622 (7)	Re2-Br2	2.619 (7)	Re3-Br3	2.632 (6)
Bonds	**Angle (°)**	**Bonds**	**Angle (°)**	**Bonds**	**Angle (°)**
N1- Re1 –N3	76.1 (8)	N4- Re2 –N6	74.5 (9)	N7- Re3 –N9	74.6 (8)
N1- Re1 –C32	94.9 (19)	N4- Re2 –C35	173.1 (19)	N7- Re3 –C38	96.5 (17)
N1- Re1 –C33	171.7 (18)	N4- Re2–C36	94.7 (15)	N7- Re3 –C39	169.0 (2)
N1- Re1 –C34	105.4 (17)	N4- Re2 –C37	166.0 (2)	N7- Re3 –C40	104.2 (18)
N1- Re1 –Br1	85.2 (5)	N4- Re2 –Br2	81.2 (5)	N7- Re3 –Br3	81.8 (5)
N3- Re1 –C32	93.8 (19)	N6- Re2–C35	173.1 (19)	N9- Re3 –C38	91.1 (18)
N3- Re1 –C33	96.1 (18)	N6- Re2 –C36	90.9 (16)	N9- Re3 –C39	95.0 (2)
N3- Re1 –C34	177.5 (18)	N6- Re2–C37	93.0 (2)	N9- Re3 –C40	178.9 (18)
N3- Re1 –Br1	87.0 (6)	N6- Re2 –Br2	87.1 (7)	N9- Re3 –Br3	85.8 (6)
C32- Re1 –C33	88.0 (2)	C35- Re2 –C36	95.0 (2)	C38- Re3 –C39	85.0 (3)
C32- Re1 –C34	88.0 (2)	C35- Re2 –C37	82.0 (3)	C38- Re3 –C40	89.0 (2)
C32- Re1 –Br1	179.1 (18)	C35- Re2 –Br2	87.7 (17)	C38- Re3 –Br3	176.8 (17)
C33- Re1 –C34	82.0 (2)	C36- Re2–C37	93.0 (2)	C39- Re3 –C40	86.0 (3)
C33- Re1 –Br1	91.5 (17)	C36- Re2 –Br2	175.8 (15)	C39- Re3 –Br3	96.0 (2)
C34- Re1 –Br1	91.1 (16)	C37- Re2 –Br2	90.8 (19)	C40- Re3 –Br3	94.0 (17)

2.27 Magnetic Moment Studies

The magnetic moments of complexes **2.1**-**2.7** were determined in d_3-acetonitrile solution at room temperature *via* the Evans' NMR method. The paramagnetic nature of these metals when co-ordinated to **L2** prevented any meaningful assignment of their corresponding ^{1}H-NMR spectra due to their broad, structureless appearance. The observed magnetic moments calculated for the compounds are displayed in Table 20, along with theoretical magnetic moments and their respective ground terms.

The observed magnetic moments provide some evidence for co-ordination of the paramagnetic metals Cu(II)-Mn(II) with **L2** but also demonstrated the ligands affinity for high spin state metal centres in solution, due to the weak field nature of the ligand. The observed magnetic moment for transition metals will vary from theoretical values depending on the contribution from orbital angular momentum. The theoretical values can be calculated using the equation: $\mu = \sqrt{[n](n+2)}$ where n is the expected number of unpaired electrons. Comparison of these theoretical values with observed values can provide reasonable evidence for the electronic configuration of the co-ordinated metal ions.

Table 20: Showing predicted and calculated magnetic moments for all non-d^{10} metals and their respective spin state.

complex	Number of Unpaired electrons	Ground term	Theoretical moment	Observed Magnetic moment μ_B	High spin/low spin
2.1 [Cr(III)]	3	^{4}F	3.87	3.98	n/a
2.2 [Mn(II)]	1 or 5	^{6}S	1.73 or 5.91	5.29	HS
2.3 [Fe(III)]	1 or 5	^{6}S	1.73 or 5.91	4.57	HS
2.4 [Fe(II)]	0 or 4	^{5}D	0 or 4.89	4.45	HS
2.5 [Co(II)]	1 or 3	^{4}F	1.73 or 3.87	3.93	HS
2.6 [Ni(II)]	2	^{3}F	2.83	2.66	n/a
2.7 [Cu(II)]	1	^{2}D	1.73	1.79	n/a

The data show that when possible the co-ordinating metal ion prefers a high-spin state arrangement which suggests that the ligand has a weak-field nature (π-donating). This is unusual as pyridines and bipys are labelled at the high-field end (π-accepting) of the spectrochemical series. However, because the donor sets of **L2** are arranged to encourage a trigonal prism geometry over an octahedral one and that a TP has a smaller orbital energy gap

(Δ) than O_h (ΔO_h = 10 Dq, ΔTP = 6⅔ Dq with the e to e energy gap in TP only 3⅓ Dq) it would be much less likely to expect low spin states from complexes with smaller energy level splittings.

Noticeably, the observed magnetic moment for **2.3** (Fe^{III}) (4.57 μ_B) is significantly lower than the expect BM = 5.91 for a HS d^5 compound, it is still presumed the complex is HS as the observed value is within a more exceptable range than compared to a low spin scenario (BM = 1.73). A possible reason for this low result could be that a proportion of the Fe(III) is actually in a low spin state possibly through spin cross over, influenced by the magnetic field in NMR machine or possibly temperatue, and hence bring down the observed magnetic moment. Complexes **2.2** and **2.4** were also observed to have slightly lower magnetic moments than predicted which could again be attributed to some spin cross over. Although the relatively small deviations in these samples could also be attributed as some error.

2.28 Conclusion

In conclusion, a novel tris pyridyl-pyrazolyl tripodal ligand has been synthesised and its co-ordination chemistry has been investigated. In general **L2** forms monomeric hexadentate complexes with many 2+ transition metals as well as stable complexes with Cr(III), Fe(III), In(III) and Re(I). Most complexes produce a hexa-imine co-ordination sphere resulting from the three pyridines and three pyrazoles, except in a couple of cases that facilitates donation from the apical OH group, complexes **2.1**, and **2.9**, with Fe(III) (compound **2.3**) being the only 3+ metal to form a hexa-imine complex.

Table 21: Showing the Bailar twist angle and co-ordinative bond lengths from crystallographic data, in the order of increasing metal ion radius.

Compound	Bailar twist angle (°). *averaged	Mean bond M···N length, Å (from Pyridine)	Mean bond M···N length, Å (from pyrazole)	Effective ionic radius of metal (pm)[b]
2.6, Ni(II)	31.74	2.049	2.105	69
2.7, Cu(II)	25.70	2.111	2.146	73
2.8, Zn(II)	24.49	2.174	2.124	74
2.5, Co(II)	25.90	2.105	2.132	74.5(hs)
2.4, Fe(II)	23.04	2.155	2.159	78(hs)
2.3, Fe(III)	21.28	2.161	2.159	78.5 (hs)
2.2, Mn(II)	11.01*	2.254	2.229	83
2.10, Cd(II)	11.80	2.360	2.284	95
2.11, Hg(II)	5.03*	2.489	2.258	102

[b] – values for ionic radii taken from reference 65.

The use of standard solid state and solution based analysis techniques such as IR spectroscopy, HR-MS, NMR spectroscopy, UV-Vis spectroscopy, Elemental analysis and X-ray crystallograghy were utilised to characterise all compounds. The UV-Vis studies show how in solution complexes **2.2-2.7** still retain some twisted conformation between TP and octahedral. However, the degree of twist in solution is suspected to be larger due to an increased amount of molecular freedom when compared to solid state analysis. The spectra were used to assign the electronic transitions occurring and where possible their ligand field splitting parameter (*Dq*), Racah parameter (*B*), and nephelauxetic ratio (*β*) were calculated (Tab. 4).

The Bailar twist angles for complexes **2.2**→**2.8** and, **2.10** and **2.11,** were calculated from crystal data and have been listed in Table 21. The amount of twist was expected to vary depending on

the stereochemical preference of the particular metal ion, where those ions with no desirable octahedral preference were expected to have less amount of Bailar twist and hence distort less away from a TP arrangement. The framework of **L2** is comparable to a previous example, tris(2,2'-bipyrid-6-yl)methanol, where three Bipy functions were used in place of three pyrid-2-yl pyrazoles, the donor arrangement of both these ligands present a strong preference to a trigonal prismatic geometry for many metal centres.[30,31] The Bailar twist angle, ϕ, varies greatly from 31.74° to 5.03° across the series of metals explored, with no discernible trend observed between the dihedral angles of the pyridyl-pyrazole units. The ionic radius of these metals can be used to explain the trend observed in Table 21 where the largest ions produce the smallest twist angle and conversely for smaller ions, such as Ni(II) where the Bailar angle is large enough such that the geometry is closer to octahedral than TP geometry. This relationship between ionic radii and Bailar twist is thought to occur due to the steric interactions between terminal methyl groups on the pyrazole backbone, this is because smaller sized metals draw in the ligand arms more, which consequently twist away from their planes to reduce steric interactions in the solid state. This is demonstrated by the much larger Bailar twist angles observed when compared with the analogous tris(2,2'-bipyrid-2-yl)methanol ligand (TBM) which has no methyl interactions.[30,31] Similarly the M-pyridine bond lengths and HP values (Fig. 24 and Tab. 22) can be used to observe how larger metal ions cannot co-ordinate as high up within the ligand cavity, thus creating a trend of geometric truncation that increases with larger metal size, due to the divergent nature of the ligand arms. Although there is a reasonable amount of Bailar twist observed in all examples they are still considered to have more TP character than octahedral, with the exception of complex **2.6** which, not only is the smallest cation, but also has a significant preference for octahedral geometry.

Table 22: Showing the distances of metal centre from higher and lower planes of the effective trigonal prism also with pyridyl-pyrazole N—N distances and bite angles.					
complex	HP (Å)	LP (Å)	N---N distance	Average Bite Angle (°)	Metal ion radius (pm)
2.6 Ni(II)	1.29	1.07	2.54	75.34	69
2.7 Cu(II)	1.36	1.09	2.55	77.28, 67.05*	73
2.8 Zn(II)	1.44	0.99	2.56	73.04	74
2.5 Co(II)	1.35	1.06	2.55	74.12	74.5(hs)
2.4 Fe(II)	1.41	1.03	2.55	72.38	78(hs)
2.3 Fe(III)	1.42	1.03	2.54	72.16	78.5
2.2 Mn(II)	1.56	1.00	2.61	71.19	83
2.10 Cd(II)	1.59	1.01	2.68	69.57	95
2.11 Hg(II)	1.80	0.81	2.65	67.55	102

*Two different angles exist due to unusual trigonal prismatic Jahn-Teller distortion, the smaller angle comes from the elongated co-ordination of one ligand arm (N1 and N3).

The Cu(II) complex **2.7** is of interest, as this compound displayed two significantly different Cu-N bond lengths, four short averaging 2.035(2) Å and two longer bonds (2.264(2) Å and 2.367(2) Å), which is indicative of a Jahn-Teller distortion, also noting that the two longer bonds are not equal in length. This is not the well-known distortion from a z-axis stretch of an octahedron but a rare Jahn-Teller distortion of a trigonal prism, see Figure 37, and has only been reported for a few examples.[34,40] This non-degenerate *cis*-distortion was attributed to a second order Jahn-Teller effect, in which the d_{yz} and p_z hybridise giving further stabilisation.

Table 23: A comparison of continuous shape measurements against Bailar twist angle. Also showing geometry deviation from the Bailar path.				
complex	Bailar twist angle (°). *averaged	S(Oct)	S(TP)	Deviation (%)
2.6 Ni(II)	31.74	6.16218	4.34233	9.3
2.7 Cu(II)	25.70	6.44979	4.75765	13.1
2.8 Zn(II)	24.49	6.74518	4.39971	12.4
2.5 Co(II)	25.90	6.17696	4.48966	10.2
2.4 Fe(II)	23.04	7.25608	4.16386	13.4
2.3 Fe(III)	21.28	7.87571	3.76070	13.8
2.2 Mn1(II)	8.95	13.0883	1.9800	21.3
Mn2(II)	13.07	11.3777	2.6003	20.1
2.10 Cd1(II)	12.15	11.88583	2.28015	19.5
Cd2(II)	11.76	11.97864	2.60559	22.3
Cd3(II)	11.48	12.05130	2.94208	25.0
2.11 Hg1(II)	8.36	14.11439	3.03387	32.9
Hg1a(II)	1.69	17.31997	2.62163	40.4

For the appropriate paramagnetic metal ions (complexes **2.2-2.5**), magnetic moment measurements were achieved using the Evans method, with data displayed in Table 20. All measured compounds were shown to adopt a high spin electronic configuration due to the trigonal prismatic arrangement of **L2**. This is attributed to poorer orbital overlap between the metal centre and the six homoleptic donors, giving the ligand a weaker field.

Using the collected SHAPE measurement data, comparisons can be made between the relative octahedron and trigonal prism configuration of each metal ion. Firstly, using Table 23, it can be confirmed that all the complexes reside closer to a trigonal prism geometry than that of an octahedron, including the Ni(II) complex (**2.6**), which displayed a large Bailar angle of 31.7°. However, none of the complexes can be said to be a near perfect trigonal prism.

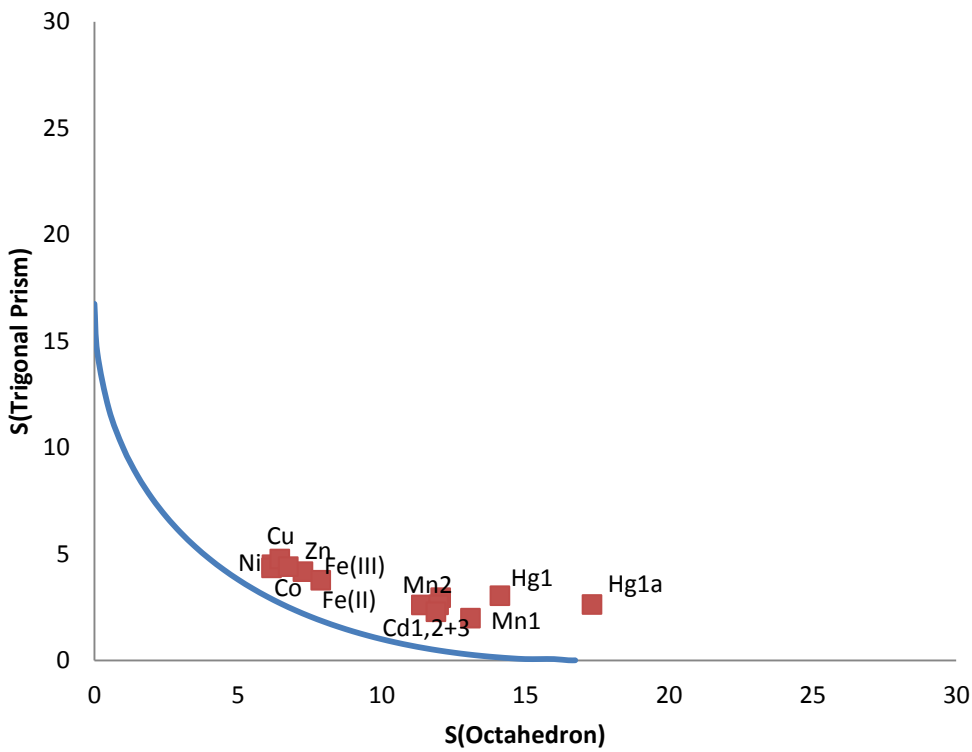

Figure 33: Shape map showing octahedral vs trigonal prismatic character of individual metal centres and their relative position from the Bailar path of interconversion (solid blue line). The deviation from the Bailar path was calculated using equation (7)

The graph in Figure 33 reveals how all of the complexes lie reasonably close to the Bailar path of interconversion from a trigonal prism to an octahedron, with exception of the Hg(II) complex which is found to have a deviation of up to 40%, see Table 23. In addition, the co-ordination spheres of **2.2** and **2.10** (Mn(II) and Cd(II)), are also observed to deviate significantly from this path. Since we are comparing the complexes to a regular trigonal prism, which has all equal sides, it is suggested that the divergent nature of the ligand arms (from being tethered at one end of the molecule), is likely to be causing this distortion from the ideal Bailar pathway. Another factor is increased ionic radius, which is found to increase the ratio between M-pyridyl and M-pyrazolyl bond lengths (Table 21). In the case of Hg(II), these M-pyridyl bonds are ~0.22Å longer than the M-pyrazolyl bonds, compared to that of the first row transition metals complexes, where the two sets of bonds remain fairly even in length. In contrast the smaller metal ions, in particular Ni(II), Co(II) and Zn(II), retain co-ordination environments that lie reasonably close to the ideal path of interconversion and consequently could be considered as trigonal metaprisms.

2.3 Experimental

General

NMR spectra were typically measured using a Bruker Av-250, Bruker AM-400 or Bruker Av-500 Plus FT-NMR spectrometer. Electrospray (ES) and high resolution (HR) mass spectra were obtained on a Waters LCT Premier XE (oa-TOF) mass spectrometer. All infrared spectra were measured on a Jasco FT-IR spectrophotometer, where each compound was pressed into a disk using an excess of dried KBr. UV-Vis absorption spectra were run using HPLC grade acetonitrile on a Perkin Elmer Lambda 2S UV-Vis spectrometer typically between 200-1100nm (optical path length 1.0 cm). Elemental analysis was carried out by MEDAC LTD analytical and chemical consultancy services or elemental analysis service, LONDON Metropolitan University.

The purity was confirmed by micro analysis of the complexes and was successfully achieved using crystals grown through vapour diffusion or using the purist possible powder samples. Overall the samples were of excellent quality. A region of error of 1% was excepted for some samples, especially in the carbon result, as carbides can be formed which are not volatile enough to be detected by this analysis. In all cases duplicate analysis were carried out to ensure consistency of the results, this required a mimimum of 5mg of sample and was carried out by MEDAC ltd or London Metropolitan University micro analysis services.

Bis(2-(6-bromopyridyl))ketone (**S1**).

2,6-dibromopyridine (5 g, 21 mmol) was dissolved in dried and degassed diethyl ether (150ml) and the resulting solution was cooled to -78°C with vigorous stirring. A solution of *n*-BuLi (14.4 ml, 23mmol, 1.6M in hexane) was added dropwise to the cooled solution. Within 5 mins a solution of diethyl carbonate (9.5mmol, 1.15ml) in diethyl ether (25 ml) was slowly added to the lithiate solution. The mixture was kept stirring at -78°C for 4h before the solution was slowly allowed to warm to ambient temperature over night. The solution was quenched with 10% HCl until acidic (pH 2-4). The resulting mixture was basified (pH 9-10) with 10% aqueous K_2CO_3, and the crude product partitioned between $CHCl_3$ and water. The aqueous layer was washed twice with $CHCl_3$ and the organic layers were combined, dried over anhydrous $MgSO_4$, decolourised with activated charcoal and the solvent was removed under reduced pressure.

The crude product was purified by column chromatography in 30/70 Hexane/DCM to give the pure product as a white solid (60-70%).

Tris(6-bromopyridin-2-yl)methanol (**S2**).

2,6-Dibromopyridine (3 g, 12.6 mmol) was dissolved in dried and degassed diethyl ether (60 mL). With vigorous stirring, the solution was cooled to -78◦C and a solution of *n*-BuLi (8.4 mL, 13.44 mmol, 1.6 M in hexane) was added dropwise. After stirring for 5 min, a cooled solution of bis(6-bromopyridin-2-yl)methanone (4.3 g, 12.6 mmol) in THF (50 mL) was slowly added to the solution of the lithiate. After stirring for 2 h at -78◦C, the reaction was allowed to warm to room temperature over night and was quenched with 10% HCl until acidic (pH 2-4). The resulting mixture was slightly basified (pH 9-10) with 10% aqueous K_2CO_3, and the crude product partitioned between $CHCl_3$ and water. The aqueous layer was washed twice with $CHCl_3$ and the organic layers were combined, dried over anhydrous $MgSO_4$, decolourised with activated charcoal and the solvent was removed under reduced pressure. The crude product was purified by column chromatography 30/70 Hexane/DCM to give the pure product as a white solid (75%).

Tris(6-hydrazinopyridin-2-yl)methanol (**S3**).

Tris(6-bromopyridin-2-yl)methanol (1.3g, 2.6 mmol) was added to hydrazine monohydrate (30ml). The solid was then dissolved by heating the mixture to 120-130°C and refluxing for 18h under a N_2 environment. The solution was then allowed to cool to room temperature and any solid formed was removed by filtration. The filtrate was reduced to dryness in *vacuo* using an external trap. The glass like solid was then washed and scratched with 20ml of ethanol until the solid retained a pale cream colour. The product was filtered off and dried under vacuum (0.395g, 43%). ^{1}H-NMR (CH_3OD; 300MHz): δ_H 7.60(t, 3H, J= 8.33Hz, C*H*), 7.11(d, 3H, J= 8.40Hz, C*H*), 6.73(d, 3H, J= 8.58 Hz, C*H*). ^{13}C-NMR ($CDCl_3$; 100MHz): δ_C 160.04 (C), 158.27 (C), 141.62 (CH), 111.94 (CH), 108.98 (CH), 78.28 (C). FT-IR (KBr/cm^{-1}) ν = 3244br, 2577br, 1974m, 1671s, 1616s, 1572s, 1495s, 1455s, 1324m, 1283m, 1162s, 1103s, 1082s, 970s, 783s. HRMS (ES-MS) *m/z* calcd. 352.16 ; exp. 535.1712 Lig + H, (72%), calcd. 322.16 ; exp. 323.1295 Lig + H – NH-NH_2, (100%).

Tris(6 - 2,4-dimethylpyrazolpyrid-2-yl)methanol (**L2**):

Tris(6-hydrazinylpyridin-2-yl)methanol (0.62g, $1.75x10^{-3}$mol) was stirred into an ethanol:methanol (2:1) solvent (30ml) and heated to roughly 60°C until the solid had dissolved. Pentane-2,4-dione (1.06g, 0.0106mol) was added to the hot solution followed by refluxing for a minimum of 4h. the reaction was then allowed to cool to room temperature and the solvent removed *in vacuo.* The remaining yellow oil was triturated with diethyl ether and the solid (by-product) filtered off. The ether solvent from filtrate was removed to produce a yellow fluffy product in high purity and good yield. (0.705g, 74%). ^{1}H-NMR ($CDCl_3$; 400MHz): δ_H 7.71(d, 3H, J=8.1Hz, C*H*), 7.69(t, 3H, J=7.4Hz, C*H*), 7.40(d, 3H, J=7.3Hz, C*H*), 6.37(s, 1H, O*H*), 5.82(s, 3H, C*H*), 2.20(s, 9H, CH_3), 2.13(s, 9H, CH_3). ^{13}C-NMR ($CDCl_3$; 100MHz): δ_C 161.20 (C), 151.86 (C), 149.94 (C), 138.92 (CH), 119.65 (CH), 114.03 (CH), 109.25 (CH), 81.89 (C), 14.49 (CH_3), 13.6 (CH_3). HRMS (ES-MS) *m/z* calcd. 545.89 ; exp. 546.2722 Lig + H, (10%), calcd. 568.25 ; exp. 568.2537 M + Na, (100%). FT-IR (KBr/cm^{-1}) ν = 3440br, 3109m, 3095m, 2977s, 2926s, 1981w, 1883w, 1794w, 1575s, 1564s, 1456br+s, 1379br+s, 1282m, 1147s, 1109s, 1073s, 973s. UV-Vis [λ_{max}, nm, (εM, $M^{-1}cm^{-1}$)] in CH_3CN: 259(43671.2), 287(41796.6)

Complexations

Cr(III) Tris(6 - 2,4-dimethylpyrazolpyrid-2-yl)methanol, $[CrC_{31}H_{31}N_9O][Cl]_3$ (**2.1**):

Chromium (III) trichloride tris tetrahydrofuran [$CrCl_3$.3THF] (49.4mg, $1.32x10^{-4}$mol) was dissolved in THF (2ml), the purple solution was then added in portions to a solution of **L2** (71.9mg, $1.32x10^{-4}$) in THF (3ml). The resulting dark orange mixture was sealed and stirred at ambient conditions for 24h eventually giving a dark green solution. The solution was reduced to a minimum (3ml) *in vacuo* and filtered through celite. Vapour diffusion of diethyl ether into a THF sample of the complex yielded dark green rhombic crystals (72mg, 78%). HRMS (ES-MS) *m/z* calcd. 631.1667 ; exp. 631.1646 $[Cr(C_{31}H_{30}N_9O)Cl]^+$, (30%), calcd. 689.1255; exp. 689.1451 $[Cr(C_{31}H_{30}N_9O)Cl_2Na]^+$, (10%). FT-IR (KBr/$cm^{-1}$) ν = 3383br+s, 3096s, 2976m, 2929m, 2865m, 1607s, 1578s, 1453s, 1364s, 1281m, 1234w, 1137m, 1059m, 992m, 814s, 782m, 748m, 721m, 657w, 626w, 538w, 432w. Found: C 47.19; H 4.84; N 15.18 (%) $CrC_{31}H_{31}N_9Cl_3.2H_2O.½CH_3CN$. Requires: C 47.29; H 4.48; N 15.77 (%). UV-Vis [λ_{max}, nm, (εM, $M^{-1}cm^{-1}$)] in CH_3CN:

254.5(31873), 289.9(23904), 452.3(170), 619.3(130). Magnetic moment (Evans method, 293K, d_3-Acetonitrile): μ_{eff} = 3.99μ_B.

Manganese(II) Tris(6 - 2,4-dimethylpyrazolpyrid-2-yl)methanol, [$MnC_{31}H_{31}N_9O$][$2ClO_4$] (**2.2**):

Manganese (II) perchlorate hexahydrate[$Mn(ClO_4)_2.6H_2O$](34.5mg, 9.54x10^{-5} mol) was dissolved in acetonitrile (5ml) and was added dropwise to a solution of **L2** (52mg, 9.54x10^{-5} mol) in acetonitrile solvent (5ml) . The resulting pale orange solution was stirred in ambient conditions for 16h. The solution was reduced to a minimum *in vacuo* and filtered through celite. Vapour diffusion of an acetonitrile/diethyl ether solvent system gave the desired complex as pale orange crystals (42mg, 55%). HRMS (ES-MS) *m/z* calcd. 699.7 ; exp. 699.15 [$MnC_{31}H_{31}N_9O[ClO_4]]^+$, (100%). FT-IR (KBr/$cm^{-1}$) ν = 3338br, 3135m, 2012w, 1604s, 1564s, 1468br, 1381s, 1362s, 1305m, 1190s, 1089br. Found: C 45.96; H 4.02; N 15.27 (%) $MnC_{31}H_{31}N_9(ClO_4)_2$. Requires: C 46.57; H 3.91; N 15.76 (%). λ_{max}, nm, (εM, $M^{-1}cm^{-1}$) in CH_3CN: 254.2(36756.76), 293.5(37837.84). Magnetic moment (Evans method, 293K, d_3-acetonitrile): μ_{eff} = 5.29μ_B.

Iron(III) Tris(6 - 2,4-dimethylpyrazolpyrid-2-yl)methanol, [$FeC_{31}H_{31}N_9O$][$3ClO_4$] (**2.3**):

A pale solution of Iron (III) perchlorate [$Fe(ClO_4)_3.4H_2O$](76.6mg, 1.80x10^{-4}mol) in acetonitrile (3ml) was added slowly to stirred solution of L2 (98mg, 1.80x10^{-4}mol) also in acetonitrile (5ml). the consequent dark orange solution was stirred for 16h before filtering through celite. The filtrate was reduced in vacuo to 4ml and set up for crystallisation by vapour diffusion of 50:50 petroleum ether and diethyl ether. The resulting orange crystals were of high purity (91mg, 57%). HRMS (ES-MS) *m/z* calcd. 300.0961 ; exp. 300.1649 [$FeC_{31}H_{30}N_9O]^{2+}$, (100%), calcd. 1144.4496 ; exp. 1144.4723 [$Fe(C_{31}H_{30}N_9O)_2]^+$, (98%). FT-IR (KBr/$cm^{-1}$) ν =3400br+s, 3242m, 3130m, 3095m, 2976m, 2927m, 1606s, 1578s, 1563m, 1471s, 1454s, 1426s, 1384m, 1364m, 1313w, 1285w, 1142s, 1109s, 1086s, 1026m, 993m, 811m, 780w, 752w, 720w. Found: C 41.35; H 3.60; N 14.04 (%) $FeC_{31}H_{31}N_9(ClO_4)_3$. Requires: C 41.36; H 3.47; N 14.01 (%). UV-Vis [λ_{max}, nm, (εM, $M^{-1}cm^{-1}$)] in CH_3CN: 260.8(32228), 288.2(34183). Magnetic moment (Evans method, 293K, d_3-acetonitrile): μ_{eff} = 4.57μ_B.

Iron(II) Tris(6 - 2,4-dimethylpyrazolpyrid-2-yl)methanol, $[FeC_{31}H_{31}N_9O][2ClO_4]$ (**2.4**):

Iron (II) perchlorate hexahydrate $[Fe(ClO_4)_2.6H_2O]$(23.4mg, 9.17x10^{-5} mol) was dissolved in acetonitrile (5ml) and was added dropwise to a solution of **L2** (50mg, 9.17x10^{-5} mol) in acetonitrile solvent (5ml) . The resulting orange solution was stirred in ambient conditions for 16h. The solution was reduced to a minimum *in vacuo* and filtered through celite. Vapour diffusion of an acetonitrile/diethyl ether solvent system gave the desired complex as yellow/orange crystals (34mg, 46%). HRMS (ES-MS) *m/z* calcd. 300.87 ; exp. 300.59 $[FeC_{31}H_{31}N_9O]^{2+}$, (100%), calcd. 700.61 ; exp. 700.15 $[FeC_{31}H_{31}N_9O[ClO_4]]^+$. FT-IR (KBr/$cm^{-1}$) ν = 3300br, 3126m, 2978w, 1604s, 1561m, 1473s, 1303m, 1190m, 1094br Found: C 47.35; H 4.18; N 15.62 (%) $FeC_{31}H_{31}N_9(ClO_4)_2$ Requires: C 46.52; H 3.90; N 15.74 (%). λ_{max}, nm, (εM, $M^{-1}cm^{-1}$) in CH_3CN: 254.9(104972.4), 284.1(91160.2), 559.8(95.85), 609.2(85.94). Magnetic moment (Evans method, 293K, d_3-acetonitrile): μ_{eff} = 4.45μ_B.

Cobalt(II) Tris(6 - 2,4-dimethylpyrazolpyrid-2-yl)methanol, $[CoC_{31}H_{31}N_9O][2ClO_4]$ (**2.5**):

Cobalt (II) perchlorate hexahydrate $[Co(ClO_4)_2.6H_2O]$(46.9mg, 1.28x10^{-4}mol) was dissolved in acetonitrile (5ml) and was added dropwise to a solution of **L2** (70mg, 1.28x10^{-4}mol) in acetonitrile solvent (5ml) . The resulting dull green solution was stirred in ambient conditions for 16h. The solution was reduced to a minimum *in vacuo* and filtered through celite. Vapour diffusion of an acetonitrile/diethyl ether solvent system gave the desired complex as greyish green crystals (43mg, 42%). HRMS (ES-MS) m/z calcd. 302.4 ; exp. 302.1, $[CoC_{31}H_{31}N_9O]^{2+}$, (100%), calcd. 703.69 ; exp. 703.14, $[CoC_{31}H_{31}N_9O[ClO_4]]^+$, (35%). FT-IR (KBr/$cm^{-1}$) ν = 3285br, 3125m, 3103m, 2996m, 2016w+br, 1604s, 1589s, 1564s, 1475br+s, 1418s, 1384s, 1367s, 1303m, 1194s, 1110br+s, 1046s, 995s, 950m, 927m, 803s, 777m, 748s, 718s, 666m, 623s UV-Vis [λ_{max}, nm, (εM, $M^{-1}cm^{-1}$)] in CH_3CN: 254.7(33098.6), 290.2(29577.5), 490.9(30.1), 630.98(17.07), 1073.6(17.4). Found: C 46.40; H 3.73; N 15.79 (%) $CoC_{31}H_{31}N_9(ClO_4)_2$. Requires: C 46.43; H 3.89; N 15.68 (%). Magnetic moment (Evans method, 293K, d_3-acetonitrile): μ_{eff} =3.93 μ_B.

Nickel(II) Tris(6 - 2,4-dimethylpyrazolpyrid-2-yl)methanol, $[NiC_{31}H_{31}N_9O][2ClO_4]$ (**2.6**):

Nickel (II) perchlorate hexahydrate $[Ni(ClO_4)_2.6H_2O]$(34.8g, 9.54x10^{-5}mol) was dissolved in acetonitrile (5ml) and was added dropwise to a solution of **L2** (52mg, 9.54x10^{-5}mol) in acetonitrile solvent (5ml) . The resulting solution was stirred in ambient conditions for 16h until

purple in colour. The solution was reduced to a minimum *in vacuo* and filtered through celite. Vapour diffusion of an acetonitrile/diethyl ether solvent system gave the desired complex as purple crystals (53mg, 69%). HRMS (ES-MS) *m/z* calcd. 704.03 ; exp. 702.14 ,$[NiC_{31}H_{31}N_9O[ClO_4]]^+$, (100%). FT-IR (KBr/cm^{-1}) ν = 3272br, 3150m, 3104m, 3001w, 1604s, 1564s, 1475s, 1366s, 1306m, 1197s, 1106br, 1045s Found: C 46.74; H 4.02; N 16.01 (%) $NiC_{31}H_{31}N_9(ClO_4)_2$. Requires: C 46.36; H 3.89; N 15.69 (%). UV-Vis [λ_{max}, nm, (εM, M^{-1}cm^{-1})] in CH_3CN: 256.3(39374.02), 289.2(30708.66), 558.1(26.01), 818.1(21.89), 963.6(35.17). Magnetic moment (Evans method, 293K, d_3-acetonitrile): μ_{eff} = 2.66μ_B.

Copper(II) Tris(6 - 2,4-dimethylpyrazolpyrid-2-yl)methanol, $[CuC_{31}H_{31}N_9O][2ClO_4]$ (**2.7**):

Copper (II) perchlorate hexahydrate $[Cu(ClO_4)_2.6H_2O]$(38mg, 1.03x10^{-4}mol) was dissolved in acetonitrile (5ml) and was added dropwise to a solution of **L2** (56mg, 1.03x10^{-4}mol) in acetonitrile solvent (5ml) . The resulting green solution was stirred in ambient conditions for 16h. The solution was reduced to a minimum *in vacuo* and filtered through celite. Vapour diffusion of an acetonitrile/diethyl ether solvent system gave the desired complex as green crystals (44mg, 52%). HRMS (ES-MS) m/z calcd. 707.1417 ; exp. 707.1459 $[CuC_{31}H_{31}N_9O[ClO_4]]^+$, (100%). FT-IR (KBr/cm^{-1}) ν = 3452br, 3114m, 2975m, 2931m, 2017w+br, 1608s, 1583s, 1466br+s, 1388s, 1367s, 1313m, 1089br+s, 992s, 930m, 809s, 750m, 624s UV-Vis [λ_{max}, nm, (εM, M^{-1}cm^{-1})] in CH_3CN: 258.8(40395.7), 287.5(37922.5), 705.2(105.8). Found: C 45.84; H 3.79; N 15.70 (%) $CuC_{31}H_{31}N_9(ClO_4)_2$. Requires: C 46.08; H 3.87; N 15.59 (%).Magnetic moment (Evans method, 293K, d_3-acetonitrile): μ_{eff} = 1.79μ_B.

Zinc(II) Tris(6 - 2,4-dimethylpyrazolpyrid-2-yl)methanol, $[ZnC_{31}H_{31}N_9O][2ClO_4]$ (**2.8**):

Zinc (II) perchlorate hexahydrate $[Zn(ClO_4)_2.6H_2O]$(32.1mg, 8.62x10^{-5}mol) was dissolved in acetonitrile (5ml) and was added dropwise to a solution of **L2** (47mg, 8.62x10^{-5}mol) in acetonitrile solvent (5ml) . The resulting pale yellow solution was stirred in ambient conditions for 16h. The solution was reduced to a minimum *in vacuo* and filtered through celite. Vapour diffusion of an acetonitrile/diethyl ether solvent system gave the desired complex as colourless crystals (38mg, 57%). ^{1}H-NMR (CD_3CN; 400MHz): δ_H 8.14(t, 3H, J = 8.15Hz, CH), 7.94(d, 3H, J = 7.79Hz, CH), 7.76(d, 3H, J = 8.5Hz, CH), 6.46(s, 1H, OH), 6.38(s, 3H, CH), 2.62(s, 9H, CH_3), 1.87(s, 9H, CH_3). ^{13}C-NMR (CD_3CN; 100MHz): δ_C 156.2, 154.0, 146.6, 145.7, 143.6, 117.91, 113.89, 111.93, 74.5 (C), 14.21 (CH_3), 11.52 CH_3). HRMS (ES-MS) *m/z* calcd. 305.64 ; exp. 304.58,

$[ZnC_{31}H_{31}N_9O]^{2+}$, (100%), calcd. 710.73 ; exp. 708.14, $ZnC_{31}H_{31}N_9O[ClO_4]]^+$, (48%). FT-IR (KBr/cm^{-1}) ν = 3303br, 3126m, 2978m, 1604s, 1562s, 1473s, 1364s, 1305s, 1192m, 1107br, 806s, 748s, 623s Found: C 45.51; H 3.79; N 15.48 (%) $ZnC_{31}H_{31}N_9(ClO_4)_2$. Requires: C 45.97; H 3.86; N 15.56 (%).

In(III) Tris(6 - 2,4-dimethylpyrazolpyrid-2-yl)methanol, $[2InC_{31}H_{30}N_9O][Cl_5.H_2O]$ (**2.9**):

Indium (III) trichloride $[InCl_3]$ (22.3mg, 1.01x10^{-4}mol) was dissolved in acetonitrile (3ml) and was added dropwise to a solution of **L2** (55mg, 1.01x10^{-4}mol) in acetonitrile solvent (5ml). The colourless complex solution was stirred for 24h. The solution was reduced to a minimum (3ml) *in vacuo* and then filtered through celite. Vapour diffusion of petrol/diethyl ether (50/50) into the complex solution yielded colourless crystals (32mg, 41%)

^{1}H-NMR (CD_3CN; 250MHz): δ_H 7.92(t, 3H, J = 7.99Hz, CH), 7.79(d, 3H, J = 8.0Hz, CH), 7.56(d, 3H, J = 5.7Hz, CH), 6.29(s, 1H, OH), 6.02(s, 3H, CH), 2.27(s, 9H, CH_3), 2.18(s, 9H, CH_3). ^{13}C-NMR (DMSO; 100MHz): δ_C 163.18, 151.70, 149.27, 141.13, 139.55, 119.87, 113.39, 109.40, 83.36, 13.95, 13.81. (ES-MS) *m/z* calcd. 694.1301 ; exp. 694.1307, $[InC_{31}H_{30}N_9OCl]^+$. FT-IR (KBr/cm^{-1}) ν = 3381br, 3132m, 3101m, 2968m, 2925m, 2856w, 1982w, 1579br+s, 1453br+s, 1383s, 1363s, 1283m, 1231w, 1145m, 1102m, 1072s, 1054m, 1027m, 993s, 972m, 812s, 782s, 745m, 709m, 657w, 629w. Found: C 37.83; H 3.25; N 12.77 (%) $In_2C_{31}H_{31}N_9OCl_6$ Requires: C 37.67; H 3.16; N 12.76 (%).

Cadmium(II) Tris(6 - 2,4-dimethylpyrazolpyrid-2-yl)methanol, $[CdC_{31}H_{31}N_9O][2ClO_4]$ (**2.10**):

Cadmium (II) perchlorate hexahydrate $[Cd(ClO_4)_2.6H_2O]$(26.3mg, 8.44x10^{-5}mol) was dissolved in acetonitrile (5ml) and was added dropwise to a solution of **L2** (46mg, 8.44x10^{-5}mol) in acetonitrile solvent (5ml) . The resulting pale yellow solution was stirred in ambient conditions for 16h. The solution was reduced to a minimum *in vacuo* and filtered through celite. Vapour diffusion of an acetonitrile/diethyl ether solvent system gave the desired complex as colourless crystals (56mg, 77%). ^{1}H-NMR (CD_3CN; 400MHz): δ_H 8.16(t, 3H, J = 8.14Hz, CH), 8.02(d, 3H, J = 7.88Hz, CH), 7.69(d, 3H, J = 8.34Hz, CH), 6.38(s, 1H, OH), 6.34(s, 3H, CH), 2.50(s, 9H, CH_3), 2.29(s, 9H, CH_3). ^{13}C-NMR (CD_3CN; 100MHz): δ_C 157.8, 153.1, 146.8, 145.2, 143.4, 119.1, 114.2, 112.4, 76.4(C), 13.8(CH_3), 13.2(CH_3). HRMS (ES-MS) *m/z* calcd. 329.15 ; exp. 329.58 ,$[CdC_{31}H_{31}N_9O]^{2+}$, (100%), calcd 757.17 ; exp. 758.12, $CdC_{31}H_{31}N_9O[ClO_4]]^+$, (60%). FT-IR

(KBr/cm^{-1}) ν = 3334br, 3130m, 2927w, 2009w, 1602s, 1565s, 1466br+s, 1433br+s, 1381s, 1361s, 1304m, 1186s, 1092br+s, 1042s, 1002s, 808m. Found: C 42.34; H 3.65; N 13.94 (%) $CdC_{31}H_{31}N_9(ClO_4)_2{\cdot}H_2O$ Requires: C 43.45; H 3.65; N 14.70 (%).

Mercury(II) Tris(6 - 2,4-dimethylpyrazolpyrid-2-yl)methanol, $[HgC_{31}H_{31}N_9O][2ClO_4]$ (**2.11**):

Mercury (II) perchlorate hexahydrate $[Hg(ClO_4)_2.6H_2O]$(42.4mg, 9.35x10^{-5}mol) was dissolved in acetonitrile (5ml) and was added dropwise to a solution of **L2** (51mg, 9.35x10^{-5}mol) in acetonitrile solvent (5ml) . The resulting pale yellow solution was stirred in ambient conditions for 16h. The solution was reduced to a minimum *in vacuo* and filtered through celite. Vapour diffusion of an acetonitrile/diethyl ether solvent system gave the desired complex as colourless crystals (54mg, 61%). ^{1}H-NMR (CD_3CN; 400MHz): δ_H 8.26(t, 3H, J = 8.1Hz, CH), 8.13(d, 3H, J = 7.5Hz, CH), 7.75(d, 3H, J = 8.2Hz, CH), 6.92(s, 1H, OH), 6.47(s, 3H, CH), 2.59(s, 9H, CH_3), 2.44(s, 9H, CH_3). ^{13}C-NMR (CD_3CN; 100MHz): δ_C 158.84, 152.49, 145.99, 144.88, 142.94, 119.64, 115.01, 112.19, 77.58, 13.52, 13.10. HRMS (ES-MS) *m/z* calcd. 372.7 ; exp. 373.6, $[HgC_{31}H_{31}N_9O]^{2+}$, (100%). calcd. 845.35 ; exp. 846.18, $HgC_{31}H_{31}N_9O[ClO_4]]^+$, (50%). FT-IR (KBr/cm^{-1}) ν = 3342br, 3129m, 2983m, 2925m, 2010w, 1599s, 1563s, 1466br+s, 1431s, 1381s, 1360s, 1304m, 1184m, 1148s, 1090br+s, 1000s, 944m, 930m, 809s, 747s, 720s, 662m, 622s Found: C 39.47; H 3.26; N 13.29 (%) $HgC_{31}H_{31}N_9(ClO_4)_2$. Requires: C 39.40; H 3.31; N 13.33 (%).

Tris(Rhenium-tricarbonylbromide)(Tris(6-2,4-dimethylpyrazolpyrid-2-yl)methanol), $3[Re(CO_3)Br][C_{31}H_{31}N_9O]$ (**2.12**):

Rhenium pentacarbonyl bromide $[ReCO_5Br]$ (111.6mg, 2.75x10^{-4}mol) and **L2** (50mg, 9.17x10^{-5}mol) were added to a flask and flushed with nitrogen. Dried and degassed toluene (50ml) was added and the mixture refluxed overnight resulting in a bright yellow precipitate being formed. The mixture was allowed to cool and filtered giving a yellow solid. The solid was washed with a small amount of toluene (2ml) followed by diethyl ether (5ml) giving the pure product in reasonable yield (92mg, 57%). The product was crystallised by slow evaporation from a $CHCl_3$ solution resulting in a sample suitable for crystallographic studies. ^{1}H-NMR (CD_3CN; 400MHz): δ_H 7.89(t, 3H, J = 8.1Hz, CH), 7.77(d, 3H, J = 7.5Hz, CH), 7.50(d, 3H, J = 7.5Hz, CH), 6.11(s, 1H, OH), 5.98(s, 3H, CH), 2.23(s, 9H, CH_3), 2.18(s, 9H, CH_3). ^{13}C-NMR (CD_3CN; 100MHz): δ_C 168.0, 156.39, 154.02, 145.86, 144.31, 124.59, 123.28, 118.05, 114.16, 18.71, 18.57. (ES-MS) *m/z* calcd. 816.2057 ; exp. 816.2114, $[(Re(CO)_3C_{31}H_{31}N_9O]^+$, (40%), calcd. 1084.1356 ; exp.

1084.1359, [2(Re(CO)$_3$)C$_{31}$H$_{30}$N$_9$O]$^+$, (55%), calcd. 1467.0482 ; exp. 1467.0455, [3(Re(CO)$_3$) C$_{31}$H$_{31}$N$_9$O.2Cl.MeCN]$^+$, (40%), calcd. 1508.0748 ; exp. 1508.0669, [3(Re(CO)$_3$) C$_{31}$H$_{31}$N$_9$O.2Cl.2MeCN]$^+$, (52%). (KBr/cm^{-1}) ν = 3360br+w, 3081w, 2985w, 2926.5w, 2021s, 1894br+s, 1604m, 1585w, 1563m, 1454s, 1421s, 1387m, 1365m, 1244w, 1154m, 1101w, 1082w, 999m, 806m, 737m, 715w, 657w, 625w, 521m. UV-Vis [λ_{max}, nm, (εM, M^{-1}cm^{-1})] in CH$_3$CN: 261.0(59215), 285.2(62010). Found: C 30.39; H 2.15; N 7.26 (%) C$_{31}$H$_{31}$N$_9$O(Re(CO)$_3$Br)$_3$. Requires: C 30.72; H 1.86; N 7.50 (%).

2.4 References

1. J. C. Bailar, *J. Inorg. Nucl. Chem.*, **1958**, 8, 165.
2. R.A.D. Wentworth, *Coord. Chem. Rev*., **1972**, 9, 171-187.
3. W.O. Gillum, R.A.D. Wentworth and R.F. Childers, *Inorg. Chem.*, **1970**, 9, 1825
4. R.A. Palmer and T.S. Piper, *Inorg. Chem.,* **1966**, 5, 864.
5. M. Pinsky and D. Avnir, *Inorg. Chem*., **1998**, 37, 5575-5582.
6. S. Alvarez, D. Avnir, P. Alemany*, Chem. Soc. Rev.,* **2005**, 34, 313-326.
7. H. Zabrodsky, S. Peleg and D. Avnir*, J. Am. Chem. Sov*, **1992**, 114, 7843-7851
8. S. Alvarez, D. Avnir, P. Alemany, D. Casanova, M. Llunell, J. Cirera*, Coord. Chem. Rev.,* **2005**, 249, 1693-1708.
9. S. Alvarez, D. Avnir, M. Llunell, M. Pinsky, *New J. Chem*., **2002**, 26, 996-1009.
10. S. Alvarez, D. Avnir, M. Pinsky, M. Llunell, *Cryst. Engineer*. **2001**, 4, 179-200.
11. M. Pinsky, K. B. Lipkowitz, D. Avnir, *J. Math. Chem*., **2001**, 30, 1, 109-120.
12. R. G. Dickinson. L. Pauling, *J. Am. Chem. Soc.,* **1923**, 45, 1466.
13. R. Eisenburg, J. A. Ibers*, J. Am. Chem. Soc.,* **1965**, 87, 3776.
14. R. Eisenburg, J. A. Ibers, *Inorg. Chem*., **1966**, 5, 411.
15. E. C. Constable, C. E. Housecroft, *Chem. Soc. Rev*., **2013**, 42, 1429.
16. A. E. Smith, G. N. Schrauzer, V. P. Mayweg, W. Heinrich, *J. Am. Chem. Soc*., **1965**, 87, 5798.
17. R. Eisenburg, E. I. Stiefel, R. C. Rosenberg, H. B. Gray, *J. Am. Chem. Soc*., **1966**, 88, 2874.
18. R. Eisenburg, H. B. Gray, Inorg. Chem., **1967**, 6, 1844.
19. E. I. Stiefel, Z. Dori, H. B. Gray, *J. Am. Chem. Soc*., 89, **1967**, 3353.
20. G. F. Brown, E. I. Stiefel*, Che., Commun*, **1970,** 725.
21. A. Sequeira, I. Bernal, *Abstr. Amer. Crystallogr., Ass Meet. Minneapolis, Minn., Summer* **1967**, 75.
22. W. O. Gillum, J. C. Huffman, W. E. Streib, R. A. D. Wentworth,. *Chem. Commun*., **1969**, 843.
23. E. B. Fleischer, A. E. Gebala, D. R. Swift,. *Chem. Commun*., **1971**, 1280.
24. E. B. Fleischer, A. E. Gebala, P. A. Tasker,. *J. Am. Chem. Soc*., **1970**, 92, 6365.
25. T. B. Karpishia, T. D. P. Stack, K. N. Raymond,. *J. Am. Chem. Soc*., **1993**, 115, 182-192.
26. R. L. Paul, A. J. Amoroso, P. L. Jones, S. M. Couchman, Z. R. Reeves, L. H. Rees, J. C. Jeffery, J. A. McCleverty, M. D. Ward*,. J. Am. Chem. Soc. Dalton. Trans*., **1999**, 1563.
27. A. J. Amoroso, J. C. Jeffery, P. L. Jones, J. A. McCleverty, P. Thornton, M. D. Ward,. *Angew. Chem. Int. Ed. Engl*., **1995**, 34, 1443.
28. M. D. Ward, *Annu. Rep. Prog. Chem. Sect A*., **2000**, 96, 345-385.
29. X. Li, C. L. D. Gibb, M. E. Kuebel, B. Gibb, *Tetrahedron*, **2000**, 57, 1175-1182.

30. J. C. Knight, *Ph.D. Dissertation, Cardiff University,* **2009**.
31. J. Knight, A. J. Amoroso, P. G. Edwards, *Dalton trans*, **2010**, 39, 3870,
32. J. Knight, A. J. Amoroso, P. G. Edwards, B. Ward, R Parabharan, *Dalton Trans*, **2010**, 39, 10031
33. J. Knight, A. J. Amoroso, P. G. Edwards, l. Ooi, R Parabharan. *Polyhedron*, **2012**, 31, 457-462.
34. J. Knight, S. Alvarez, A. Amoroso, P. Edwards, N. Singh,. *Dalton. Trans*., **2010**, 39, 3870–3883
35. D. L. Lewis, E. Dixon Estes, D. J. Hodgson*, J. Cryst. Mol. Struct*., **1975**, 5, 67-74 (perchlorate IR ref)
36. D. J. Parker., *Spectrochimica Acta*, **1983**, 39A, 5, 463-476.
37. D. F. Shriver and P. W. Atkins, *3rd Edition, Inorganic Chemistry, Oxford press*, **1999**.
38. E.Farkas, E. A. Enyedy, L. Zekany, G. Deak, *J. Inorg. Biochem*., **2001**, 83, 107-114.
39. P. Krumholtz, *J. Am. Chem. Soc*., **1953**, 75, 2163.
40. J. Echeverrıa, E. Cremades, A. J. Amoroso, S. Alvarez. *Chem. Commun*., **2009**, 4242-4244.
41. E. Brunet, O. Jaunes, *Tet. Lett.*, **2007**, 48 1353-1355.
42. M. D. Ward, J. A. McCleverty, *Coord. Chem. Rev*., **2001**, 222, 251-272.
43. M. D.Ward, Annu. *Rep. Prog. Chem.,sect. A*, 2000, 96, 345-385.
44. X. Jin, Z. Wang and S. Cao,. *Acta. Cryst*. **2011**. E67, m1492.
45. X.M.Chen, R.Q. wang, Z.T. Xu, *Acta. Cryst.*, **1995**, C51, 850
46. R. Van Gorkum, F. Buda, H. Kooijman, A. L. Spek, E. Bouwman, J. Reedijk,. *Eur. J. Inorg. Chem.* **2005**, 2255–2261.
47. Bao Huo Niu, Tao Li, *Acta. Cryst.* **2010**. E66, m201.
48. J. C. Zhaung, F. L. Hu, X. H. Yin, Q. L. Wu, Z. R. Luo, Y. Zhaung,. *J. Chem. Crystallogr*., **2011**, 41, 787-790.
49. A. X. Zheng, J. Si, X. Y. Tang, L. L. Miao, M. Yu, K. P. Hou, F. Wang, H. X. Li, J. P Lang,. *Inorg. Chem*. **2012**, 51, 10262−10273.
50. Y. Yang, P. Yanga, C. Zhanga, G. Lia, X. J. Yanga, B. Wua, C. Janiak,. *Journal of Molecular Catalysis A: Chemical.* **2008**, 296, 9–17.
51. G. F. Liu, Z. G. Ren, H. X. Li, Y. Chen, Q. H. Li, Y. Zhang, J. P. Lang,. *Eur. J. Inorg. Chem.* **2007**, 5511–5522.
52. X. H. Yin, K. Zhao, Y. Fenga, J. Zhub,. *Acta. Cryst.*, **2007**, E63, m2926.
53. M. D. Ward, K. L. V. Mann, J. C. Jeffery, J. A. McCleverty, *Acta. Cryst*., **1998**, C54, 601-603.
54. K. Das, S. Konar, A. Jana, A. K. Barikc, S. Roy, S. K. Kar, *Journal Molecular Structure*, **2013**, 1036, 392–401.
55. Ç. Hopa, R. Kurtaran, A. Azizoğlu, M. Alkan, N. B. Arslan, C. Kazak,. *Z. Anorg. Allg. Chem.* **2011**, 637, 1238–1245.
56. L. A. Lytwak, J. M. Stanley, M. L. Mejia, B. J. Holliday,. *Dalton Trans.,* **2010**, 39, 7692–7699.

57. Y. Sasaki., *Bulletin Institute Chemical Research, Kyoto. Univ.*, **1980**, 58(2), 182-192.
58. S. Liu, R. Pattacini, P. Braunstein, *Organometallics*, **2011**, 30, 3549-3558.
59. L. R. Grey, A. L. Hale, W. Lavason, F. P. McCullough, M. Webster. *J. Chem. Soc. Dalton. Trans*., **1984**, 47-53.
60. M. A. Estervelas, A. M. Lopez, L. Mendez, M. Olivan, E. Onate. *Organometallics*, **2003**, 22, 395-406.
61. N. Cloete, H. G. Visser, A. Roodt*, Acta. Cryst.*, **2007**, E65, m45-m47.
62. J. Hurtado, D. Mac-Leod. Carey, A. Muñoz-Castro, R. Arratia-Pérez, R. Quijada, G. Wud, R. Rojas, M. Valderrama,. *J. Org. Met. Chem.*, **2009**, 694, 2636–2641.
63. C. Bachmann, M. Guttentag, B. Spingler, R. Alberto,. *Inorg. Chem*., **2013**, 52, 6055-6061.
64. V. Amani, N. Safari, H. R. Khavasi, P. Mirzaei,. *Polyhedron*, **2007**, 26, 4908-4914.
65. R. D. Shannon, *Acta. Cryst.*, **1976**, A32, 751-767.

Table 1A: Crystallographic data for complexes with **L2**.						
Compound	2.1	2.2	2.3	2.4	2.5	2.6
Chemical formula	$[CrC_{31}H_{31}N_9O][Cl]_3.3CH_3CN$	$[MnC_{31}H_{31}N_9O][ClO_4]_2$	$[FeC_{31}H_{31}N_9O][ClO_4]_3$	$[FeC_{31}H_{31}N_9O][ClO_4]_2$	$[CoC_{31}H_{31}N_9O][ClO_4]_2$	$[NiC_{31}H_{31}N_9O][ClO_4]_2$
Mr, g/mol	827.16	799.49	899.85	800.40	803.48	803.26
Crystal system	Triclinic	Monoclinic	Trigonal	Monoclinic	Monoclinic	Monoclinic
Space Group	P-1	P21/c	R-3	P21/c	P21/c	P21/c
T (k)	150 (2)	293 (2)	293 (2)	293 (2)	150 (2)	150 (2)
a, Å	15.1834 (10)	19.9034 (9)	15.089 (4)	11.9100 (3)	11.7018 (7)	11.5504 (2)
b, Å	15.6209 (10)	19.4985 (9)	15.089 (4)	11.0013 (4)	11.1342 (7)	11.2121 (2)
c, Å	20.1600 (9)	16.9122 (7)	26.927 (5)	25.6063 (8)	25.6402 (9)	25.6038 (6)
α, deg	105.848 (4)	90.00	90.00	90.00	90.00	90.00
β, deg	97.921 (4)	92.675 (2)	90.00	98.503 (2)	98.690 (3)	98.4470 (10)
γ, deg	111.397 (3)	90.00	120.00	90.00	90.00	90.00
V, $Å^3$	4129.5 (4)	6556.2 (5)	5310 (2)	3318.20 (18)	3302.3 (3)	3279.83 (11)
Z	4	8	6	4	4	4
D_c g/cm^3	1.330	1.620	1.689	1.602	1.616	1.656
μ(Mo K α), mm^{-1}	0.516	0.637	0.734	0.686	0.752	0.826
Observed Reflections	8552	9508	2021	7902	7520	8008
Reflections collected	14973	17686	7604	20120	17269	15241
R_{int}	0.0646	0.0928	0.1037	0.0898	0.0732	0.0605
R_I [I>2σ(I)]	0.0701	0.1742	0.1118	0.1023	0.0692	0.0814
wR_2 (all data)	0.1686	0.4379	0.3077	0.2113	0.1852	0.2060

Table 1B: Crystallographic data for complexes with **L2**.						
Compound	2.7	2.8	2.9	2.10	2.11	2.12
Chemical formula	$[CuC_{31}H_{31}N_9O][ClO_4]_2$	$[ZnC_{31}H_{31}N_9O][ClO_4]_2$	$[In_2C_{31}H_{31}N_9O][OH][Cl]_5$	$[CdC_{31}H_{31}N_9O][ClO_4]_2$	$[HgC_{31}H_{31}N_9O][ClO_4]_2$	$[(Re(CO)_3Br)_3C_{31}H_{31}N_9O].2CHCl_3$
Mr, g/mol	808.09	809.92	969.55	856.95	945.14	1834.80
Crystal system	Monoclinic	Monoclinic	Orthorhombic	Monoclinic	Monoclinic	Triclinic
Space Group	P21/c	P21/c	Pccn	Cc	Cc	P-1
T (k)	150 (2)	150 (2)	150 (2)	150 (2)	293 (2)	150 (2)
a, Å	11.687 (2)	11.8415 (2)	28.7018 (4)	19.7559 (7)	19.5246 (14)	10.4560 (10)
b, Å	11.0822 (2)	11.05360 (10)	13.8724 (2)	29.2938 (8)	9.8912 (5)	15.6112 (17)
c, Å	25.8550 (4)	25.6249 (3)	18.3745 (2)	17.0749 (6)	17.1758 (11)	20.482 (2)
α, deg	90.00	90.00	90.00	90.00	90.00	81.442 (6)
β, deg	98.5590 (10)	98.5310 (10)	90.00	92.558 (3)	91.818 (5)	80.497 (7)
γ, deg	90.00	90.00	90.00	90.00	90.00	87.845 (5)
V, $Å^3$	3311.39 (10)	3316.96 (7)	7316.04 (17)	9871.8 (6)	3315.4 (4)	3260.4 (6)
Z	4	4	8	12	4	2
D_c g/cm^3	1.621	1.622	1.760	1.730	1.894	1.869
μ(Mo K α), mm^{-1}	0.892	0.972	1.670	0.897	4.874	7.691
Observed Reflections	7459	8216	9111	20421	6739	6671
Reflections collected	12546	15961	16846	33756	11052	10326
R_{int}	0.0347	0.0396	0.0363	0.0667	0.0762	0.1492
R_I [I>2σ(I)]	0.0488	0.0646	0.0490	0.1382	0.0902	0.1529
wR_2 (all data)	0.1264	0.1662	0.1265	0.3946	0.2004	0.3987

Chapter 3:

A Tripodal Pyridyl Diphenyl-Pyrazole Framework and its Co-ordination Complexes with Various Transition Metals

3.0 Abstract

Presented in this chapter is the novel tripodal ligand **L3** (Tris(6 – 3,5-diphenylpyrazolpyrid-2-yl)methanol) and its co-ordination chemistry with a range of transition metals including Zn(II), Cu(II), Ni(II), Co(II), Fe(II), Mn(II), Cd(II), Hg(II), Y(III) and Re(I). The introduction of phenyl groups to the pyrazole backbone make this ligand more sterically demanding upon complexation compared with analogous methyl-substituted tripods such as **L2** described in chapter 2. The ligand and complexes have been studied and characterised using UV-Vis, IR, NMR spectroscopies, mass spec, magnetic susceptability and X-ray crystallography.

3.1 Introduction

As discussed in chapter 4, the co-ordination chemistry of N-heterocylic donors has become increasingly topical in recent decades, especially those containing pyridine and pyrazoles units, due to their rich diversity in metal co-ordination and vast ability to be functionalised.[1,2] Chelating ligands based around pyrazole rings has been extensively developed in recent years for their broad applicability in many fields, such as supramolecular arrays,[3,4] catalysis,[5,6] and magnetic properties.[7,8]

Substitution of pyrazoles around the 3- and 5-positions allows investigations into the nature of their co-ordination and provides different steric and electronic qualities into the resulting structures of such complexes. Pons *et. al*. have extensively studied the co-ordination chemistry of simple functionalised pyrazoles over recent years, using groups such as CH_3, CF_3 and pyridines, with particular interest in their applications as palladium Heck catalysts.[9a,b] In a more recent study, they have characterised a diphenyl-substituted pyrazole ligand (2-(3,5-diphenyl-1H-pyrazol-1-yl)ethanol), and investigated its different co-ordination behaviour with the transition metals Pd(II), Zn(II) and Cu(II) (Sch. 1).[10] The Pd(II) complex was found to coordinate two ligands in a *trans*-fashion through their pyrazole N-donors. This gives a traditional square planar complex, with the other two *trans*-donors being chlorides (Sch. 1). The isolated Zn(II) complex however, was found to bind in a tetrahedral manner with only one ligand. This facilitated both the nitrogen and the alcohol donors, creating a six membered metallocycle ring, and again retained co-ordination of its two chloride counter ions. In contrast the Cu(II) complex

presented a dinuclear structure, where one Cu centre is bound with two ligands, in a head to head arrangement (due to the restricted sterics of the appending phenyl groups), creating two six membered metallocycles. The loss of both hydroxyl protons allows the *cis*-co-ordination of the second Cu centre to the same oxygens, on the end of the structure, with both metals presenting distorted square planar geometries (Sch. 1). In summary, this demonstrates the range of co-ordinating abilities of just one ligand and the diverse structures simple functionalised pyrazoles can form.

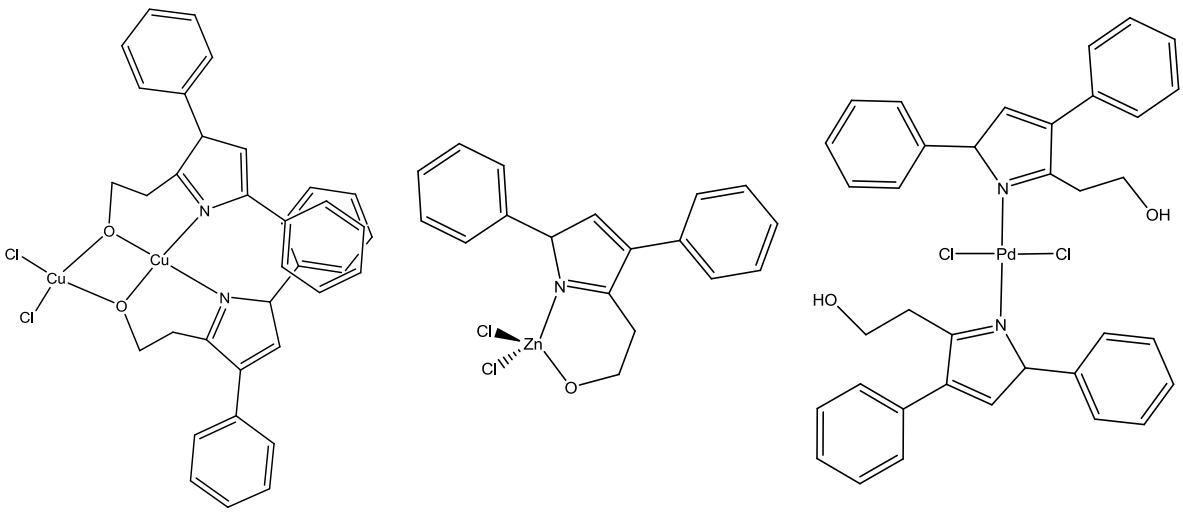

Scheme 1: Showing the three different co-ordination modes of 2-(3,5-diphenyl-1H-pyrazol-1-yl)ethanol.[10]

The linking of pyridine moieties to pyrazole creates a potentially bidentate chelating ligand with a preposition for efficient co-ordination to transition metals. Campo *et. al*., in their search for good supramolecular arrangements, have developed two ligands of this type, with the addition of oxygen containing pendent groups to the pyrazole backbone, L^{OBu} (3,5-bis(4-butoxyphenyl)-1-(pyridin-2-yl)-1H-pyrazole) and L^{OPh} (3,5-bis(4-phenoxyphenyl)-1-(pyridin-2-yl)-1H-pyrazole).[11] These ligands have been successfully complexed with Cu(I) and Cu(II) showing versatile co-ordinating abilities. With both ligands, Cu(II) was found to form six co-ordinate complexes utilising two ligands for every copper centre. In the case of complexation with $CuCl_3$ starting material, both L^{OBu} and L^{OPh} produced complexes with a *cis* arrangement. By contrast they found that instead, by using $Cu(BF_4)_2$, complexation with L^{OBu} gave a *trans*-arranged structure, which could not be seen using the bulkier ligand L^{OPh} (Sch. 2). Alternatively, by using $Cu(PF_6)$, both ligands produced square planar structures, each co-ordinating two ligands in a similar

fashion. Additionally it was found that the complex $[Cu(L^{OBu})_2][PF_6]$, if left in DCM and open to air, would oxidise to form a five co-ordinate Cu(II) complex in which a chloride has been adopted as the fifth donor set.

The ligand L^{OBu} has also been investigated by Gallego *et.al* using Ag(I), where it was found to form either four or five co-ordinate structures depending on the stoichiometry of ligand used. They were also interested in supramolecular arrays and found that these complexes formed 1D and 2D networks, through hydrogen bonding, in the solid-state.[12]

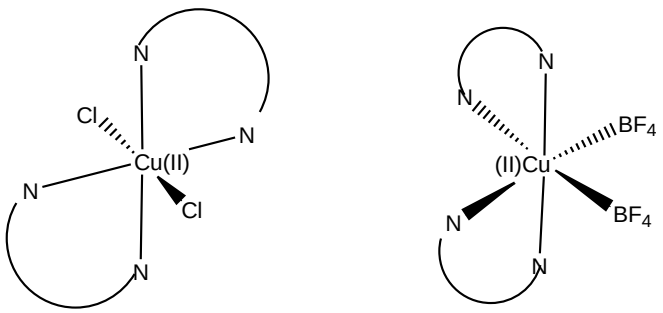

L^{OBu} and L^{OPh} L^{OBu}

Scheme 2: Showing the possible *cis* and *trans* arrangements of L^{OBu} with Cu(II).[11]

The use of sterically encumbered pyrazoles has also been investigated with regard to catalysis. In general these are also linked to other heterocycles to create rigid multidentate ligands that are suitable for forming stable complexes with tuneable activity. For example, Yang *et. al.* have developed a series of trigonal bipyramidal nickel(II) halide complexes bearing a tridentate 2-pyrazolyl substituted 1,10-phenanthroline unit (Sch. 3).[13]

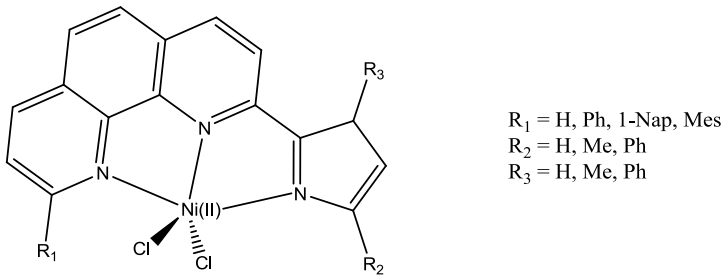

Scheme 3: Nickel complex with the 2-pyrazolyl substituted 1,10-phenanthroline ligand unit.[13]

The purpose of this study was to gauge the reactivity of these complexes, in ethylene oligomerization, with different pendent groups. In summary, their investigations found that all of the complexes showed a significant level of oligomerization, however, it was clear that bulkier substituted pyrazoles (R2 and R3 = Ph) produced the highest activities. Bulky groups substituted to the 9-position on the phenanthroline were also employed which were found to further improved catalytic ability, with the ligand 2-(3,5-diphenylpyrazol-1-yl)-9-mesityl-1,10-phenanthroline, showing the overall highest reactivity. The success of the bulkier substituted ligands was owed to the formation of a reaction channel around the nickel centre, see Scheme 4, which was said to enhance the probability of insertion over dissociation once an ethylene was already bound to the Ni centre.

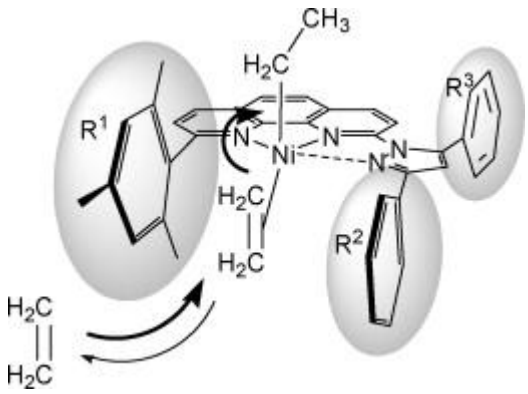

Scheme 4: Representation which highlights the reaction channel formed by bulkier substituted groups on the ligand framework, which promotes C-C formation and decreases ethylene dissociation.[13]

Another set of Ni(II) complexes has been described by Cheng *et. al.* using the ligand 2,7-bis(3,5-di-R-pyrazol-1-yl)-1,8-naphthyridine (R = H, Me or Ph).[14] In this example they investigated the catalytic ability of di-nickel complexes in the homo-coupling of various terminal alkynes. These complexes have metal centres which are now hexa-coordinate, where two Ni(II) ions bind with a single ligand in a bidentate fashion, possessing strong octahedral geometries, see Scheme 5. Various catalysis experiments were performed using the modified pyrazole ligands and different terminal alkynes. All of the modified ligands were found to be significantly more active than any previous mono-nuclear species. In addition, the activity of the di-nickel complex was improved in the more sterically substituted ligand (R = Ph). Although the product yields of the

un-substituted pyrazole ligand (R =H) compared closely to that of the di-Phenyl ligand, the much lower reaction times observed with the bulkier ligand was of significant improvement. Similarly to the previous example, this was owed to the steric presents of the phenyl moieties, which is suggested to accelerate the reductive elimination step in catalysis.

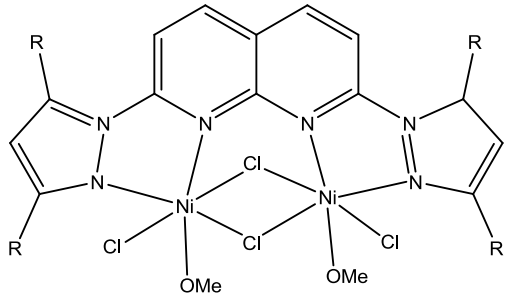

R= H, Me, Ph

Scheme 5: The di-nickel complex with 2,7-bis(3,5-di-R-pyrazol-1-yl)-1,8-naphthyridine ligand.[14]

The following chapter introduces the novel ligand Tris(6–(3,5-diphenylpyrazol-1-yl)pyrid-2-yl)methanol (**L3**). This is an analogue of **L2** which incorporates different appendages in the form of phenyl groups to the 3- and 5-positions of the pyrazole backbone, in replacement of the methyl functions used in **L2**. The addition of these phenyl groups was employed to investigate the co-ordination ability of this new system with various transition metals, with the ultimate goal that the phenyl groups could potentially be further functionalised. Employing nitro, amine or acid groups to the *para*-position of these pendent phenyls could allow the linking of useful biologically active conjugates, which may aid the targeting and accumulation of these probes in assays of living systems.

3.2 Results and Discussion

3.21 Ligand synthesis

The starting material **S3** was synthesised via compounds **S1** and **S2** which are described in chapter 2 for the ligand **L2** (Page 35) giving the building block for the tripodal framework. **S3** was condensed with 3.2eq of 1,3-diphenyl-1,3,-propanedione in an ethanol/methanol (2:1) solvent system by refluxing for 20 hours. This resulted in cyclisation of 1,3-diphenyl-1,3,-propanedione with the pendent hydrazido-moieties of **S3** to give a ligand system (**L3**) analogous to that of **L2** in which the appending 3,5-methyl groups are replaced by larger phenyl moieties (Sch. 6).

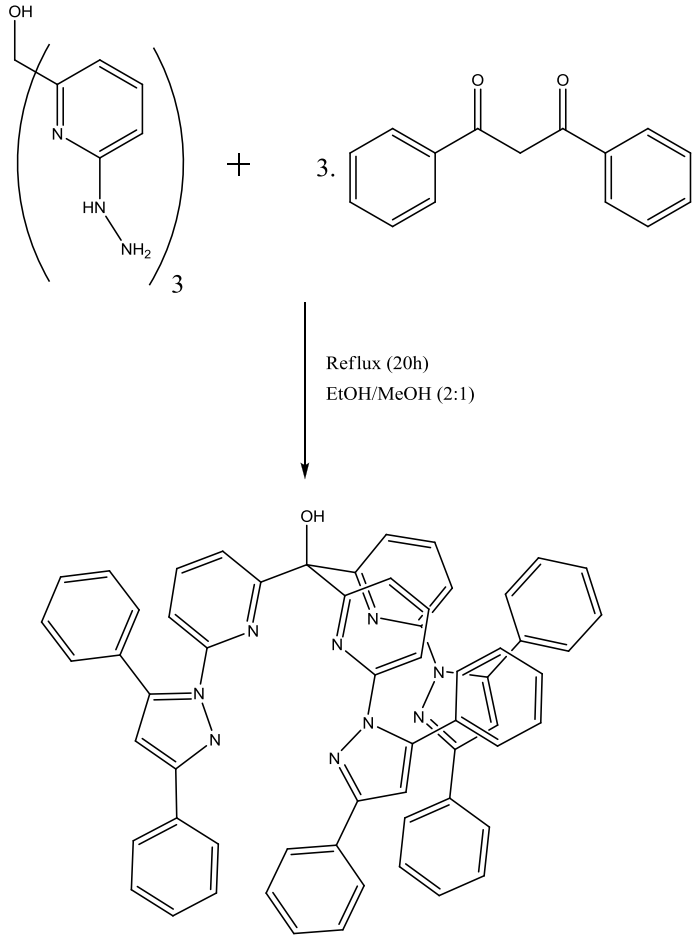

(**L3**)

Scheme 6: Synthetic route to ligand Tris(6–(3,5-diphenylpyrazol-1-yl)pyrid-2-yl)methanol **L3**.

3.22 Synthesis of Complexes

Following on from the previous chapter, the complexes with **L3** were synthesised in a similar fashion to those of **L2**. A series of transition metal perchlorate salts (with exception of **3.9** which started as $Re(CO)_5Br$), see Table 1, were dissolved in acetonitrile (typically 2-3ml) and the solutions were added slowly to a warm solution of **L3** in acetonitrile (typically 0.1mmol in 3ml). Heating was often required as **L3** is less soluble than **L2** in the chosen solvent. Generally a colour change was observed (with exception of compounds **3.6**-**3.8** due to their d^{10} nature) and the mixtures were allowed to equilibrate for 3h before filtration through celite. All of the complexes remained in solution upon cooling and are more soluble than the free ligand **L3**. All the complexes (**3.1**-**3.8**, Sch. 7) were reacted in a 1:1 equivalents ratio with exception of compound **3.9** which was refluxed in toluene from $Re(CO)_5Br$ in a 3:1 metal:ligand ratio, and is comparable to complex **2.12** in the previous chapter.

Table 1: Showing complex label with the corresponding metal ion used

Complex label	Ion used with **L3**
3.1	Mn(II)
3.2	Fe(II)
3.3	Co(II)
3.4	Ni(II)
3.5	Cu(II)
3.6	Zn(II)
3.7	Cd(II)
3.8	Hg(II)
3.9	Re(I)

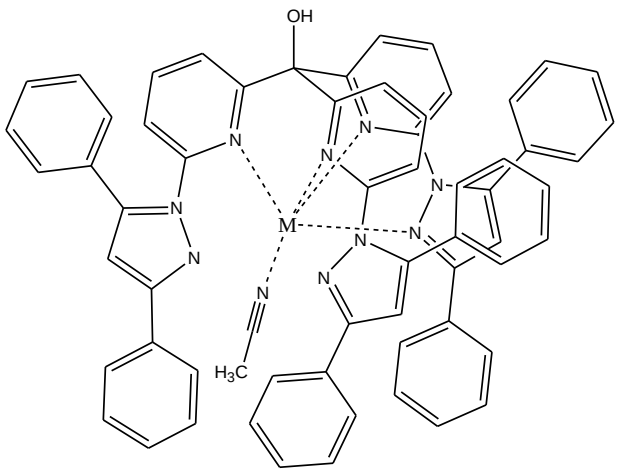

Scheme 7: Schematic diagram showing the general co-ordination mode of **L3** with various transition metals. M= Mn(II), Fe(II), Co(II), Ni(II), Cu(II), Cd(II) and Hg(II).

3.23 Vibrational spectroscopy

The IR spectra of **L3** and all the synthesised complexes were collected in the solid-state using KBr discs, with the data displayed in Table 2. The phenyl and pyridyl ring stretches of complexes **3.1-3.9** are typically seen between 1610cm^{-1} and 1350cm^{-1}. These peaks shift only slightly across the series of complexation with the largest change seen in the highest energy band at around 1600cm^{-1}. Typical ν(O-H) and ν(C-H) stretches (3350cm^{-1} and 3080cm^{-1} respectively) were observed for all samples. Interestingly the Zn(II) compound (**3.6**) was observed to have the highest energy ν (O-H) stretch, which could be attributed to the formation of a dimer, which is shown in crystallographic data, Page 132. This complex utilises bridging oxygens from the apical OH groups. The π(C-H) vibrations are a good identification of this ligand (**L3**), as they are well separated, strong absorptions. However, there are no discernible trends observed in these peaks between the free ligand and complexes. There are only two stretches observed in the perchlorate frequency regions for all of the complexes, a strong broad peak at approximately 1090cm^{-1} and a sharper equally strong peak around 622cm^{-1}. As discussed in the previous chapter (Page 39), this refers to un-coordinated perchlorate counter ions, which are also confirmed by crystallographic data from complexes **3.3, 3.5** and **3.6**.

Complex **3.9** is a rhenium compound and does not contain any perchlorate counter ions. Instead the complex can be identified by three very strong carbonyl absorptions from 1870cm^{-1}

to 2030cm^{-1}. These CO stretches are typical of M-CO complexes and the lower energy shift observed by one peak set is indicative of Re-*fac*-tricarbonyl co-ordination.

Table 2: Showing characteristic vibrational modes of **L3** and complexes					
compound	Aromatic ν(C-H)	ν (O-H)	ν (C=N) and (C=C)	π(C-H)	ν (Cl-O) ν (C≡O)*
L3	3059.0(m), 3044.8(m)	3358.9 (m)	1592.9(s), 1575.6(s), 1550.9(m) & 1485.9(s), 1452.6(s), 1362.0(s)	813.8(s), 760.8(s), 693.8(s)	n/a
3.1	3058.1(m), 3040.0(m)	3389.8 (br+s)	1603.5(s), 1575.1(s), 1543.4(m) & 1485.9(s), 1451.7(s), 1361.5(s)	814.8(m), 762.7(s), 695.2(s)	1088.6(br+s) 625.3(s)
3.2	3125.6(m), 3051.3(m)	3434.1 (br+m)	1605.9(m), 1572.7(s), 1557.4(m) & 1484.9(s), 1452.6(s), 1360.5(s)	818.2(m), 763.7(s), 695.7(s),	1090.6(br+s), 624.8(m)
3.3	3121.7(m), 3061.4(m)	3434.1 (br+m)	1610.3(m), 1586.2(m), 1558.7(m) & 1486.9(m), 1471.9(s), 1408.8(w), 1358.6(m)	808.0(w), 763.7(s), 696.2(s)	1091.0(br+s), 622.4(s)
3.4	3115.9(m), 3061.4(m)	3376.3 (br+m)	1610.8(s), 1586.2(s), 1558.7(s) & 1464.7(br+s), 1408.8(s), 1361.0(s)	808.0(m), 761.3(s), 695.2(s)	1089.1(br+s), 621.0(s)
3.5	3105.9(m), 3060.0(m)	3323.5 (w)	1608.8(s), 1581.3(s), 1561.4(m) & 1486.4(s), 1466.6(s), 1455.0(s), 1408.3(m), 1363.43(s)	817.2(m), 761.3(s), 698.1(s)	1087.7(br+s), 622.9(s)
3.6	3120.7(m), 3053.3(m)	3479.9 (w)	1613.9(m), 1575.1(s), 1557.7(m) & 1485.9(s), 1455.5(s), 1411.8(m), 1361.0(s)	814.3(m), 765.1(s), 696.2(s)	1091.5(br+s), 622.9(s)
3.7	3117.9(w), 3059.5(w)	3378.2 (w)	1594.4(s), 1575.1(s), 1553.4(s) & 1485.9(s), 1456.0(br+s), 1405.9(s), 1361.5(s)	814.3(s), 764.2(s), 694.7(s)	1095.4(br+s), 623.4(s)
3.8	3130.4(m), 3061.9(m)	3357.5 (m)	1660.9(m), 1582.8(s), 1556.8(s) & 1485.9(s), 1456.0(br+s), 1407.8(s), 1348.0(s)	804.7(s), 767.5(s), 699.6(s), 668.2(s)	1086.2(br+s), 621.9(s)
3.9	3063.4(w), 3044.1(w)	3445.7 (w)	1604.0(s), 1569.8(m), 1554.4(m) & 1488.3(s), 1467.1(s), 1402.5(w), 1362.0(s)	826.3(m), 809.5(m), 758.37(s), 694.2(s), 685.6(s)	2030.2(s)*, 20.13.2(s)*, 1916.9(br+s)*, 1876.9(br+s)*

3.24 NMR spectroscopy

Proton and carbon NMR data were collected for **L3** and complexes **3.6-3.9** using CD_3CN solvent. The ^{1}H-NMR for **L3** gave seven peaks all within the aromatic region (6.7-8ppm) with integrations in a ratio of 3:6:9, indicating the symmetrical three fold nature of the compound. The ^{1}H-NMR for complexes **3.6-3.9** all show some degree of shift in relation to the free ligand, which provides evidence that co-ordination has occurred (Fig. 1-4). Insufficient solubility in deuterated solvents meant that collecting solution-state data was difficult, and as a result, most carbon NMR data were poorly resolved. The complexes **3.7** (Cd^{2+}, Fig. 2) and **3.8** (Hg^{2+}, Fig. 3) have similar proton NMR spectra to that of **L3** (Appendix Fig. 1A) in that they contain only 7 aromatic proton environments with integrations of the same ratios. In general all of the peaks in both complexes are seen to have shifted down field, with exception of the peak at 6.7ppm. This shifting and the similarities of the spectra of **L3** suggest that these complexes form fairly symmetrical monomeric structures, similar to that observed in the X-ray data for **3.3** and **3.5** (Fig. 11 and 14 respectively). However, it must be noted that this is a solution based study and not necessarily comparable to the solid-state information obtained from single crystal X-ray diffraction studies.

The Zn(II) complex (**3.6**) has a more complicated ^{1}H-NMR spectrum than of the previous d^{10} metals, and shows 14 aromatic proton environments (Fig. 1). The large number of peaks suggests that an unsymmetrical structure is present. The integrations of these peaks are also more complicated than those observed for **L3**, **3.7**, **3.8** and **3.9** (Fig. 4). Altogether these results suggest that one ligand arm per tripodal ligand is experiencing a different environment to the other two arms (displaying a 1:2 integration ratio). Interestingly this evidence is also reflected in the X-ray data of **3.6** (Fig. 16) where a dimer forms, which involves the coming together of two ligands and two Zn(II) centres, where four ligand arms co-ordinate and the other two remain pendant. From the ^{1}H-NMR data collected, it is assumed that the dimer structure (**3.6**, Fig. 1) observed from crystallographic data may also be stable in solution.

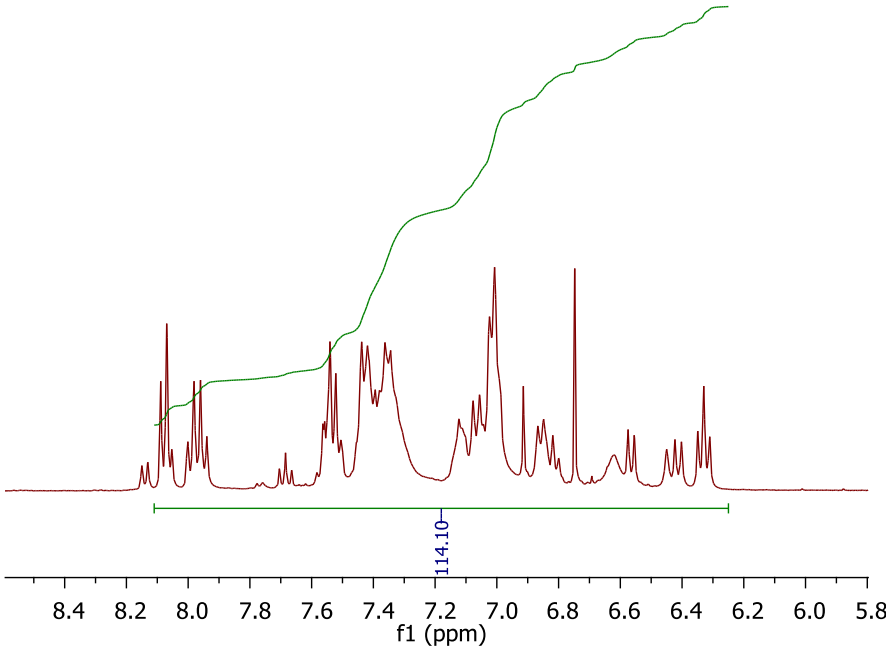

Figure 1: Aromatic region of ^{1}H-NMR spectrum for compound **3.6** $[2[Zn(C_{61}H_{42}N_9O)][(ClO_4)_2]$.

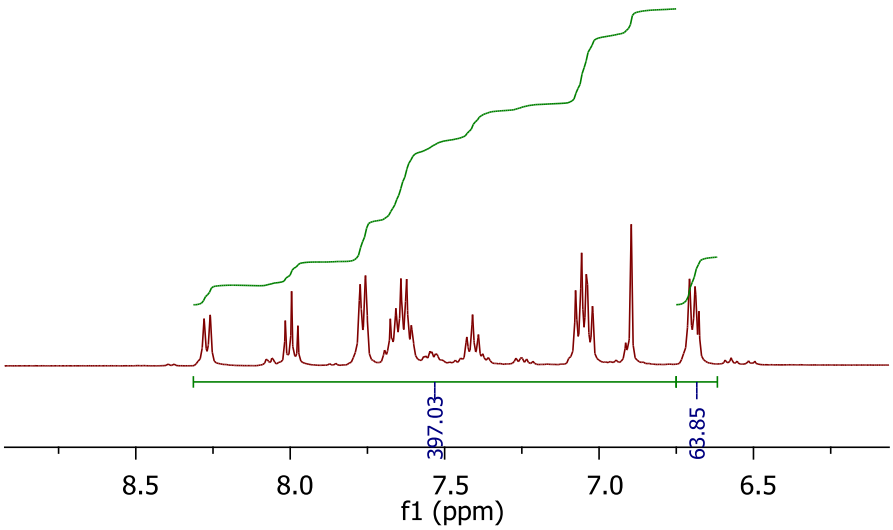

Figure 2: Aromatic region of ^{1}H-NMR spectrum for compound **3.7**. $[CdC_{61}H_{42}N_9O][2ClO_4]$.

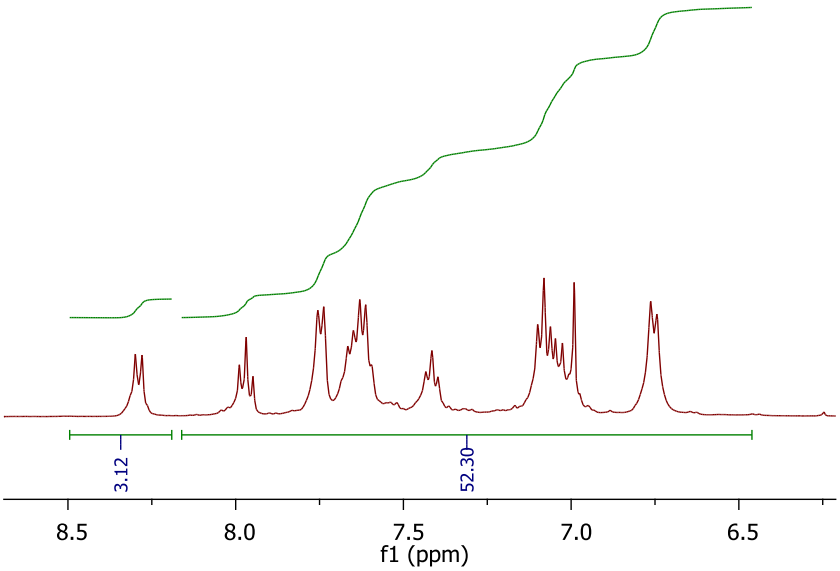

Figure 3: Aromatic region of ^{1}H-NMR spectrum for compound **3.8** $[HgC_{61}H_{42}N_9O][2ClO_4]$.

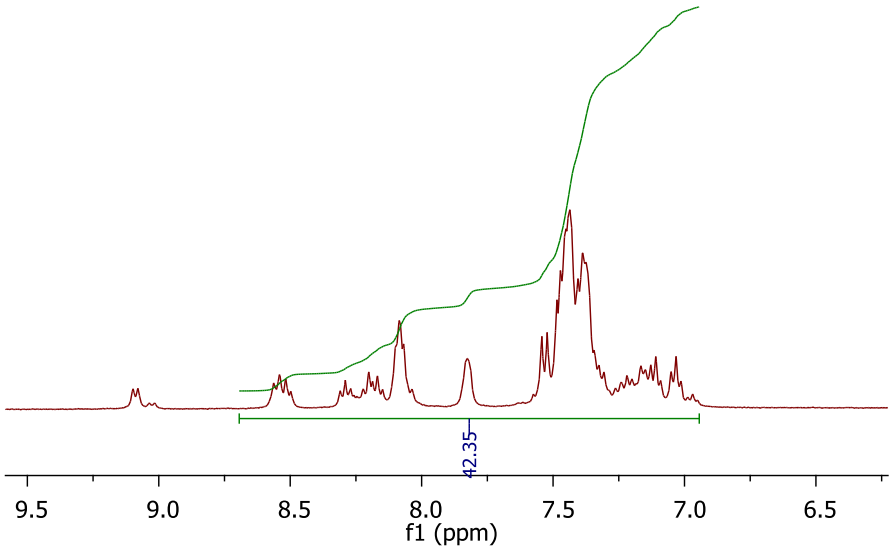

Figure 4: Aromatic region of ^{1}H-NMR spectrum for compound **3.9** $[(Re(CO)_3)_3C_{61}H_{42}N_9O]$ in DMSO. Refer to Appendix Fig. 1A (page 148).

3.25 Electronic absorption spectroscopy

The electronic absorption spectra of **L3** and complexes **3.1-3.5** and **3.9** have been measured in the solution-state with the data displayed in Table 3. All of the compounds were investigated in acetonitrile at various concentrations (ranging from 2.4 $x10^{-6}$ to 2.0 $x10^{-3}$ mol dm^{-3}). The absorption spectra of **L3** and all of its complexes possess two strong bands between 254nm and 298nm which are characteristic of intra-ligand π-π* transitions. The spectra of **L3** did not reveal any additional transitions within the range 200-1100nm.

Table 3: Electronic absorption spectral assignments

compound	π-π* transitions / λ (nm)	MLCT λ (nm)	d-d transitions / λ (nm)
L3	259(60,952), 297(60,599)	–	–
3.1 (Mn2+)	277(54,602), 295(65,523)	~406 (shoulder)(5850)	Not observed
3.2 (Fe2+)	254(43,818), 294(40,130)	~397 (shoulder)(2170)	838(217), 1044(325)
3.3 (Co2+)	284(57,535), 298(54,796),	~345 (shoulder)(2064)	510(41), 531(39), 637(8.8), 1177(8.3)
3.4 (Ni2+)	275(60,669), 296(58,159),	hidden	566(25.3), 770(16), 874(20.1), 1034(23)
3.5 (Cu2+)	277(51167), 292(48992),	hidden	746(115), 861(107).
3.9 (Re+)	275(44,642)	~373 (shoulder)(3212)	-

Compound 3.1 The Mn(II) complex **3.1** did not reveal any observable d-d transitions within the measured range. However, there is the presence of an MLCT band at approximately 24,631 cm^{-1} (406nm), the majority of which is being obscured by the intense π-π* ligand bands. As mentioned previously, the molar extinction coefficient for octahedral Mn^{2+} is very small (typically 10^{-2} – 10^{-1} $dm^3mol^{-1}cm^{-1}$) making it difficult to identify any d-d absorptions. Limits in the amount of available sample and solubility of the complex meant that it was not possible for the d-d transitions to be observed.

Compound 3.2 The absorption spectra of the Fe(II) complex **3.2** reveal two strong intra-ligand π-π* bands, one MLCT band (25,189 cm^{-1}) and only two weak d-d transitions in the visible region, occurring at 11,933 and 9579 cm^{-1}. No crystallographic data could be collected for this complex, so no initial co-ordination number could be predicted. However, the complex was found to have a magnetic moment of 4.92 BM, highlighting the four unpaired electrons within the system and confirming the high spin nature of **3.2**. In the case of a high spin octahedral co-ordination geometry there is only one spin-allowed transition corresponding to $(t_{2g})^4(e_g)^2 \rightarrow (t_{2g})^3(e_g)^3$, ($^5E_g \leftarrow {}^5T_{2g}$). However generally, this excited state is split into $^5A_1$ + $^5B_1$ (often seen as two peaks or a broad band containing a shoulder peak) resulting from either a Jahn-Teller or tetragonal distortion. This is shown clearly by the HS complex Iron(II) bis 1,10-phenanthroline dithiocyanate [Fe(o-phen)$_2$(NCS)$_2$], which produces bands at 12,050 and 9,800 cm^{-1} and compares reasonably well with peaks observed for **3.2**.[15,16]

High spin trigonal bipyramidal complexes also typically present two d-d bands at low energy (ca ≤5,820 cm^{-1} ($^5E' \leftarrow {}^5E''$) and 8,000-10,000cm^{-1}($^5A_1 \leftarrow {}^5E''$).[16] These energies are clearly far more red shifted than those observed for **3.2**, where the lower energy transition ($^5E' \leftarrow {}^5E''$) is likely to be unobservable within the experimental range used. This is confirmed by the related tripodal ligand tris(3,5-dimethyl-pyrazolyl-methyl)amine (MeTPyA) which produces peaks at 5400 and 9000 cm^{-1} in the complex [Fe(MeTPyA)Cl][BPh$_4$] and therefore suggests that a trigonal bipyramidal geometry is less likely to be occurring.[17] It must be noted however, that in the case of a,a',a''-tri-imine, 2-6, (dibenzothiazol-2-yl)-pyridine, Fe(NNN)X$_2$, two d-d bands are observed at significantly higher energy than previous examples, 8500-9600 and 15,300-17,000cm^{-1}, casting some reasonable doubt over the actual conclusion.[18]

High spin square pyramidal complexes do exist for Fe(II),[19-21] however, they are less common than its trigonal bipyramidal counterpart. These complexes again typically present two d-d bands due to the $^5A_1 \leftarrow {}^5T_2$ and $^5B_1 \leftarrow {}^5T_2$ transitions, with some observed at very low energies, *ca* ~4,500 and ~11,000 cm^{-1}.[16] Again the lowest energy band ($^5A_1 \leftarrow {}^5T_2$) is likely to occur beyond the range of the experiment, >1100nm, and is therefore unobservable, expecting only one visible peak in the spectra which is not consistent with the observed data. Unfortunately due to the lack of comparative absorption spectra for SP complexes, a satisfactory conclusion is not possible. The evidence presented suggests that the observed spectra of **3.2** best fits that of a

high spin octahedral (possibly trigonally distorted) geometry in solution. This is supported by similar comparisons with known HS O_h complexes. However both high spin SP and TBP complexes are also expected to have two d-d transitions, although in both cases, one band is expected to be at too low energy to be observed, suggesting that these geometries are less likely to be observed. Moreover, the contradicting values for the Fe(NNN)X_2 complex, and the lack of supporting data for a HS square pyramidal Fe(II) complex means that ruling these two geometries out is not possible. The amount of steric interaction between phenyl groups of complex **3.2** would suggest that a six co-ordinate structure is less favourable than a five co-ordinate. However, it is considered that in solution, acetonitrile solvent molecules could potentially be filling the empty co-ordination sites and may be allowing for a hexa-donated Fe(II) centre.

<u>Compound 3.3</u> The visible region of electronic spectra for complex **3.3** displays three observable bands with the highest energy absorption splitting into two discrete peaks, occurring at 19,608, 18,832, 15,699 and 8,496cm^{-1}(Fig. 5). The solid-state data for this complex suggests that the Co(II) centre is five co-ordinate, one acetonitrile and four ligand N-donors adopting a distorted square pyramidal geometry. It is also known that in solution the complex is high spin, μ = 4.09 BM, and therefore it could be assumed that this geometry is retained in solution. HS square pyramidal complexes of Co(II) are best regarded as analogues of tetragonally distorted six co-ordinate species with weak axial field strengths. This enables the assignment of the visible peaks as $^4E_g(P)\leftarrow{}^4E_g, {}^4A_{2g}$, $^4B_{1g}\leftarrow{}^4E_g, {}^4A_{2g}$, $^4E_g\leftarrow{}^4E_g$ and $^4A_{2g}$ in decreasing energy,[22] which correspond reasonably well with the peaks observed for Cobalt(II) 1,1,7,7-Tetraethyldiethylenetriamine [Co(Et_4dien)CL3] observed at 19,200, 18,300, 15,300 and 11,000 cm^{-1},[23] noting that this complex is also known to possess a distorted square pyramidal geometry similar to that of **3.3**. Note that the ground state is labelled as ^4E_g and $^4A_{2g}$. This is due to the $^4T_{1g}(F)$ term splitting and it is impossible to determine the true ground term based on the data collected.

The doublet feature of the spectra, seen at *ca*. 18,800-19,800 cm^{-1} is another characteristic feature of tetragonal or square pyramidal complexes corresponding to the single transition $^4E_g(P)\leftarrow{}^4E_g, {}^4A_{2g}$, and is thought to be primarily due to the admixture of spin forbidden states to doublet states.[22] Unfortunately the high energy transition $^4A_{2g}(P)\leftarrow{}^4E_g, {}^4A_{2g}$ is not observed in

the spectra for **3.3**. This transition is usually considered to be quite weak, sometimes appearing as a shoulder, and appears to be hidden under the intense intra-ligand absorptions for this compound. Similarly, the lowest energy transition ($^4B_{2g}\leftarrow{}^4E_g,{}^4A_{2g}$) can also not be seen as it is believed to be very low in energy, appearing beyond the range of the experiment. Another example is that of tetrakis(μ-benzoato-O,O'-bis(quinoline)dicobalt(II), $[Co_2(bz)_4(quin)_2]$, which again has a similar peak pattern to **3.3**, however, all of the absorptions are shifted to slightly lower energy, 18,800, 17,400, 13,500 and 8,100 cm^{-1},[24] possibly as a consequence of this complex not being as distorted as **3.3** or $Co(Et_4dien)CL3$.

Square pyramidal spectra do not vary much from those of HS trigonal bipyramidal, since both absorb in the NIR and visible regions, especially in the case of $Co(Et_4dien)CL3$ where the spectra can be assigned with respect to either geometry.[23,25] For this reason, the spectra of **3.3** could alternatively be assigned with respect to a trigonal bipyramidal as $^4E''(P)\leftarrow{}^4A_{2g}$, $^4A_2'(P)\leftarrow{}^4A_{2g}$ and $^4E'\leftarrow{}^4A_{2g}$ in decreasing energy.

Although both scenarios are considered possible it is generally known that square pyramidal systems have lower intensities (often <100 $dm^3mol^{-1}cm^{-1}$) than those of trigonal bipyramidal spectra, where **3.3** gives extinction coefficient values all <42 $dm^3mol^{-1}cm^{-1}$. On that basis it is thought most likely that, for complex **3.3**, a more square pyramidal geometry exsists in solution.

As mentioned, the spectra of **3.3** are also representative of a tetragonally distorted six co-ordinate system, which would give the same assigned transitions as for a square pyramidal geometry. This makes it difficult to unequivocally rule out either geometry based on electronic spectra alone. However, given the lack of evidence for six co-ordinate systems with **L3** (except with Zn(II)) and with its potential steric boundaries from the phenyl groups, the data continues to suggest the five co-ordinate square pyramidal system is most likely.

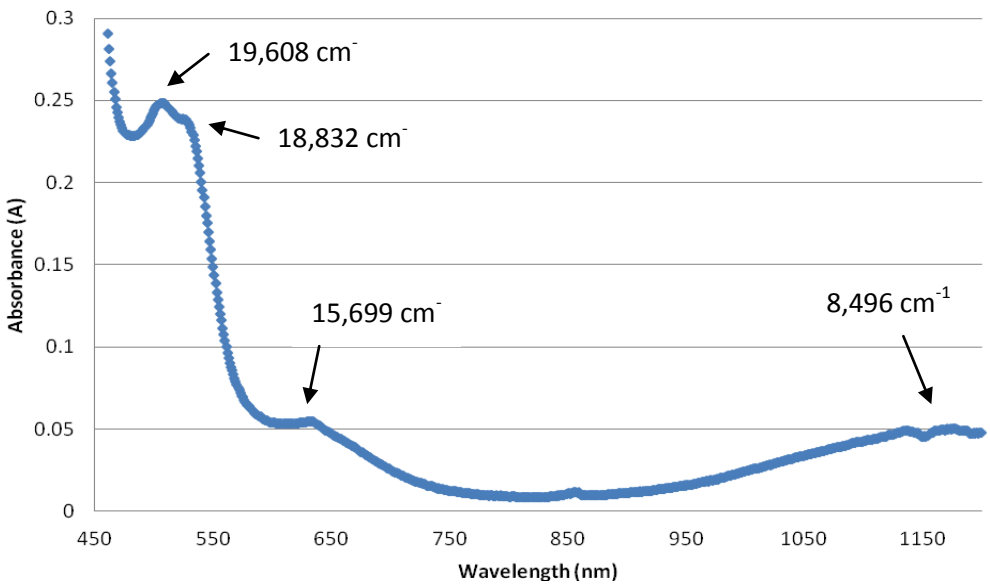

Figure 5: Visible region of the electronic spectra for the Co(II) complex **3.3**.

<u>Compound 3.4</u> There are three clear d-d transitions observed in the spectra of compound **3.4** which appear at 9,671, 11,442 and 17,986 cm^{-1}, with a possible shoulder peak observed at approximately 13,000 cm^{-1} (Fig. 6). Unfortunately there are no crystallographic data for complex **3.4** meaning that no initial predictions about the metal geometry could be made. However, nickel(II) (d^8) is known to have a strong preference for octahedral geometry which can also result in three observable bands in the visible region. From this first assumption, the three bands are assigned to an octahedral model as $^3T_{2g}\leftarrow{}^3A_{2g}$, $^3T_{1g}(F)\leftarrow{}^3A_{2g}$ and $^3T_{1g}(P)\leftarrow{}^3A_{2g}$ in increasing energy. This was applied to the appropriate d^8 O_h Tanabe Sungano diagram in which Dq was found to be 961 cm^{-1}, and *B* to be <193 cm^{-1}. The value of *B* is very much lower than is typical for octahedral Ni(II) complexes, ($[Ni(bipy)_3]CL3.7H_2O$, *B* = 672 cm^{-1} and $[Ni(2\text{-}(2\text{-pyridyl})imidazole)_2](NO_3)_2.2H_2O$, *B* = 747 cm^{-1}),[26] and therefore, does not support the presence of an octahedral centre in this Ni(II) complex. Further comparison however, revealed that the spectra for [Ni(**L2**)][ClO_4]$_2$, compound **2.6** (Chapter 2, Page 49), has a very similar absorption pattern (10,377, 12,223 and 17,917cm^{-1}) as that recorded for **3.4**. Since compound **2.6** was found to be six co-ordinate with a high degree of trigonal prismatic character, the same rationale was applied to the spectra for **3.4**. The peaks of **3.4** could now be assigned as a spin-allowed $^3E'\leftarrow{}^3A_2'$, a spin-forbidden $^1E'\leftarrow{}^3A_2'$ and a spin-allowed $^3E''(P)+{}^3A_2'(P)\leftarrow{}^3A_2'$ transition in increasing energy. Using the appropriate Sugano Tanabe diagram,[27] the spectroscopic

parameters were calculated as Dq = 1064 cm^{-1} and B = 691 cm^{-1} (Dq/B = 1.54)* , $\Delta_1 = \Delta_2 = 3\frac{1}{3}Dq$ = 3546 cm^{-1} and β = 0.64 (assuming free ion [Ni^{II}], B =1080 cm^{-1}).[28] These values now strongly agree with existing compounds rather than the alternative octahedral scenario.

There is some difficulty excepting the possible trigonal prismatic arrangement of **3.4** due to the large amount of steric influence (presented by the appending phenyl rings), as seen in the solid-state data of the analogous five co-ordinate complexes, **3.3** and **3.5** (Pages. 127 + 130). These other metals simply cannot co-ordinate more than four N-donors from the same ligand due to this steric bulk. However, if this complex has formed some sort of dimeric structure, as demonstrated by the Zn(II) complex **3.6**, then the possibility of a six co-ordinate species would be more likely.

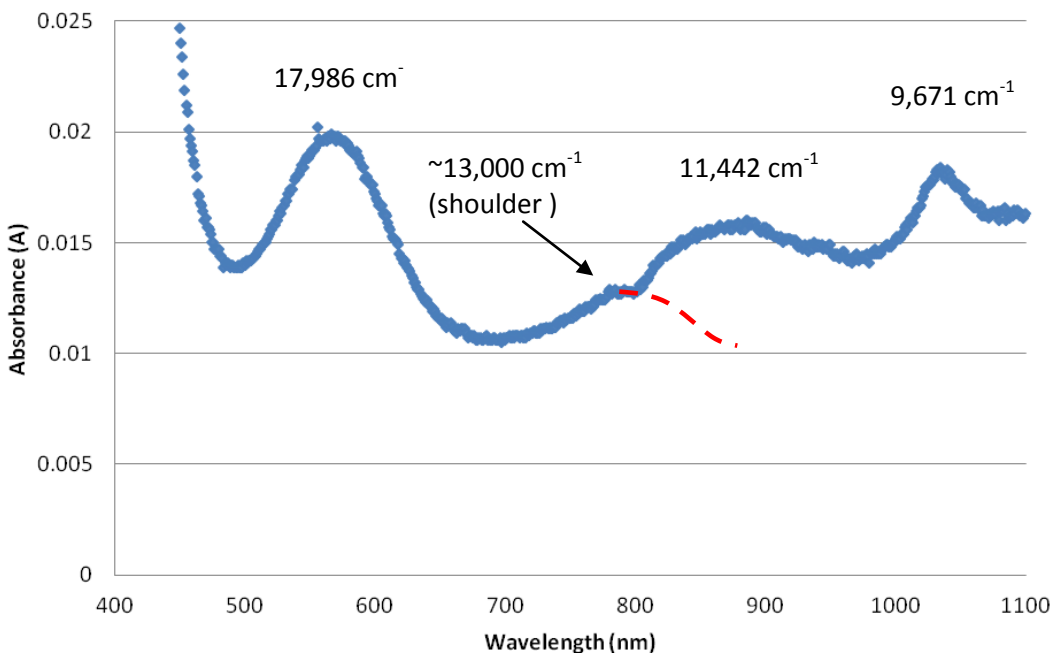

Figure 6: Visible region of the electronic absorption spectrum for **3.4** [Ni(**L3**)(CH_3CN)][ClO_4]$_2$. Showing three distinct peaks and one weak shoulder around 13,000cm^{-1}.

The spectra were compared to trigonal bipyramidal and square pyramidal scenarios. The magnetic moment of **3.4** was measured as 2.96 BM, confirming that the complex contains two unpaired electrons and is therefore high spin in these two geometries. Caimpolini has calculated energy level diagrams for such five co-ordinate Ni(II) compounds with weak field ligands (**L3** is considered weak field), allowing a comparison with **3.4** (Fig. 7).[29] If μ = 5.0 for a

TBP geometry, then five spin allowed peaks at approximately 7000, 14000, 15,000, 22,000 and 26,000 cm^{-1}, and three spin forbidden peaks at 7,000, 14,000 and 19,000cm^{-1} could be observed. The same is true for a SP geometry which should produce four spin allowed (9000, 11,000, 13,000 and 20,000cm^{-1}) and four spin forbidden transitions (7,000, 19,000, 21,000 and 22,000cm^{-1}).[30] From the two sets of approximate peak values, the SP geometry appears to fit most accurately with the observed spectra, noting that the high energy transitions of **3.4** would be obscured by the intense ligand absorptions. In Figure 6, it is clear to see how the four observed bands of **3.4** correlate well with the calculated energy levels of a square pyramidal geometry at μ = 4.9. On this basis the observed bands could be tentatively assigned as the four spin allowed transitions $^3E(1)\leftarrow{}^3B_1$, $^3B_2\leftarrow{}^3B_1$, $^3A_2\leftarrow{}^3B_1$ and $^3E(2)\leftarrow{}^3B_1$ in increasing energy (Fig. 6). This argument is strengthened by a reasonable peak comparison with those of nickel(II) 1,1,7,7-tetraethyldiethylenetriamine dichloride, [Ni(Et_4dien)CL3], also known to exist as a square pyramid, giving peaks at 10,200, 11,700, 13,100 and 18,900cm^{-1}.[31,32] In conclusion, the Ni(II) centre of complex **3.4** has shown the potential to be either a 6 co-ordinate trigonal prism or a 5 co-ordindate square pyramid through comparisons of energy level diagrams. From spectra alone, it would be unreasonable to speculate the conformation of **3.4** as being either geometry. However, due to the inevitable steric clashing created by a six co-ordinate structure, it is deemed more likely that a square pyramidal structure exists in solution, where the fifth N-donor comes from an acetonitrile solvent molecule. It is also accepted that in reality, the metal centre is unlikely to be a perfect TP or SP, and so distortion of the observed spectra will result in bands displaced slightly relative to those of ideal geometries.

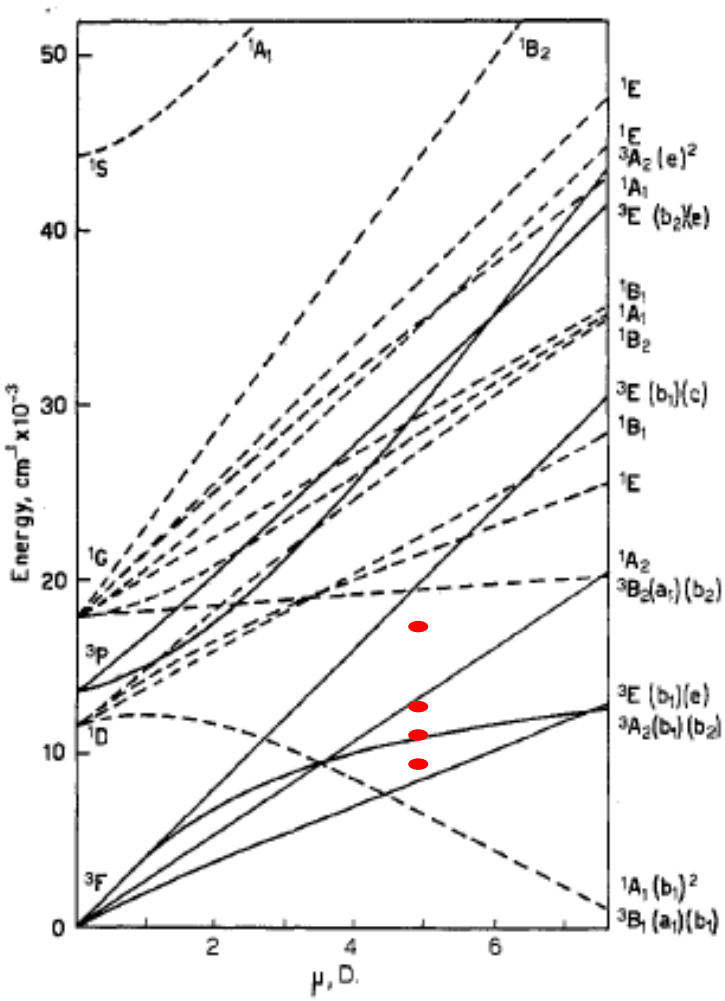

Figure 7: Energy level diagram of a Ni(II) 5-coordinate square pyramidal configuration.[29] The red dots mark the relative positions of observed d-d bands for complex **3.4** at μ = 4.9

* in theory the two lowest energy bands of a TP could swap positions which would alter the calculated spectroscopic parameters as *Dq* = 1284 cm^{-1} and *B* = 608cm^{-1} (*Dq/B* = 2.12), giving β = 0.56 and $\Delta_1 = \Delta_2 = 3⅓Dq$ = 4280 cm^{-1} assuming a perfect trigonal prism.

<u>Compound 3.5</u> The electronic absorption spectrum for complex **3.5** $[Cu^{II}(\mathbf{L3})][ClO_4]_2$ contains two broad absorptions within the visible region, located at 13,404cm^{-1} and 11,614cm^{-1} (Fig. 8). Single crystal X-ray diffraction data indicates that the metal centre is five co-ordinate with a geometry between trigonal bipyramidal and square pyramidal. The absorption pattern expected for a trigonal bipyramidal Cu(II) complex ranges from 10,500 – 14,600 cm^{-1} and consists of two bands, $^2E'' \leftarrow {}^2A_1'$ and $^2E' \leftarrow {}^2A_1'$ in decreasing energy. The higher energy transition ($^2E'' \leftarrow {}^2A_1'$) is formally forbidden and is therefore weaker in intensity than its lower energy counterpart, usually appearing as a shoulder as demonstrated by $Cu(NH_3)_2Ag(SCN)_3$.[33] A

square pyramidal absorption spectrum would lead to a similar band envelop, which typically ranges 11,400 – 15,000 cm^{-1}, however in this arrangement the expected peak intensities are reversed, with the higher energy bands generally being more intense,[32] represented well by the asymmetric band in the spectra of the square pyramidal $[CuCl_5]^{2-}$ ion,[32,34] or more appropriately, the example $(NH_4)Cu(NH_3)_5(ClO_4)_3$, which has N-donors.[35] The Latter trend, corresponding to a square pyramidal geometry, best fits the observed peak trend, along with the solid state structure which shows the fifth N-donor of the complex (Cu-N7) is bonded at a 0.3 (2) Å greater bond length compared to the 'in plane' donors; also indicative of a more square-pyramidal geometry. However, it has been stated that some intermediates of the two stereochemical forms exhibit twin peaks in the spectra.[32] This is clearly demonstrated by the twin peak absorption patterns of $[Cu(bipy)_2Cl][ClO_4]$ and $[Cu(bipy)_2(NCS)][BF_4]$, giving bands at 10,100 and 14,160 cm^{-1} and 11,170 and 14,120 cm^{-1} respectively.[36,37] These compare well with the bands observed in compound **3.5**, which occur at 11,610 and 13,400 cm^{-1}, and most notably the example $[Cu(bipy)_2(NCS)][BF_4]$, which has a peak splitting energy (2950 cm^{-1}) closest to that of **3.5** (1790 cm^{-1}). Therefore from the observed spectra and the available comparisons, it seems most reasonable to assign compound **3.5** as a distorted square-based pyramid in the solution-state.

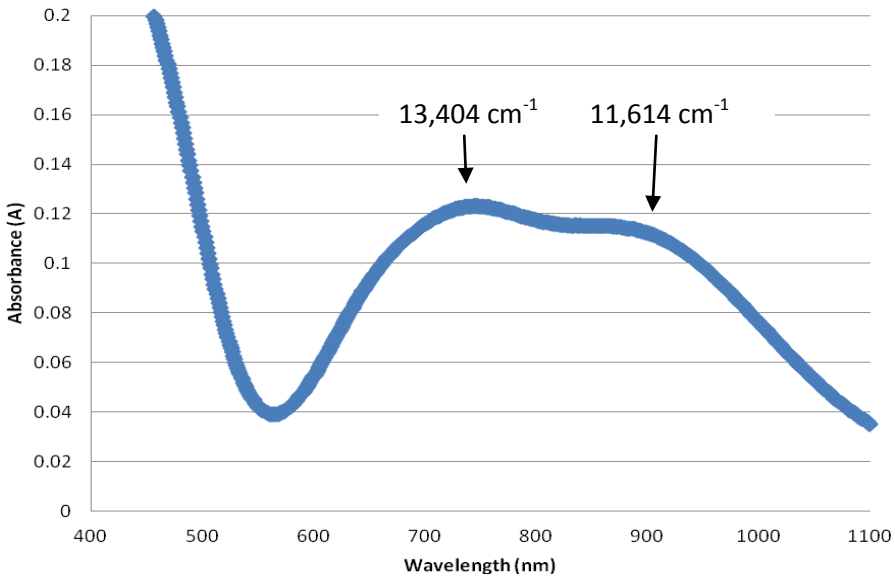

Figure 8: Visible region of the electronic absorption spectrum for **3.5** $[Cu(\mathbf{L3})(CH_3CN)][ClO_4]_2$.

Compound 3.9 The electronic absorption spectrum for the rhenium compound **3.9** revealed only one strong broad band at 36,364 cm^{-1} which is attributed to the π→π* transitions of the hetero-aromatic rings. A slight shoulder is also displayed, occurring at lower energy, which approximately resolves as a peak at 26,810cm^{-1} (373nm)(Fig. 9). This is confidently assigned as a MLCT band that is commonly seen in rhenium diimine complexes such as 3-chloromethylpyridyl bipyridine *fac*-tricarbonyl rhenium (MLCT = 380nm).[38] No crystal data could be obtained for this complex, and therefore, no solid state comparisons can be made. However, the compound was synthesised in an identical way to that of **2.12** (previous chapter with **L2**), where three equivalents of $Re(CO)_5Br$ were reacted with each ligand molecule (structure shown in Fig. 10). In evaluation the data for **2.12**, it is possible to predict that replacement of the methyl groups for phenyl substituents, would not greatly restrict the formation of a trimetallic species. Therefore, this compound is regarded as forming a similar structure to that of **2.12,** where an octahedral $Re(CO)_3Br$ unit occupies each of the three bidentate ligand arms.

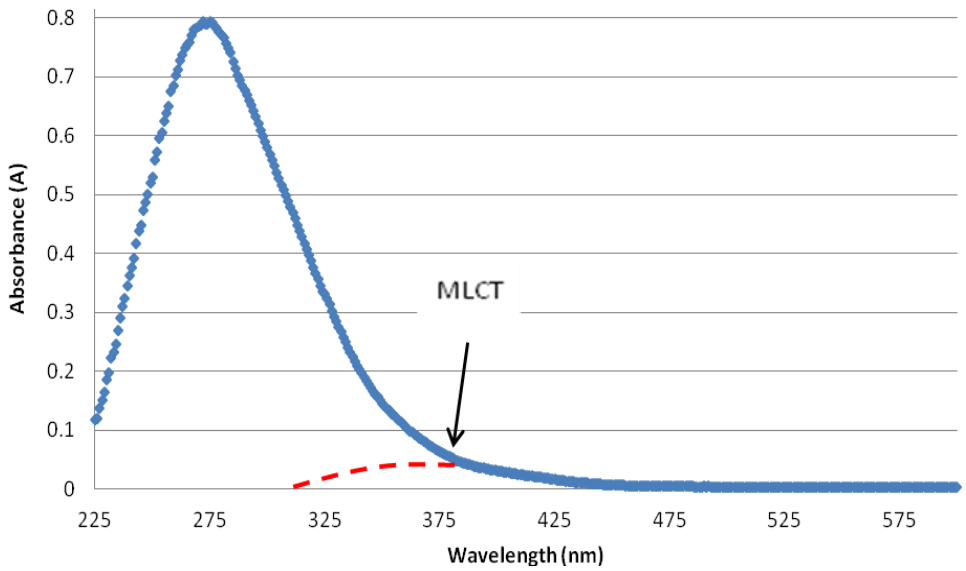

Figure 9: Visible region of the electronic absorption spectrum for **3.9** [3($ReCO_5Br$)(**L3**)].

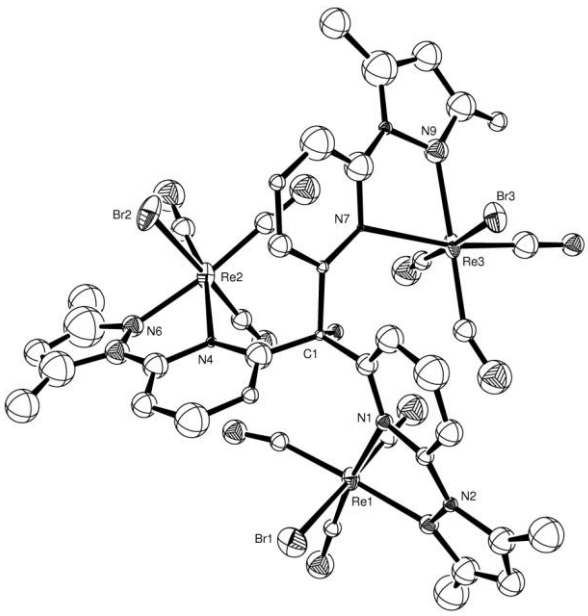

Figure 10: Crystal structure of compound **2.12,** used to compare with compound **3.9** [3($ReCO_5Br$)(**L3**)]. It can be seen how the addition of phenyl rings to pyrazole backbone would not greatly impede the potential formation of a similar structure by alternatively using **L3**.

3.26 X-ray crystallography

Crystal Structure of [Co(L3)][ClO_4]$_2$ (3.3)

The complex [Co(**L3**)][(ClO_4)$_2$] formed orangey/red coloured crystals, grown by the vapour diffusion of diethyl ether into a concentrated acetonitrile solution of the complex. The compound crystallises in the orthorhombic space group $P2_12_12_1$ (Flack parameter) and contains only one dicationic complex and two perchlorate counter ions per asymmetric unit with the overall molecular symmetry being best described as C_1. The Co^{II} centre exists in a geometry between square pyramidal and trigonal bipyramidal where four available imines (three pyridyl (N1, N4 and N7) and one pyrazolyl (N3)) are involved in coordination along with an axially donating acetonitrile (N10) solvent molecule. Coordination of one bulky pyridine-pyrazolyl arm (N1 and N3) to the Co centre prevents adequate rotation of the other two phenyl-pyrazole groups, only allowing coordination through the pyridine donors of those arms (Fig. 11). Orbital overlap with the pyrazoles is not posible due to clashing of their terminal phenyl rings, so the ligand is rendered tetra-dentate with two pendant pyrazole functions plus the acetonitrile moiety giving Co its 5-donor coordination sphere (Fig. 12).

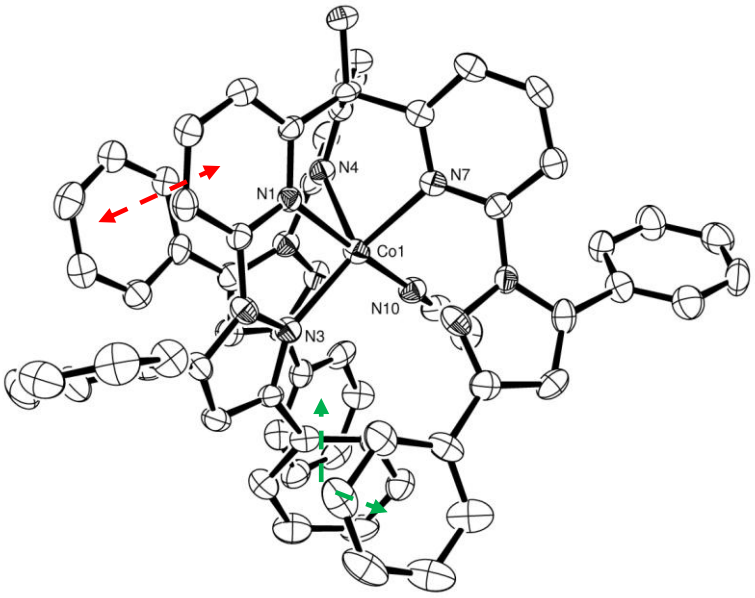

Figure 11: ORTEP Perspective view of the asymmetric unit for $[Co^{II}(\mathbf{L3})][(ClO_4)_2]$ with atom labelling. Displacement ellipsoids are shown at 50% probability with H atoms and two perchlorate counterions have been excluded for clarity. The red line showing π-stacking between a pyridyl and a phenyl moiety. The green line shows weaker potential stacking between three phenyls groups.

It is worth noting that the resulting, parallel like, stacking of the aromatic groups, within the structure (seen more clearly in Fig. 11), may aid to reduce the overall energy of the complex in the solid-state, and perhaps compensates for the lack of donation observed by the sixth ligand donor group. There is at least one example of face to face π-stacking, present in this complex, between the pyridyl ring containing N1 and the terminal phenyl function of the neighbouring ligand arm, highlighted by the red arrow (Fig. 11). The structure reveals a π-π distance of 3.887 Å and is below the accepted distance of 4 Å, typical for this type of stacking. There are also three phenyl rings showing some degree of alignment which could tentatively be assigned as weak π-stacking, represented by the green line in Figure 13. However these have larger separations (4-5 Å) and greater angles between the phenyl planes which reduce their continuity for stacking.

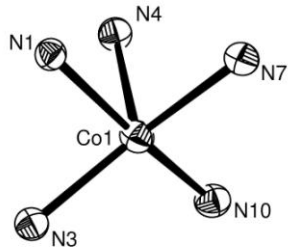

Figure 12: ORTEP Perspective view of the metal centre for **3.3** with atom labelling. Displacement ellipsoids are shown at 50% probability.

The average Co-N bond length for ligand nitrogens is 2.110(4) Å (Tab. 4), which is in keeping with the other complexes of this ligand and the analogous hexa-coordinate complex **2.5** (mean Co-N bond length 2.118(4) Å) in length. The bonds are also comparable, although slightly shorter, to that of a Co(II) bis 2,6-dipyrazol-1-ylpyridine complex which gives Co-N bond lengths of 2.126(3)Å,[39] perhaps due to more effiecient orbital overlap in the 6 co-ordinate species allowing for longer bonds. The fifth co-ordination site of Co(II) is occupied by an acetonitrile molecule, most likely due to its small linear shape, which allows it to fit amongst the large bulky groups which are restricted from binding. This gives a typical Co-N bond length of 2.042(5) Å (Tab. 4), which is closely comparable to 2.046(3) Å seen for the complex $[Co(TMPA)*(CH_3CN)]^{2+}$.[40] *TMPA = tris(2-pyridylmethyl)amine).

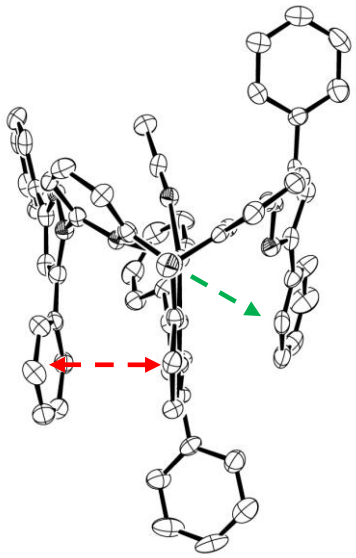

Figure 13: ORTEP Perspective view of **3.3** from above emphasizing the parallel packing of some aromatic groups.

Table 4: Selected bond Distances (Å) and Angles (°) for complex **3.3**			
Bond	Length (Å)	Bond	Length (Å)
Co1-N1	2.071 (4)	Co1-N7	2.111 (4)
Co1-N3	2.091 (4)	Co1-N10	2.042 (5)
Co1-N4	2.166 (4)		
Bonds	Angle (°)	Bonds	Angle (°)
N1-Co1-N3	77.30 (16)	N3- Co1-N7	141.26 (16)
N1-Co1 –N4	80.87 (16)	N3- Co1-N10	106.41 (16)
N1- Co1-N7	84.42 (16)	N4- Co1-N7	89.56 (15)
N1- Co1-N10	170.21 (17)	N4- Co1-N10	89.51 (17)
N3- Co1-N4	120.18 (16)	N7- Co1-N10	97.36 (17)

Crystal Structure of [Cu(L3)][ClO_4]$_2$ (3.5)

Green rhombic crystals were grown by vapour diffusion of diethyl ether into a concentrated acetonitrile solution of the complex **3.5**. This provided crystals of suitable quality to allow a crystallographic data set to be collected for the compound [Cu(**L3**)][(ClO_4)$_2$]. This molecule crystallises in the orthorhombic space group $P2_12_12_1$, with one complex and two perchlorate counter ions per asymmetric unit (Fig. 14). There is very little symmetry in the structure and the overall molecular symmetry is denoted C_1. To all intents and purposes, the Cu(II) complex **3.5** is identical to that of **3.3**, described previously, in solid state. They are both 5 co-ordinate (Fig. 15) with a geometry between square pyramidal and trigonal bipyramidal. The Cu(II) co-ordinates through the same units within the ligand (three pyridyl and one pyrazolyl) and also adopts the binding of an acetonitrile molecule, identical to **3.3** (Fig. 11). The same two aromatic rings seen in **3.3** are again involved in face-face π-stacking, indicated by the red line in Figure 14. This gives a stacking distance of 3.874 Å which is very similar to that seen for the Co(II) complex (3.887 Å)(Tab. 5).

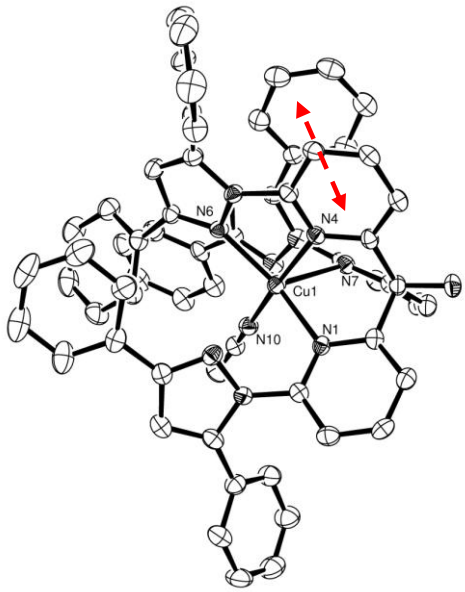

Figure 14: ORTEP Perspective view of the asymmetric unit for [Cu(**L3**)][$(ClO_4)_2$] with atom labelling. Displacement ellipsoids are shown at 50% probability with H atoms and two perchlorate counterions being excluded for clarity. The red line shows π-stacking between the pyridyl and phenyl moiety.

There are also some dissimilar features in this complex, notably amongst the co-ordinating bond lengths. The average Cu-N bond length from **L3** nitrogen donors (2.099(2) Å) does not vary much from **3.3** (mean Co-N ligand bond length is 2.110(4) Å), however, their bonds are longer when compared to the 5 co-ordinate complex $[Cu(bdmpp)(MeCN)_2]^{2+}$ (bdmpp = 2,6-bis(3,5-dimethyl-1H-pyrazol-1-yl)pyridine) where the mean ligand Cu-N bond length is 1.965(2) Å.[41] In contrast the Cu-Acetonitrile bond in **3.5** (1.967(2) Å) is significantly shorter than those in $[Cu(bdmpp)(MeCN)_2]^{2+}$ (2.108(3) Å)(Tab. 5).[41] Interestingly, the Cu-N7 bond in **3.5** is approximately 0.3 Å longer than other co-ordinating bonds in this complex. The remaining four bonds, which could be considered in a plane (Fig. 15), are on average 0.1 Å shorter when compared to the same bonds in the Co(II) example. This gives an image of compression around the plane and elongation along the z-axis (Cu-N7 bond). This is characteristic of a Jahn-Teller distortion which is expected in the co-ordination of d^9 copper. Interestingly, the elongated Cu-N7 bond does not appear to affect the π-stacking distance measured, which is in fact smaller than that measured in **3.3** although this difference in negligible. Also it is notable that the Cu1—N3 distance is 2.815(2) Å (of the free pyrazole in Figure 14) and could possibly be binding with the metal centre. However, this would alter the geometry of the Copper from square pyramidal to a distorted octahedral which seems unlikely when considering the two 'z-axis' donors. These

trans-bonds would not be linear (free prazole not point directly at metal centre) with respect to each other, and also, their lengths would also vary by 0.5Å, decreasing the overall symmetry.

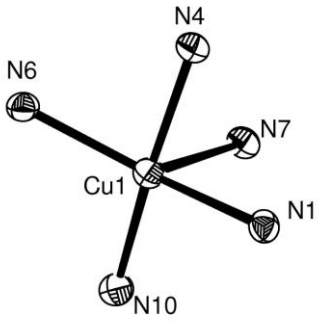

Figure 15: ORTEP Perspective view of the Cu(II) co-ordination sphere for **3.5** with atom labelling. Displacement ellipsoids are shown at 50% probability.

Table 5: Selected bond Distances (Å) and Angles (°) for complex **3.5**			
Bond	Length (Å)	Bond	Length (Å)
Cu1-N1	2.071 (2)	Cu1-N7	2.331 (2)
Cu1-N4	1.955 (2)	Cu1-N10	1.967 (2)
Cu1-N6	2.037 (2)		
Bonds	Angle (°)	Bonds	Angle (°)
N1-Cu1-N4	87.38 (9)	N4- Cu1-N7	80.13 (8)
N1-Cu1 -N6	147.28 (8)	N4- Cu1-N10	167.25 (9)
N1- Cu1-N7	89.57 (8)	N6- Cu1-N7	118.10 (8)
N1- Cu1-N10	95.90 (9)	N6- Cu1-N10	102.00 (9)
N4- Cu1-N6	81.16 (9)	N7- Cu1-N10	87.57 (9)

Crystal Structure of $[Zn_2(L3)_2][(ClO_4)_2]$(3.6)

Crystals suitable for X-ray crystallographic studies of the complex $[Zn_2(\mathbf{L3})_2][ClO_4]_2$ were obtained through vapour diffusion of diethyl ether into a concentrated acetonitrile solution of the complex, yielding colourless needle-like crystals. The complex crystallised in a P-1 Triclinic space group with the asymmetric unit containing two dimeric complexes and two perchlorate counter-anions (bond-lengths and angles are provided for each dimer in Tables 6a and 6b). The overall molecular symmetry of the compound is close to C_2 with each discrete complex containing two ligands and two Zn(II) centres. All the metal centres have virtually identical

binding *via* two bridging OH groups and two bidentate pyridyl-pyrazole donors, leaving a third un-coordinated arm on both ligands (see Fig. 16).

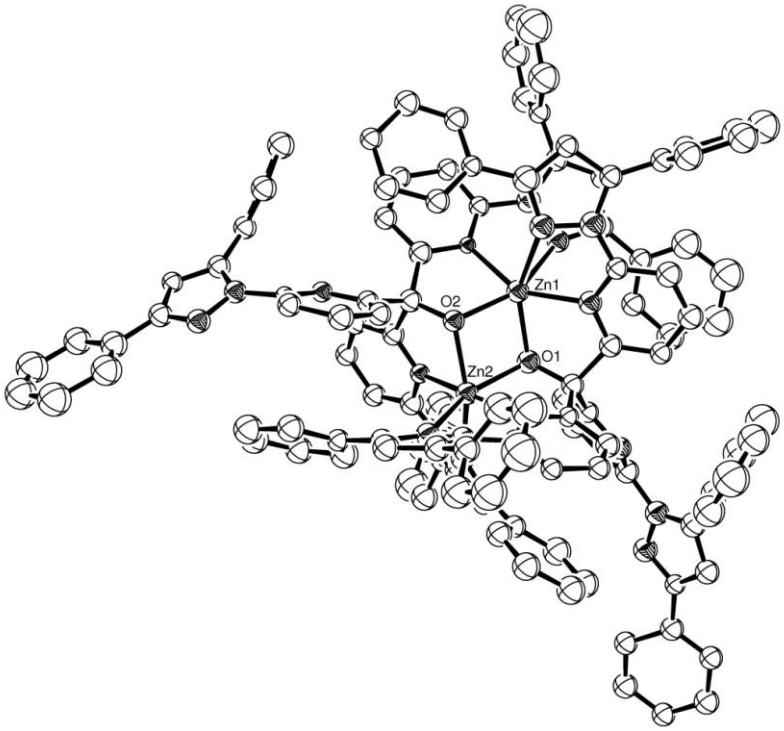

Figure 16: ORTEP Perspective view of the asymmetric unit for $[Zn_2(\mathbf{L3})_2][(ClO_4)_2]$ with atom labelling. Displacement ellipsoids are shown at 50% probability with H atoms and two perchlorate counterions have been excluded for clarity.

As a result, unlike the previous two monomeric examples, the zinc prefers to form a dimer utilising bridging oxygens from the apical hydroxyl function of each ligand (Fig. 17), giving an average Zn-µO bond length of 2.055(18) Å, where the oxygens are equidistant from each Zn(II) ion. This is a feature seen in many zinc complexes within literature; for example, the Zn(II) dimeric complex with the compound Bis(2,2'-bipridin-6'-yl)(methoxy)methanol,[42] which creates a similar bridging oxygen dimer to **3.6**, but instead has two co-ordinating bipyridine functions around each metal centre (with an average Zn-µO bond length of 2.103(2) Å). Each zinc centre of **3.6** binds with two separate ligand arms that originate from different parent ligands, perhaps to keep steric interactions at a minimum. As a result, the pyridyl N-donors present much shorter bond lengths (mean Zn-N_{pyr} bond length is 2.05(2) Å, Table 6a and 6b) compared to the Zn-N bonds from the pyrazole moieties (mean Zn-N_{pyz} bond length is 2.337(19) Å, Table 6a,b). This is also noted in, and compares well with, the zinc bis(2,2'-bipridin-6'-yl)(methoxy)methanol

complex, which gives Zn-N_{pyr} and Zn-N_{pyz} bond lengths as 2.060(2) and 2.268(2) Å respectively. The different Zn-N bond lengths are probably due to the sp^3 hybridized carbon atoms (attached to the OH groups) restraining its adjacent pyridine rings and preventing them from adopting larger bond distances. The average Zn-O-Zn angle of **3.6** is 97.3(8)°, whilst the average O-Zn-O angle is 81.5(7)°, which creates a diamond core, is also mentioned in literature, and compares well with the known Zinc dimer which has angles of 95.93(7)° and 84.07(7)° respectively.[42]

This dimeric feature could be explained by a combination of two things. The Zn(II) being slightly harder than the previous metals (Co^{II}, Cu^{II}), hence preferentially binding to oxygen, and the reduced geometric constraints with d^{10} metals which allows more rotation in the ligand so it can envelop the metal centre more efficiently to allow space for coordination of a sixth donor, resulting in a hexadentate co-ordination sphere. This is unlike the 5 co-ordinate Co(II) and Cu(II) complexes seen previous using the same ligand (compounds **3.3** and **3.5** respectively). Although both metal centres in each dimer are 6 co-ordinate, they do not share the same geometry. One is a slightly distorted octahedral (Zn2 and Zn3) with its neighbour possessing a much more distorted arrangement (Fig. 17). This is attributed to ligand strain formed from having two ligands and metals within close proximity, preventing one Zn centre from having a more ideal geometry.

Reports of bonding between two Zn centres in a dimer is present in literature, however, to consider these as bonding interactions, the Zn-Zn distances would have be less than 2.5 Å.[43] This is a lot shorter than the observed average Zn-Zn distance in this complex (3.11 Å), and therefore removes this as a possible consideration, despite it correlating well with the Zn-Zn distances in the Bis(2,2'-bipridin-6'-yl)(methoxy)methanol complex discussed previously (Zn-Zn distance 3.1241(8) Å).

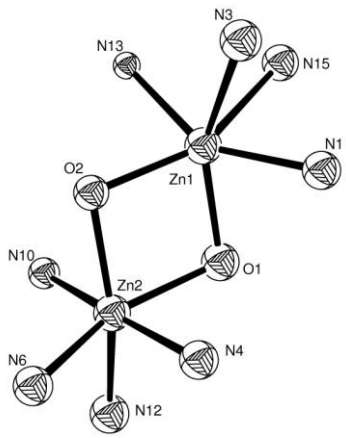

Figure 17: ORTEP Perspective view of the Zn(II) dimer co-ordination sphere for **3.6** with atom labelling. Displacement ellipsoids are shown at 50% probability.

Table 6a: Selected bond Distances (Å) and Angles (°) for the first dimer of **3.6** in the asymmetric unit

Bond	Length (Å)	Bond	Length (Å)
Zn1-N1	2.07 (2)	Zn2-N4	2.05 (2)
Zn1-N3	2.32 (2)	Zn2-N6	2.28 (2)
Zn1-N13	2.050 (18)	Zn2-N10	2.021(19)
Zn1-N15	2.46 (2)	Zn2-N12	2.29 (2)
Zn1-O1	2.053 (18)	Zn2-O1	2.079 (18)
Zn1-O2	2.027 (17)	Zn2-O2	2.050 (17)
Bonds	**Angle (°)**	**Bonds**	**Angle (°)**
N1- Zn1-N3	71.2 (9)	N4- Zn2-N6	75.6 (9)
N1- Zn1 –N13	147.6 (8)	N4- Zn2 –N10	171.3 (10)
N1- Zn1 –N15	80.8 (8)	N4- Zn2 –N12	100.0 (9)
N1- Zn1 –O1	78.5 (8)	N4- Zn2 –O1	76.2 (8)
N1- Zn1 –O2	131.2 (8)	N4- Zn2 –O2	106.9 (8)
N3- Zn1 -N13	88.1 (8)	N6- Zn2 –N10	111.2 (8)
N3- Zn1 –N15	81.8 (8)	N6- Zn2 –N12	93.4 (8)
N3- Zn1 –O1	147.2 (7)	N6- Zn2 –O1	151.3 (7)
N3- Zn1 –O2	109.3 (8)	N6- Zn2 –O2	102.7 (8)
N13- Zn1 –N15	71.6 (8)	N10- Zn2 –N12	74.7 (8)
N13- Zn1 –O1	124.7 (7)	N10- Zn2 –O1	97.3 (8)
N13- Zn1 –O2	78.5 (7)	N10- Zn2 –O2	77.4 (7)
N15- Zn1 –O1	105.9 (8)	N12- Zn2 –O1	96.8 (8)
N15- Zn1 –O2	147.8(7)	N12- Zn2 –O2	151.3 (7)
O1- Zn1 –O2	81.4 (7)	O1- Zn2 –O2	80.2 (7)

Table 6b: Continued: Selected bond Distances (Å) and Angles (°) for the second dimer of **3.6** in the asymmetric unit

Bond	Length (Å)	Bond	Length (Å)
Zn3-N22	2.03 (2)	Zn4-N19	2.10 (2)
Zn3-N24	2.29 (2)	Zn4-N21	2.39 (2)
Zn3-N28	2.05 (2)	Zn4-N34	2.03 (2)
Zn3-N30	2.23 (2)	Zn4-N36	2.437 (19)
Zn3-O3	2.057 (16)	Zn4-O3	2.066 (19)
Zn3-O4	2.105 (19)	Zn4-O4	2.005 (16)
Bonds	**Angle (°)**	**Bonds**	**Angle (°)**
N22- Zn3-N24	75.6 (8)	N19- Zn4-N21	71.4 (8)
N22- Zn3 –N28	174.2 (10)	N19- Zn4 –N34	146.8 (8)
N22- Zn3 –N30	109.0 (9)	N19- Zn4 –N36	84.4 (7)
N22- Zn3 –O3	78.0 (7)	N19- Zn4 –O3	79.2 (8)
N22- Zn3 –O4	98.8 (8)	N19- Zn4 –O4	129.7 (7)
N24- Zn3 –N28	100.9 (8)	N21- Zn4 –N34	83.4 (8)
N24- Zn3 –N30	93.7 (8)	N21- Zn4 –N36	83.2 (7)
N24- Zn3 –O3	152.9 (7)	N21- Zn4 –O3	149.0 (7)
N24- Zn3 –O4	97.2 (8)	N21- Zn4 –O4	107.9 (7)
N28- Zn3 –N30	75.6 (9)	N34- Zn4 –N36	71.2 (8)
N28- Zn3 –O3	104.9 (7)	N34- Zn4 –O3	127.6 (8)
N28- Zn3 –O4	76.9 (8)	N34- Zn4 –O4	78.1 (8)
N30- Zn3 –O3	100.4 (8)	N36- Zn4 –O3	103.9 (7)
N30- Zn3 –O4	151.8 (7)	N36- Zn4 –O4	145.9 (7)
O3- Zn3–O4	81.1 (7)	O3- Zn4 –O4	83.3 (7)

Crystal parameters and details of the data collection, solution and refinement for complexes **3.3**, **3.5** and **3.6** are presented in Table 7.

Table 7: Crystallographic data for complexes of Tris(6 - 2,4-diphenylpyrazolpyrid-2-yl)menthanol (**L3**).			
Compound	**3.3**	**3.5**	**3.6**
Chemical formula	$[(CoC_{63}H_{46}N_{10}O)][2ClO_4]$ $.CH_3CN$	$[(CuC_{63}H_{46}N_{10}O)][2ClO_4]$ $.CH_3CN$	$[ZnC_{61}H_{43}N_9O)][2ClO_4]$
Mr, g/mol	1257.98	1262.59	1182.31
Crystal system	orthorhombic	orthorhombic	Triclinic
Space Group	$P2_12_12_1$	$P2_12_12_1$	P-1
T (k)	293 (2)	150 (2)	293 (2)
a, Å	11.5506 (5)	11.52650 (10)	19.9646 (7)
b, Å	19.9429 (8)	19.9566 (2)	22.1018 (10)
c, Å	24.7128 (5)	24.7278 (4)	31.3506 (15)
α, deg	90.00	90.00	96.848 (2)
β, deg	90.00	90.00	99.524 (3)
γ, deg	90.00	90.00	104.283 (3)
V, $Å^3$	5692.7 (4)	5688.13 (12)	13034.4 (10)
Z	4	4	2
D_c g/cm^3	1.468	1.474	0.301
μ(Mo K α), mm^{-1}	0.467	0.550	0.129
Observed Reflections	8205	15717	24946
Reflections collected	22450	15717	39533
R_{int}	0.0813	0.001	0.1614
R_I [I>2σ(I)]	0.0555	0.0531	0.2629
wR_2 (all data)	0.1288	0.1242	0.5906

3.27 Magnetic moments

The magnetic moments of complexes **3.1**-**3.5** were determined in a d_3-acetonitrile solution at room temperature *via* the Evans' NMR method, at a typical concentration of 8.5×10^{-3}moldm^{-3}. Assignment of the various ^{1}H-NMR data was not possible with these complexes due to their paramagnetic nature, giving broad and structureless spectra. The observed magnetic moments calculated for the compounds are displayed in Table 8, along with theoretical magnetic moments and their respective ground terms. The theoretical values can be calculated using the equation: $\mu = \sqrt{[n(n+2)]}$ where n is the expected number of unpaired electrons. Comparison of these theoretical values with observed values can provide reasonable evidence for the electronic configuration of the co-ordinated metal ions.

Table 8: Showing predicted and calculated magnetic moments for all non-d^{10} metals and their respective spin state.

Complex	Number of Unpaired electrons	Ground term	Theoretical moment	Observed Magnetic moment μ_B	High spin/low spin
3.1 [Mn(II)]	1 or 5	^{6}S	1.73 or 5.91	5.91	HS
3.2 [Fe(II)]	0 or 4	^{5}D	0 or 4.89	4.92	HS
3.3 [Co(II)]	1 or 3	^{4}F	1.73 or 3.87	4.09	HS
3.4 [Ni(II)]	2	^{3}F	2.83	2.96	n/a
3.5 [Cu(II)]	1	^{2}D	1.73	1.22	n/a

The data displayed in Table 8 show how 3d transition metals, when possible, favour a high spin state arrangement when co-ordinated with **L3**. This is good evidence for the ligand having a small energy gap in the crystal field splitting pattern and is therefore labelled as weak field in nature (π-donating). This is to be expected as similar results were seen for the analogous ligand **L2** (Chapter 2 Page. 83), which also has a weak field effect. The steric bulk of **L3**, namely due to phenyl rings, is thought to restrict the ligand arms and reduce the number of available N-donors to a single metal centre. This is suspected to create a poorer orbital overlap between the co-ordinative bonds and hence reducing the complex field strength. Unusually the magnetic moment collected for **3.5** was much lower than expected from theoretical calculations. The value of 1.22BM still provides strong evidence for the presence of a d^9 Cu(II) centre, however, the low value is most likely attributed to human error or impure sample.

3.28 Conclusion

Reported in this chapter is the synthesis, complexation and characterisation of a novel tripodal ligand, tris(6 - 2,4-diphenylpyrazolpyrid-2-yl)methanol (**L3**). Successful complexations involved 3d transitions metals Zn(II)→Mn(II) and Re(I) with all producing high spin state compounds where possible. **L3** is structurally analogous to the ligand **L2**, the only difference being the replacement of the methyl substituents with phenyl groups on each pyrazole back bone. **L3** has six N-donors and one potential O-donor similar to **L2**, however the co-ordination of these two ligands with 3d transition metals are very different. X-ray crystal structure data has shown, in some cases (complexes **3.3** and **3.5**), that **L3** preferably forms five co-ordinate structures compared with the unanimous six co-ordinate species formed by complexation of **L2**. Interestingly, in the cases of **3.3** and **3.5**, only four of the co-ordination sites are occupied by the ligand donors with the fifth coming from an acetonitrile molecule. This gives these two complexes an intermediate geometry between square pyramidal and trigonal bipyramidal. This is supported by UV-Vis data that suggests complex **3.5** retains a predominantly square pyramidal geometry even in solution. This is thought to be attributed to the large phenyl rings interacting strongly when the ligand arms are pulled inwards upon complexation. This prevents the neat arrangement of donors, like those seen for complexes of **L2**, around the metal centre, limiting **L3** as a tetradentate chelate. A similar conclusion is thought most likely for the Ni(II) complex **3.4**, again based on evidence from the electronic absorption spectra, suggesting a more square pyramidal arrangement in solution. As for the Fe(II) complex **3.2**, limited data restricts the determination of the favoured structure. Mass spectroscopy confirmed a monomeric species was present with the UV-Vis data tentatively describing **3.2** as an octahedral or trigonally distorted six co-ordinate centre. If this determination is accurate, then the six co-ordinate structure is perhaps possible, due to Fe(II) having a slightly larger ionic radius (78pm) than previous 2+ metals, which may allow an extra ligand donor or even acetonitrile to bind with iron. Unfortunately little conclusive data could be collected about the Mn(II) complex, **3.1**. As anticipated the UV-Vis data revealed no observable d-d transitions, with the mass spectrum giving the only evidence of complexation, which appears to be monomeric. A similar story arises for the Cd(II) and Hg(II) complexes (**3.7** and **3.8**), which appear to be monomeric, based on mass spectrometry, and the high symmetry, observed from ^{1}H-NMR

data. The symmetrical nature of these two complexes, is reminiscent to the complexes of **L2** and may again be attributed to the large size of these ions, pushing out the ligand arms and perhaps allowing all three to be involved in co-ordination. However more data would be needed to confirm such postulates. The most intriguing complex is that of Zn(II) (compound **3.6**), which was confirmed as a dimer by crystallographic information and NMR spectroscopy. Both zinc centres are found to be six co-ordinate, utilising four N-donors and two bridging oxygen donors, unlike any of the other complexes. The ^{1}H-NMR spectra shows a much more complicated and unsymmetrical peak pattern compared with those of **3.7** and **3.8**. This correlates well with the crystal data which reveals how, for each ligand, two ligand arms co-ordinate whilst the third remains pendent, also suggesting that this structure is stable in solid and solution state. It must also be noted that the two Zn(II) centres, although both six c-ordinate, possess slightly different geometries with Zn(1) being more distorted form a octahedron. This is suggested to be a result of trying to constrain two ligands around two metal centres which matters least to Zn(II) due to its d^{10} nature. Interestingly, most evidence for the Cu(II) complex, **3.5**, suggests it has a five co-ordinate structure, with exception of its mass spectrum which shows the existence of a monomeric and dimeric species, suggesting that a dimeric compound, similar to that of the Zn(II) complex **3.6,** may also be possible under the right conditions.

Lastly, the yellow Re(I) complex **3.9**, was prepared in a 3:1 metal ligand ratio in the same way as for compound **2.12** (Chapter 2, Page 38). The starting material $Re(CO)_5Br$ is well known for its binding affinity to bidentate bipy-type ligands which lead to the trimetallic species seen in the crystal structure (Fig. 10). All three rhenium centres are strongly octahedral as anticipated, with the ^{1}H-NMR also showing a single symmetrical species which also suggests that **3.9** is stable in the solid and solution state.

3.3 Experimental

Tris(6–(3,5-diphenylpyrazol-1-yl)pyrid-2-yl)methanol (**L3**):

Tris(6-hydrazinylpyridin-2-yl)methanol (**S3**) (1.1g, $3.12x10^{-3}$mol) was stirred into an ethanol:methanol (2:1) solvent (45ml) and heated at roughly 60°C until all the solid had dissolved. 1,3-diphenyl-1,3-propanedione (2.23g, $9.96x10^{-3}$mol) 3.2eq was then added to the hot solution, flushed with N_2, and then refluxed for a minimum of 20h. The mixture was allowed to cool to RT producing pure product as an off white precipitate. The solid was filtered *in vacuo* and the filtrate reduced to dryness. The dried filtrate was then triturated with ethanol (5ml) to produce more off white product. The products were combined to give **L3** in reasonable yield and high purity. (876mg, 31%).

^{1}H-NMR (CD_3CN; 400MHz): δ_H 7.95(6H, d, J= 5.2Hz, CH), 7.67(6H, m, CH), 7.49(6H, t, J= 7.7Hz, CH), 7.40(3H, d, J= 7.4Hz, CH), 7.22(6H, d, J= 7.0Hz, CH), 7.13(9H, m, CH), 6.89(3H, s, CH), 6.69(3H, d, J= 7.4Hz, CH). ^{13}C-NMR ($CDCl_3$; 400MHz): δ_C 160.00(C), 152.20(C), 150.31(C), 145.06(C), 138.63(CH), 132.85(C), 131.65(C), 128.72(CH), 128.42(CH), 128.27(CH), 128.09(CH), 127.92(CH), 125.92(CH), 121.43(CH), 115.68(CH), 106.96(CH), 80.46(C). FT-IR (KBr/cm^{-1}) ν = 3359br+m, 3059m, 1593s, 1576s, 1551m, 1486s, 1453s, 1406m, 1362s, 1307m, 1284m, 1215m, 1187m, 1153m, 1118w, 1064m, 1027m, 1003m, 993m, 955s, 914w, 814s, 761s, 694s, 616w, 502w. HRMS (ES-MS) *m/z* calcd. 940.3488 ; exp. 940.3495 $[C_{61}H_{43}N_9ONa]^+$, (80%), calcd. 956.3228 ; exp. 956.3231 $[C_{61}H_{43}N_9OK]^+$, (100%). UV-Vis [λ_{max}, nm, (εM, $M^{-1}cm^{-1}$)] in CH_2CL3 : 258.9(60952), 296.9(60599). Found: C 76.19; H 4.41; N 13.02 (%) $C_{61}H_{43}N_9O.2.5H_2O$ Requires: C 76.06; H 5.03; N 13.10 (%).

General Complex synthesis

The ligand **L3** (1 equivalent, generally about 0.1 mmol) was dissolved in a minimum amount of acetonitrile (typically 2-3ml) with stirring and requiring heating to 60°C to remain in solution. The required metal perchlorate salt (1 equivalent) was then also dissolved in acetonitrile (2ml) and added slowly to the stirred solution of **L3**. The resulting complexes were more soluble than the parent ligand allowing the solutions to be stirred at room temperature for 3 hours. After stirring the solutions were filtered through celite and concentrated (typically to 2-3ml) before

purification. Recyrstallisation involved diffusion of diethyl ether or Petrol ether into a concentrated acetonitrile solution of the complex.

Note: perchlorate metal salts are potentially explosive, and care should be taken when handling these solids (use a plastic spatula).

Manganese(II) Tris(6 - 2,4-diphenylpyrazolpyrid-2-yl)methanol (**3.1**):

L3 (49mg, 0.053mmol) was added to $Mn(ClO_4)_2.6H_2O$ (19mg, 0.053mmol). Crystallisation yielded pale wool like crystals (43%, 27mg). HRMS (ES-MS) *m/z* calcd. 486.1486; Exp. 486.7234, $[MnC_{61}H_{43}N_9O]^{2+}$, (100%). calcd. 1071.2456; exp. 1071.2437, $\{[MnC_{61}H_{43}N_9O][ClO_4]\}^+$, (50%). calcd. 971.2893; exp. 971.7734 $[MnC_{61}H_{42}N_9O]^+$, (50%). FT-IR (KBr/cm^{-1}) ν = 3390br+s, 3058m, 2924m, 2852w, 1715w, 1604s, 1575s, 1486s, 1452s, 1361s, 1307m, 1276m, 1218m, 1147s, 1089s, 993m, 955m, 916w, 815m, 763s, 695s, 625s. UV-Vis [λ_{max}, nm, (εM, M^{-1}cm^{-1})] in CH_3CN: 277(54602), 295(65523). Magnetic moment (Evans method, 293K, Acetonitrile): μ_{eff} = 5.91μ_B. Found: C 56.96; H 4.55; N 9.65 (%) $MnC_{61}H_{43}N_9O(ClO_4)_2.7H_2O$ Requires: C 56.43; H 4.43; N 9.72 (%).

Iron(II) Tris(6 - 2,4-diphenylpyrazolpyrid-2-yl)methanol (**3.2**):

L3 (57mg, 0.062mmol) was added to $Fe(ClO_4)_2.6H_2O$ (23mg, 0.062mmol). Crystallisation yielded dark orange powder (77%, 56mg). HRMS (ES-MS) *m/z* calcd. 486.6469; exp. 486.6507, $[FeC_{61}H_{43}N_9O]^{2+}$, (85%), calcd. 1072.2425; exp. 1072.2462 $\{[FeC_{61}H_{43}N_9O][ClO_4]\}^+$, (10%). FT-IR (KBr/cm^{-1}) ν = 3434br+s, 3126m, 3051m, 2923s, 2851m, 1606m, 1573s, 1485s, 1453s, 1360s, 1309w, 1223w, 1091br+s, 1027m, 955w, 818m, 764s, 696s, 625s. UV-Vis [λ_{max}, nm, (εM, M^{-1}cm^{-1})] in CH_3CN: 265(43818), 294(40130), 397(2170). Magnetic moment (Evans method, 293K, Acetonitrile): μ_{eff} = 4.92μ_B.

Cobalt(II) Tris(6 - 2,4-diphenylpyrazolpyrid-2-yl)methanol (**3.3**):

L3 (48mg, 0.052mmol) was added to $Co(ClO_4)_2.6H_2O$ (19mg, 0.052mmol). Crystallisation yielded pale orangey/red crystals (34%, 21mg). HRMS (ES-MS) *m/z* calcd. 488.1461; exp. 488.1275, $[CoC_{61}H_{43}N_9O]^{2+}$, (100%), calcd. 1075.2408; exp. 1075.2384, $\{[CoC_{61}H_{43}N_9O][ClO_4]\}^+$, (25%). FT-IR (KBr/cm^{-1}) ν = 3434br+m, 3122m, 3061m, 1610m, 1586m, 1559m, 1487s, 1472s, 1409m, 1359s, 1303w, 1282w, 1223w, 1183w, 1091br+s, 1029m, 960m, 926w, 808m, 764s, 696s, 622s.

UV-Vis [λ_{max}, nm, (εM, $M^{-1}cm^{-1}$)] in $CHCl_3/CH_3CN$(50/50): 284(57,535), 298(54,796), 345(2064), 510(41), 531(39), 637(8.8), 1177(8.3). Magnetic moment (Evans method, 293K, Acetonitrile): μ_{eff} = 4.09μ_B. Found: C 58.52; H 3.86; N 10.17 (%) $CoC_{61}H_{43}N_9O(ClO_4)_2.4H_2O$ Requires: C 58.69; H 4.12; N 10.10 (%).

Ni(II) Tris(6 - 2,4-diphenylpyrazolpyrid-2-yl)methanol (**3.4**):

L3 (51mg, 0.056mmol) was added to $Ni(ClO_4)_2.6H_2O$ (20mg, 0.056mmol). Crystallisation yielded pale green non-crystalline solid (64%, 42mg). HRMS (ES-MS) *m/z* calcd. 487.6472; exp. 487.6495, $[NiC_{61}H_{43}N_9O]^{2+}$, (100%). calcd. 1074.2429; exp. 1074.2448, $\{[NiC_{61}H_{43}N_9O][ClO_4]\}^+$, (12%). FT-IR (KBr/$cm^{-1}$) ν = 3376br+m, 3116m, 3061m, 2978w, 1611s, 1586s, 1559s, 1516w, 1465br+s, 1409s, 1361s, 1305m, 1282m, 1223m, 1183m, 1089br+s, 1001s, 960m, 926m, 808s, 761s, 695s, 621s. UV-Vis [λ_{max}, nm, (εM, $M^{-1}cm^{-1}$)] in CH_3CN: 275(60669), 296(58159), 566(25.3), 874(20.1), 1034(23). Magnetic moment (Evans method, 293K, Acetonitrile): μ_{eff} = 2.96μ_B. Found: C 60.90; H 3.75; N 10.39 (%) $NiC_{61}H_{43}N_9O(ClO_4)_2.2H_2O$ Requires: C 60.45; H 3.91; N 10.41 (%).

Cu(II) Tris(6 - 2,4-diphenylpyrazolpyrid-2-yl)methanol (**3.5**):

L3 (69mg, 0.075mmol) was added to $Cu(ClO_4)_2.6H_2O$ (28mg, 0.075mmol). Crystallisation yielded pale green crystals (46%, 41mg). HRMS (ES-MS) *m/z* calcd. 980.2887; exp. 980.2856, $2[CuC_{61}H_{42}N_9O]^{2+}$, (100%), calcd. 1015.2575; exp. 1015.2648, $[CuC_{61}H_{42}N_9O][Cl]^+$, (30%). FT-IR (KBr/$cm^{-1}$) ν = 3323w, 3106m, 3060m, 1609s, 1581s, 1517w, 1486s, 1467s, 1455s, 1408m, 1363s, 1267w, 1223w, 1180m, 1088br+s, 1002m, 924w, 817m, 761s, 698s, 623s. UV-Vis [λ_{max}, nm, (εM, $M^{-1}cm^{-1}$)] in CH_3CN: 277(51167), 292(48992), 746(115), 861(107). Magnetic moment (Evans method, 293K, Acetonitrile): μ_{eff} = 1.22μ_B. Found: C 61.85; H 3.78; N 10.75 (%) $CuC_{61}H_{43}N_9O(ClO_4)_2$ Requires: C 62.05; H 3.67; N 10.68 (%).

Zinc(II) Tris(6 - 2,4-diphenylpyrazolpyrid-2-yl)methanol (**3.6**):

L3 (69mg, 0.075mmol) was added to $Zn(ClO_4)_2.6H_2O$ (28mg, 0.075mmol). Crystallisation yielded colourless crystals (58.5%, 52mg). ^{1}H-NMR (CD_3CN; 400MHz): δ_H 8.07(2H, t, J=7.2Hz, CH), 7.95(2H, dd, J=8.2Hz, CH), 7.54(4H, t, J=7.0Hz, CH), 7.40(12H, br.m, CH), 7.11(2H, br.s, CH), 7.07(3H, d, J=7.5Hz, CH), 7.00(6H, d, J=8.3Hz, CH), 6.92(1H, s, CH), 6.84(2H, m, CH), 6.74(2H, s,

CH), 6.62(1H, d, J=8.7Hz, CH), 6.58(1H, d, J=8.0Hz, CH), 6.43(2H, t, J=9.5Hz, CH), 6.34(2H, t, J=7.7Hz, CH). HRMS (ES-MS) *m/z* calcd. 490.6441; exp. 490.6498, $[ZnC_{61}H_{42}N_9O]^{2+}$, (100%), calcd. 1080.2367; exp. 1080.2318, $[ZnC_{61}H_{42}N_9O][ClO_4]^+$, (28%). FT-IR (KBr/cm^{-1}) ν = 3480br, 3121w, 3053w, 2924m, 2853m, 1713m, 1575s, 1558s, 1486s, 1456br+s, 1361s, 1308m, 1275m, 1226m, 1092br+s, 1029s, 998m, 969m, 954m, 920m, 814s, 765s, 696s, 623s. Found: C 61.86; H 3.72; N 10.60 (%) $ZnC_{61}H_{43}N_9O(ClO_4)_2$ Requires: C 61.95; H 3.67; N 10.67 (%).

Cadmium(II) Tris(6 - 2,4-diphenylpyrazolpyrid-2-yl)methanol (**3.7**):

L3 (63mg, 0.069mmol) was added to $Cd(ClO_4)_2.6H_2O$ (26mg, 0.069mmol). Crystallisation yielded colourless crystals (35%, 29.5mg). ^{1}H-NMR (CD_3CN; 400MHz): δ_H 8.27(3H, d, J=7.9Hz, CH), 8.00(3H, t, J=8.2Hz, CH), 7.78(6H, d, J=6.8Hz, CH), 7.65(9H, m, CH), 7.41(3H, t, J=8.1Hz, CH), 7.04(9H, dd, J=7.9Hz, CH), 6.89(3H, s, CH), 6.69(6H, d, J=7.3Hz, CH). ^{13}C-NMR (CD_3CN; 100MHz): δ_C. 158.33(C), 157.38(C), 148.92(C), 148.60(C), 142.77(CH), 131.02(CH), 129.94(C), 129.82(2xCH), 129.45(C), 129.21(CH), 128.69(CH), 126.76(CH), 120.12(CH), 116.64(CH), 114.70(CH), 74.98(C). HRMS (ES-MS) *m/z* calcd. 515.6312; exp. 515.7110, $[CdC_{61}H_{42}N_9O]^{2+}$, (100%), calcd. 1126.2106; exp. 1126.2151, $[CdC_{61}H_{42}N_9O][ClO_4]^+$, (10%). FT-IR (KBr/cm^{-1}) ν = 3378br+m, 3118w, 3059m, 2957w, 2932w, 2858w, 1966w, 1888w, 1810w, 1717m, 1575s, 1553s, 1516w, 1486s, 1456s, 1361s, 1307m, 1274m, 1223m, 1178m, 1157m, 1095br+s, 1026s, 993s, 955s, 917m, 814s, 764s, 695s, 623s, 502w. Found: C 55.96; H 3.11; N 9.79 (%) $CdC_{61}H_{43}N_9O(ClO_4)_2.⅔CHCl_3$ Requires: C 56.43; H 3.37; N 9.66 (%).

Mercury(II) Tris(6 - 2,4-diphenylpyrazolpyrid-2-yl)methanol (**3.8**):

L3 (57mg, 0.062mmol) was added to $Hg(ClO_4)_2.6H_2O$ (28mg, 0.062mmol). Crystallisation yielded colourless crystals (47%, 35mg). ^{1}H-NMR (CD_3CN; 400MHz): δ_H 8.31(3H, d, J=7.8Hz, CH), 7.97(3H, t, J=8.1Hz, CH), 7.74(6H, d, J=7.0Hz, CH), 7.62(9H, m, J=7.1Hz, CH), 7.40(3H, t, J=7.3Hz, CH), 7.06(9H, m, J=7.4Hz, CH), 7.01(3H, s, CH), 6.78(6H, d, J=7.2Hz, CH). ^{13}C-NMR (CD_3CN; 100MHz): δ_C. 157.89(C), 149.35(C), 147.34(C), 142.42(CH), 131.10(CH), 130.18(CH), 129.79(CH), 129.30(CH), 129.09(C), 128.84(CH), 128.66(C), 126.71(CH), 120.47(CH), 116.97(CH), 114.64(CH), 75.77(C). HRMS (ES-MS) *m/z* calcd. Mass spectroscopic data could not be obtained due to decomposition of the sample. FT-IR (KBr/cm^{-1}) ν = 3357br+m, 3130m, 3062m, 1977w, 1898w, 1661m, 1583s, 1557s, 1516w, 1486s, 1456s, 1408s, 1348s, 1304m, 1222m, 1180s, 1086br+s,

999s, 960s, 923s, 805s, 768s, 699s, 668m, 622s, 524w. Found: C 51.36; H 3.45; N 8.98 (%) $HgC_{61}H_{43}N_9O(ClO_4)_2.CHCl_3$ Requires: C 51.80; H 3.09; N 8.78 (%).

Tris-Rhenium(I) Tris(6 - 2,4-diphenylpyrazolpyrid-2-yl)methanol (**3.9**):

L3 (61mg, 0.067mmol) was added to $Re(CO)_5Br$ (81mg, 0.20mmol) and refluxed in toluene overnight. Crystallisation yielded yellow crystals (68%, 89mg). ^{1}H-NMR (CD_3CN; 400MHz): δ_H 8.54(2H, t, J=9.1Hz, CH), 8.29(2H, t, J=8.1Hz, CH), 8.18(2H, t, J=8.2Hz, CH), 8.09(4H, t, J=5.9Hz, CH), 7.83(2H, br.s, CH), 7.55(2H, d, J=8.2Hz, CH), 7.44(12H, m, CH), 7.37(9H, m, CH), 7.21(3H, t, J=8.4Hz, CH), 7.15(2H, t, J=7.6Hz, CH), 7.03(2H, t, J=7.4Hz, CH). ^{13}C-NMR (CD_3CN; 100MHz): δ_C. 143.00(CH), 142.53(C), 141.51(C), 128.98(CH), 128.91(CH), 128.82(CH), 128.70(CH), 128.60(CH), 128.56(CH), 128.33(CH), 127.78(CH), 127.47(CH), 126.12(CH), 125.88(CH), 125.76(CH), 124.87(CH), 123.08(C), 122.97(C), 106.55(C), 105.66(C), 104.54(C). HRMS (ES-MS) *m/z* calcd. 1499.2588; exp. 1499.2942, $[2(Re(CO)_3)C_{61}H_{42}N_9O.CH_3CN]^+$, (100%), calcd. 1542.2094; exp. 1542.3122, $[C_{61}H_{43}N_9O.(Re(CO)_3Cl).(Re(CO)_2(CH_3CN)Cl]^+$, (20%), calcd. 1931.0126; exp. 1931.0817, $[C_{61}H_{43}N_9ONa.2(Re(CO)_3Br).(Re(CO)(CH_3CN)Cl]^+$, (15%). FT-IR (KBr/cm^{-1}) ν = 3445br+m, 3063m, 2030s, 2015s, 1917s, 1877s, 1604m, 1570m, 1488s, 1467s, 1402w, 1362m, 1218w, 1179w, 1098w, 1075m, 1064m, 1027m, 952m, 916w, 826m, 809m, 758s, 694s, 686s, 668w, 657w, 604w, 533m, 524m. UV-Vis [λ_{max}, nm, (εM, M^{-1}cm^{-1})] in CH_3CN: 275(44642). Found: C 48.52; H 2.48; N 6.96 (%) $3(Re(CO)_3Cl)C_{61}H_{43}N_9O.CH_3OH$) Requires: C 48.41; H 2.69; N 7.16(%).

3.4 References

1. C. Pettinari, R. Pettinari, *Coord. Chem. Rev*., **2005**, 249, 663.
2. A. L. Gavrilova, B Bosnich, *Chem. Rev*. **2004**, 104, 349−383.
3. S. Derossi, L. Brammer, C. A. Hunter, M. D. Ward, *Inorg. Chem.*, **2009**, 48(4), 1666.
4. L. Cronin, *Angew. Chem. Int. Ed.*, **2006**, 45(22), 3576.
5. F. Zeng, Z. Yu, *Organometallics*, **2009**, 28(6), 1855.
6. M. Jia, A Steifert, W. R. Thiel, *Chemistry of materials*, **2003**, 15(11), 2174.
7. M. A. Halcrow, *Coord. Chem. Revs.*, **2009**, 253, 2493.
8. M. A. Halcrow, *Coord. Chem. Revs.*, **2005**, 249, 2880.

9a. V. Montoya, J. Pons, V. Branchadell, J. García-Antón, X. Solans, M. FontBardia, J. Ros, *Organometallics*, **2008**, 27, 1084.

9b. V. Montoya, J. Pons, V. Branchadell, J. García-Antón, X. Solans, M. FontBardia, J. Ros, *Organometallics*, **2007**, 26, 3183.

10. S. Muñoz, J. Pons, J. Ros, M. Font-Bardia, C. A. Kilner, M. A. Halcrow., *Inorg. Chim. Acta,* **2001**, 373, 211–218.
11. J. A. Campoa, M. Canoa, J. V. Heras, M. C. Lagunas, J. Perlesa, E. Pinilla, M. R. Torres, *Helv. Chim. Acta*, **2002**, 85, 1079.
12. M. L. Gallego, M. Cano, J. A. Campo, J. V. Heras, E. Pinilla, M. R. Torres, P. Cornago, R. M. Claramunt, *Eur. J. Inorg. Chem.* **2005**, 4370–4381.
13. Y. Yang, P. Yang, C. Zhang, G. Li, X-J. Yang, B. Wu, C. Janiak, *J. Mol. Catal. A- Chem.*, **2008**, 296, 9–17.
14. T-P. Cheng, B-S. Liao, Y-H. Liu, S-M. Peng, S-T. Liu, *Dalton. Trans.,* **2012**, 41, 3468.
15. K. Madeja, E. Konig,. *J. Inorg. Nucl. Chem*. **1963**, Vol. 25, 377.
16. A. B. P. lever,. *Inorganic electronic spectroscopy*, 2nd Ed, p458-461.
17. F. Mani, G. Scapacci,. *Inorg. Chim. Acta*, **1980**, 38, 151-155.
18. S. E. Livingstone, J. D. Nolan, *J. Chem. Soc. Dalton*. *Trans*., **1972**, 218.
19. A. K. Patra, E. Bill, E. Bothe, K. Chlopek, F. Neese, T. Weyhermuller, K. Stobie, M. D. Ward. J. A. McCleverty, K. Wieghardt,. *Inorg. Chem*., **2006**, 45, 7877.
20. T. A. Fiedler, H. L. Halfen, J. A. Halfen, T. C. Brunold,. *J. Am. Chem. Soc*., **2005**, 127(6), 1675-89.

21. S. H. Lapidus, P. W. Stephens, E. Shurdha, J. G. DaSilva, J. S. Miller, *Polyhedron*, **2013**, 52, 713-718.

22. A. B. P. lever, *Inorganic electronic spectroscopy*, 2nd Ed, p480-495.

23. J. L. Burmeister, T. P. O'Sullivan, K. A. Johnson., *Inorg. Chem*., **1971**, 10, 1803.

24. A. Bencini, C. Benelli, D. Gatteschi., *Inorg. Chem*., **1978**, 17, 3313.

25. Z. Dori, H. B. Gray,. *Inorg. Chem*., **1968**, 7, 889.

26. Y. Sasaki., *Bulletin. Institute. Chemical. Research., Kyoto. Univ.*, **1980**, 58(2), 182-192

27. W.O. Gillum, R.A.D. Wentworth and R.F. Childers, *Inorg. Chem.*, **1970**, 9, 1825

28. D. F. Shriver and P. W. Atkins, 3rd Edition, Inorganic Chemistry, Oxford press, **1999**.
29. M. Ciampolini, *Inorg. Chem*., **1966**, 5, 35.
30. M. Nemiroff, S. L. Holt,. *Inorg. Chem*., **1973**, 12, 2032.
31. J. L. Burmeister, T. P. O'Sullivan, K. A. Johnson,. *Inorg. Chem*., **1971**, 10, 1803.
32. A. B. P. lever,. Inorganic electronic spectroscopy, 2nd Ed, p568.

33. Slade, A. A. G. Tomlinson, B. J, Hathaway, D. E. Billling,. *J. Chem. Soc*. *(A), Inorg. Phys. Theor*., **1968,** 61.

34. B. J. Hathaway, D. E. Billng *Coord. Chem Rev*, 5, **1970**, 143-207.

35. A. A. G. Tomlinson, B. J, Hathaway,. *J. Chem. Soc*. *(A), Inorg. Phys. Theor*., **1968,** 1905.

36. W. D. Harrison, D. M. Kennedy, M. Power, R. Sheahan, B. J. Hathaway,. *J. Chem. Soc. Dalton. Trans., 1981*, 1556.

37. S. Tyagi, B. J. Hathaway,. J. Chem. Soc. Dalton., 1981, 2029.

38. A. J. Amoroso, R. J. Arthur, M P. Coogan, J. B. Court, V. Fernandez-Moreira, A. J. Hayes, D. Lloyd, C. Millet, S. J. A. Pope, *New J. Chem*., **2008**, 32, 1097–1102.

39. J. M. Holland, C. A. Kilner, M. Thornton-Pett, M. A. Halcrow,. *Polyhedron*, **2001**, 20, 2829–2840.

40. A. Nanthakumar, S. Fox, N. N. Murthy, K. D. Karlin,. *J. Am. Chem. Soc.* **1997,** *119,* 3898-3906.

41. G. F. Liu, Z. G. Ren, H. X Li, Y. Chen, Q. H. Li, Y. Zhang, J. P. Lang,. *Eur. J. Inorg. Chem*. **2007**, 5511–5522.

42. J. C. Knight, A. J. Amoroso, P. G. Edwards, R. Prabaharan, N. Singh,. *Dalton Trans*., **2010**, 39, 8925–8936.

43. Y. Wang, B. Quillian, P. Wei, H. Wang, X. J. Yang, Y. Xie, R. B. King, P. V. R. Schleyer, H. F. Schaefer, G. H. Robinson,. *J. Am. Chem. Soc.* **2005**, 127, 11944-11945.

Appendix

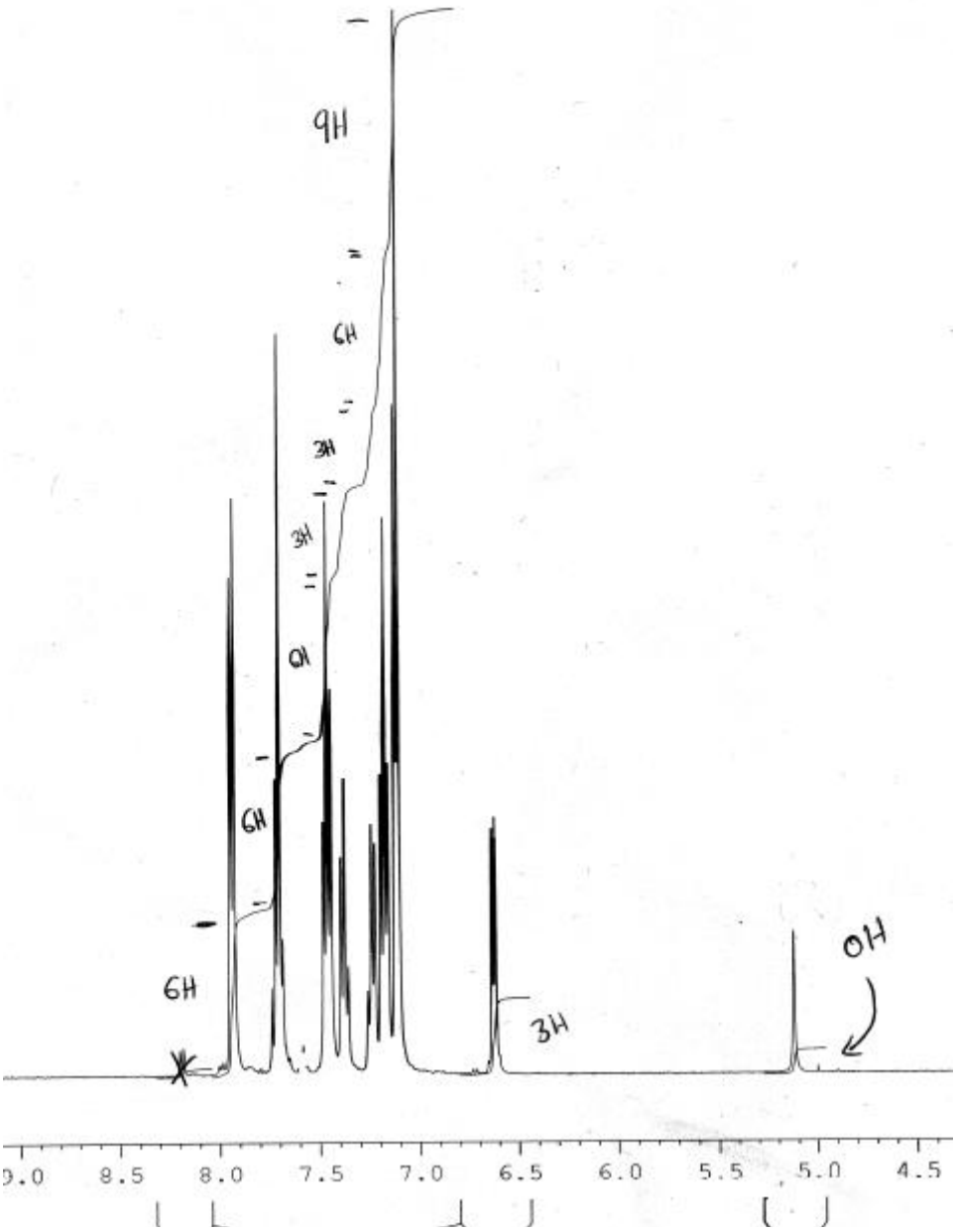

Figure 1A: Aromatic region of H-NMR for **L3** in the solvent DMSO.

Chapter 4:

Bipodal Bis-pyridyl Dimethylpyrazole Framework and Co-ordination with Various Transition Metals

4.0 Abstract

A planar and potentially tetradentate ligand 6,6'-bis(dimethylpyrazole)-2,2'-bipyridine has been synthesised (**L4**). The ligand has also been complexed with a series of transition metal perchlorate salts from Manganese(II) to Zinc(II) as well as Mercury(II). The following compounds have all been analysed using IR, NMR, electronic absorption spectroscopy, Mass spectrometry, X-ray crystallography and magnetic susceptibility measurements. Crystallographic data was achieved for all of the compounds with exception of complex **4.5** (Zn(II)). The data showed that all analysed metals form six co-ordinate distorted octahedral structures in the solid state. The co-ordination generally involves four ligand N-donors and two perchlorate O-donors, correlating with IR data, with exception of the Ni(II) complex that utilises six N-donors from two ligands leaving a pendent pyrazole per ligand. All appropriate complexes were found to be high spin. Their UV-Vis studies suggest the complexes retain such geometries in solution and are in agreement with crystallographic data.

4.1 Introduction

Nitrogen containing heterocyclic ligands and their co-ordination complexes is a vast subject and has proven very fruitful over the past few decades. The different ring sizes (5- and 6-membered) and variable donor properties of these ligands make them ideal for investigating the co-ordination chemistry of such systems. Their richness of possible organic modifications and the huge number of available metals makes the diversity of this area appear infinite. These frameworks have set precedence in many areas of chemistry, for example, the formation of supramolecular arrays,[1-4] and their use in catalytic,[5-6] optical[7-8] and magnetic applications.[9-12]

Variation of the conjugation in these molecules allows the electronic properties of the resulting complexes to be tuned, and the communication between different donors or metal centres to be investigated. The ability of ligands to be multidentate and/or multinuclear due to co-ordination through bridging ligands has meant that much attention has been spent studying heterocycles, especially by those interested in poly-nuclear assemblies, such as helicates,[13] cages[14,15] and catalysts.[23] By linking heterocyclic groups together it is possible to synthesise chelating ligands, which are less common, but have developed rapidly in recent years. Bidentate ligands such as 2,2'-bipyridine and 2-pyridyl-pyrazole are well established, putting these donor groups in good stead for further development. Phillips *et. al.* have discussed

ligands with linked bidentate groups, such as bipyridines and pyrazolyl-pyridines, which themselves provide a platform for the formation of multinuclear systems such as compounds (1)-(3) in Figure 1.[16] These highly conjugated ligands allow strong metal-metal interactions to be explored due to the relatively close proximity of coordinated metal cations.[17-21] For example, Phillips *et. al.* have synthesised two dinuclear complexes with ligand (2) (Fig. 1), one with $PdCl_4$, which was poorly soluble, and the other with $Ru(II)(bipy)_2Cl_2$ which forms two six co-ordinate Ru(II) centres each surrounded by three bipyridine units and linked together through the 4,4'-bipyridine moiety. This complex was observed to contain some metal-metal communication through the pi system, however, this interaction was found to be weak, most likely due to the free rotation in the 4',4" linking bond.[22]

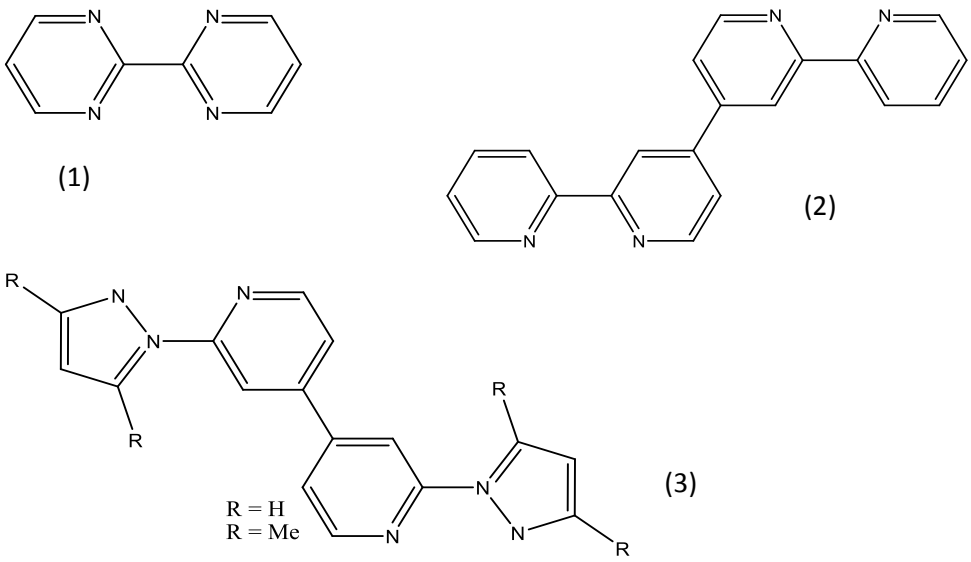

Figure 1: Doubly bidentate ligands developed by Phillips *et. al.* for multi nuclear co-ordination arrays. 2,2'-bipyrimidine (1), 2,2':4',4":2",2"'-quaterpyridine (2) and 2,2'-bis(pyrazol-1-yl)4,4'-bipyridine (3).[16]

Ward *et. al*. have also described similar frameworks in their quest to study metallosupramolecular compounds, however these have less conjugation due to the incorporation of more flexible spacers, see Figure 2, to aid the formation of multi-nuclear bidentate systems.[1,2,14,25] They have developed a series of dinucleating and trinucleating bridging ligands which contain two or three pyrazolyl-pyridine units and co-ordinate to relatively "soft" natured metals such as Ag(I) and Hg(I), due to their preference for low co-ordination numbers and relatively strong metal-metal interactions.[24] For example, the complex $[Ag(L^{mPh})(BF_4)(^iPr_2O)]_\infty$ creates a one dimensional helical co-ordination polymer (Fig. 2), where

each Ag(I) centre is bound, in a tetrahedral geometry, to two bidentate pyrazoyl-pyridine units each from a separate ligand molecule. This co-ordination polymer was shown to have a two-fold rotation creating a helical structure in the solid state. This in turn allows for inter-ligand π-π stacking (3.2-3.5Å) between the phenyl spacers and a pyrazole moiety from the adjacent ligand which further stabilizes the structure. The Ag(I) complex, $[Ag_2(L^{mTol})_2(ClO_4)_2]$ however, gives a discrete dinuclear 'mesocate' structure where two ligands span two Ag(I) ions (Fig. 2). The simple addition of a methyl substituent to the vacant *meta*-position of L^{mPh} (discussed *vide infra*), prevents the formation of the helicate polymer system through unfavourable steric interactions, which in this case highlights the importance of steric bulk when trying to create discrete complexes over co-ordination polymers.

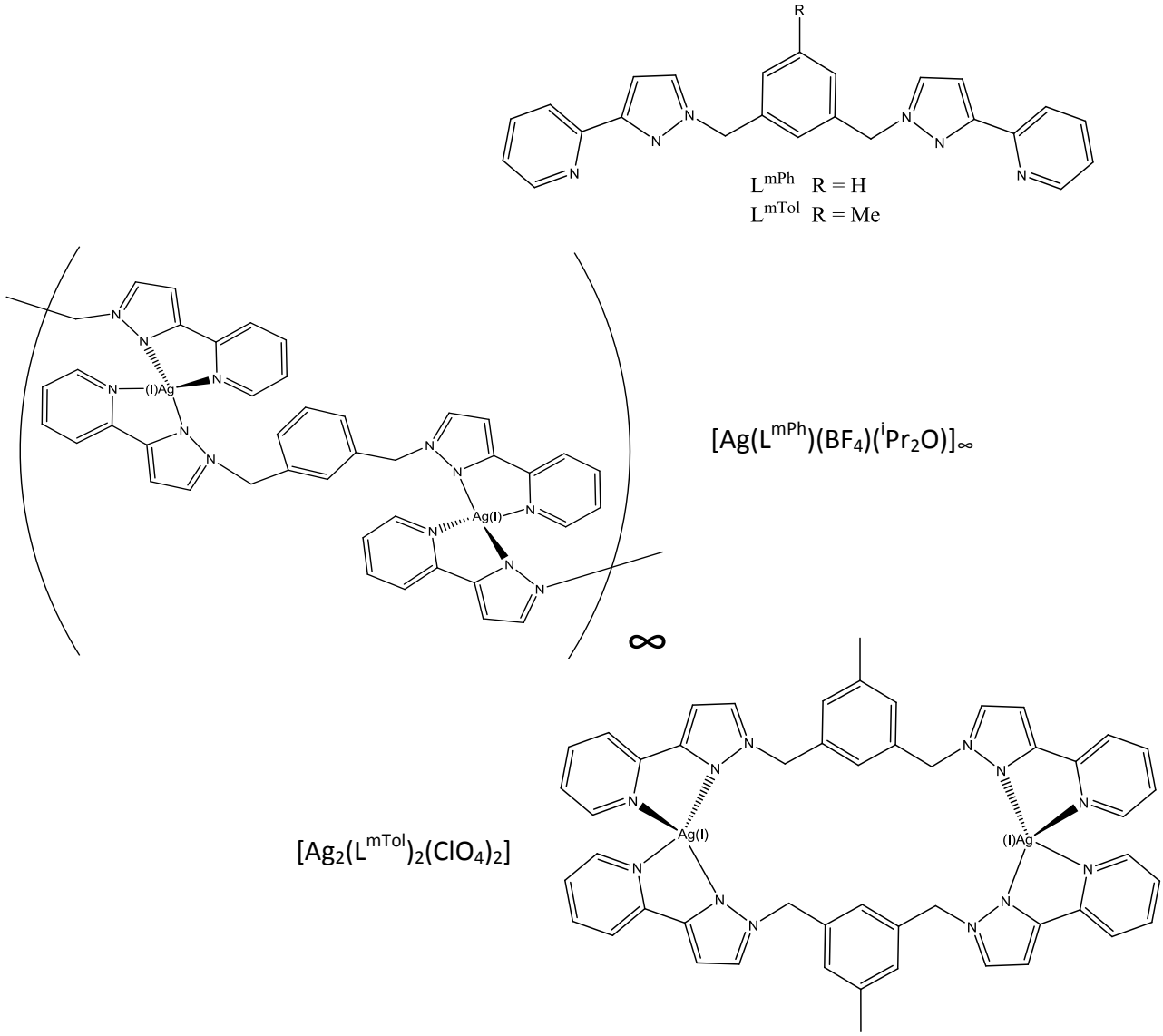

Figure 2: Some of the ligands and complexes discussed by Ward *et. al*. where $Ag(L^{mPh})(BF_4)(^iPr_2O)]$ forms a helical co-ordination polymer and $[Ag_2(L^{mTol})_2(ClO_4)_2]$ forms a more discrete dimetallic structure.[24]

A very similar ligand (L^{oPh}), also developed by Ward *et. al.*, has been shown to co-ordinate readily with first row transition metals such as cobalt(II) and zinc(II), producing six co-ordinate metal centres that form tetrahedral cages of the formula $[M_4(L^{oPh})_6]^{8+}$.[25,26] However, the same ligand, when treated with $Hg(ClO_4)_2$, was found to form an individual dimetallic complex (Fig. 3) displaying a metal-metal bond (Hg-Hg = 2.518(2) Å). This close proximity is thought to have facilitated the reduction of Hg(II) to Hg(I) allowing the crystallisation of the Hg_2 unit. Faster crystallisation of the same system did afford a mononuclear Hg(II) complex where L^{oPh} now acts as a tetradentate chelate (Fig. 3), noting that the flexible linker twists perpendicular to the ligand rings to bring the two pyrazolyl-pyridine moieties closer together. This reveals how shorter bridge groups would be more suitable for the synthesis of discrete mononuclear compounds.

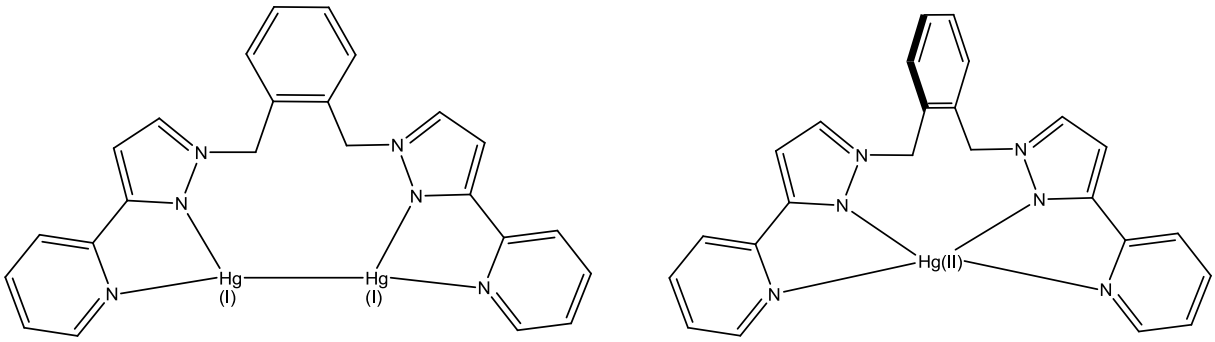

Figure 3: Structures of the dinuclear and mononuclear complexes $[Hg_2(L^{oPh})(MeNO_2)_2][ClO_4]_2$ (left) and $[Hg(L^{oPh})][ClO_4]_2$ (right) respectively .[24]

The group of Toshihiro Ise *et. al.* have synthesised a series of similar sized ligand frameworks where two pyrazolyl-pyridine units are bridged by either a 5,5'-(1,1'-biphenyl) group, or a shorter iso-propyl linker, and both show tetradentate co-ordination of the ligands to a single Zn(II) centre (Fig. 4). Many other analogous compounds of this type are being developed and investigated for their interesting electroluminescent properties.[27] These examples demonstrate that even first row transition metals, with octahedral preferences, can also utilise the donor abilities of two chelating pyrazolyl-pyridine units to form mononuclear complexes.

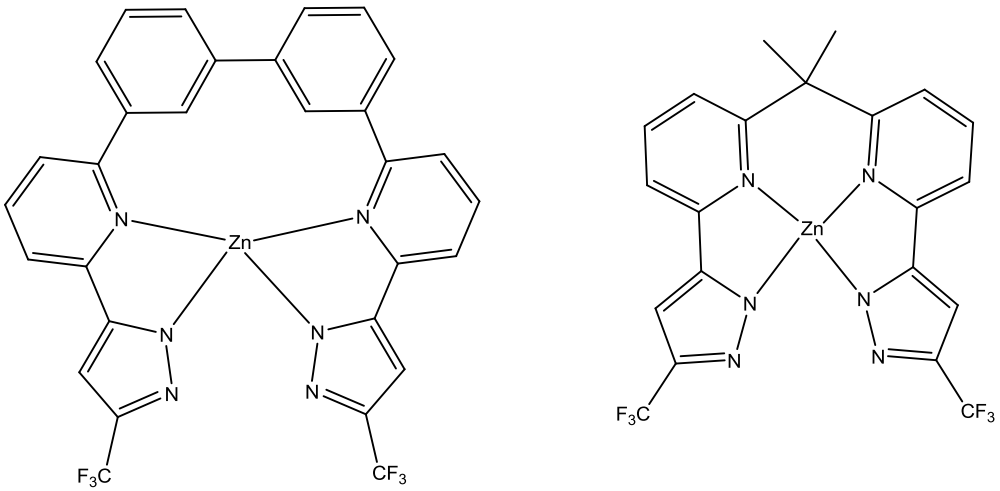

Figure 4: Structures of mononuclear complexes [Zn(II)(5,5'-(1,1'-biphenyl)bis(pyrazolyl-pyridine)] and [Zn(II)((isopropyl)-bis(pyrazolyl-pyridine))] respectively.[27]

Couchman *et. al*. have synthesised another potentially tetradentate ligand, 6,6'-bis(3-pyrazolyl)-2,2'-bipyridine, where the two pyrazolyl-pyridine moieties are now directly linked through the 2-positions of the pyridine units.[28] This was complexed with Cu(I) and Ag(I) which formed the familiar discrete dimetallic double helicate structure, where two 6,6'-bis(3-pyrazolyl)-2,2'-bipyridine ligands are bridged by two Ag(I) or Cu(I) ions, which is a consequence of Cu(I) and Ag(I) having a preference for *pseudo*-tetrahedral co-ordination geometries. Oxidation of the Cu(I) dimer complex however, resulted in the formation of a mononuclear Cu(II) complex (Fig. 5), where the copper centre now has a preference for a five co-ordinate donor set. The Cu(II) centre shows a typical square pyramidal geometry which allows the two pyrazolyl-pyridine donor sets to exist in a co-planar arrangement.

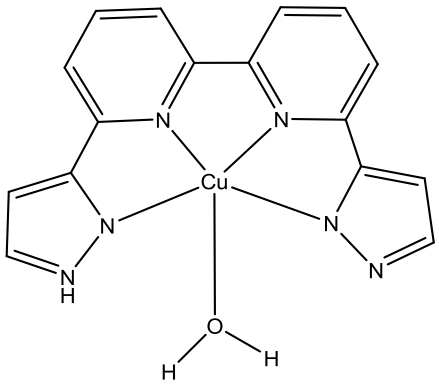

Figure 5: Structure of [Cu(II)(6,6'-bis(3-pyrazolyl)-2,2'-bipyridine).H_2O].[28]

Chi *et. al*. have discussed a more rigid ligand framework 2,9-Bis(1H-pyrazol-1-yl)-1,10-phenanthroline (dpphen) which was synthesised by the reaction of 2,9-dichloro-1,10-phenanthroline with pre-made pyrazole.[29] This ligand is slightly different in structure to previous examples as now the pyrazole functions are bonded to the phenanthroline (pyridyl units) *via* one of its nitrogen moieties (Fig. 6). Subsequently this ligand was reacted with $Ni(ClO_4)_2$, followed by the addition of NaSCN, where the ligands strong chelating abilities and large conjugation planes are named as ideal properties for investigating intermolecular ferro- and anti-ferromagnetic interactions, using variable temperature magnetic susceptibility experiments.[29] The resulting complex gave a Ni(II)-N_6 slightly distorted octahedral co-ordination geometry as a mononuclear complex, with the formula $[Ni(dpphen)(NCS)_2]$(Fig. 6). Addition of methyl or phenyl groups to the 3 and 5 positions of the pyrazole backbone have also recently been explored, and until now, only the $[Cd(dpphen)(NCS)_2]$ structure of the methyl substituted complex has been published giving a similar, but more distorted, Cd-N_6 octahedral co-ordination geometry.[30,31]

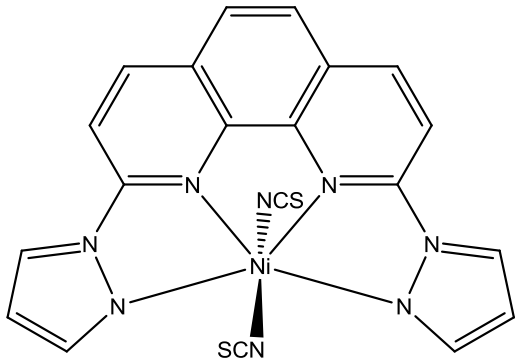

Figure 6: Structure of $[Ni(dpphen)(NCS)_2]$.[29]

Equatorial binding of the two pyrazolyl-pyridine N-donor sets in these complexes reveals that the ligands are perfectly suited to allow the formation of six co-ordinate, octahedral, transition metal complexes that can strongly co-ordinate all the donors within these tetradentate systems, in addition to their proven ability to give stable crystalline products.

Lewis *et. al.* have exploited the strong binding affinities of relatively low oxidation state transition metals, to pyrazolyl-pyridine ligands, to facilitate ring closure reactions.[32,33] This was demonstrated by first isolating the Ni(II) complex of 6,6'-dihydrazino-2,2'-bipyridine, and subsequently reacting this complex with substituted beta-diketone precursors to form the functionalised bispyrazole-bipyridine ligands which retain the Ni(II) centre (Fig. 7). Only limited

characterisation of this early work was obtained, and no further complexes have been reported.

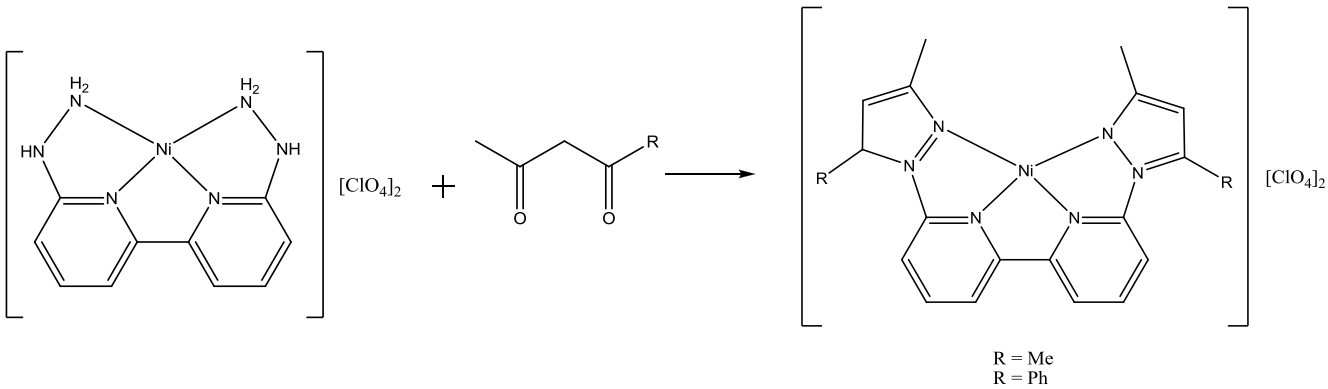

Figure 7: Reaction of 6,6'-dihydrazino-2,2'-bipyridyl Nickel(II) perchlorate with a β-diketone to form [Nickel(II) 6,6'-Bis(3,5-dimethylpyrazol-1-yl)-2,2'-Bipyridine]perchlorate.[32,33]

In this chapter, a new synthetic approach to this ligand has been developed, without the need to pre-form the 6,6'-dihydrazino-2,2'-bipyridine metal complex prior to cyclisation. This has allowed the preparation of several novel transition metal complexes, which have been fully characterised. Solution-state characterisation of their electronic and magnetic properties has been performed and solid-state structural studies via single crystal X-ray diffraction have been used to investigate their coordination geometries.

4.2 Results and Discussion

4.21 Ligand synthesis

The 6,6'-dibromo-2,2'-Bipyridine (**S1**) starting material was synthesised by the homocoupling of two equivalents of mono-lithiated 2,6-dibromopyridine.

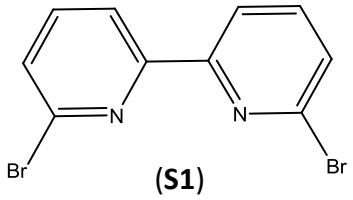

Figure 8: 6,6'-dibromo-2,2'-Bipyridine (**S1**).

As discussed in Chapter 2, the enhanced reactivity of the bromides on the C-N π-bond in each pyridyl unit, allows the treatment of 6,6'-dibromo-2,2'-bipyridine (**S1**) with hydrazine hydrate. Hydrazine was used as a solvent and refluxing this mixture in a nitrogen atmosphere for approximately 14 hours (Sch. 1) allowed direct displacement of the bromides giving the bis(hydrazino)-2,2'-bipyridine species (**S2**).

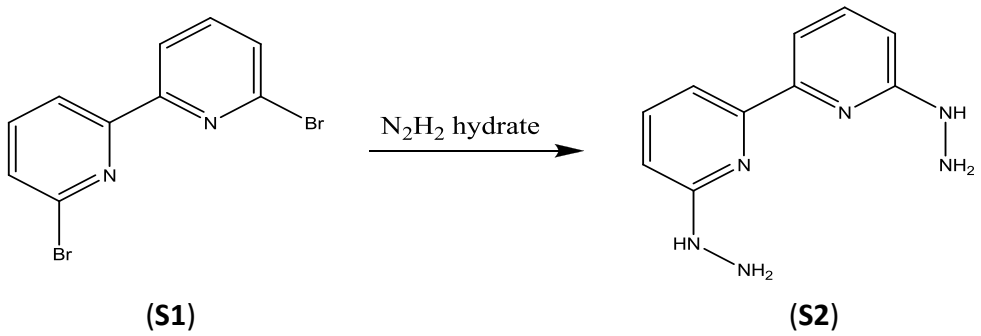

Scheme 1: Synthesis of the intermediate 6,6'-Dihydrazino-2,2'-Bipyridine (**S2**).

Upon cooling of the reaction some precipitate developed (impure product) which could be filtered off under reduced pressure giving a pure solution of the hydrazino product. Using an external trap, the hydrazine solvent was removed from the filtrate by gentle heating *in vacuo* producing a sticky solid. The dull yellow solid was triturated with distilled water, to remove any excess hydrazine solvent, until a paler, powdery solid was achieved, often requiring sonication. The pale solid was filtered off and washed with a small amount of ethanol to further remove any remaining water. A final wash with a minimum of $CHCl_3$ was needed to dry the product,

which was done in a N_2 atmosphere as the product was found to be hygroscopic, which again is reasonable to expect for a compound containing such pendent amines. The desired product was isolated in high purity and confirmed by ^{1}H-NMR spectroscopy, where the two aromatic doublets are shown to have shifted upfield relative to starting material, and LR-mass spectrometry which achieved the expected molecular ion signal at 239.10 m/z for the sodium cation of **S2**.

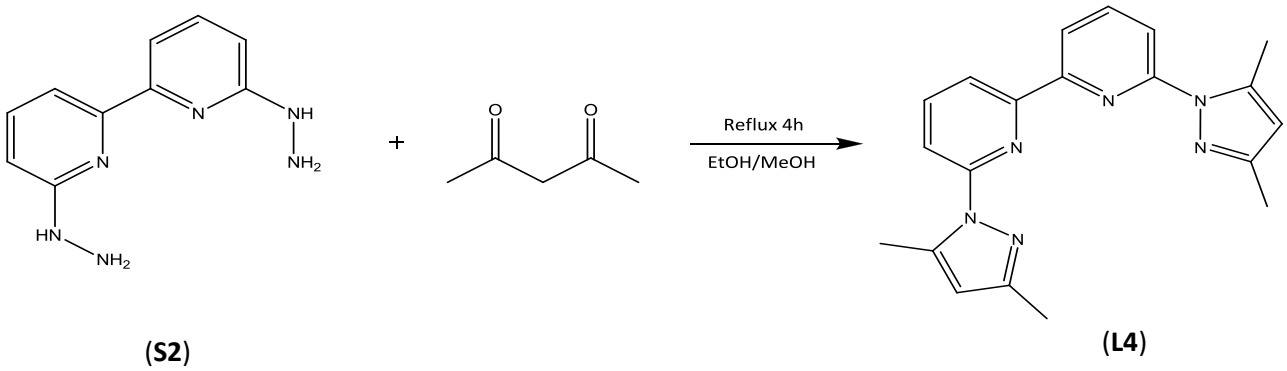

Scheme 2: synthesis of ligand 6,6'-Bis(dimethylpyrazole)-2,2'-Bipyridine

The new product 6,6'-dihydrazino-2,2'-Bipyridine (**S2**) was then reacted readily with 2.2 equivalents of pentane-2,4-dione by heating in an ethanol/methanol (2:1) solvent at reflux for a minimum of 4 hours (Sch. 2). Upon cooling the reaction to room temperature, a small amount of precipitate developed (pure product **L4**), and further cooling over night in -25°C allowed the collection of the second crop of product. The pale yellow solid was filtered *in vacuo*, washed with a small amount of fresh ethanol and allowed to dry in air giving the desired compound in high purity. More product could be extracted from the filtrate by reducing the solvent volume and again cooling it to -25°C overnight followed by washing any filtered solid with fresh ethanol. The product 6,6'-bis(dimethylpyrazole)-2,2'-bipyridine was isolated with an 85% combined yield and was confirmed by NMR spectroscopy, mass spectrometry and X-ray crystallography.

4.22 Synthesis of complexes

The ligand (**L4**) was complexed with a variety of transition metal perchlorates giving complexes **4.1**-**4.6**, see Table 1**.** The general procedure involved stirring a solution of **L4** (typically 0.1mmol) in 4 ml of a chloroform/acetonitrile (1:1) mixture aided by warming, followed by the slow addition of a metal salt solution dissolved in acetonitrile or THF (typically 3-4ml). A colour change was usually seen upon complexation, with the exception of **4.5** and **4.6** which were d^{10} and therefore show no significant colour change. Unfortunately isolation of the Fe(II) complex was not achieved, with all attempts recovering only free ligand.

Table 1: displaying the various complex numbers and their corresponding metal ion.

Complex number	Metal ion used
4.1	Mn (II)
4.2	Co(II)
4.3	Ni(II)
4.4	Cu(II)
4.5	Zn(II)
4.6	Hg(II)

The complexes are found to be more soluble than the free ligand which meant continuous warming was not necessary during formation. All of the complex solutions were allowed to equilibrate for 24h and were filtered through celite before attempting crystalisation. All of the complexes were made in a 1:1 (metal:ligand) ratio and could be isolated from a variety of organic solvents via the method of vapour diffusion, often giving samples of suitable quality for X-ray crystallographic study. However if precipitation proceeded too quickly, colourless cotton wool like crystals of free ligand would form, which was confirmed by X-ray diffraction.

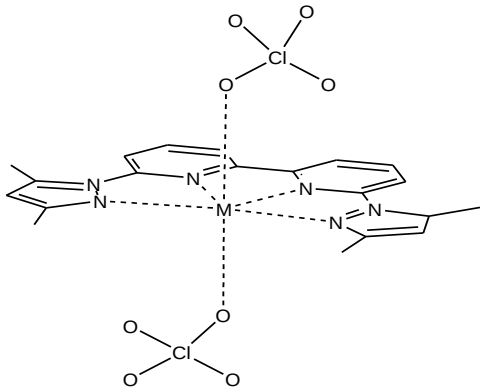

M = Ni(II), Cu(II), Zn(II), Co(II), Mn(II) and Hg(II)

Figure 9: Diagram showing the general co-ordination of **L4** with different dicationic transition metals.

4.23 Vibrational spectroscopy

Assignment of IR spectral bands can prove useful in helping to determine a ligands mode of co-ordination, and Table 2 lists some of the characteristic stretches seen for these molecules. In the free ligand, two bands are seen around 1575cm^{-1}, one of which is fairly broad (hiding a third band) whereas in complexes **4.1**-**4.6**, three distinct stretching modes are seen. The newly appearing peak, *ca*. 1600cm^{-1}, of the complexes comes from a strong band shifting to a higher frequency which is indicative of pyridyl co-ordination. Complex **4.3** shows a fourth but weaker stretch (1621cm^{-1}) which suggest less symmetry in the compound. This correlates with X-ray data as two C=N environments for the pyrazoles are also seen (co-ordinating and non co-ordinating), unlike the other complexes in which they are all co-ordinating. It is possible to predict the environment of perchlorate counter ions from the number of bands present in the IR spectrum. If two bands are observed at ~1100cm^{-1} and ~620cm^{-1}, this suggests a symmetrical non-coordinating counter ion which has been noted for complexes **4.2**, **4.3** and **4.5**. However, the appearance of six bands from four regions suggests de-symmetrisation of the tetrahedral counter ions, which implies co-ordination through one of its oxygens, and correlates with bands observed in complexes **4.1**, **4.4** and **4.6** (Ref: 35 Chapter 2, Pg. 100). These IR results compared well with the X-ray data collected for these compounds, with exception of **4.5** where suitable crystals could not be obtained. However, from the IR data it is concluded that the Zinc complex

is analogous to **4.2** in solid state, where only three C=N stretches are seen and that the perchlorate counterions are non co-ordinating.

Table 2: Some key IR stretching frequency modes for **L4** and complexes **4.1**-**4.6**.

Compound	Aromatic ν(C-H)	ν(C=N) and (C=C)	π(C-H)	N (Cl-O)*
L4	3113.03(m), 3051.8(m)	1589.54(s), 1566.4(br+s) and 1479.13(s), 1441.05(s) 1431.4(s)	775(s), 797.72(s)	n/a
4.1	3114.5(m), 3091.3(m), 2923.6(m)	1598.2(s), 1581.82(s), 1562.1(s) and 1482.03(s), 1444.9(s), 1418.87(s)	797.9(s), 780.1(m)	1110.31(s), 1087.7(s), 912.2(m), 636.9(s), 625.8(s), 481.96(w)
4.2	3134.24(m), 3110.62(br +m),	1602.56(s), 1583.75(s), 1566.4(s) and 1486.37(s), 1449.24(s), 1426.58(s)	794.5(s), 781.0(m)	1121.89(s), 615.7(s)
4.3	3098.08(m), 2981.41(m)	1620.7(m), 1605.45 (s), 1589.54 (s), 1569.77 (s), and 1491.67(s), 1452.14(s), 1429.48(s)	794.05(s), 760.3(m)	1129.12(s), 624.82(s)
4.4	3135.21(m), 3110.14(m), 3089.89(m)	1606.9(s), 1583.75(s), 1571.2(s) and 1489.26(s), 1449.24(s), 1430.44(s)	795.5(s), 780.07(m)	1120.92(split), 930.0(m), 620.0(split), 479.6(w)
4.5	3142.9(m), 3100(m), 2930.8(m),	1603.0(s), 1585.2(s), 1568.81(s) and 1486.85(s), 1451.65(s), 1428.99(s)	795.01(s), 781.9(m)	1110.8(s), 623.86(s)
4.6	3150(m), 3101.9(m), 2920.2(m)	1597.7(s), 1580(s), 1563.5(s) and 1477.21(s), 1447.8(s), 1420.3(s)	797.4(s), 732.3(w)	1107.9(s+split), 920.4(m), 636.49(m), 625.3(s) ,465.2(w)

*Assignments for Cl-O perchlorate stretches and bonding modes were determined from reference 34.

4.24 ^{1}H NMR and ^{13}C NMR spectroscopy

The ^{1}H and ^{13}C NMR spectra of **L4** and **4.5** and the ^{1}H NMR of **4.6** have all been determined. At ambient temperature the ligand displays a straightforward spectrum as a consequence of its simple and symmetric structure, with only six identifying peaks corresponding to three aromatics, two methyls and one from the pyrazole backbone. The complexes display similarly simplistic spectra confirming that some form of symmetrical co-ordination is occurring. Since the complexes were not soluble in chloroform comparisons were made from DMSO solutions. Downfield shifting of all of the peaks was observed for compound **4.6** relative to the spectrum of **L4** (approximately 0.3-0.5ppm for the aromatic protons and 0.5ppm for the pyrazole back bone)(see figure 10+11), however, no such shifting could be identified for the Zn(II) complex **4.5**. The identical spectra of **4.5** and **L4** may suggest that the Zn(II) complex is less stable, especially in a DMSO solution, and could therefore be dissociating into the free ligand and a solvated cation. However evidence for the zinc complex was confirmed by ^{1}H-NMR spectroscopy when **4.5** was alternatively dissolved in CD_3CN, giving the spectrum shown in figure 13. This spectrum was compared to that of **L4** (which is poorly soluble in acetonitrile, see figure 12) showing a small down field shift in all of the peaks, with exception of the aromatic triplet and pyrazole backbone protons which have shifted downfield by 0.5ppm, noting that the aromatic triplet has now become the most downfield peak.

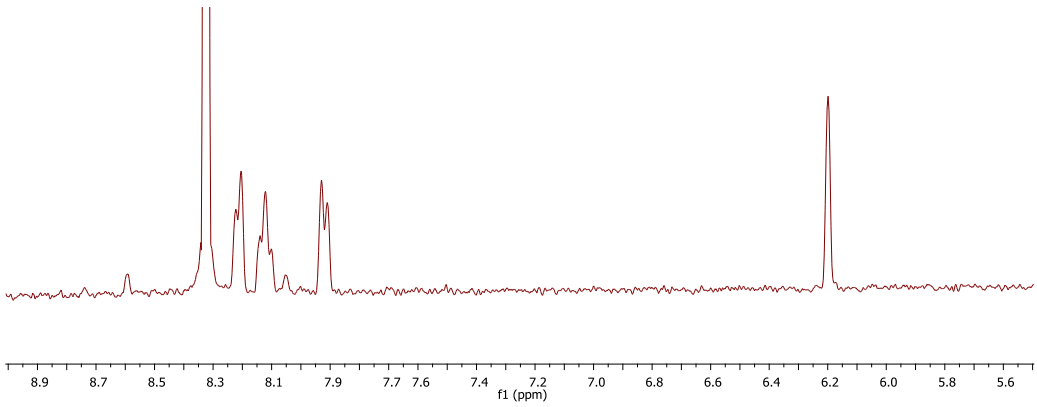

Figure 10: Down field region of the ^{1}H NMR for **L4** in DMSO.

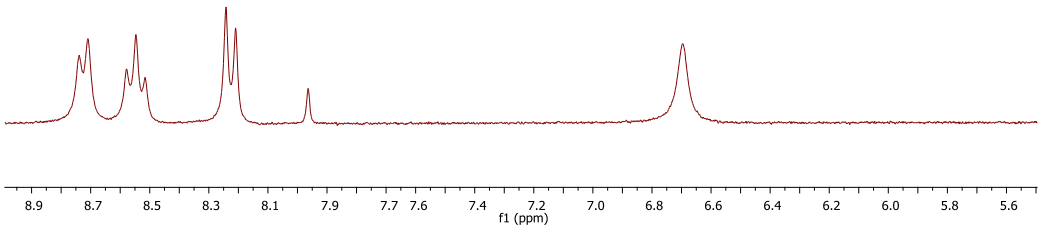

Figure 11: Down field region of the ^{1}H NMR for compound **4.6** in DMSO.

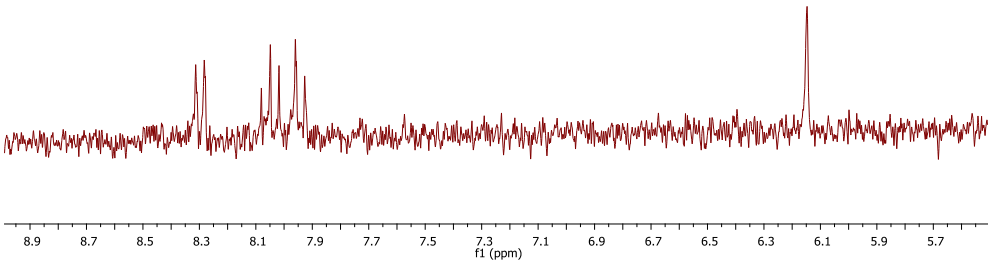

Figure 12: Down field region of the ^{1}H NMR for the parent Ligand **L4** in CD_3CN

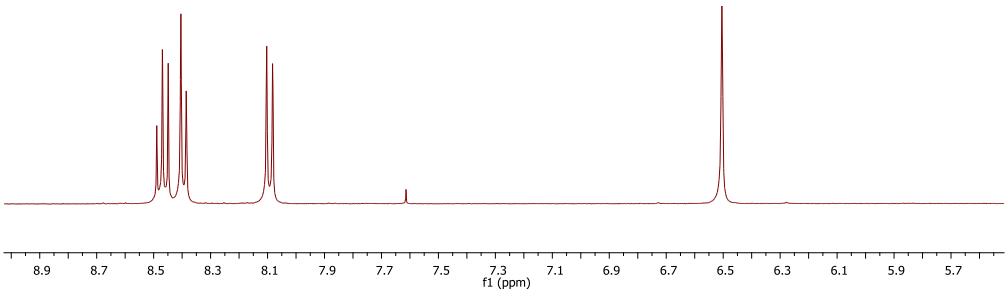

Figure 13: Down field region of the ^{1}H NMR for compound **4.5** in CD_3CN

4.25 Electronic absorption spectra

The electronic absorption spectra of **L4** and complexes **4.1**-**4.5** have been measured with data displayed in Table 3. All of the spectra were analyzed in an acetonitrile:chloroform (50:50) solvent mixture in a 1cm quartz cuvette at concentrations ranging from 3.9×10^{-6} to 1.3×10^{-3} mol dm^{-1}. The use of a solvent mixture was necessary due to the lower solubility of the ligand in neat acetonitrile, compared to **L2**. All of the spectra have two broad and intense band structures between 260-370nm, with peaks sometimes showing splitting, and are attributed to the intra-ligand π→π* transitions. The lower energy of these bands is some 40-70nm longer in wavelength than the equivalent band of **L2** (~290nm), possibly due to **L4** being a single more conjugated unit.

Table 3: Electronic spectral assignments for **L4** and complexes.

compound	π-π* transitions/ λ nm (ε)	MLCT / λ nm (ε)	d-d transitions/ λ nm (ε)	Dq	B (cm^{-1})	β
L4	270(20698), 314(12581)	n/a	n/a	-	-	-
4.1 (Mn)	267(26,570), 344(15,182)	unobservable	unobservable	-	-	-
4.2 (Co)	267(30,465), 326(9,704), 344(8,865)	~350 (hidden)	~440(53) 535(15.1), >1145(11)	996	873	0.75
4.3 (Ni)	269(20,400), 336(11,300), 345(10,769)	~350 (hidden)	407(19), 556(16), 819(18), 888(23)	1126	840	0.78
4.4a*(Cu)	270(17,355),301(9034), 347(12,423),360(13,323)	~360 (shoulder) (807)	685(134)	-	-	-
4.5 (Zn)	269(40,296), 314(23,187)	n/a	n/a	-	-	-

* compound **4.4a** was used in replacement of **4.4** due to solubility issues, perchlorate ions were exchanged for hexafluorophosphate ions.

Compound **4.1**: Within the visible region there are no observable d-d transitions for the Mn(II) complex. This is typical for such compounds due to manganese having low molar extinction coefficients of the spin forbidden transitions (between 10^{-2}-10^{-1} $dm^3mol^{-1}cm^{-1}$). To observe such weak transitions, concentrations of >10M would be required. Unfortunately however, stronger concentrations of this compound were not possible due to the poorer solubility of these complexes compared to those of **L2** and **L3**.

Compound **4.2**: The visible and NIR regions of the electronic absorption spectra of compound **4.2** only reveal two of the possible three transitions expected for a typical octahedral d^7 geometry, appearing at 8,734 and 18,690 cm^{-1}, labelled ν_1 and ν_2 respectively. The three spin allowed transitions are assigned as $^4T_{2g}\leftarrow{}^4T_{1g}$, $^4A_{2g}\leftarrow{}^4T_{1g}$ and $^4T_{1g}(P)\leftarrow{}^4T_{1g}$ in increasing energy, where the second transition, $^4A_{2g}\leftarrow{}^4T_{1g}$, is known to be relatively weak compared to ν_3.[35] The third band, $^4T_{1g}(P)\leftarrow{}^4T_{1g}$, is obscured by charge-transfer and intra-ligand absorptions, however, it is possible to see the slight shoulder of this peak around 440nm. The ν_2/ν_1 ratio = 2.14 which lies nicely within the range 1.9-2.2 expected for high spin d^7 octahedral species.[35] From this information *via* the appropriate d^7 Tanabe-Sugano diagram, a tentative prediction of the Dq and B values can be calculated, giving Dq = 996 cm^{-1} and B = 840 cm^{-1} (Δ/B = 10.1). This allows the calculation of the nephelauxetic ratio which equals β = 0.75 (assuming free ion [Co^{II}], B = 1120 cm^{-1}), showing that complexation has occurred but with a relatively small amount of covalency in bonding, which is also shown in the Ni(II) complex **4.3**. Comparable results were observed for the Co(II) complex of 1,3-bis[3-(2-pyridyl)pyrazol-1-yl]propane, a similar bis-pyridyl-pyazoyl compound, which gave peaks at 9,794, 18,692 and 21,367 cm^{-1}.[36]

Compound **4.3**: The electronic absorption spectra of the Ni(II) complex reveals two distinct peaks and two extra shoulder peaks within the visible region, see figure 15. The peak pattern of this complex is very typical of an octahedral species which is also in agreement with the crystal data, which shows **4.3** to have a slightly distorted octahedral centre.[37] This allows the peaks 11,261, 12,210, 17,986 and 24,570 cm^{-1} to be assigned as follows $^3T_{2g}\leftarrow{}^3A_{2g}$, $^1Eg\leftarrow{}^3A_{2g}$ (spin forbidden), $^3T_{1g}(F)\leftarrow{}^3A_{2g}$ and $^3T_{1g}(P)\leftarrow{}^3A_{2g}$ respectively. The crystal structure of **4.3** reveals how each nickel centre has two surrounding ligands, each of which are tridentate. This represents a co-ordination sphere similar to that of octahedral nickel(II) bis-terpyridine $[Ni(terpy)_2][ClO_4]_2$ and has a visible absorption spectrum (12,600 and 19400 cm^{-1}, ν_1 and ν_2 respectively), which compares reasonably well with **4.3**.[38] Another example is that of nickel(II) bis-6-(2″-pyridylthio)-

2,2'-bipyridine $[Ni(L2)_2][(SbF_6)_2]$, another octahedral bis-tridentate system, see figure 14, which has displayed peaks at 11,493, 12,579, and 18,622 cm^{-1} in the visible region and compares very well with **4.3**, supporting the presence of an octahedral bis-ligand arrangement in solution.[39]

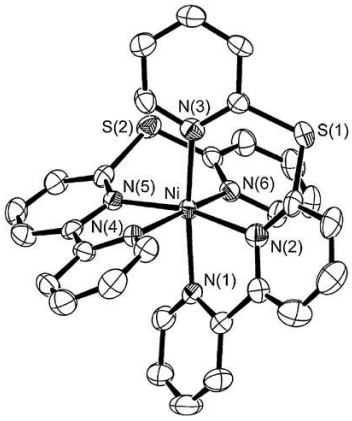

Figure 14: X-ray crystal structure of nickel(II) bis 6-(2″-pyridylthio)-2,2'-bipyridine $[Ni(\mathbf{L2})_2][(SbF_6)_2]$, showing its similarity in co-ordination with **4.3**.

The spin forbidden transition ($^1Eg \leftarrow {}^3A_{2g}$) lies very close in energy to the allowed band ν_1 and is not resolved, but may possibly be observed as a slight shoulder to higher energy of ν_1 (see Fig. 15). As a result, extensive mixing of the two states can occur probably giving rise to the relatively high intensity of the spin forbidden transition. A second spin forbidden transition can sometimes be observed between ν_2 and ν_3, however it appears be obscured in this example. A similar story is seen for ν_3 where the strong intra-ligand and charge transfer absorptions almost overwhelm this transition, leaving only a small shoulder. Using the appropriate d^8 Tanabe-Sugano diagram and knowing $\nu_{2/}\ \nu_1$ = 1.60, it is possible to approximate the *Dq* and Racah parameter, *B*, which calculate as *Dq* = 1126 cm^{-1} and *B* = 840 cm^{-1} (Δ_o/B = 13.4). This data allows the calculation of the nephelauxetic ratio β = 0.78 (assuming free ion $[Ni^{II}]$, *B* = 1080 cm^{-1}), and reveals that there is not a great deal of covalency in the M-N bonds of the complex. The high value also indicates the lack of electron delocalisation, from the metal over **L4**, and suggests **L4** is a relatively hard ligand compared to **L2** and **L3**.

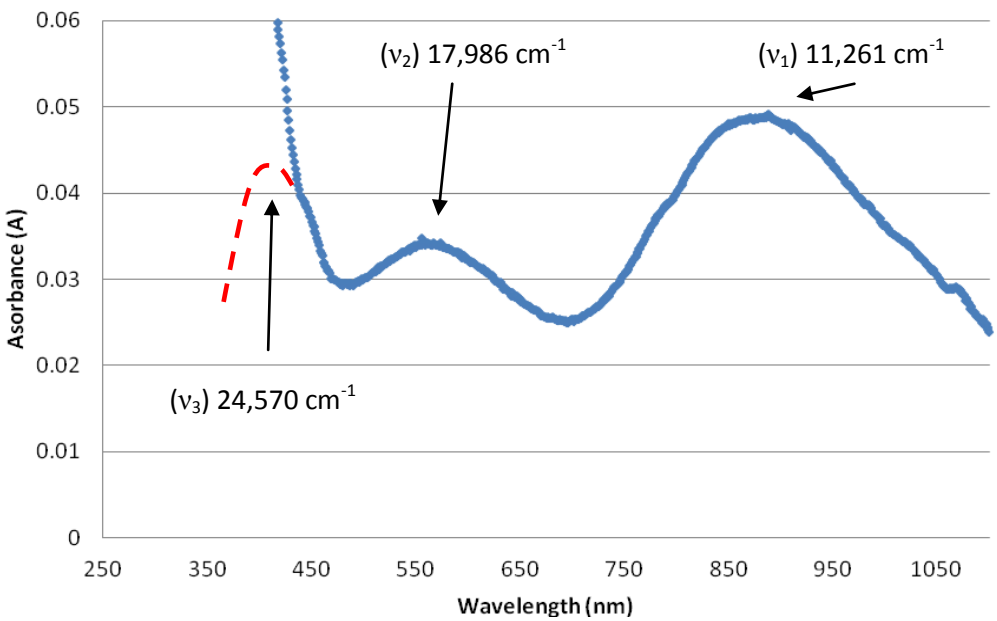

Figure 15: Visible region of the electronic absorption spectrum for compound **4.3** $[Ni(\mathbf{L4})_2][ClO_4]_2$. The dotted red lines highlight the approximate curve of any obscured shoulder peaks.

<u>Compound **4.4a**:</u> Cu(II): the visible region of the absorption spectra for the complex **4.4a** shows one broad asymmetric band, observed at 14,600 cm^{-1} (Fig. 16). The X-ray data for compound **4.4a** (Fig. 23, Page 174) reveals a six co-ordinate structure containing an N_4O_2 chromophore giving a tetragonally distorted octahedral geometry with approximate D_{4h} symmetry. The broad spectrum observed is quite typical of Cu(II) complexes with such symmetry. The elongation noted for the Cu-O bonds (approximately 0.4 Å longer than Cu-N bonds), causes a tetragonal distortion which splits the t_{2g} and e_g sub sets, theoretically producing three transitions, xz, yz→x^2-y^2 , xy→x^2-y^2 and z^2→x^2-y^2.[40] The lowest energy of these, (z^2→x^2-y^2) corresponding to the $^2A_{1g}$ ←$^2B_{1g}$ transition, is thought to occur in the NIR region. The remaining two transitions, are known to lie relatively close in energy, and are considered to be the contributing factors of the asymmetric peak observed at 14,600 cm^{-1} and are labelled as $^2B_{2g}$ ←$^2B_{1g}$ and ^2E_g ←$^2B_{1g}$.

These results compare nicely to the spectra of Cu^{II}(bis(2,2'-bipyrid-6'-yl)ketone), a similar six co-ordinate compound also with approximate D_{4h} symmetry, which gives an asymmetric peak at around 16100 cm^{-1}.[41] The higher energy maxima of Cu^{II}(bis(2,2'-bipyrid-6'-yl)ketone) compared with **4.4a** could possibly be due to the amount of Cu-O elongation present in the complex (tetragonal distortion). In the bis(2,2'-bipyrid-6'-yl)ketone example, the Cu-O bonds are up to 0.7Å longer compared to only 0.4 Å in complex **4.4**. This larger degree of elongation gives the

x^2-y^2 orbital more anti-bonding character and hence blue shifts its transitions relative to those of **4.4a**.

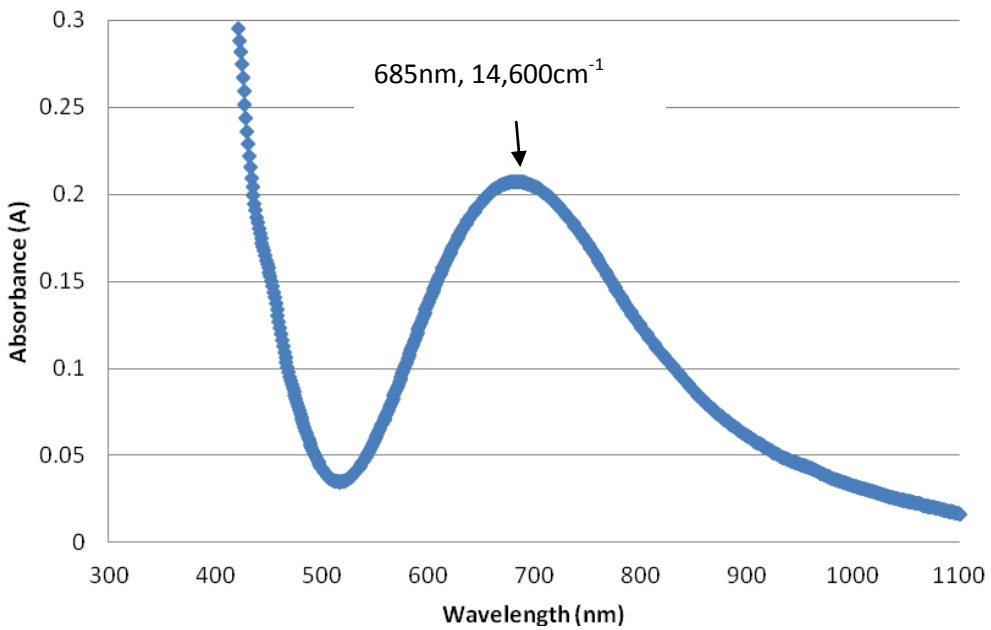

Figure 16: Visible region of the electronic absorption spectrum for compound 4.4a $[Cu^{II}(L4)(ClO_4)_2]$ in 50:50 $CHCl_3$:CH_3CN.

<u>Compound **4.5**</u>: As expected, the visible region of this d^{10} complex bares no d-d transition due to its completely filled orbitals, typical of a colourless metal complex. The only features present in this spectrum are the high energy intra-ligand π→π* transitions observed below 320nm.

4.26 X-ray crystallography

Described below is the X-ray diffraction data for the ligand **L4** and complexes **4.1-4.4** and **4.6**, with details of crystal parameters and data collection presented in Table A1 of the appendix, page 190.

Crystal structure of 6,6'bis(dimethylpyrazolyl)2,2'-Bipyridine (L4)

Colourless needle like crystals of **L4** were collected from a concentrated acetonitrile solution by slow evaporation. The compound crystallised in the monoclinic space group C2/c. In the solid state the ligand packs efficiently in a 180° twisted conformation to reduce repulsion between the lone pairs of the two pyridyl N-donors, giving it a C_2 molecular symmetry, see figure 17, with only half the molecular structure present in the asymmetric unit (Fig. 18). All C-C bond lengths (1.380(5) -1.487(5) Å), C-N bond lengths (1.333(5) - 1.432(5) Å) and N-N bonds lengths (1.353(4) Å) of **L4** are typical and compare well with those of the isostructural compound 2,2'-bis(pyrazol-1-yl)4,4'-bipyridine (C-C = 1.372(2) – 1.477(2) Å, C-N = 1.320(2) – 1.405(1) Å and N-N = 1.357(1) Å).[16]

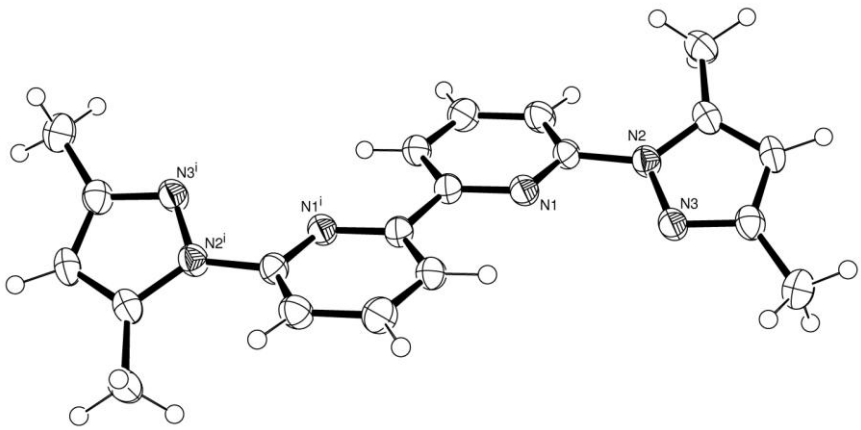

Figure 17: ORTEP Perspective view of the ligand **L4** with some atom labelling. Displacement ellipsoids are shown at 50% probability with H atoms included as spheres of arbitrary radius.

Crystal structure of $[Mn(L4)][ClO_4]_2$ (4.1)

Compound **4.1** crystallised by slow vapour diffusion of petroleum ether into a concentrated acetonitrile solution of the complex. The complex crystallises in a monoclinic $P2_1/n$ space group creating pale yellow needles suitable for data collection.

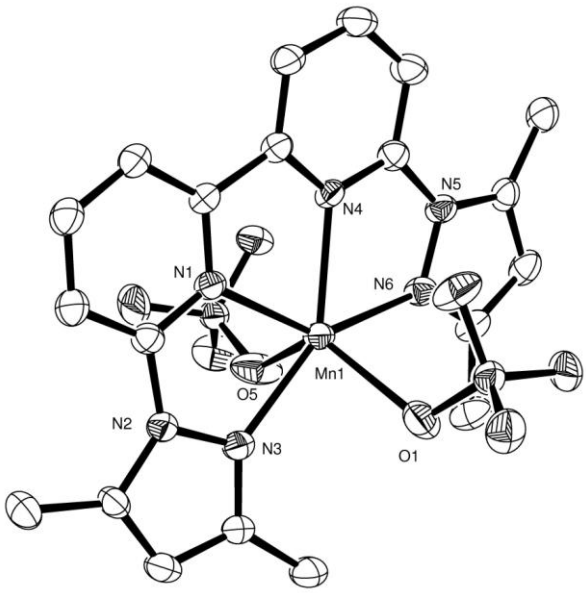

Figure 18: ORTEP Perspective view of the complex [Mn(**L4**)][ClO_4]$_2$ with the co-ordinated atoms labelled. Displacement ellipsoids are shown at 50% probability with H atoms excluded for clarity.

The asymmetric unit contains one mononuclear complex where all ligand N-donors are utilised including two perchlorate counter ions that are also involved in co-ordination. The overall molecular symmetry of the complex is C_{2V} where the manganese centre is six co-ordinate, presenting a distorted octahedral geometry constructed from two O-donors (perchlorates) and four N-donors (two pyridyl and two pyrazolyl), see Figure 18. Restrictions in the ligand framework appear to prevent adequate wrapping of the N-donors around the equatorial plane of the complex and cause the distorted effect. As a result the N3-Mn1-N6 angle becomes 149.46 (9) degrees which is much larger than the ideal 90° in a perfect octahedron. To compensate, the less efficient orbital overlap from this restriction, the two 'axial' donors (perchlorates) bend towards each other reducing the O1-Mn1-O5 co-ordination angle to 121.46(10)° (Fig. 19).

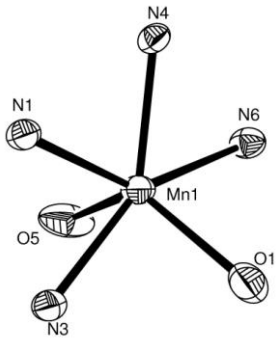

Figure 19: View of complex core showing only the co-ordinating atoms. Displacement ellipsoids are shown at 50% probability.

The octahedral distortion of the manganese centre is thought to be increased due to the relatively large ionic radius of Mn(II), compared to other 3d transition metals studied in this chapter. The Mn-N pyridine bonds are noted to be longer than those to the pyrazoles, however, only by a mean distance of 0.03 Å. The Mn-N bond lengths range from 2.216(2) to 2.267(2) Å, and fall within the range observed for comparable complexes. For example, the complex [Mn(DPP)$(NCS)_2$] (DPP = 2-(3,5-dimethyl-1H-pyrazol-1-yl)-1,10-phenanthroline) which has been found to have Mn-N bond lengths ranging from 2.172(6) to 2.273(6) Å.[42] The relatively large radius of Mn(II) is thought to prevent closer bonding to the pyridine moieties, which consequently reduces the pyridine-pyrazole bite angles (average angle = 69.98°) compared to those of the analogous cobalt and copper complexes (compounds **4.2** and **4.4**), which have average bite angles of 74.3° and 78.8° respectively.

Table 4: Selected bond Distances (Å) and Angles (°) for complex **4.1**

Bond	Length (Å)	Bond	Length (Å)
Mn1-N1	2.267 (2)	Mn1-N6	2.216 (2)
Mn1-N3	2.250 (2)	Mn1-O1	2.238 (2)
Mn1-N4	2.257 (2)	Mn1-O5	2.208 (2)
Bonds	**Angle (°)**	**Bonds**	**Angle (°)**
N1- Mn1 -N3	69.69 (8)	N3- Mn1 –O5	81.07 (9)
N1- Mn1 -N4	70.61 (8)	N4- Mn1-N6	70.28 (8)
N1- Mn1 -N6	140.69 (9)	N4- Mn1-O1	119.57 (8)
N1- Mn1 –O1	120.01 (9)	N4- Mn1-O5	110.25 (9)
N1- Mn1 –O5	103.52 (10)	N6- Mn1-O1	83.36 (9)
N3- Mn1 -N4	140.25 (9)	N6- Mn1-O5	86.37 (10)
N3- Mn1-N6	149.46 (9)	O1- Mn1-O5	121.46 (10)
N3- Mn1-O1	79.77 (9)		

Crystal structure of $[Co(L4)(CH_3CN)_2][ClO_4]_2$ (4.2)

The complex $[Co(\mathbf{L4})(CH_3CN)_2][ClO_4]_2$ produced dark yellow crystals suitable for X-ray crystallographic data collection. These were obtained *via* vapour diffusion of diethyl ether into a concentrated acetonitrile solution of **L4.** The compound crystallised in the monoclinic space group $P2_1/n$ with the asymmetric unit containing one complete complex with two co-ordinating acetonitrile molecules and two unco-ordinating perchlorate counter ions. The cobalt adopts a six co-ordinate system possessing a slightly distorted octahedral geometry (Fig. 20+21) with the molecular symme

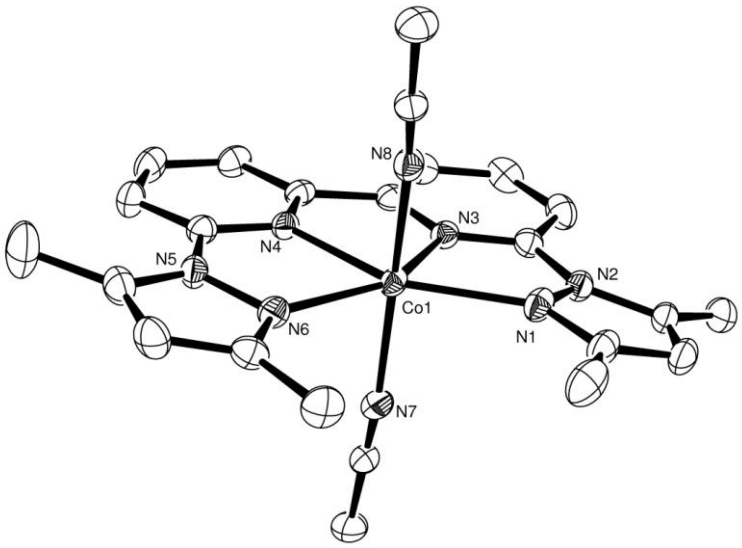

Figure 20: ORTEP Perspective view of the complex $[Co(\mathbf{L4})(CH_3CN)_2][ClO_4]_2$ with the co-ordinated atoms labelled. Displacement ellipsoids are shown at 50% probability with perchlorate counter ions and H atoms excluded for clarity.

The metal ion is equatorially bound to all of the available N-donors of **L4**, and axially with two acetonitrile molecules. Interestingly, compound **4.2** is the only complex in this series that utilises two acetonitrile solvent donors instead of the two perchlorate molecules which is seen in compounds **4.1**, **4.4** and **4.6**. The angle between the axial donors is much more ideal (170.87°) compared to that of the manganese complex which has an angle of 121.5°. Also it is important to note that the pyridyl-pyrazole bite angle to the Co(II) centre (average 74.26(6)°) is the second largest observed within its analogous complexes. The Co-N bond lengths range from 2.1074(16) Å to 2.1714(16) Å in which the shortest co-ordinative bonds, from the two pyridines, are on average only 0.0461(2) Å shorter than those to the pyrazole donors. This feature is also seen in the Cu(II) complex **4.4** however, not in the manganese example. This is possibly due to

their relatively small ionic radii allowing them to fit further into the planar cavity and bond closer to the pyridine donors as a result. The Co(II) co-ordinative bond lengths to a similarly constructed ligand bis(2,2'-bipyrid-6'-yl)ketone, which facilitates four pyridyl units, compares well to those observed for compound **4.2** (Co-N bonds range 2.097(5)-2.130(5) Å).[43] It is also noted in the bis(2,2'-bipyrid-6'-yl)ketone example that co-ordinative bonds to the bridged pyridyl moieties present shorter bonds than those of the appending pyridyls, a feature also seen in **4.2**. However, the difference in bond lengths between the two sets of donor units is larger for compound **4.2**. This is likely a result of reducing the bridge length (from one carbon to zero) and therefore reducing flexibility in the ligand framework, altering the donating angle of the nitrogen groups.

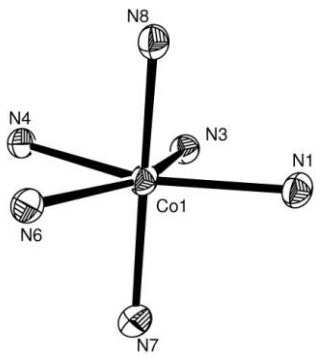

Figure 21: View of complex core showing only the co-ordinating atoms. Displacement ellipsoids are shown at 50% probability.

Table 5: Selected bond Distances (Å) and Angles (°) for complex **4.2**

Bond	Length (Å)	Bond	Length (Å)
Co1-N1	2.1714 (16)	Co1-N6	2.1371 (16)
Co1-N3	2.1074 (16)	Co1-N7	2.1133 (17)
Co1-N4	2.1090 (15)	Co1-N8	2.1219 (17)
Bonds	**Angle (°)**	**Bonds**	**Angle (°)**
N1- Co1 -N3	74.25 (6)	N3- Co1 –N8	99.87 (6)
N1- Co1 -N4	148.38 (7)	N4- Co1-N6	74.26 (6)
N1- Co1 -N6	137.33 (6)	N4- Co1-N7	93.78 (6)
N1- Co1 -N7	89.66 (6)	N4- Co1-N8	91.33 (6)
N1- Co1 –N8	89.95 (6)	N6- Co1-N7	87.87 (6)
N3- Co1 -N4	74.41 (6)	N6- Co1-N8	86.24 (6)
N3- Co1-N6	148.18 (6)	N7- Co1-N8	170.87 (6)
N3- Co1-N7	88.80 (6)		

Crystal structure of $[Ni(L4)_2][ClO_4]_2$ (4.3)

Crystals suitable for X-ray crystallographic studies of the complex $[Ni(\mathbf{L4})_2][(ClO_4)_2]$ were obtained by vapour diffusion of 40/60 petroleum ether into a concentrated chloroform/DMF (50/50) solution of the complex, yielding greyish-blue needle like crystals. The complex crystallised in a P-1 space group with the asymmetric unit containing one complex, two perchlorate counter ions and a petrol solvent molecule. The Ni(II) centre lies close to octahedral in geometry, co-ordinating to six nitrogens from two ligands, where the bond lengths and angles are presented in Table 6. Both ligands co-ordinate *via* only three nitrogens, each leaving a pendent pyrazole moiety, which twists perpendicular to the rest of the ligand plane, mainly to reduce steric interactions. Like the other complexes in this series, **4.3** was made in a 1:1 ligand:metal reaction ratio, however in the solid state, Ni(II) seems to be more stable in a 2:1 conformation giving the structure seen in Figure 22. This structure type is most likely to have occurred due to the different solvent system needed in order to obtain suitable crystals, where the 2:1 system crystallised more readily than the expected 1:1 complex in a chloroform/DMF environment, and could not be explained through conventional arguments of sterics, electronics or cation size.

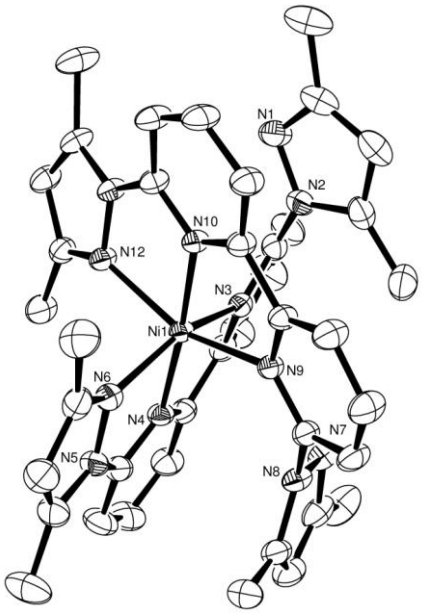

Figure 23: ORTEP Perspective view of the complex $[Ni(\mathbf{L4})_2][ClO_4]_2$. Showing how two ligands surround one Ni(II) centre with the co-ordinated atoms labelled. Displacement ellipsoids are shown at 50% probability with two perchlorate counter ions, a petrol molecule and H atoms excluded for clarity.

The Ni-N pyridyl bonds range from 2.004(2) Å to 2.012(2)Å and are comparable, although slightly shorter, to the pyridyl bonds of the complex [Ni(dpphen)$(NCS)_2$] which has an equivalent bond length of 2.0430(17) Å.[29] In comparison, the Ni-pyrazolyl bond lengths (2.107(2) to 2.190(2) Å) are found to be much shorter than the same bonds measured in [Ni(dpphen)$(NCS)_2$], which has a Ni-N bond length of 2.3570(19) Å.[29] This is most likely due to the **L4** only acting as a tridentate donor, compared to dpphen which is tetradentate, and is therefore likely to experience more steric strain in trying to gain the best donation angle. The two shorter bonds from N4 and N10 (pyridyl donors) are the only set of *trans*-donors that are not constrained to same ligand allowing them to co-ordinate closer to the metal centre, creating a compression along the z-axis. This is because bending the ligand to allow the equatorial nitrogen donors to bind more closely is considered far more unfavourable.

Table 6: Selected bond Distances (Å) and Angles (°) for complex **4.3**

Bond	Length (Å)	Bond	Length (Å)
Ni1-N3	2.178 (2)	Ni1-N9	2.190 (2)
Ni1-N4	2.004 (2)	Ni1-N10	2.012 (2)
Ni1-N6	2.107 (2)	Ni1-N12	2.129 (2)
Bonds	**Angle (°)**	**Bonds**	**Angle (°)**
N3-Ni1-N4	77.69 (9)	N4- Ni1-N12	98.99 (9)
N3-Ni1 –N6	154.82 (10)	N6- Ni1-N9	86.51 (9)
N3- Ni1-N9	101.84 (9)	N6- Ni1-N10	101.34 (10)
N3- Ni1-N10	103.68 (9)	N6- Ni1-N12	97.04 (10)
N3- Ni1-N12	85.72 (9)	N9- Ni1-N10	77.00 (9)
N4- Ni1-N6	77.16 (10)	N9- Ni1-N12	154.25 (9)
N4- Ni1-N9	106.65 (9)	N10- Ni1-N12	77.30 (9)
N4- Ni1-N10	175.86 (10)		

Crystal structure of [Cu(L4)]$[ClO_4]_2$ (4.4)

Bright green needle-like crystals for the complex [Cu(**L4**)]$[ClO_4]_2$ were collected by vapour diffusion of diethyl ether into a concentrated acetonitrile solution of the complex. The complex crystallised in a triclinic P-1 space group with the asymmetric unit containing one complex including two co-ordinating perchlorate counter ions. The Cu(II) complex forms in a 1:1 ligand to metal ratio with all four possible ligand nitrogen donors co-ordinating to the metal centre. As there are no more available ligand donors, the two perchlorate counterions bond to the Cu(II)

centre in the axial positions allowing the metal centre to fulfil a hexa-coordinated geometry. The overall molecular geometry is close to C_{2v} and the co-ordination of Cu(II) forms a trigonally distorted octahedral geometry, where the co-ordinated counter ions form the stretched z-axis, indicative of d^9 systems (Fig. 23+24).

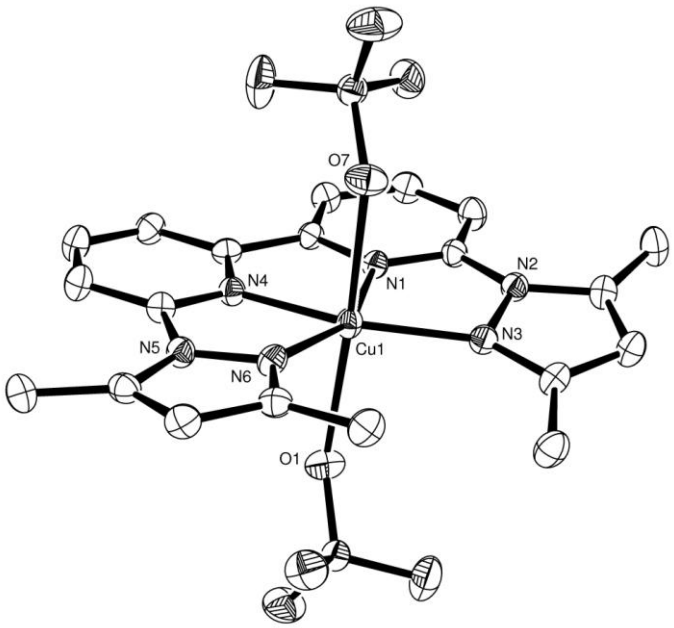

Figure 23: ORTEP Perspective view of the complex [Cu(**L4**)][ClO_4]$_2$ with the co-ordinated atoms labelled. Displacement ellipsoids are shown at 50% probability with H atoms excluded for clarity.

Copper(II) is the smallest cation to form this type of structure (1:1 ligand to metal ratio) amongst the metals analysed. As a result, the copper fits further into the planar cavity giving it the smallest M-pyridine bond lengths (1.970(2) Å) and the largest pyridyl-pyrazolyl bite angle (78.8°) compared to analogous complexes in this chapter. The angle between axial donors (O1-Cu1-O7 = 172.87°) is also the largest seen in this series. Again, as observed in compound **4.2**, the pyridyl donors exhibit the shorter co-ordinative bonds (1.968(2) and 1.971(2) Å) compared to those of the pyrazoles (2.061(2) and 2.046(2) Å). This pattern of bond lengths is also observed in the Cu(II) complex of bis(2,2'-bipyrid-6'-yl)ketone, where the pyridines closer to the bridging ketone group also exhibit shorter bonds (1.968(3) Å compared to 1.991(3) Å) however, to a much smaller extent.[43] The Cu-N bond lengths of **4.4** also compare well to that of di-μ-bromo-bis{[2,6-bis(pyrazol-1-yl)pyridine]perchloratocopper(II)} ($Cu_2(bPP)_2$) which also has a tetragonally stretched copper centre (Cu-N bond range of 1.962(6) - 2.016(6) Å).[44]

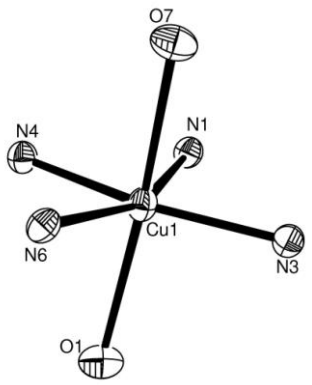

Figure 24: View of complex core showing only the co-ordinating atoms.
Displacement ellipsoids are shown at 50% probability.

Also noted for $Cu_2(bPP)_2$ is the Cu-perchlorate bond length, that also reside on the trigonally stretched axis due to Jahn Tellar distortion (average bond length = 2.515(6) Å),[44] which correlate reasonably with those of **4.4** (2.421(2) Å). However, in the bis(2,2'-bipyrid-6'-yl)ketone example, these equivalent bonds are larger again (average bond length 2.628(3) Å).[43]

Table 6 : Selected bond Distances (Å) and Angles (°) for complex **4.4**

Bond	Length (Å)	Bond	Length (Å)
Cu1-N1	1.968 (2)	Cu1-N6	2.046 (2)
Cu1-N3	2.061 (2)	Cu1-O1	2.401 (2)
Cu1-N4	1.971 (2)	Cu1-O7	2.441 (2)
Bonds	**Angle (°)**	**Bonds**	**Angle (°)**
N1-Cu1-N3	78.64 (9)	N3- Cu1-O7	91.69 (8)
N1-Cu1 -N4	78.68 (9)	N4- Cu1-N6	79.01 (9)
N1- Cu1-N6	156.65 (9)	N4- Cu1-O1	87.88 (9)
N1- Cu1-O1	97.73 (9)	N4- Cu1-O7	91.70 (9)
N1- Cu1-O7	89.15 (9)	N6- Cu1-O1	88.24 (9)
N3- Cu1-N4	157.01 (9)	N6- Cu1-O7	84.69 (9)
N3- Cu1-N6	123.95 (9)	O1- Cu1-O7	172.87 (8)
N3- Cu1-O1	91.45 (9)		

Crystal structure of $[Hg(L4)][ClO_4]_2$ (4.6)

Colourless crystals of complex $[Hg(\mathbf{L4})][(ClO_4)_2]$ were grown *via* vapour diffusion, using a concentrated acetonitrile solution of the complex and diethyl ether. The compound crystallised in the monoclinic $P2_1/n$ space group with the asymmetric unit containing one complex with two co-ordinating perchlorate counter ions. The d^{10} Hg^{II} ion has no stereochemical preference, and typically, the geometry follows the most stable steric conformation allowed by the ligand. The asymmetric unit contains one discrete complex with two co-ordinating perchlorate counter ions. The overall molecular symmetry of the structure is C_{2v} with the molecular structure of the mercury complex shown in Figure 25. The geometry of the Hg(II) centre is best described as a distorted octahedral (Fig. 26) and resembles a geometry similar to the Mn(II) complex (compound **4.1**), where the co-ordination sphere consists of two axial O-donors and four equatorial N-donors. The Hg-N bond lengths range from 2.148(4) to 2.429(4) Å lying within an acceptable range on comparison to similar complexes. For example, the complex $[MeHg(Npypyz)]NO_3$ (Npypyz = 1-(2-pyridyl)pyrazole) has Hg-N bonds ranging 2.21(3)-2.61(5) Å and also the complex $Hg(L^{oPh})[ClO_4]_2$ (L^{oPh} = [1,2-bis(1-methyl-3-(2-pyridyl)pyrazole)benzene]) by Ward *et. al.*, has bonds ranging 2.157(4)-2.458(5) Å.[45,24]

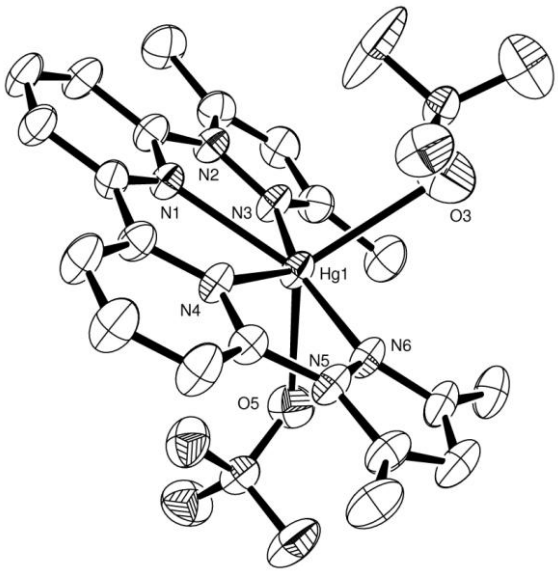

Figure 25: ORTEP Perspective view of the complex $[Hg(\mathbf{L4})][ClO_4]_2$ with the co-ordinated atoms labelled. Displacement ellipsoids are shown at 50% probability with H atoms excluded for clarity.

Although the overall Hg-N bond lengths compare well, compound **4.6** is the only structure observed where the Hg-pyridyl bonds (Hg-N_{pyr} average = 2.428(4) Å) are longer than those to the pyrazoles (Hg-N_{pyz} average = 2.155(4) Å). In the case of compound **4.6** this is likely to be a result of the large ionic radius of Hg(II), preventing the cation from sitting further within the planar cavity as discussed previously for complex **4.1**. It must also be noted that the Hg-O bonds in **4.6** are significantly longer (average = 2.678(5) Å) than those to N-donors, which is a common feature seen amongst co-ordinating perchlorates.[24]

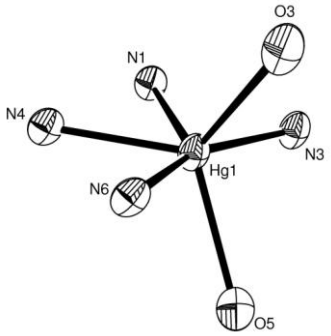

Figure 26: View of complex core showing only the co-ordinating atoms. Displacement ellipsoids are shown at 50% probability.

The bite angles N1-Hg1-N3 and N4-Hg1-N6 where found to be 68.73(15) and 69.50(16) degrees respectively, which are the smallest observed within this series of complexes and is indicative of the size of mercury ions. This also relates to the angle between the axial donors (O3-Hg1-O5 = 119.17(16)°) which is even smaller than that observed in **4.1** (121.46°), showing **4.6** to have a more distorted geometry.

Table 7: Selected bond Distances (Å) and Angles (°) for complex **4.6**			
Bond	Length (Å)	Bond	Length (Å)
Hg1-N1	2.429 (4)	Hg1-N6	2.148 (4)
Hg1-N3	2.162 (4)	Hg1-O3	2.731 (5)
Hg1-N4	2.427 (4)	Hg1-O5	2.625 (5)
Bonds	Angle (°)	Bonds	Angle (°)
N1- Hg1 -N3	68.73 (15)	N3- Hg1 –O5	85.24 (16)
N1- Hg1 -N4	65.31 (14)	N4- Hg1-N6	69.50 (16)
N1- Hg1 -N6	134.75 (15)	N4- Hg1-O3	115.72 (16)
N1- Hg1 –O3	113.12 (15)	N4- Hg1-O5	114.19 (15)
N1- Hg1 –O5	117.88 (15)	N6- Hg1-O3	84.29 (16)
N3- Hg1 -N4	133.98 (16)	N6- Hg1-O5	82.60 (16)
N3- Hg1-N6	156.51 (17)	O3- Hg1-O5	119.17 (16)
N3- Hg1-O3	84.25 (16)		

4.27 Magnetic moments

The magnetic moments of all of the potentially paramagnetic complexes have been collected and are shown in Table 8. The results were determined at room temperature by the Evans method using ^{1}H-NMR spectroscopy and d_3-acetonitrile solutions of the complexes. Solubility in this set of complexes was problematic, and in the case of **4.4**, a suitable solution could not be obtained. As a result, the perchlorate counter ions of **4.4** were exchanged for two hexafluorophosphate anions, by reaction with excess NH_4PF_6 in water, giving the same desired copper product **4.4a** but with more solubility and thus allowing a more accurate measurement.

Table 8: Showing predicted and calculated magnetic moments for all non-d^{10} metals and their respective spin state.				
complex	Number of Unpaired electrons	Theoretical moment	Observed Magnetic moment μ_B	High spin/ low spin
4.3 [Ni(II)]	2	2.83	2.70	n/a
4.4a [Cu(II)]	1	1.73	1.15	n/a
4.2 [Co(II)]	1 or 3	1.73 or 3.87	3.98	HS
4.1 [Mn(II)]	1 or 5	1.73 or 5.91	5.24	HS

The results show that the ligand **L4** must impose a weak field on the complexes due to the high spin states of compounds **4.1** and **4.2**. This is a feature seen throughout the series of ligands using the basic pyridine and pyrazole moieties.

4.28 Conclusion

In conclusion, the solid and solution based structural properties of **L4** and its complexes with Mn(II), Co(II), Ni(II), Cu(II), Zn(II) and Hg(II) have been characterized and their co-ordination chemistry has been studied. Overall, **L4** readily forms complexes with transition metals, although, poor solubility of the free ligand required mixtures of solvents to achieve pure compounds. The high spin state of complexes **4.1** and **4.2** reveals the weak field nature of **L4**, a property previously observed in **L2** and **L3**.

From the observed data, **L4** generally forms mononuclear complexes, as expected from the stoichiometry used. All four N-donors of **L4** are involved in co-ordination in an equatorial fashion around the metal centre, where the axial donors are fulfilled by bound perchlorate counter ions (with exception to **4.2** which utilises two acetonitrile molecules). This gives the metal centres an octahedral geometry, where in the case of the larger cations Mn(II) and Hg(II), they become strongly distorted. An exception to this was found for the Ni(II) complex (**4.3**) where the crystal data reveals a ratio of two ligands per Ni(II) centre. This complex still forms an octahedral type geometry using only three N-donors per ligand leaving two pyrazoles pendent and is considered a result of faster crystallisation within a different solvent system.

The electronic absorption studies of these compounds (**4.1**-**4.4**) confirm the octahedral or near octahedral geometry of these complexes in solution. In the cases of Co(II) and Ni(II), Dq and β values could be calculated, Dq = 996 cm^{-1} and 1126 cm^{-1} and β = 0.74 and 0.78 respectively. These high nephelauxetic ratio values reveal the lack of covalency within the complex bonding, suggesting that they may not be as stable as complexes in previous chapters. Donors in this ligand have difficult donation angles towards a metal centre which is probably reducing orbital overlap.

In solid state the 1:1 complexes (**4.1**, **4.2**, **4.4** and **4.6**) show a trend between relative octahedral distortion, bite angles, pyridyl bond lengths and the relative ionic radii of the cation involved. The pattern suggests that the smaller ions e.g. copper(II) can co-ordinate closer to the pyridyl units within the planar cavity of the ligand. This in turn, produces larger bite angles to the pyridyl-pyrazole moieties and also larger angles between axial donors. which results in metal geometries being closer to an ideal octahedron, data displayed in Table 9.

Table. 9: Comparison of cation radius with various bond lengths and angles within complex.					
complex	Ionic size, Å[46]	Pyr-pyz bite angle, average °	Angle between axial donors, °	M-N pyridine bond length, average Å	M-N pyrazole bond length, average Å
4.4 (Cu(II))	73	78.8(9)	172.87(8)	1.970(2)	2.054(2)
4.2 (Co(II))	74.5(HS)	74.26(6)	170.87(6)	2.1082(16)	2.1543(16)
4.1 (Mn(II))	83	69.98(8)	121.46(10)	2.262(2)	2.233(2)
4.6 (Hg(II))	102	69.12(16)	119.17(16)	2.428(4)	2.155(4)

4.3 Experimental

General

NMR spectra were typically measured using a Bruker Av-500 Plus, Bruker AM-400 or Bruker Av-250 FT-NMR spectrometers. Electrospray (ES) and high resolution (HR) mass spectra were obtained on a Waters LCT Premier XE (oa-TOF) mass spectrometer. All infrared spectra were measured on a Jasco FT-IR spectrophotometer, where each compound was pressed into a disk using an excess of dried KBr. UV-Vis absorption spectra were run using HPLC grade acetonitrile on a Perkin Elmer Lambda 2S UV-Vis spectrometer typically between 200-1100nm (optical path length 1.0 cm). Elemental analyses were carried out by MEDAC LTD analytical and chemical consultancy services or elemental analysis service, LONDON metropolitan university.

6,6'-Dibromo-2,2'-Bipyridine (**S1**)

2,6-dibromopyridine (5g, 21.1mmol) was dissolved in dried degassed diethyl ether (80ml) and the resulting mixture was cooled to 195k (-78°C) with vigorous stirring. A solution of n-BuLi (7.26ml, 11.6mmol, 1.6M in hexane) was added dropwise via syringe to the cooled solution. The mixture was kept stirring at -78°C for 4h before the solution was slowly allowed to warm to ambient temperature over night to allow homo-coupling. The solution was quenched with 10% HCl until acidic (pH 2-4). The resulting mixture was basified (pH 9-10) with 10% aqueous K_2CO_3, and the crude product partitioned between $CHCl_3$ and water. The aqueous layer was washed twice with $CHCl_3$ and the organic layers were combined, dried over anhydrous $MgSO_4$ and the solvent was removed under reduced pressure. The crude product was purified by column chromatography in 20/80 Hexane/DCM to give the pure product as a white solid (0.96g, 29%). ^{1}H-NMR ($CDCl_3$; 400MHz): δ_H 8.31(d, 2H, J=7.7Hz, *CH*), 7.59(t, 2H, J=7.8Hz, *CH*), 7.43(d, 2H, J=7.8Hz, *CH*).

6,6'-Dihydrazino-2,2'-Bipyridine (**S2**)

(**S1**) 6,6'-dibromo-2,2'-Bipyridine (1g, 3.2mmol) was added directly to degassed hydrazine monohydrate (20ml) solvent. The solid was dissolved by stirring and heating to 130°C which was left to reflux for 14h under a nitrogen atmosphere. The yellow solution was then allowed to cool to room temperature forming a precipitate. The solid was filtered off and the filtrate

reduced to dryness *in vacuo* giving a sticky solid. This solid was then washed in distilled water (2x20ml) and filtered leaving a pale solid which was further washed in ethanol (15ml) and then finally in a minimum of chloroform (5ml) giving the product in high purity (0.69g, 56%).^{1}H-NMR (DMSO; 250MHz): δ_H 7.63(m, 4H, J=7.7Hz, *CH*), 7.47(s, 4H, *NH$_2$*), 6.76(d, 2H,J=7.5Hz, *CH*). LRMS (ES-MS) *m/z* calcd. 239.102; exp. 239.10 $[C_{10}H_{12}N_6Na]^+$, (100%); calcd. 217.12 ; exp. 217.12 $[C_{10}H_{13}N_6]^+$, (15%).

6,6'-Bis(dimethylpyrazole)-2,2'-Bipyridine (**L4**)

(**S2**) 6,6'-dihydrazino-2,2'-Bipyridine (0.4g, 1.85mmol) was stirred into an ethanol:methanol (2:1) solvent (20ml) and was heated to roughly 60°C until the solid had dissolved. Pentane-2,4-dione (408mg, 4.07mmol) was added to the hot solution followed by refluxing for a minimum of 4h. The reaction was then allowed to cool to room temperature with further cooling at 0°C for 1h yielding an off-white precipitate. The solid was filtered and washed with a minimum of diethyl ether giving the product in high purity (0.54g, 85%). ^{1}H-NMR ($CDCl_3$; 400MHz): δ_H 8.14(d, 2H, J=7.0Hz, CH), 7.86(m, 4H, J=7.2Hz, CH), 5.99(s, 2H, CH), 2.76(s, 6H, CH_3), 2.27(s, 6H, CH_3). ^{13}C-NMR ($CDCl_3$; 100MHz): δ_C 153.74(C), 153.08(C), 149.94(C), 141.39(C), 139.29(CH), 117.69(CH), 115.68(CH), 109.27(CH), 15.28(CH_3), 13.71(CH_3). HRMS (EI-MS) *m/z* calcd. 344.1749; exp. 344.1749 $[C_{20}H_{20}N_6]^-$, (85%). FT-IR (KBr/cm^{-1}) ν = 3113w, 2976m, 2966m, 2917m, 1590s, 1566br+s, 1479s, 1441br+s, 1431br+s, 1419m, 1393m, 1381s, 1362s, 1287m, 1148w, 1101m, 1077m, 1045m, 988m, 972s, 797s, 775m, 732w, 703s, 635m, 591w. λ_{max}, nm, (εM, M^{-1}cm^{-1}) in CH_3CN:$CHCl_3$ (1:1): 270(20698), 314(12581). Found: C 67.21; H 5.67; N 23.63 (%) $C_{20}H_{20}N_6.0.5H_2O$ Requires: C 67.95; H 5.99; N 23.79 (%).

Mn(II) 6,6'-bis(dimethylpyrazole)-2,2'-Bipyridine, $[MnC_{20}H_{20}N_6][2ClO_4]$ (**4.1**):

Manganese(II) perchlorate hexahydrate $[Mn(ClO_4)_2.6H_2O]$(49mg, 1.45x10^{-4}mol) was dissolved in THF (2ml) and was added dropwise to a warm solution of **L4** (50.0mg, 1.45x10^{-4}mol) in $CHCl_3$ (4ml). Addition of the manganese immediately produced a pale yellow precipitate which was filtered and dried using diethyl ether (2ml). The complex was purified by crystallisation from acetonitrile and vapour diffusion of petroleum ether giving pale yellow crystals of high purity (73mg, 74%). HRMS (ES-MS) *m/z* calcd. 498.0615; exp. 498.0631 $[MnC_{20}H_{20}N_6[ClO_4]]^+$, (40%). FT-IR (KBr/cm^{-1}) ν = 3531br+m, 3464br, 3115m, 3091m, 2994m, 2924m, 1598s, 1582m, 1562s, 1482.0s, 1445s, 1419s, 1382m, 1359s, 1324m, 1305m, 1264m, 1145br+s, 1110br+s, 1088br+s,

1033m, 1001m, 912w, 820w, 798s, 780m, 709m, 675m, 637s, 626s. λ_{max}, nm, (εM, $M^{-1}cm^{-1}$) in CH_3CN: 267(26,570), 344(15,182). Found: C 39.82; H 3.41; N 13.93 (%) $MnC_{20}H_{20}N_6(ClO_4)_2$. Requires: C 40.14; H 3.37; N 14.05 (%). Magnetic moment (Evans method, 293K, Acetonitrile): μ_{eff} = 5.24μ_B.

Co(II) 6,6'-bis(dimethylpyrazole)-2,2'-Bipyridine, $[CoC_{20}H_{20}N_6][2ClO_4]$ (**4.2**):

Cobalt(II) perchlorate hexahydrate $[Co(ClO_4)_2.6H_2O]$(53mg, 1.45x10^{-4}mol) was dissolved in acetonitrile (2ml) and added dropwise to a warm solution of **L4** (50.0mg, 1.45x10^{-4}mol) in a $CHCl_3$:CH_3CN (50:50) solvent (4ml). The mixture was stirred for 24h and allowed to cool to ambient conditions yielding a mustard yellow solution. The solution was then filtered through celite and diethyl ether was added to the filtrate precipitating a dull yellow solid. The solid was then filtered under gravity and dried with 3ml of diethyl ether giving the desired complex in high purity (77g, 88%). HRMS (ES-MS) *m/z* calcd. 502.0567; exp. 502.0550 $[CoC_{20}H_{20}N_6[ClO_4]]^+$, (97%), calcd. 201.5541 ; exp. 201.5538 $[CoC_{20}H_{20}N_6]^{2+}$, (12%). FT-IR (KBr/cm^{-1}) ν = 3399br, 3134m, 3111m, 1603s, 1584s, 1566s, 1486s, 1449s, 1427s, 1387s, 1366s, 1333m, 1310m, 1273w, 1122br+s, 1083s, 1036s, 1024s, 991s, 916m, 795s, 710m, 616s. λ_{max}, nm, (εM, $M^{-1}cm^{-1}$) in CH_3CN: 267(30,465), 326(9,704), 344(8,865), 555(15.1), 650(9), 762(6.8). Found: C 39.77; H 3.56; N 13.98 (%) $CoC_{20}H_{20}N_6(ClO_4)_2$. Requires: C 39.87; H 3.35; N 13.96 (%). Magnetic moment (Evans method, 293K, Acetonitrile): μ_{eff} = 3.98μ_B.

Ni(II) 6,6'-bis(dimethylpyrazole)-2,2'-Bipyridine, $[NiC_{20}H_{20}N_6][2ClO_4]$ (**4.3**):

Nickel (II) perchlorate hexahydrate $[Ni(ClO_4)_2.6H_2O]$(29.7mg, 8.13x10^{-5}mol) was dissolved in acetonitrile (4ml) and was added dropwise to a stirring solution of **L4** (28mg, 8.13x10^{-5}mol) in acetonitrile: $CHCl_3$ (50:50) solvent (4ml). The resulting pale blue solution was stirred for 24h in ambient conditions. Diethyl ether (8ml) was added to the solution yielding a precipitate. The green/blue solid was then filtered and dried. A portion of the solid was dissolved in DMF: $CHCl_3$ (50:50) (4ml) and the solution filtered through celite. Vapour diffusion of diethyl ether into the solution yielded greyish-blue crystals of the desired complex in high purity (49mg, 86%). HRMS (ES-MS) *m/z* calcd. 201.0551; exp. 201.0514 $[NiC_{20}H_{20}N_6]^{2+}$ (100%), calcd. 501.0588 ; exp. 501.0593 $[NiC_{20}H_{20}N_6[ClO_4]]^+$, (80%). FT-IR (KBr/$cm^{-1}$) ν = 3399br, 3141m, 3098m, 1605s, 1589s, 1570s, 1492s, 1452s, 1429s, 1387s, 1366s, 1335s, 1314m, 1280m, 1197m, 1183m, 1129br+s, 1037s, 994s, 928m, 854w, 808m, 794s, 760w, 710m, 688m, 651m, 625s. λ_{max}, nm, (εM, $M^{-1}cm^{-1}$)

in CH_3CN: 268.78 (20401.5), 335.50 (11300.2), 556.06 (16.02), 887.93 (22.65). Found: C 39.31; H 3.19; N 13.82 (%) $NiC_{20}H_{20}N_6(ClO_4)_2.0.5H_2O$ Requires: C 39.30; H 3.47; N 13.76 (%). Magnetic moment (Evans method, 293K, Acetonitrile): μ_{eff} = 2.70μ_B.

Cu(II) 6,6'-bis(dimethylpyrazole)-2,2'-Bipyridine, $[CuC_{20}H_{20}N_6][2ClO_4]$ (**4.4**):

Copper(II) perchlorate hexahydrate $[Cu(ClO_4)_2.6H_2O]$(49.6mg, 1.34x10^{-4}mol) was dissolved in THF (4ml) and added slowly to a stirring solution of **L4** (46.1mg, 1.34x10^{-4}mol) in warm $CHCl_3$ (5ml). The immediate green precipitate was allowed to cool and stir for 3h before filtering. The dried green solid was dissolved in a minimum of DMF (3ml) and filtered through celite. Vapour diffusion of diethyl ether into the filtrate yielded bright green crystals of high purity (54.4mg, 67%). HRMS (ES-MS) *m/z* calcd. 203.5523; exp. 203.5497 $[CuC_{20}H_{20}N_6]^{2+}$, (50%), calcd. 506.0531 ; exp. 506.0530 $[CuC_{20}H_{20}N_6[ClO_4]]^+$, (40%). FT-IR (KBr/cm^{-1}) ν = 3135m, 3110m, 3090m, 1607s, 1584s, 1571s, 1489br+s, 1475s, 1449s, 1430s, 1415s, 1389s, 1370s, 1342s, 1313s, 1278m, 1241m, 1121br+s, 1052br+s, 1039s, 1026s, 991s, 924m, 909m, 838m, 818w, 795s, 780m, 708m, 694w, 654m, 620s. Found: C 39.79; H 3.20; N 13.92 (%) $CuC_{20}H_{20}N_6(ClO_4)_2$. Requires: C 39.57; H 3.32; N 13.85 (%).

Cu(II) 6,6'-bis(dimethylpyrazole)-2,2'-Bipyridine, $[CuC_{20}H_{20}N_6][2PF_6]$ (**4.4a**):

A saturated solution of ammonium hexafluorophosphate $[NH_4.PF_6]$ (3ml) was added slowly to a stirring solution of complex **4.2** (25mg, 4.12x10^{-5}mol) dissolved in DMF (3ml) forming a fine green precipitate. The mixture was allowed to stir for 1h before removal of solvents *in vacuo*. The solid was then washed (2 x 6ml) with distilled water and left to settle before decanting off the liquid. Next the remaining green solid washed and dried using diethyl ether giving the desired complex in high purity (23mg, 81%). (ES-MS) *m/z* calcd. 224.0655; exp. 224.0615 $[CuC_{20}H_{20}N_6(CH_3CN)]^{2+}$, (100%), calcd. 506.0531 ; exp. 552.0686 $[CuC_{20}H_{20}N_6[PF_6]]^+$, (15%). λ_{max}, nm, (εM, M^{-1}cm^{-1}) in CH_3CN: 270(68133), 347(27265), 360(28538), 685(134). Found: C 34.51; H 3.04; N 11.97 (%) $CuC_{20}H_{20}N_6(PF_6)_2$. Requires: C 34.40; H 2.89; N 12.04 (%). Magnetic moment (Evans method, 293K, Acetonitrile): μ_{eff} = 1.15μ_B.

Zn(II) 6,6'-bis(dimethylpyrazole)-2,2'-Bipyridine, $[ZnC_{20}H_{20}N_6][2ClO_4]$ (**4.5**):

Zinc(II) perchlorate hexahydrate $[Zn(ClO_4)_2.6H_2O]$(54.1mg, 1.45x10^{-4}mol) was dissolved in acetonitrile (3ml) and added dropwise to a solution of **L4** (50.0mg, 1.45x10^{-4}mol) in a $CHCl_3$:CH_3CN (75:25) solvent (5ml). The mixture was stirred for 24h allowing some of the $CHCl_3$ solvent to evaporate which yielded a white precipitate. The solid was filtered off under gravity then washed and dried using diethyl ether giving the complex in high purity (40mg, 45%). ^{1}H-NMR (CD_3CN; 250MHz): δ_H 8.46(t, 2H, J=8.0Hz, *CH*), 8.38(d, 2H, J=7.6Hz, *CH*), 8.09(d, 2H, J=8.3Hz, *CH*), 6.51(s, 2H, *CH*), 2.68(s, 6H, *CH$_3$*), 2.61(s, 6H, *CH$_3$*). ^{13}C-NMR ($CDCl_3$; 100MHz): δ_C 152.02 (C), 147.29(C), 146.03(C), 144.96(CH), 143.95(C), 119.41(CH), 114.70(CH), 112.83(CH), 14.30(CH_3), 13.45(CH_3). HRMS (ES-MS) *m/z* calcd. 507.0526; exp. 507.0534 $[ZnC_{20}H_{20}N_6[ClO_4]]^+$, (96%), calcd. 204.0520; exp. 204.0521 $[ZnC_{20}H_{20}N_6]^{2+}$, (11%). FT-IR (KBr/cm^{-1}) ν = 3399br, 3143w, 3105w, 2931w, 1603s, 1585s, 1569s, 1487s, 1452s, 1429s, 1386m, 1363s, 1333m, 1313m, 1278w, 1195w, 1184w, 1111br+s, 1037s, 1011m, 993m, 929w, 919w, 808w, 795s, 782w, 711m, 682m, 644m, 624s. λ_{max}, nm, (εM, M^{-1}cm^{-1}) in CH_3CN: 269(40,296), 314(23,187). Found: C 38.09; H 3.07; N 12.98 (%) $ZnC_{20}H_{20}N_6(ClO_4)_2{\cdot}0.25CHCl_3$. Requires: C 38.07; H 3.20; N 13.16 (%).

Hg(II) 6,6'-bis(dimethylpyrazole)-2,2'-Bipyridine, $[HgC_{20}H_{20}N_6][2ClO_4]$ (**4.6**):

Mercury(II) perchlorate hexahydrate $[Hg(ClO_4)_2.6H_2O]$(79.5mg, 1.57x10^{-4}mol) was dissolved in acetonitrile (3ml) and added dropwise to a solution of **L4** (54.0mg, 1.57x10^{-4}mol) in $CHCl_3$:acetonitrile (50:50) (5ml). The colourless mixture was stirred for 24h and then filtered through celite. The filtrate was reduced *in vacuo* to 4ml and vapour diffusion of diethyl ether into the solution produced colourless crystals of high purity (75mg, 64%). ^{1}H-NMR (DMSO; 250MHz): δ_H 8.72(d, 2H, J=7.4Hz, *CH*), 8.55(t, 2H, J=8.2Hz, *CH*), 8.23(d, 2H, J=8.1Hz, *CH*), 6.70(s, 2H, *CH*), 2,87(s, 6H, *CH$_3$*), 2.54(s, 6H, *CH$_3$*). (ES-HRMS) *m/z* calcd. 444.1954; exp. 444.1521 $[Hg(C_{20}H_{20}N_6)_2]^{2+}$ (60%), calcd. 644.1970; exp. 644.0913 $[HgC_{20}H_{20}N_6[ClO_4]]^+$ (30%). FT-IR (KBr/cm^{-1}) ν = 3580m, 3527br+m, 3151m, 3102m, 2975br+m, 2920m, 8031m, 1654m, 1597s, 1590s, 1564s, 1477s, 1448s, 1420s, 1382s, 1355s, 1324m, 1307m, 1269w, 1108br+s, 1045s, 1012s, 920m, 839w, 797s, 709w, 703m, 675w, 637m, 625s. Found: C 32.22 H 2.82; N 11.22 (%) $C_{20}H_{20}N_6HgCl_3O_8$ Requires C 32.27; H 2.71; N 11.30 (%).

References

1- M. D. Ward., *Annu. Rep. Prog. Chem. Sect A. Inorg. Chem.,* **2002**, 98, 285-320.

2- S. Derossi, L. Brammer, C. A. Hunter, M. D. Ward., *Inorg. Chem*., **2009**, 48(4), 1666-1677.

3- L. Cronin, *Angew. Chem. Int. Ed*., **2006**, 45(22), 3576-3578.

4- V. Balamugan, J. Wilson, M. Jhumpa, M. Rabindranath, *Cryst. Eng. Comm*., **2004**, 6, 396-400.

5- F. Zeng, Z. Yu., *Organometallics.,* **2009**, 28(6), 1855-1862.

6- M. Jia, A. Seifert, W. R. Thiel., *Chem. Mater.,* **2003**, 15(11), 2174-2180.

7- S. Wang., *Coord. Chem. Revs*., **2001**, 215, 79-98.

8- R. Ziessel, L. J. Charbonniere., *J. Alloy. Compd*., **2004,** 374, 284-288.

9- M. A. Halcrow., *Coord. Chem. Revs*., **2009**, 253, 2493-2514.

10- H-R. Wen, Y-Z. Tang, C-M. Liu, J-L. Chen, C-L. Yu., *Inorg. Chem*., **2009**, 48(21), 10177-10185.

11- M. A. Halcrow., *Coord. Chem. Revs*., **2005**, 249, 2880–2908.

12- S. S. Tandon, L. K. Thompson, M. E. Manuel, J. N. Bridson, *Inorg. Chem*., **1994,** 33(24), 5555-5570.

13- C. R. K. Glasson, L. F. Lindoy, G. V. Meehan, *Coord. Chem. Revs*., **2008**, 252(8+9), 940-963.

14- M. D. Ward., *Chem. Commun***., 2009**, 4487-4499.

15- M. Yoshizawa, M. Tamura, M. Fujita*., J. Am. Chem. Soc*., **2004**, 126, 6846-6847.

16- I. G. Phillips, P. J. Steel., *Aust. J. Chem*., **1995**, 48, 1617-1624.

17- V. E. Dose, L. Wilson., *Inorg. Chem.,* **1978,** 17, 2660.

18- D. P. Rillema, B. K. Mack,. *Inorg. Chem.,* **1982,** 21, 3849.

19- D. E. Ernst, W. Kaim., *Inorg. Chem.,* **1989,** 28, 1520.

20- D. B. Macqueen, J. D. Peterson., *Inorg. Chem.,* **1990,** 29, 2313.

21- J. B. Cooper, D. B. MacQueen, J. D. Peterson, D. W. Wertz., *Inorg. Chem.,* **1990,** 29, 3701.

22- A. J. Downard, G. E. Honey, L. F. Philiips, P. J. Steel,. *Inorg. Chem*. **1991,** 30, 2259-2260.

23- J. García-Antón, R. Bofill, L. Escriche, A. Llobet, X. Sala,. *Eur. J. Inorg. Chem*. **2012**, 4775–4789.

24- S. P. Argent, H. Adams, T. Riis-Johannessen, J. C. Jeffery, L. P. Harding, W. Clegg, R. W. Harrington, M. D. Ward., *Dalton. Trans***., 2006**, 4996-5013.

25- J. S. Fleming, K. L. V. Mann, C. A. Carraz, E. Psillakis, J. C. Jeffery, J. A. McCleverty, M. D. Ward, *Angew. Chem. Int. Ed.,* **1998**, 37, 1279.

26- R. L. Paul, Z. R. Bell, J. C. Jeffery, J. A. McClevertly, M. D. Ward, *Proc. Natl. Acad. Sci. U. S. A.,* **2002**, 99, 4883.

27- Toshihiro. Ise, Seiji. Ichijima., US7754347, 2007.

28- S. M. Couchman, J. C. Jeffery, M. D. Ward., *Polyhedron*, **1999**, 18, 2633–2640.

29- Y-H. Chi, W. Wei, J-M Shi, Y-Q. Zhang, S. Liu., *J. Coord. Chem*., **2012**, (65) 13, 2379–2390.

30- L. Y. Zhenga, Y. H. Chib., *Acta Cryst*., **2011**, E67, m68.

31- T. Tatsuo; K. Rie, K. Eisaku, K. Hiroshi, (2010), JP 2010238880, 2010.

32- J. Lewis, K. P. Wainwright., *Chem. Comm.,* **1974**, 169-170.

33- J. Lewis, K. P. Wainwright., *Dalton. Trans.,* **1978**, 440-446.

34- D. L. Lewis, E. Dixon, D. J Hodgson*., J. Cryst. Mol. Struct*., **1975**, Vol 5, issue 1, p-67-74.

35 - A.B.P. Lever., *Inorganic. Electronic. Spectroscopy*. 2nd Ed, p479-486.

36 - V. Mishra, F. Lloret, R. Mukherjee., *Inorg. Chim. Acta.,* **2006,** 359, 4053–4062.

37- A.B.P. Lever., *Inorganic. Electronic. Spectroscopy*. 2nd Ed, p507-516.

38- A. T. Baker, D. C. Craig, A. D. Rae, *Aust. J. Chem.* **1995**, 48, 1373.

39- M. Hirotsu, Y. Tsukahara, I. Kinoshita*., Bull. Chem. Soc. Jpn*., **2010**, 83(9) 1058-1066.

40- A.B.P. Lever., *Inorganic. Electronic. Spectroscopy*. 2nd Ed, p554-567.

41- J. C. Knight, A. J. Amoroso, P. G. Edwards, R. Prabaharan, N. Singh., *Dalton Trans*., **2010**, 39, 8925–8936.

42 – L. Yu, J-M. Shi, Y-Q. Zhang, Y-Q. Wanga, Y-N. Fana, G-Q. Zhanga, W. Shi, P. Cheng., *J. Mol. Struct*., **2011**, 987, 138-143.

43- J. C. Knight, A. J. Amoroso, P. G. Edwards, R. Prabaharan, N. Singh., *Dalton Trans*., **2010**, 39, 8925–8936.

44 –S. Chakrabarty, R. K. Roddar, R. D. Poulsen, A. L. Thompsom, J. A. K. Howard,. *Acta. Cryst*., **2004**, C60, m628-m630.

45- A. J. Canty, C. V. Lee, N. Chalchit, B. M. Gatehouse,. *Acta Cryst*., **1982**, B38, 743-748.

46 – R. D. Shannon, Acta. Crystallogr. ,1976, A32, 751-767.

Table A1: Crystallographic data for 6,6'-Bis(dimethylpyrazole)-2,2'-Bipyridine (**L4**) and complexes.						
Compound	**L4**	**4.1**	**4.2**	**4.3**	**4.4**	**4.6**
Chemical formula	$[C_{20}H_{22}N_6][2ClO_4]$	$[MnC_{20}H_{20}N_6][2ClO_4]$	$[CoC_{20}H_{20}N_6(CH_3CN)_2][2ClO_4]$	$[Ni(C_{20}H_{20}N_6)_2][2ClO_4].C_5H_{10}$	$[CuC_{20}H_{20}N_6][2ClO_4]$	$[HgC_{20}H_{20}N_6][2ClO_4]$
Mr, g/mol	545.34	598.26	684.36	1016.58	606.86	743.91
Crystal system	Monoclinic	Monoclinic	Monoclinic	Triclinic	Triclinic	Monoclinic
Space Group	C2/c	$P2_1/n$	$P2_1/n$	P-1	P-1	$P2_1/n$
T (k)	150 (2)	150 (2)	293 (2)	293 (2)	150 (2)	293 (2)
a, Å	17.2930 (6)	9.1993 (2)	15.2640 (2)	8.7125 (2)	8.0759 (2)	9.0497 (3)
b, Å	10.1821 (6)	14.6318 (4)	9.8112 (2)	12.8234 (3)	11.5440 (4)	14.4708 (7)
c, Å	13.2668 (7)	17.4288 (4)	19.0858 (4)	21.2605 (6)	12.2970 (3)	18.4253 (7)
α, deg	90.00	90.00	90.00	91.496 (2)	82.287 (1)	90.00
β, deg	101.511 (3)	100.249 (2)	94.7040 (10)	99.200 (1)	83.847 (1)	101.822 (3)
γ, deg	90.00	90.00	90.00	92.454 (2)	88.244 (2)	90.00
V, $Å^3$	2289.0 (2)	2308.52 (10)	2848.63 (9)	2341.29 (10)	1129.36 (6)	2361.73 (17)
Z	4	4	4	2	2	4
D_c g/cm^3	1.582	1.721	1.596	1.442	1.785	2.092
μ(Mo K α), mm^{-1}	0.346	0.866	0.853	0.595	1.267	6.805
Observed Reflections	2778	5668	7402	12211	5953	6267
Reflections collected	4505	9265	11870	17304	8777	9975
R_{int}	0.0470	0.0323	0.0255	0.0273	0.0267	0.0288
R_I [I>2σ(I)]	0.0720	0.0533	0.0404	0.0593	0.0504	0.0440
wR_2 (all data)	0.2132	0.1474	0.1026	0.1715	0.1315	0.1009

Chapter 5:

Tripodal Bis-quinoline Bromo-benzyl Framework and Co-ordination with Various Transition Metals

5.0 Abstract

This chapter discusses the preparation and isolation of a novel bis-quinoline tripodal ligand system, namely bis(2-quinoline)(4-bromo-phenyl)menthanol (**L5**). Complexes of this ligand were isolated with various divalent first row transition metals (Co→Zn) which have been fully characterized via solution and solid state techniques. Additionally a complex of **L5** with $[Re(CO)_3]^+$ was also achieved giving a stable compound with potential luminescent and PET active properties. All compounds formed six co-ordinate octahedral structures where **L5** acts as a facial tridentate donor, with exception to **5.3** which is square pyramidal. The Cu(II) complex (**5.3**) is also unique in that it forms a 3:3 trimer structure in the solid state, involving a capping perchlorate molecule across the three copper centres.

5.1 Introduction

The usefulness of heteraromatic groups such as pyridines and pyrazoles in their structural capabilities and broad binding affinities has already been proven in previous work. Quinoline is another example of a similar heteroaromatic group which has additional photophysical properties, due to its high conjugation. Early literature has shown its potential in co-ordination chemistry[1,2] and luminescent properties, which have been exploited for applications such as Zinc cation sensing.[3-5]

Linking quinoline groups together to form chelating ligands has its advantages in creating more stable metal complexes. An early and simple example of this was first synthesised by Scheibe *et. al.* in 1921, which involved linking two quinoline moieties *via* a methylene bridge through the 2,2' quinoline positions (Fig. 1).[6] This was done by the reaction of 2-methylquinoline with 2-chloroquinoline in a sealed system. More recently (1960), Scheibe *et. al.* was able to isolate Co(II), Cd(II) and Hg(II) complexes of this system, revealing its ability to co-ordinate transition metals of varying ionic radius.[7]

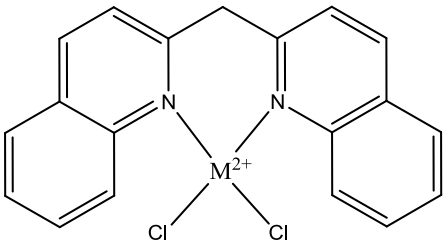

M= Co(II), Cd(II), Hg(II) and Zn(II)

Figure 1: Ligand di(2-quinolyl)methane and coordination mode[7] its Zn(II) complex also being achieved.[8]

This same system was later adopted by Liangyou He *et. al.* who were investigating the interesting luminescent and structural properties of trivalent lanthanide complexes. In this research they managed to isolate a myriad of mononuclear lanthanide perchlorate complexes, where two ligands surround one metal centre (Fig. 2).[9]

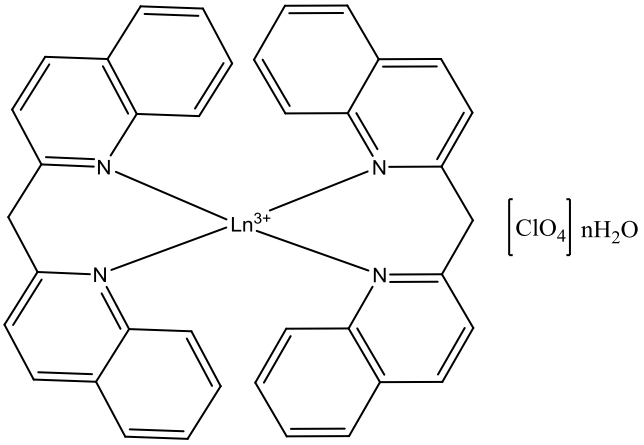

Ln = La, Lu, Yb, Gd, Tm, Er, Ho, Dy, Tb, Sm, Eu and Nd

Figure 2: The 2:1 co-ordination mode of di(2-quinolyl)methane with various trivalent lanthanide metals, n= 0-4 water molecules.[9]

Black *et. al*. were investigating metal template reactions which allowed them to create the Co(II) and Ni(II) 2,2'-quinadilic acid ([Ni(qda)(OH)(H_2O)]) complexes, shown in Figure 3.[10] They achieved this by a base catalysed rearrangement of a bis-quinoline α-diketone molecule, which undergoes a group migration to give the ligand 2,2'-quinaldilic acid (qda) (*c.f.* benzilic acid rearrangement). This was subsequently added to metal acetate salts and was shown to co-ordinate in a tridentate fashion, giving mononuclear complexes. These complexes have shown

the ability of metals to interact with additional groups within the ligand. The functionalisation of the bridging group increases the chelating ability of the ligands and thus improves their stability as discrete structures.

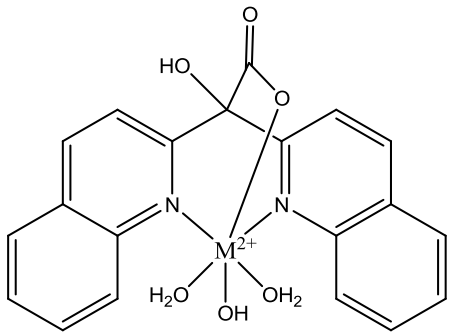

M = Co(II) or Ni(II)

Figure 3: Showing the co-ordination mode of the complex $[M(qda)(OH)(H_2O)_2]$.[10]

A very successful ligand framework related structurally to the work described previously, was that of 8-hydroxyquinaldine and 2,2'-(2,2-Propanediyl)-bis(8-hydroxyquinoline), developed by Deraeve *et. al* (Fig. 4).[11] They were interested in the ability of 8-hydroxylquinoline groups to strongly co-ordinate first row transition metals, especially Cu(II) and Zn(II) ions. These metals are important with respect to research into Alzheimer's disease as they readily form toxic plaques around neurons when complexed with β-type amyloid peptides (Aβ) which are associated with the disease .[12a-c] It has been shown that some metal-chelating agents are able to promote the dissolution of Aβ deposits through the removal of these bound metal ions, giving these compounds great therapeutic potential.[13,14] Deraeve *et. al* discussed the strong chelating ability of their bis-quinoline ligands showing how they form mononuclear complexes with distorted square pyramidal geometries. In the case of many bis-8-hydroxyquinoline ligands, they found a 10,000 times increased binding affinity for Cu(II) and Zn(II) compared to that of monomeric 8-hydroxy quinolines.[11] Moreover, their one atom linked ligands were found to have the most efficient binding for these metals, and therefore, in the case of Cu(II) best prevents the formation of Aβ-Cu complexes, giving the highest inhibition of H_2O_2 production (formed by the oxidative stresses from the accumulation of redox active metal ions).

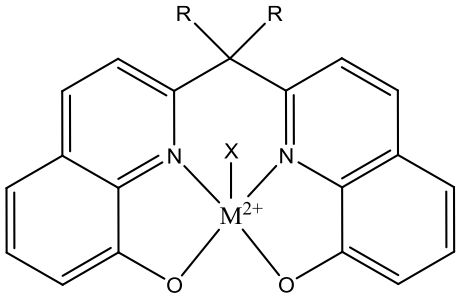

M = Cu(II) and Zn(II)
R = H or Me
X = O or Cl-

Figure 4: 8-hydroxyquinaldine or 2,2'-(2,2-Propanediyl)-bis(8-hydroxyquinoline) complexation with Z(II) and Cu(II).[11]

The group of Zubieta have extensively studied the biological application of Re-bis quinoline systems.[15a-c] For example Gasse *et. al*. have described the formation of a PNA (poly nucleic acid) conjugated $[Re(CO)_3$bis-quinoline$]^+$ complex (Fig. 5) which can be used for *in vitro* fluorescence microscopy of cancerous cells.[16] They successfully demonstrate the uptake of such compounds, and their binding affinity for DNA. *In vitro* binding was shown to not affect its essential photophysical properties with little cytotoxic effects observed, indicating the high stability of these organometallic species in biological media.

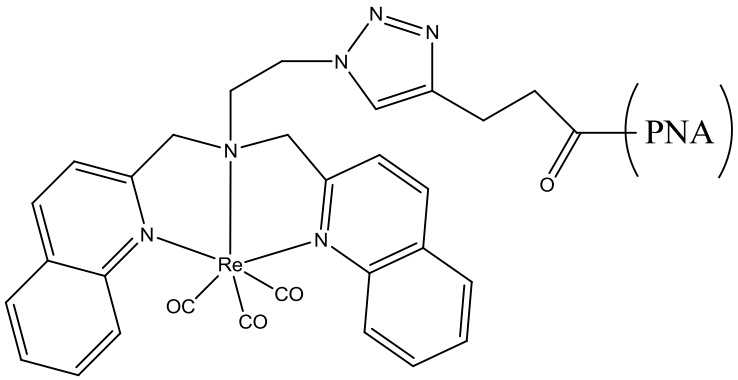

Figure 5: Structure of $Re(CO)_3]$-PNA.[16]

Viola-Villegas *et. al.* report the synthesis of a similar Re(I) bis-quinoline complex, B_{12}-BQBA-$[Re(CO)_3]^+$, that is now conjugated to a vitamin B_{12} unit (Fig. 6).[17] Confocal microscopy studies demonstrate cell uptake of the Re-conjugate and its binding ability to the Cubilin receptor (a receptor which is over expressed in malignancies). Moreover the photophysical characteristics (emission wavelength and intensity) upon binding to the Cublin receptor are retained, and it therefore presents a suitable biomarker for cancers of gastrointestinal and renal tissues. Alberto *et. al.* have also demonstrated how the ^{99m}Tc analogue can also be prepared for the

evaluation of its PET and fluorescence bimodal applications[18,19] giving Re(I) bis-quinoline type systems great prospects within biomedical imaging.

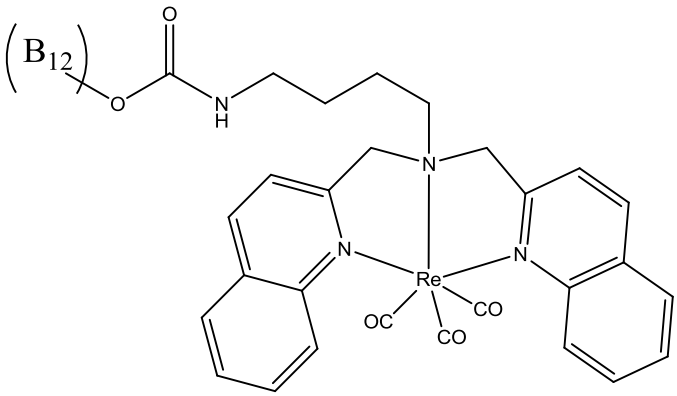

Figure 6: Structure of B_{12}-BQBA-$[Re(CO)_3]^+$ a conjugate for targeting malignacies.[17]

In view of these findings it is of great interest to develop novel tripodal based bis-quinoline ligands with a one carbon linker (due to their strong binding affinity), and to investigate their co-ordinative properties with transition metals such as Zn(II), Cu(II) and Re(I). The increased biomedical applications involving these particular metals still need further refinement, demanding new systems. The use of Re(I) in replacement of ^{99m}Tc is a cheaper, safer and quicker way of developing potential bimodal PET/fluorescence imaging probes which is a fast growing and increasingly desirable field of research.

5.2 Results and Discussion

5.21 Ligand synthesis

The starting material Bis(2-quinoline)methanone (**S1**) was synthesised according to the literature method described by Burns *et al* (see scheme 1).[20] Some minor synthetic modifications were adopted during the reaction, in which the crude mixture was stirred for 16h, instead of the stated 2h, allowing the temperature to slowly to reach ambient conditions. The purification was also simplified by dissolving the crude reaction solid with a minimum of methanol followed by addition of diethyl ether which produced a dry white solid (**S1**) with high purity and give a yield comparable to that in the literature (59%).

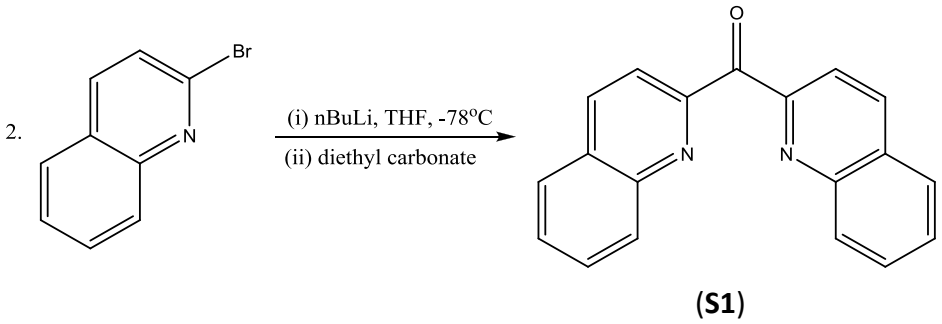

Scheme 1: Synthesis of Bis(2-quinoline)methanone (**S1**).[18]

The compound bis(2-quinoline)(4-bromo-phenyl)menthanol (H**L5**) was synthesised by slow addition of the quinoline-ketone to a 1.02eq solution of lithiated 4-Iodo-1-bromobenzene, in THF at -78°C, resulting in an intense pink solution. The reaction can be worked up in the same manner as **S1** and simply washing the brown solid with diethyl ether gives the product in high purity (see scheme 2). The resulting ligand again follows the traditional C_3 scaffold with a tertiary alcohol group however the addition of the para substituted benzene provides potential for the addition of different functional groups. The use of quinolines in this ligand provides more aromaticity to the system compared with pyridines and gives rise to luminenscent properties upon complexation with Re(I) (see compound **5.5**).

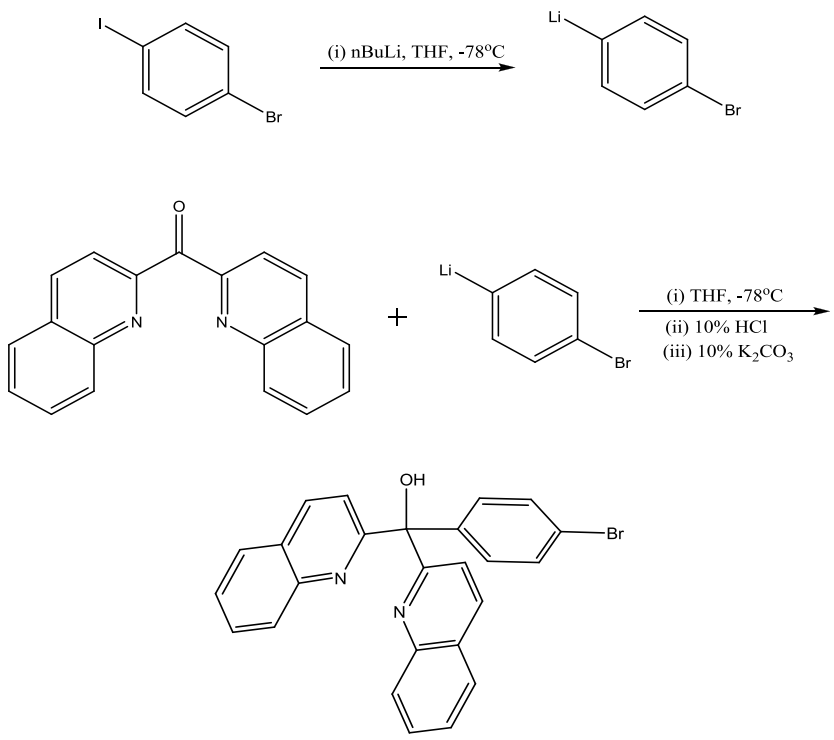

(**L5**)

Scheme 2: Synthesis of bis(2-quinoline)(4-bromo-phenyl)menthanol (H**L5**).

5.22 Synthesis of complexes

The ligand H**L5** is readily soluble in DCM or hot acetonitrile and can form complexes with several divalent transition metals (Co→Zn) as well as $[Re(CO)_3]^+$ (Tab. 1). Complexes **5.1** – **5.4** were all prepared in a 1:1 stoichiometry. Preparation involved the slow addition of metal perchlorate salt in acetonitrile to a stirred solution of H**L5** generally producing a solution colour change. Compound **5.5** ($Re(CO)_3$(**L5**)) was prepared differently by refluxing H**L5** with rhenium penta-carbonyl bromide in toluene overnight, forming product as a dark yellow precipitate.

Table 1: List of metal ions successfully complexed	
Compound number	Associated metal ion
5.1	Co(II)
5.2	Ni(II)
5.3	Cu(II)
5.4	Zn(II)
5.5	Re(I)

5.23 Vibrational spectroscopy

The IR spectra of H**L5** and complexes **5.1-5.5** were studied in the solid state as KBr discs, with their key bond absorptions listed in Table 2. For the quinoline functions typically four stretching modes were observed in all complexes, between 1620cm^{-1} and 1480cm^{-1}. These values do fluctuate compared with H**L5** and no discernible pattern relating to co-ordination could be concluded. The aromatic C-H stretches around 3070cm^{-1} are seen to have increased energy within the complexes compared to free ligand. This is possibly due to the effects of co-ordination changing the electron density within the aromatic rings and altering the C-H bond strength. In the finger print region there is a set of 3 or 4 absorptions between 826cm^{-1} and 750cm^{-1} seen in all samples. These represent the C-H bending modes of a para-disubstituted benzyl function giving an undisturbed and clear indicator for this molecule. For compounds **5.1**→**5.4** only two perchlorate absorptions were observed, ~1100cm^{-1} and 625cm^{-1}, suggesting that the counter ions are unco-ordinated which corresponds with the X-ray crystallographic data. However, in the case of compound **5.3** a broad strong shoulder at 960.4cm^{-1}, along with a medium strength absorption at 493.2cm^{-1}, suggest the presence of a co-ordinating perchlorate group and does correlate well with the X-ray data of **5.3**. As expected three strong CO absorptions are observed for the Rhenium complex **5.5,** due to the symmetric and asymmetric stretching modes of three facial CO donors. These peaks are of lower energy than the CO stretches observed in the Rhenium starting material, which has resulted from changing their trans donors and a clear indication of co-ordination with **L5**.

Table 2: Showing characteristic vibrational modes of H**L5** and complexes						
compound	Aromatic ν(C-H)	ν (O-H)	ν (C=N) and (C=C)	ν (C-H) bend. para-disubstituted benzyl ring	ν (C-O)	ν (Cl-O) or (C≡O)
H**L5**	3058.6 (m), 3043.8 (m)	3388.3 (m)	1617.0 (m), 1596.8 (s), 1566.9 (m) and 1500.5 (s), 1486.9 (m)	826.8 (s), 802.2(s), 786.8 (m), 770.4 (w), 753.5 (s)	1172.5 (m)	n/a
5.1 (Co^{II})	3066 (m)	3399.9 (br+s)	1619.4 (m), 1598 (m) and 1508.1 (m), 1486.4 (w)	826.3 (m), 804.2 (m), 756.9 (m)	1145 (s)	1089.6 (br+s), 625.8 (s)
5.2 (Ni^{II})	3059.5 (m)	3418.7 (br+s)	1656.1 (s), 1620.9 (s), 1592.9 (s) and 1510.0 (s), 1489.3 (s)	824.4 (s), 784.4 (s), 764.6(s)	unobserved	1093.9(br+s), 624.3(s)
5.3 (Cu^{II})	3084.6 (m)	3372.4 (br+m)	1621.8 (m), 1596.8 (s) and 1510.0 (s), 1484.4(s)	824.9 (s), 807.5 (s), 781.0 (m), 754.0 (s)	unobserved	1108.9 (br+s), 960.4(Br+s), 638.0(s), 625.3 (s) 474.9(m)
5.4 (Zn^{II})	3100.0 (m)	3475.1 (br+s)	1621.4 (s), 1596.8 (s), 1532.7 (w), 1507.6 (s), 1484.9(m)	823.9 (s), 806.1 (s), 782.9 (m), 754.5 (m)	1142.6 (s)	1108.4 (br+s), 625.8 (s)
5.5 (Re^{I})	3072.1 (w)	3446.2 (br+m)	1618.9 (w), 1593.4 (m) and 1508.1 (s), 1489.7 (m)	823.9 (m), 808.9 (w), 779.1 (m), 758.9 (m), 732.3 (m)	1144.6 (w)	2009.0 (s), 1979.8(s), 1868.2(s)

5.24 NMR spectroscopy

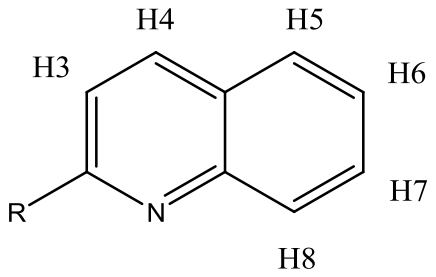

Scheme 3: Proton labelling of the quinoline moieties.

Ligand H**L5** – Protons H9 and H10 of the phenyl bromide function are thought to be the two upfield doublets (7.41ppm and 7.52ppm, appendix Fig. 1, page 228) as these values match well with related compounds and starting material as well as the evidence of strong roofing the two peaks have towards each other, demonstrating their close connection. The remaining six peaks (two triplets and four doublets) are all downfield respective to the phenyl bromide peaks and belong to the quinoline function. The peak separations are all fairly even with exception of the doublet at 8.36ppm which, due to resonace effects, possibly relates to H4 on the quinoline moieties.

Compound **5.4** – Due to the d^{10} diamagnetic nature of Zn(II) a ^{1}H-NMR spectra of complex **5.4** was collected. The broad spectra shows seven discrete peaks with the central doublet integrating to twice that of the remaining peaks, see appendix Figure 2, (page 228). The doublet at 8.78ppm, attributed to H4, is seen to have shifted 0.4ppm downfield relative to the free ligand. This is most likely due to the complexation of zinc drawing electron density away from the quinoline ring which further de-shields H4. The same is true for the remaining aromatic peaks which are seen to have shifted downfield, with the exception of one triplet (now at 7.85 ppm). H6 of the quinolines is likely to be the most upfield of the two possible triplets, this is based on resonance effects and its larger distance from the N-donor (four bonds as opposed to only three bonds for H7, see scheme 3).

Compound **5.5** - The bright yellow rhenium complex (d^6) gave a sharp spectra containing 6 peaks including two multiplets, three doublets and interestingly, an OH peak (appendix Fig. 3, page 229). All of the peaks shift downfield relative to the free ligand. The multiplet at 7.73 ppm is attributed to the overlap of a triplet (H6) and a doublet (H10) as these are expected to have the most upfield environment. The second multiplet at 8.08 ppm is likely due to the overlap of two doublets and the other triplet (H3, H5 and H6). The two closely spaced downfield doublets are therefore attributed to H4 and H8. One of these doublets, thought to be H8, has shifted at least 0.7ppm compared to the free ligand. This is likely due to the change in spatial environment upon complexation, as the proton would now be pointing towards the carbonyls of the metal centre.[21] In addition there is only a two bond bridge between H8 and the N-donor and the electronic pull through the nitrogen could therefore be adding to the amount of shift observed. Lastly to note is the unexpected presence of an OH peak at 8.31 ppm. Interestingly, crystal data suggested that the oxygen moiety was co-ordinated to the rhenium centre which, in solution, appears to be either: bound to both rhenium and a proton or that the oxygen has become unco-ordinated, residing as an alcohol group. Conversely in the analogous complex **6.2** no OH peak in DMSO was observed, possibly suggesting that **5.5** is less stable in solution than **6.2**.

As a result of observing an OH proton environment in the spectra of **5.5** a small sample was washed with excess triethyl amine (Compound **5.5a**). The spectra was then run again revealing the loss of the OH peak however, no observable shifts in the aromatic peaks were observed suggesting that the oxygen moiety may always be bound to rhenium, protonated or not. The lack of shifting observed is however, unexpected as even adding/removing H^+ to the oxygen should change its charge density and casts doubt over the origin of the OH environment.

5.25 Electronic Absorption Spectra

The electronic absorption spectra of H**L5** and complexes **5.1-5.3** and **5.5** have been measured and displayed in Table 3. All the samples were run from an acetonitrile solution in a 1cm quartz cuvette at concentrations from $8x10^{-6}$ $moldm^{-3}$ to $2.8x10^{-3}$ $moldm^{-3}$. At least two intense spectral bands were observed between 230 nm and 320 nm for all complexes with **L5**, which are attributed to the intra-ligand π-π* quinoline transitions. Where as for the free ligand H**L5**, four absorptions below 320nm were observed, three sharp and one broad.

Table 3: Electronic absorption spectral assignments

compound	π-π* transitions / λ (nm)	MLCT λ (nm)	d-d transitions / λ (nm)	Dq (cm^{-1})	B (cm^{-1})	B^b
HL5	240(24532), 270(12904), 302(11879), 316(13929)	-	-	-	-	-
5.1(Co2+)	243(19917), 302(10430)	331(3268)	436(26), 1032(5.2)	969	788	0.7
5.2(Ni2+)	279(12122), 315(10302)	~400(16.4)	581(9.4), 964(7.1)	1037	864	0.8
5.3(Cu2+)	244(32843), 316(22927)	406(860)	787(79)	1271	-	-
5.5(Re1+)	255(36857), 310(20126)	338(8810), 416(440)	-	-	-	-

Compound **5.1** - For the Cobalt(II) complex **5.1,** one relatively high energy, observable band is present in the visible region of the spectrum at 22,936cm^{-1} and could be a contribution of two transitions, v_3 and v_2 ($^4A_{2g}(F) \leftarrow {}^4T_{1g}$ and $^4T_{1g}(P) \leftarrow {}^4T_{1g}$) see Figure 7. A second, but weak, band at 9690cm^{-1} (v_1) can be faintly observed and can be attributed to the $^4T_{2g}(F) \leftarrow {}^4T_{1g}$ transition. A similar shape spectra was observed for the high spin complex $(isoquinoline)_2Co(NO_3)_2$ (nitrates are bidentate) where an intense high energy band is seen around 20,000cm^{-1} (obscured in spectra for **5.1**) followed by a weak broad low energy band around 9100cm^{-1}.[22] At higher concentrations the v_3/v_2 band becomes obscured and forms a shoulder on the strong MLCT peak at 30,211cm^{-1}. From crystal data each Co(II) centre is slightly distorted octahedral and surrounded by two ligands giving the complex a C_{2h} symmetry, this would lead to an expected three absorptions and it is likely that the middle energy band v_2 ($^4T_{1g}(P) \leftarrow {}^4T_{1g}$) is obscured

under the higher energy absorptions of v_3 and MLCT. Using the appropriate d^7 Tanabe-Sugano diagram and with ratio v_3/v_1 = 2.3 the Δ/B value was measured as 12.3, which reveals that the two higher energy transitions (v_2 and v_3) are similar in energy and strengthens the possibility that the band at 22,936cm is actually a contribution of v_2 and v_3. This allowed *Dq* and *B* to be approximately calculated as 969cm^{-1} and 788cm^{-1} respectively. The nephlauxetic ratio, β = 0.70 (assuming free ion [Co^{II}], *B* =1120cm^{-1}),[23] shows the metal centre to have some degree of covalency within bonding however, this value maybe high due to the two electrostatic O$^-$ donors making the ligand 'harder'.

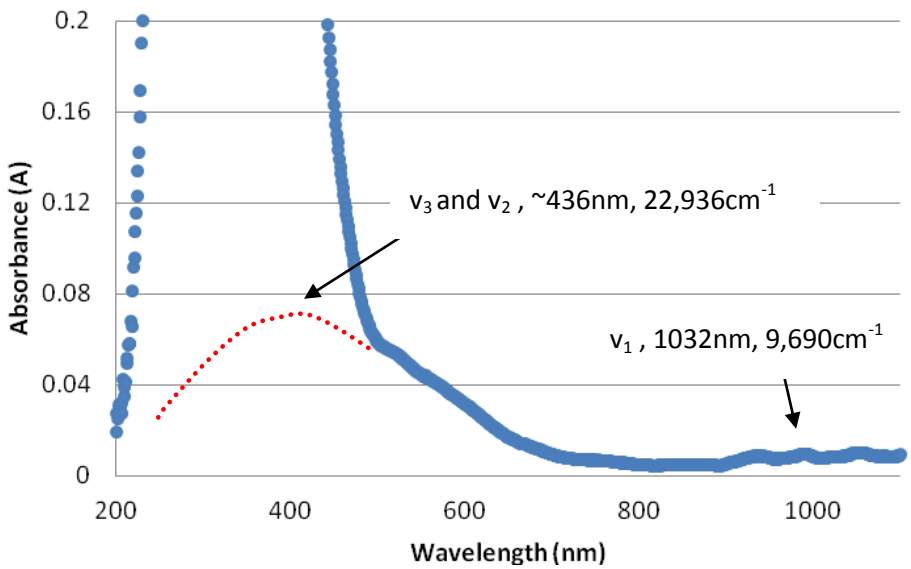

Figure 7: Visible region of the electronic absorption spectrum for **5.1** [Co(**L5**)$_2$].

As mentioned earlier the symmetry of **5.1** is C_{2h} and actually presents a more tetragonally distorted octahedral geometry (Co-N_4O_2) than an ideal octahedral. This raises concerns over the assignments given previous and the calculated Dq and B values. Another example [Co-(L-histidine)$_2$(H_2O)$_2$] which has a similarly tetragonal distortion, again from a Co-N_4O_2 donor arrangment, also gives a spectra comparable to **5.1**.[24] In the solution spectra peaks were observed at 20,500 cm^{-1}, 19,300 cm^{-1} and 10,100 cm^{-1}, and assigned as $^4A_2 \leftarrow {}^4B_1$, $^2T_1 \leftarrow {}^4B_1$ and $^4A_2$,$^4A_1 \leftarrow {}^4B_1$ respectively. The symmetry change from tetragonal distortion causes degenerate orbitals to split, including $^4T_{1g}$(F), which results in the new ground state ($^4B_1$).

<u>Compound **5.2**</u> There are two clear bands (v_1 = 10,373cm^{-1} and v_2 = 17,212cm^{-1}) in the visible region of the spectra for complex **5.2** (Fig. 8). There is also one obscured band (v_3 = ~25,000cm^{-1} that is mostly hidden due to the strong intra-ligand absorptions at around 30,000cm^{-1}, which is similar in character to the Ni(II) 8-(*p*-toluenesulfonamino)-quinoline complex absorption spectra.[25] Nickel(II) is d^8 with general preference for octahedral geometry, which is strongly supported by the crystal data of this complex. On this basis the three bands were assigned from the appropriate octahedral d^8 Tanabe-Sugano diagram where; v_1 = $^3T_{2g}\leftarrow{}^3A_{2g}$, v_2 = $^3T_{1g}(F)\leftarrow{}^3A_{2g}$ and v_3 = $^3T_{1g}(P)\leftarrow{}^3A_{2g}$. Using this information the v_2/v_1 = 1.66 ratio was used to measure the Δ/B value of 1.20 which allows *Dq* to be calculated as 1037cm^{-1} and therefore *B* to equal 864cm^{-1}. From this data the obscured band v_3 can be predicted to appear at 27,302cm^{-1} (366nm), which is only slightly higher in energy than the estimated 25,000cm^{-1} (400nm) value collected from the spectra. Finally the nephlauxetic ratio, β = 0.80 (assuming free ion [Ni^{II}], *B* =1080cm^{-1})[23] shows that the complex has a small amount of covalency within the coordinative bonds, less so than the previous Co(II) complex. These relatively high β values for **5.1** and **5.2** suggest that **L5** is a weak field ligand, which was predicted by magnetic moment measurements which revealed a high spin arrangement.

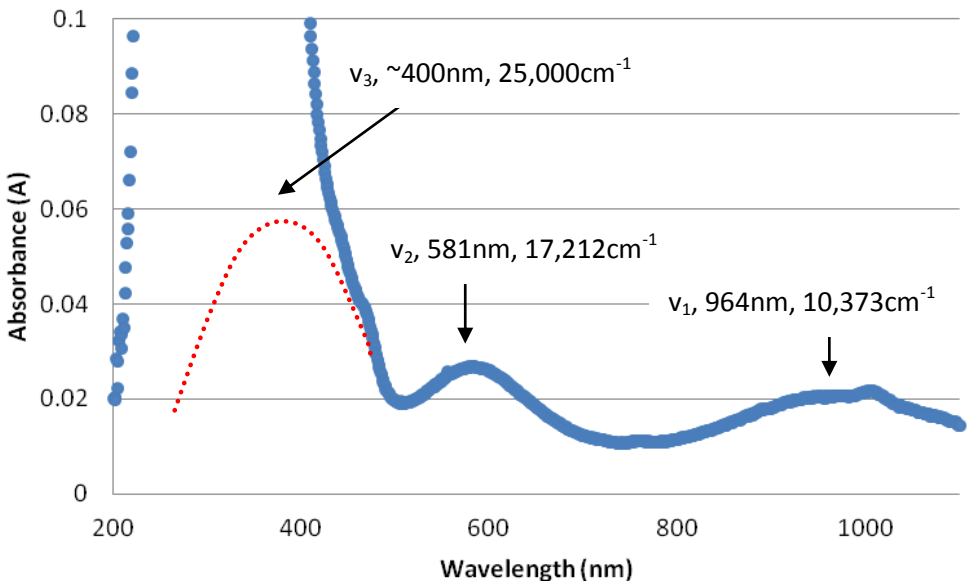

Figure 8: Visible region of the electronic absorption spectrum for **5.2** [Ni(**L5**)(CH_3CN)$_3$][ClO_4].

<u>Compound **5.3**</u> The copper(II) complex **5.3** presents only one broad asymmetric band in the visible region, common in Jahn-Tellar distorted Cu(II) complexes, which is situated at 12707cm^{-1} (787nm). Each complex is considered as a trimer containing three metals, three ligands and a co-ordinating perchlorate molecule with each copper centre having a predominantly square pyramidal geometry. This leads to a splitting of both the ^2E_g and $^2T_{2g}$ terms into ($^2B_{1g}$ and $^2A_{1g}$) and ($^2B_{2g}$ and ^2E_g) respectively (Fig. 9). This is expected to produce three absorption bands where all three are considered to be contributing to the single asymmetric band, which have been tentatively labelled as v_1 = $^2A_{1g}\leftarrow{}^2B_{1g}$, v_2 = $^2B_{2g}\leftarrow{}^2B_{1g}$ and v_3 = $^2E_g\leftarrow{}^2B_{1g}$ or ($d_z^2\rightarrow d_{x-y}^2$), ($d_{xy}\rightarrow d_{x-y}^2$) and ($d_{xz}, d_{yz}\rightarrow d_{x-y}^2$) respectively.

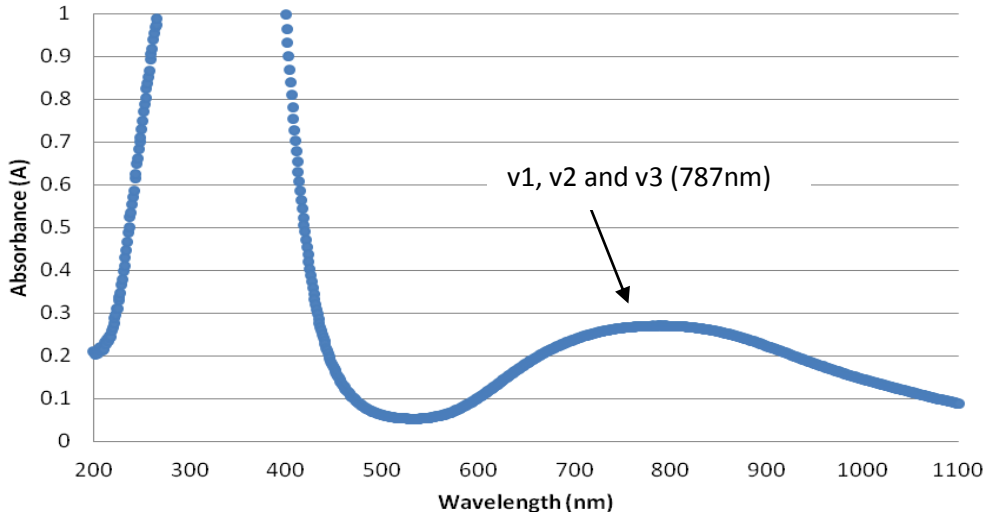

Figure 9: Visible region of the electronic absorption spectrum for **5.3** $[Cu_3(\mathbf{L5})_3(ClO_4)][ClO_4]_2$.

<u>Compound **5.5**</u> The spectra for complex **5.5** shows two strong bands at 39,216cm^{-1} and 32,258cm^{-1} (Fig. 10) which occur from the π→π* transitions of the ligand, there is also the presence of a slight shoulder occurring at approximately 29,586cm^{-1} (~338nm) which is attributed to the MLCT transition in the complex. Rhenium(I) is a d^6 low spin metal and as a result has no readily observable d-d transitions present in the spectra.

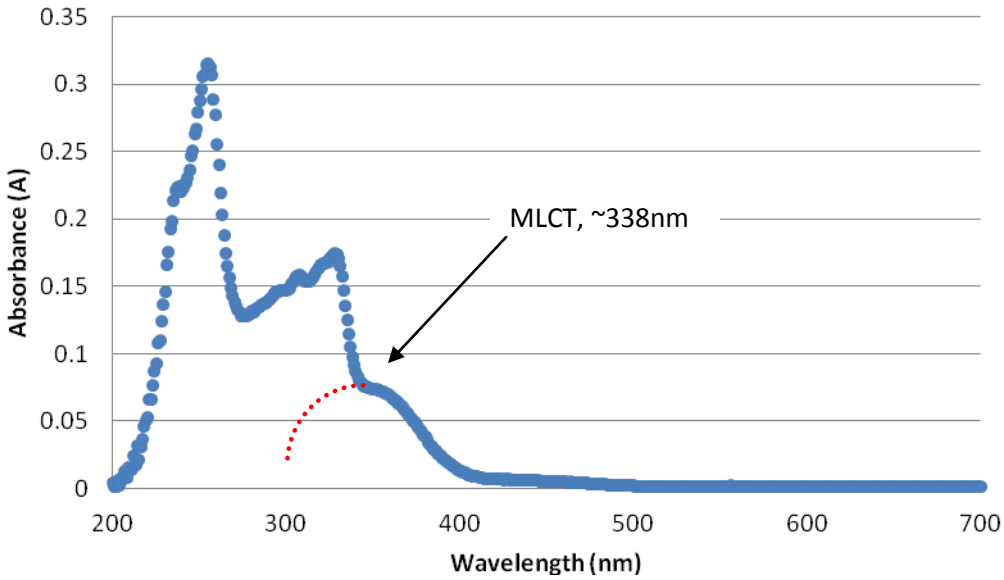

Figure 10: Visible region of the electronic absorption spectrum for **5.5** [Re(CO)$_3$(**L5**)].

5.26 X-Ray Crystallography Data

Disscussed below is the single crystal X-ray diffraction data for the ligand **HL5** and complexes **5.1**-**5.3** and **5.5**, with all details of crystal parameters and data collection displayed in Table 1A of the appendix (page 230).

Crystal Structure of (HL5):

Crystals of ligand H**L5** were obtained from a pure NMR sample in acetonitrile. The compound crystallises in the orthorhombic space group Pbcm with only half the ligand per asymmetric unit. The overall molecular symmetry of the ligand in solid state is C_S as there is only one mirror plane (Fig. 11). The bridge head carbon is shown to form a tetrahedral geometry where all the pending functions are separated equally to minimize steric strain. In the case of free ligand the quinoline groups are rotated away from the direction of the tertiary alcohol group, unlike what is seen for complexes of this ligand. Interestingly the nitrogen donors from the quinolines are both positioned pointing towards the centre of the potential cavity and not skewed by repulsive interactions demonstrating its potential to form a bidentate pincer in co-ordination.

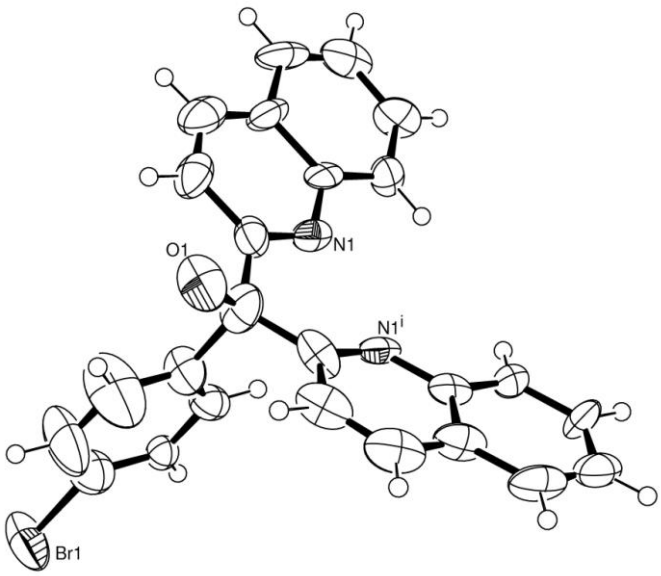

Figure 11: ORTEP Perspective view of the symmetric unit for the ligand H**L5.** Displacement ellipsoids are shown at 50% probability with H atoms included. One diethyl ether solvent molecule has been removed for clarity. Note a proton should be present on alcohol group (O1).

Crystal Structure of $[Co(L5)_2][Co(L5)(HL5)][ClO_4]$ (5.1):

The complex $[Co(\mathbf{L5})_2][Co(\mathbf{L5})(H\mathbf{L5})][ClO_4]$ formed orange coloured rhombic crystals, grown by the vapour diffusion of diethyl ether into a concentrated acetonitrile solution of the complex. The compound crystallises in the triclinic space group P-1 and contains two complexes per asymmetric unit (Fig. 12), the overall molecular symmetry of the discrete complex is very close to C_{2h}. The metal centre retains a slightly distorted octahedral geometry with each Co(II) centre co-ordinating with two tri-dentate ligands (one hydroxyl and two quinoline donors per ligand)(Fig. 13). The complex was prepared in a 1:1 metal:ligand ratio however upon crystallisation Co(II) prefers the donation of two ligands. The coblt centres accommodate two donating oxygen moieties, which co-ordinate *trans* to each other in order to reduce steric interactions between ligands, and likely favoured through the trans effect. The presence of only one disordered perchlorate counter ion between both Co(II) centres in the asymmetric lattice suggest that one of the four O-donors may be protonated.

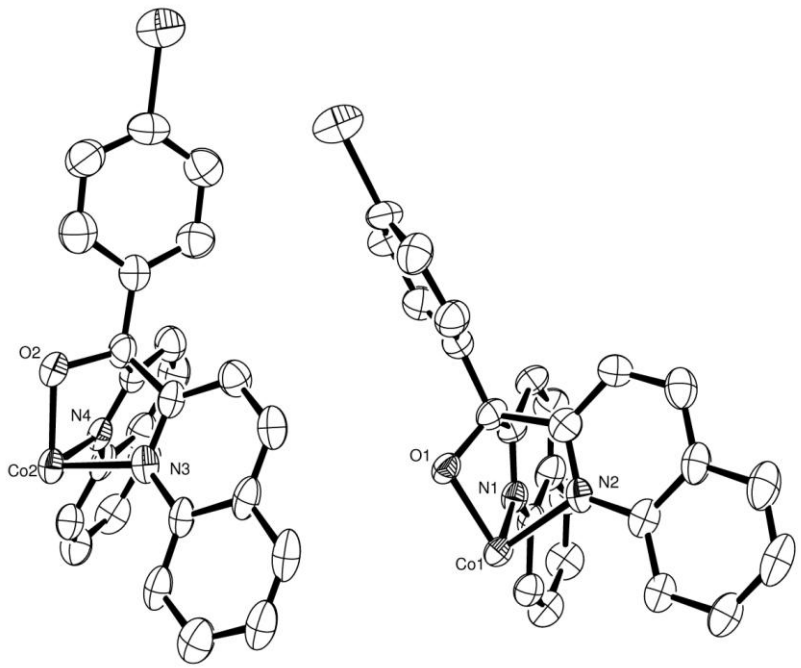

Figure 12: ORTEP Perspective view of the asymmetric unit for $[Co^{II}(\mathbf{L5})_2]_2[ClO_4]$ showing two halves of the complete complex. Displacement ellipsoids are shown at 50% probability with H atoms and solvent excluded for clarity.

Figure 13 shows two different views of the Co(II) complex with both surrounding ligands. It is possible to see how the ligands co-ordinate in opposite directions to reduce steric interactions and increase symmetry within the crystal lattice. The average Co-N bond length is 1.995(6) Å which is shorter but still comparable to 2.064(2) Å that derives from a Co(II)-quinoline bond of the complex $[Co(Cl)_3(quin)]^-$,[26] the shorter bond most likely occurs due to the chelating effect of **L5** pulling in the donors towards the metal centre. The Co-O bond distances in both complexes within the unit are identical giving a shorter bond value of 1.877(6) Å which is comparable to the complex $Co[Py)_2C(OH)_2]_2$ which presents a very similar donor set to **5.1**, giving an average Co-O bond length of 1.883(7) Å.[27] The average Co-N_{Py} bond length from this complex (1.930(8) Å)[27] are also comparable to the equivalent Co-N_{quin} bonds in **5.1**. The shorter Co-O bonds are associated with the electrostatic charge on oxygen increasing bond strength.

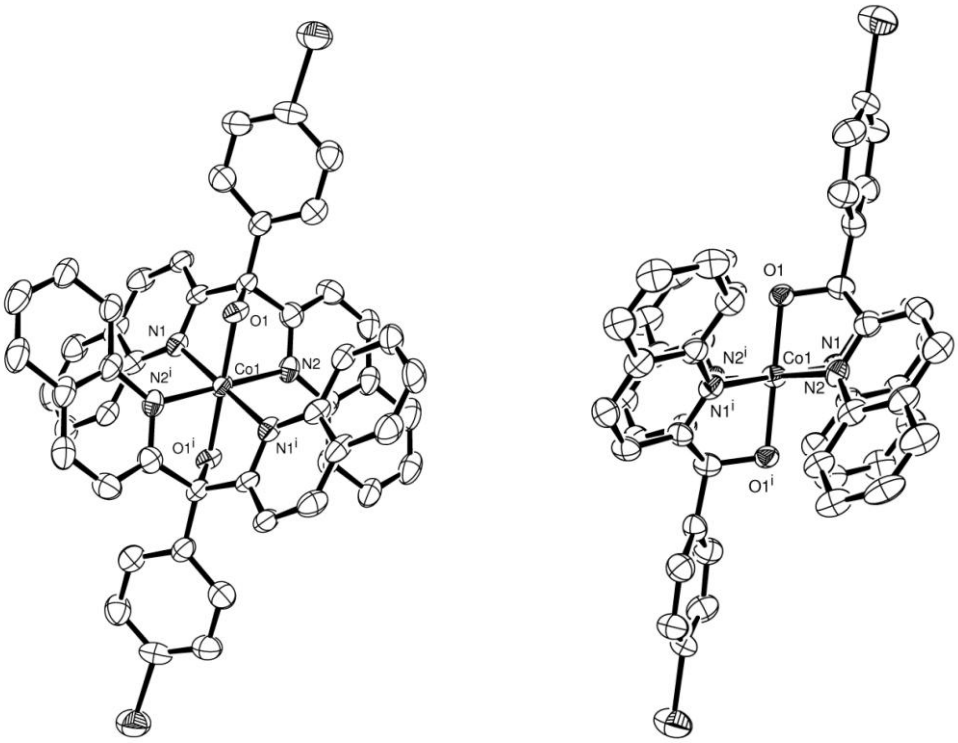

Figure 13: Two ORTEP Perspective views of the complete complex $[Co^{II}(\mathbf{L5})_2]$ showing how two ligands surround one octahedral Cobalt centre. Displacement ellipsoids are shown at 50% probability with H atoms, counter ions and solvent excluded for clarity.

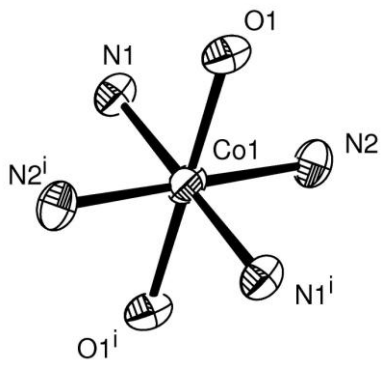

Figure 14: ORTEP Perspective view for the octahedral centre of the complex $[Co^{II}(\mathbf{L5})_2[ClO_4]]$. Showing only co-ordinating atoms.

Table 4: Selected bond Distances (Å) and Angles (°) for **5.1**

Bond	Length (Å)	Bond	Length (Å)
Co1-N1	2.007 (6)	Co2 – N3	1.999 (6)
Co1-N2	2.003 (6)	Co2 –N4	1.989 (7)
Co1-O1	1.877 (5)	Co2 –O2	1.876 (6)
Co1-N1^{i}	2.007 (6)	Co2 – N3^{i}	1.999 (6)
Co1- N2^{i}	2.003 (6)	Co2 – N4^{i}	1.989 (7)
Co1- O1^{i}	1.877 (5)	Co2 – O2^{i}	1.876 (6)
Bonds	**Angle (°)**	**Bonds**	**Angle (°)**
N1- Co1 –N2	87.8 (3)	N3- Co2 –N4	88.5(3)
N1- Co1 –O1	81.4 (2)	N3- Co2 –O2	82.1 (3)
N1- Co1 – N1^{i}	180.00 (1)	N3- Co2 – N3^{i}	180.0 (4)
N1- Co1 – N2^{i}	92.2 (3)	N3- Co2 – N4^{i}	91.5 (3)
N1- Co1 – O1^{i}	98.6 (2)	N3- Co2 – O2^{i}	97.9 (3)
N2- Co1 –O1	81.9 (3)	N4- Co2 –O2	82.2 (3)
N2- Co1 – N1^{i}	92.2 (3)	N4- Co2 – N3^{i}	91.5 (3)
N2- Co1 – N2^{i}	180.00 (1)	N4- Co2 – N4^{i}	180.0 (4)
N2- Co1 – O1^{i}	98.1 (3)	N4- Co2 – O2^{i}	97.8 (3)
O1- Co1 – N1^{i}	98.6 (2)	O2- Co2 – N3^{i}	97.9 (3)
O1- Co1 – N2^{i}	98.1 (3)	O2- Co2 – N4^{i}	97.8 (3)
O1- Co1 – O1^{i}	180.00 (19)	O2- Co2 – O2^{i}	180.0 (3)
N1^{i} - Co1 – N2^{i}	87.8 (3)	N3^{i} – Co2 – N4^{i}	88.5 (3)
N1^{i} - Co1 – O1^{i}	81.4 (2)	N3^{i} – Co2 – O2^{i}	82.1 (3)
N2^{i} - Co1 – O1^{i}	81.9 (3)	N4^{i} – Co2 – O2^{i}	82.2 (3)

Crystal Structure of $[Ni(HL5)(CH_3CN)_3]_2[ClO_4]_4$ (5.2):

The compound $[Ni(H\mathbf{L5})(CH_3CN)_3]_2[ClO_4]_4$ was crystalised by slow vapour diffusion of diethyl ether into a concentrated acetonitrile solution of the complex. The compound crystallised in a triclinic P-1 space group yielding blueish/grey rhombic like crystals suitable for data collection. The complex is mononuclear with two complexes and four perchlorate counter ions present in the asymmetric unit. The overall molecular symmetry of each complex is C_S with the ligand co-ordinating in a *fac* arrangement (Fig. 15) giving an octahedral geometry (Fig. 16). The presence of two counter ion per Ni(II) centre suggest that now the ligand is acting as a neutral donor unlike the previous Co(II) species (**5.1**).

Uniquely **5.2** has remained as a discrete 1:1 ratio complex with three acetonitrile solvent molecules for its remainder donor sites, rather than a second ligand seen previous in complex **5.1**. It is difficult to determine exactly why the two structures vary however, the mass spectrum for **5.2** did detect a significant amount of the $[Ni(\mathbf{L5})_2]$ species. It is therefore possible that solubility or crystal packing forces could have caused the 1:1 nickel complex to crystallizes faster thus giving this structure.

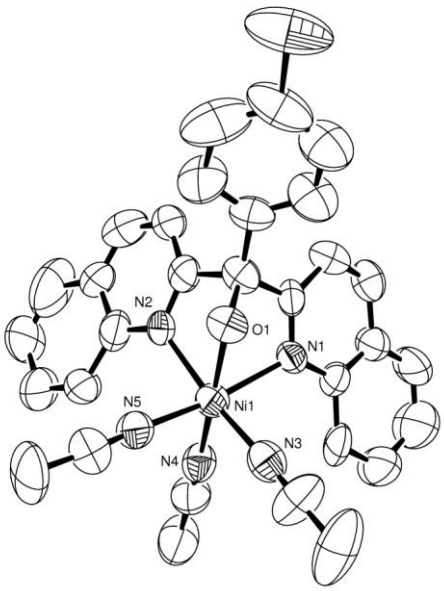

Figure 15: ORTEP Perspective view of the asymmetric unit for the complex **5.2** $[Ni^{II}(\mathbf{L5})(CH_3CN)_3[ClO_4]]$. Displacement ellipsoids are shown at 50% probability with H atoms, counter ions and solvent excluded for clarity.

It is common, and clear to see, that the Ni(II) centre is very close to octahedral in geometry. The Ni-N_{quin} bond lengths do not vary much and average 2.1445(10) Å. Interestingly this is approximately 0.15 Å longer than the equivalent bonds in the Co(II) structure, however are similar to the Ni-N_{quin} bond length of 2.779(14) Å from the Ni[Bis(methanol- κO)bis(quinoline-2-carboxylato-κ^2N,O)] complex.[28] The Ni-$N_{solvent}$ bonds are shorter than those measured for the quinoline donors giving an average length 2.0445(14) Å, most likely due to reduced sterics in the linear solvent molecules allowing closer interactions and hence strengthening the Ni- $N_{solvent}$ bonds. These bonds fit well with a series of Ni(II) complexes with tetradentate tripodal 4N ligands such as N,N-dimethyl-N',N'-bis(pyrid-2-ylmethyl)ethane-1,2-diamine which have Ni-$N_{Acetonitrile}$ bonds lengths ranging 2.031(4)-2.0735(19) Å.[29]

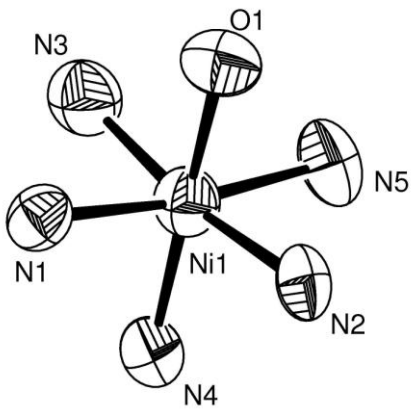

Figure 16: ORTEP Perspective view for the octahedral centre of the complex $[Ni^{II}(\mathbf{L5})(CH_3CN)_3[ClO_4]]$. Showing only co-ordinating atoms.

Table 5: Selected bond Distances (Å) and Angles (°) for **5.2**			
Bond	Length (Å)	Bond	Length (Å)
Ni1-N1	2.152 (9)	Ni2-N6	2.141 (10)
Ni1-N2	2.135 (10)	Ni2-N7	2.150 (10)
Ni1-N3	2.064 (14)	Ni2-N8	2.023 (14)
Ni1-N4	2.045 (12)	Ni2-N9	2.055 (15)
Ni1-N5	2.036 (11)	Ni2-N10	2.044 (11)
Ni1-O1	2.053 (10)	Ni2-O2	2.041 (10)
Bonds	Angle (°)	Bonds	Angle (°)
N1- Ni1 –N2	87.0 (3)	N6- Ni2 –N7	86.9 (3)
N1- Ni1 –N3	91.5 (4)	N6- Ni2 –N8	169.1 (4)
N1- Ni1 – N4	98.0 (4)	N6- Ni2 – N9	100.2 (4)
N1- Ni1 –N5	169.7 (4)	N6- Ni2 –N10	91.7 (4)
N1- Ni1 –O1	75.9 (4)	N6- Ni2 –O2	75.3 (4)
N2- Ni1 – N3	169.2 (4)	N7- Ni2 – N8	90.0 (4)
N2- Ni1 –N4	98.0 (4)	N7- Ni2 –N9	98.4 (4)
N2- Ni1 –N5	90.2 (4)	N7- Ni2 –N10	170.4 (4)
N2- Ni1 – O1	74.7 (3)	N7- Ni2 – O2	76.2 (3)
N3- Ni1 –N4	92.7 (4)	N8- Ni2 –N9	90.6 (5)
N3- Ni1 –N5	89.3 (4)	N8- Ni2 –N10	89.6 (5)
N3- Ni1 – O1	94.6 (3)	N8- Ni2 – O2	93.8 (3)
N4- Ni1 –N5	92.1 (4)	N9- Ni2 –N10	91.2 (4)
N4- Ni1 –O1	170.6 (4)	N9- Ni2 –O2	173.0 (4)
N5- Ni1 – O1	93.8 (4)	N10- Ni2 – O2	94.3 (4)

Crystal Structure of $[(Cu(L5))_3(ClO_4)][ClO_4]_2$(5.3):

Crystals suitable for X-ray crystallographic studies of the complex $[(Cu(\mathbf{L5}))_3(ClO_4)][(ClO_4)]_2$ were obtained through vapour diffusion of petroleum ether into a concentrated acetonitrile solution of the complex, yielding bright green crystals. The complex crystallised in the monoclinic space group $P2_1/c$ with the asymmetric unit containing two identical trimer species with their molecular symmetry closely representing C_3. As seen in Figure 17 each trimer is constructed of three ligands and three Cu(II) centres all interacting through the bridging O^- of the apical hydroxyl group on each ligand, forming a six membered Cu-O ring.

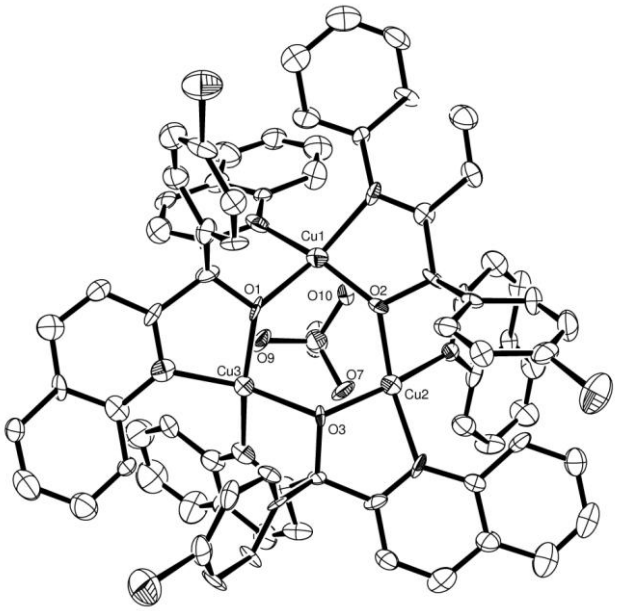

Figure 17: ORTEP Perspective view of the asymmetric unit for the complex **5.3 -** $3[Cu^{II}(\mathbf{L5})[ClO_4]]$. Displacement ellipsoids are shown at 50% probability with H atoms, counter ions and solvent excluded for clarity.

This type of trinuclear copper structure has been seen previous using tridentate schiff base ligands (see Fig. 18) giving an average Cu-µO bond length of 1.985(4) Å[30] which is comparable to the observed average Cu-µO bond length 1.943(14) Å. Existing Cu-µO tetramer cores are more common and have bonds ranging from 1.901-2.573 Å.[31]

In **5.3**, all the Cu(II) centres are 5 co-ordinate and identically made up of two Cu-N, two Cu-(µ-O) and one Cu-O bonds resulting in a solid state geometry close to square pyramidal, seen more

clearly in Figure 19. The two quinoline donors on each Cu(II) centre originate from separate ligands and give a Cu-N average bond length of 2.006(18) Å, slightly longer than the bridging oxygen bonds, possibly due to the nitrogens being neutral donors These bond lengths are within range of values found in similar systems.[31]

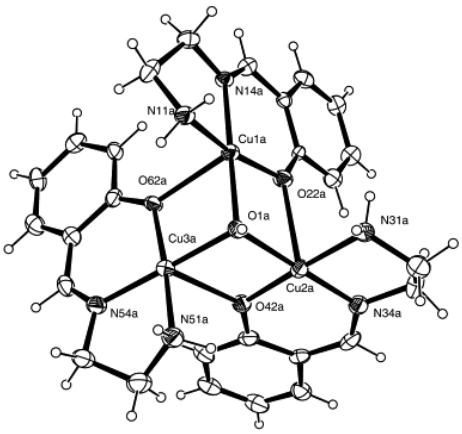

Figure 18: ORTEP image of (Cu(2-[(2-amino-ethylimino)-methyl]-phenol))$_3$(μ_3-OH)](ClO_4)$_2$·3.75H_2O.[30]

Another interesting feature is the presence of a capping perchlorate anion which is seen to co-ordinate with all three copper centres (Fig. 19), this is unusual and also seen in the analogous Cu(II) complex with **L5** discussed later (complex **6.1**). Previous examples of co-ordinating perchlorates in clusters only involve one of the Cu(II) environments weakly bonding to a perchlorate across the lattice, between discrete complexes, with bond lengths averaging 2.652(14) Å. In this example the average Cu-O bond length to the capping perchlorate is 2.611(14) Å which is much longer and presumably weaker than other bonds within the complex.

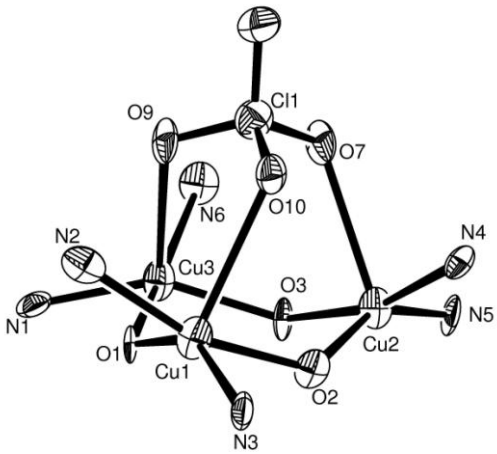

Figure 19: ORTEP Perspective view of the co-ordinating centre for the trimer complex 3[Cu^{II}(**L5**)[ClO_4]]. All Copper centres are 5 co-ordinate with a geometry between a square based pyramid and trigonal bipyramidal. Note the capping perchlorate counter ion.

An interesting part of this perchlorate binding is how each copper co-ordinates to its own oxygen from the anion creating a capping type structure. This is an unusual species with only a few cases reported in literature, for example in the development of single molecule magnets (SMM's) using (Mn_3O(Me-salox)$_3$($MeOH$)$_3$(ClO_4)]-MeOH) trimers, figure 20.[32] Also as potential catalysts in Cu(I) 2,4,6-tris(1-benzyenzimidazol-2-yj)benzene tetramers, $(Cu_4L5)^{4+}$,[33] or the Cu(II) trimer [Cu_3(NHDEPO)$_3$(ClO_4)O] NHDEPO = 3-[3-(diethylamino)proplimino]butan-2-one oxime),[34-36] see Figure 20.

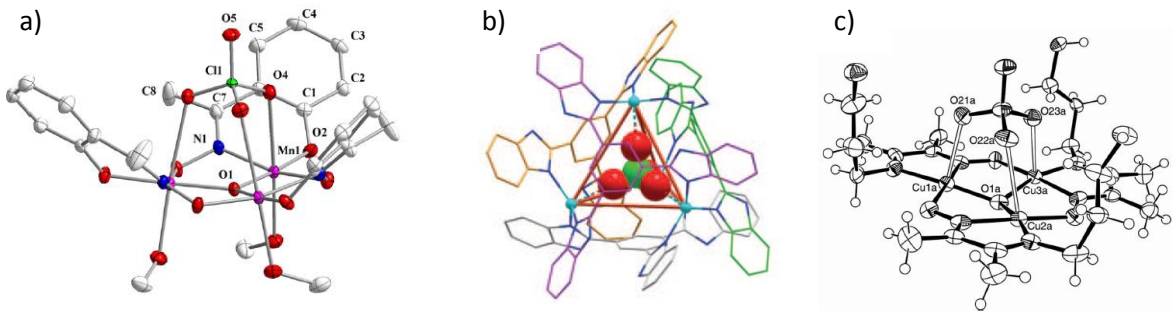

Figure 20: Showing examples of capping perchlorate ions. (a) Mn_3O(Me-salox)$_3$($MeOH$)$_3$(ClO_4)]-MeOH trimer (b) (Cu_4(2,4,6-tris(1-benzyenzimidazol-2-yj)benzene)$_4$ tetramer and (c) [Cu_3(NHDEPO)$_3$(ClO_4)O].[32-36]

Table 6: Selected bond Distances (Å) and Angles (°) for **5.3**

Bond	Length (Å)	Bond	Length (Å)	Bond	Length (Å)
Cu1-N2	1.967 (19)	Cu2-N4	1.966 (18)	Cu3-N1	1.996 (18)
Cu1-N3	2.037 (18)	Cu2-N5	2.038 (17)	Cu3-N6	2.030 (20)
Cu1-O1	1.967 (14)	Cu2-O2	1.955 (13)	Cu3-O1	1.920 (14)
Cu1-O2	1.897 (13)	Cu2-O3	1.920 (13)	Cu3-O3	1.996 (18)
Cu1-O10	2.588 (14)	Cu2-O7	2.593 (14)	Cu3-O9	2.652 (14)
Bonds	**Angle (°)**	**Bonds**	**Angle (°)**	**Bonds**	**Angle (°)**
N2-Cu1-N3	106.6 (7)	N4-Cu2-N5	104.5 (8)	N1-Cu3-N6	107.6 (8)
N2-Cu1-O1	84.0 (7)	N4-Cu2-O2	84.6 (7)	N1-Cu3-O1	83.2 (7)
N2-Cu1-O2	161.8 (7)	N4-Cu2-O3	164.1 (7)	N1-Cu3-O3	147.3 (7)
N2-Cu1-O10	81.5 (7)	N4-Cu2-O7	81.4 (7)	N1-Cu3-O9	108.3 (7)
N3-Cu1-O1	146.8 (7)	N5-Cu2-O2	149.9 (7)	N6-Cu3-O1	159.3 (7)
N3-Cu1-O2	83.5 (7)	N5-Cu2-O3	81.9 (7)	N6-Cu3-O3	83.6 (8)
N3-Cu1-O10	106.5 (7)	N5-Cu2-O7	104.9 (7)	N6-Cu3-O9	78.1 (7)
O1-Cu1-O2	95.8 (6)	O2-Cu2-O3	97.1 (6)	O1-Cu3-O3	96.9 (6)
O1-Cu1-O10	106.1 (7)	O2-Cu2-O7	104.7 (7)	O1-Cu3-O9	81.7 (7)
O2-Cu1-O10	81.1 (7)	O3-Cu2-O7	82.9 (7)	O3-Cu3-O9	104.0 (7)

Crystal Structure of $[Re(CO)_3(L5)]$ (5.5):

Slow evaporation of acetonitrile from a complex solution produced small pale yellow crystals suitable for crystallographic studies. The crystal forms in the triclinic space group P-1 with two complete complexes per asymmetric unit. All available donor groups of the ligand, two quinolines and a hydroxyl, are involved in co-ordination where they bind in a *fac* arrangement which is expected by the topography of the ligand (Fig. 21). This gives a molecular symmetry of C_S for the complex. Stabilisation through π-backbonding to the carbonyl groups explain the relative shortness of the Re-CO bonds. These bonds vary little and average at 1.925(4) Å which is perfectly comparable to similar Re-CO compounds with bonds ranging from 1.896 Å to 1.969 Å.[16,37]

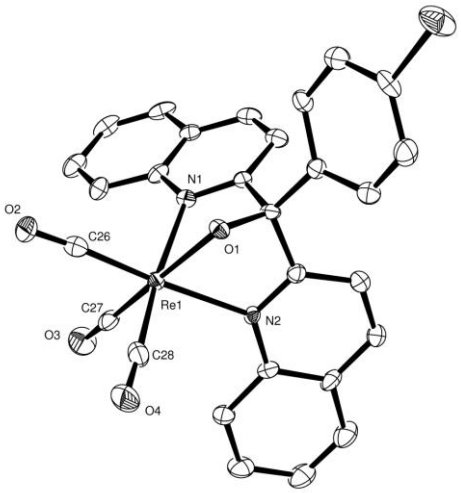

Figure 21: ORTEP Perspective view of the asymmetric unit for the complex **5.5** $[Re(CO)_3(L5)]$. Showing the *fac* co-ordination of the ligand. Displacement ellipsoids are shown at 50% probability with H atoms and solvent removed for clarity.

The Re-N bonds are the longest within the complex ranging from 2.221-2.244(4) Å and are comparable to 2.223(8) Å which are the Re-N bond lengths from a related bis-quinoline compound $[Re(CO)_3(L–N_3)]Br$, $L-N_3$ = (2-azido-N,N-bis((quinolin-2-yl)methyl)ethanamine), see figure 5.[16] The Re-O bonds are shorter than those to the quinoline by 0.2 Å, possibly due to the electrostatic attraction involved from the oxygen, as its considered to have a negative charge, therefore keeping the overall complex neutral. As a consequence of using the oxygen moiety the pendent benzyl-bromide group moves to the apical position of the complex, this allows for

the potential to use this group, through coupling reactions such as Heck, Negishi Suzuki, Stille, Kumada and Sonogashira etc, to create a library of new functionalized ligands, represented in Figure 22 with a Heck coupling.

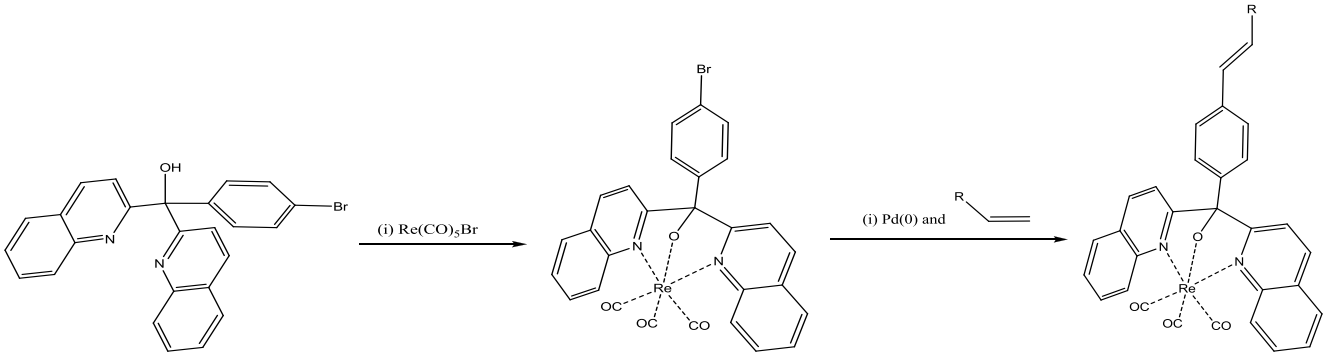

Figure 22: Scheme showing apical positioning of phenyl bromide group in **L5** upon co-ordination with Re(I). The second stage represents an example for the library of precursors that **L5** could potentially couple with.

Table 7: Selected bond Distances (Å) and Angles (°) for **5.5**

Bond	Length (Å)	Bond	Length (Å)
Re1-N1	2.228 (4)	Re2-N3	2.237 (4)
Re1-N2	2.244 (4)	Re2-N4	2.221 (4)
Re1-O1	2.076 (4)	Re2-O5	2.077 (4)
Re1-C26	1.921 (6)	Re2-C54	1.919 (6)
Re1-C27	1.923 (6)	Re2-C55	1.932 (6)
Re1-C28	1.920 (6)	Re2-C56	1.934 (7)
Bonds	Angle (°)	Bonds	Angle (°)
N1-Re1-N2	81.77 (15)	N3-Re2-N4	82.39 (16)
N1-Re1-O1	74.21 (15)	N3-Re2-O5	74.07 (16)
N1-Re1-C26	98.2 (2)	N3-Re2-C54	95.2 (2)
N1-Re1-C27	96.7 (2)	N3-Re2-C55	167.9 (2)
N1-Re1-C28	172.9 (2)	N3-Re2-C56	99.7 (2)
N2-Re1-O1	74.46 (15)	N4-Re2-O5	73.85 (16)
N2-Re1-C26	173.3 (2)	N4-Re2-C54	175.8 (2)
N2-Re1-C27	99.63 (19)	N4-Re2-C55	93.6 (2)
N2-Re1-C28	93.7 (2)	N4-Re2-C56	97.5 (2)
O1-Re1-C26	99.1 (2)	O5-Re2-C54	102.1 (2)
O1-Re1-C27	169.6 (2)	O5-Re2-C55	93.9 (2)
O1-Re1-C28	99.4 (2)	O5-Re2-C56	169.79 (19)
C26-Re1-C27	87.0 (2)	C54-Re2-C55	88.0 (2)
C26-Re1-C28	85.6 (2)	C54-Re2-C56	86.3 (3)
C27-Re1-C28	89.4 (3)	C55-Re2-C56	92.1 (3)

5.27 Conclusion

A series of transition metal complexes with the tridentate ligand bis(2-quinoline)(4-bromo-phenyl)menthanol (H**L5**) have been synthesised and structurally characterized.

All the compounds were synthesised in a 1:1 stoichiometry from solutions of acetonitrile with only complexes **5.2**, **5.4** and **5.5** resulting in expected monomeric structures. The Co(II) complex (**5.1**) was also monomeric but was found to preferentially form a 1:2 metal:ligand species in solid state. However, from the collected data it is not possible to confirm the same structure in solution. In all compounds, **L5** is seen to bond through the apical alcohol moiety and in most cases acts as an anionic donor, with exception of **5.2** which has two perchlorates present for each Ni(II) centre. In the case of **5.1** the two donating ligands counteract the 2+ metal centre giving the complex a neutral overall charge. The same also applies to the Re(I) complex **5.5** which only requires one anionic ligand for neutral formation. The Cu(II) complex (**5.3**) is unique in that it forms a trimer species constructed from three ligand molecules around three copper(II) centres, with a capping perchlorate molecule co-ordinating over the three metal centres. In this compound each ligand unit is co-ordinated to two copper centres once through each quinoline and secondly through a bridging oxygen. This resulted in the formation of a six membered ring made from three coppers and three bridging oxygens. It should also be noted that all the Cu(II) centres are five co-ordinate with a near square-pyramidal geometry. This is contrary to all other complexes which were found to be hexa co-ordinated and strongly octahedral. The ligand is considered to be weak-field in nature, which was confirmed by magnetic susceptibility measurements found by the Evans method, where the ^{1}H-NMR resulted in a high spin complex for **5.1** (μ_{eff} = 3.99μ_B). This is also supported by the relatively high nephlauxetic parameter's calculated for compounds **5.1** and **5.2** (β = 0.7 and 0.8 respectively), characteristic of 'hard' or weak-field ligands. Also of note from the available data is that L5 appears to triply donate in a *fac* arrangement relative to the metal centre, which is unsurprising when considering the positions of donors within the ligand.

5.3 Experimental

Bis(2-quinoline)methanone ($C_{19}H_{12}N_2O$) (**S1**):

The synthesis of **S1** was achieved following literature published by Burns et al with a modified purification.[20] The crude product was washed with a minimum amount of methanol followed by a minimum amount of diethyl ether giving a white solid of high purity (59%). ^{1}H-NMR (DMSO; 300MHz): δ_H 8.29(d, 2H, J=8.5Hz, *CH*), 8.16(d, 2H, J=8.5Hz, *CH*), 8.11(d, 2H, J=8.5Hz, *CH*), 7.83(d, 2H, J=8.2Hz, *CH*), 7.69(t, 2H, J=7.7Hz, *CH*), 7.58(t, 2H, J=7.5Hz, *CH*).

Bis(2-quinoline)(4-bromo-phenyl)menthanol ($C_{25}H_{17}N_2OBr$) (**HL5**):

1-bromo-4-iodobenzene (274mg, 0.97mmol) was dissolved in dried and degassed THF (250ml) then cooled to -78°C with continuous stirring under inert atmosphere. nBuLi (0.62ml, 0.99mmol, 1.6M in hexane) was then added dropwise to the pre-cooled solution over a period of 10 minutes. After lithiation a pre-cooled (-20°C) solution of **S1** (270mg, 0.95mmol) in THF (40ml, dried and degassed) was slowly transferred, in portions, into the mixture forming an intense pink solution. The solution was left to stir for 16h and allowed to slowly warm to RT. Next the reaction was quenched with a 10% HCl solution until pH3 followed then by a solution of 10% K_2CO_3 until the mixture was pH9. The crude product was then extracted into chloroform (3x60ml), dried over $MgSO_4$ and reduced to dryness *in vacuo*. The product was obtained as a brown solid in high purity by washing in a minimum of diethyl ether (320mg, 76%). ^{1}H-NMR (DMSO; 300MHz): δ_H 8.36(d, 2H, J=8.5Hz, CH), 7.98(d, 2H, J=8.5Hz, CH), 7.91(d, 2H, J=8.5Hz, CH), 7.80(d, 2H, J=8.5Hz, CH), 7.72(t, 2H, J=7.5Hz, CH), 7.60(t, 2H, J=7.5Hz, CH), 7.52(d, 2H, J=8.5Hz, CH), 7.45(s, 1H, OH), 7.41(d, 2H, J=8.5Hz, CH). ^{13}C-NMR ($CDCl_3$; 100MHz): 162.30(C), 145.85(C), 145.16(C), 136.41(CH), 131.17(CH), 129.74(CH), 129.53(CH), 129.20(CH), 127.51(CH), 127.38(C), 126.76(CH), 121.67(C), 121.30(CH), 80.59(C). HRMS (AP-MS) *m/z* calcd. 441.0602 ; exp. 441.0613 $[C_{25}H_{17}N_2OBr]^+$ (100). FT-IR (KBr/cm^{-1}) ν = 3388Br, 3059m, 3044m, 1617m, 1597s, 1567m, 1500s, 1487s, 1424m, 139m, 1351m, 1330m, 1306m, 1173m, 1069s, 1013m, 962w, 927w, 842m, 827s, 802s, 787m, 770w, 754s, 621w, 578m, 545br+w. UV-Vis [λ_{max}, nm, (εM, M^{-1}cm^{-1})] in CH_3CN: 240(24532), 270(12904), 302(11879), 316(13929). Found: C 67.93; H 3.88; N 6.28 (%) $C_{25}H_{17}N_2OBr$ Requires: C 68.02; H 3.88; N 6.35 (%).

Co(II) bis(2-quinoline)(4-bromo-phenyl)menthanol $[CoC_{25}H_{16}N_2OBr][ClO_4]_2$ (**5.1**):

A solution of Co(II) perchlorate hexahydrate $[Co(ClO_4)_2.6H_2O]$ (11.8mg, 0.0322mmol) in acetonitrile (1ml) was added in portions to a stirring solution of H**L5** (14.2mg, 0.0322mmol) in DCM (2ml). The resulting orange mixture was stirred overnight allowing the temperature to return to ambient. A brown/orange precipitate was obtained upon addition of diethyl ether, filtered and dried in air. A portion of the solid was dissolved in acetonitrile (3ml) and filtered through celite, vapour diffusion of diethyl ether yielded bright orange crystals of high purity. (16mg, 62%). HRMS (ES-MS) *m/z* calcd. 519.4901; exp. 519.4874 $[2(CoC_{25}H_{16}N_2OBr)CH_3CN]^{2+}$ (30%); calcd. ; exp. 640.9599 $[(CoC_{25}H_{16}N_2OBr)(ClO_4)CH_3CN]^+$ (15%); calcd. 599.9322; exp. 599.9313 $[(CoC_{25}H_{16}N_2OBr)(ClO_4)]^+$ (12%). IR (KBr/cm^{-1}) ν = 3400br+s, 3066m, 2980m, 1619m, 1598m, 1508m, 1486w, 1431w, 1381w, 1145s, 1120s, 1090s, 1009m, 826m, 804m, 757m, 626s, 476m. UV-Vis [λ_{max}, nm, (εM, M^{-1}cm^{-1})] in CH_3CN: 243(19917), 302(10430), 331(3268), 436(26). Magnetic moment (Evans method, 293K, Acetonitrile): μ_{eff} = 3.99μ_B. Found: C 40.64; H 2.84; N 3.99 (%) $C_{25}H_{16}N_2OBrCo(2ClO_4).2H_2O$ Requires: C 40.88; H 2.75; N 3.82 (%).

Ni(II) bis(2-quinoline)(4-bromo-phenyl)menthanol $[Ni(C_{25}H_{16}N_2OBr)(CH_3CN)_3][2ClO_4]$ (**5.2**):

A solution of Ni(II) perchlorate hexahydrate $[Ni(ClO_4)_2.6H_2O]$ (12.4mg, 0.034mmol) in acetonitrile (3ml) was added in portions to a stirring solution of H**L5** (15mg, 0.034mmol) in hot acetonitrile (4ml). The resulting dark yellow mixture was stirred overnight maintaining the temperature at 50°C. The yellow solution was reduced by half *in vacuo*, filtered through celite and purified by vapour diffusion using diethyl ether. yielding the pure product as blueish/grey coloured crystals (13mg, 47%). HRMS (ES-MS) *m/z* calcd. 1097.4606; exp. 1097.2512 $[2(NiC_{25}H_{16}N_2OBr)ClO_4]^+$ (100%); calcd. 1017.5571; exp. 1017.3569 $[Ni_2(C_{25}H_{16}N_2OBr)(C_{25}H_{16}N_2O)(2ClO_4)]^+$ (45%). calcd. 1138.2174; exp. 1138.3313 $[Ni(C_{25}H_{16}N_2OBr)_2.2ClO_4]^+$ (30%). calcd. 939.4056; exp. 939.3171 $[Ni(C_{25}H_{16}N_2OBr)_2]^+$ (5%). IR (KBr/cm^{-1}) ν = 3419br+s, 3060m, 3006m, 2980m, 2936m, 2712w, 2021w, 1656s, 1621s, 1593s, 1574m, 1510s, 1489s, 1435s, 1378s, 1340m, 1307m, 1245w, 1218m, 1094br+s, 992 s, 950s, 934m, 879w, 839s, 824s, 784s, 765s, 729w, 624s, 579m, 493m, 467w. UV-Vis [λ_{max}, nm, (εM, M^{-1}cm^{-1})] in CH_3CN: 238(25078), 279(12122), 315(10302), 400(16.4), 581(9.4), 964(7.1), 1006(7.5). Magnetic moment (Evans method, 293K, Acetonitrile): μ_{eff} = 2.77μ_B.

Cu(II) bis(2-quinoline)(4-bromo-phenyl)menthanol $[(CuC_{25}H_{16}N_2OBr)_3(ClO_4)][ClO_4]_2$ (**5.3**):

A solution of Cu(II) perchlorate hexahydrate $[Cu(ClO_4)_2.6H_2O]$ (46.2mg, 0.125mmol) in hot (50°C) acetonitrile (3ml) was added in portions to a stirring solution of H**L5** (55mg, 0.125mmol) in hot acetonitrile (4ml). The resulting green mixture was stirred overnight allowing the temperature to return to ambient. A light green precipitate was obtained upon addition of diethyl ether, filtered and dried in air. A portion of the solid was dissolved in acetonitrile (3ml) and filtered through celite, vapour diffusion of petroleum ether yielded bright green crystals of high purity. (52mg, 51%). HRMS (ES-MS) *m/z* calcd. 524.4888; exp. 524.4855 $[2(CuC_{25}H_{16}N_2OBr)CH_3CN]^{2+}$ (100%); calcd. 544.0086; exp. 544.0107 $[(CuC_{25}H_{16}N_2OBr)CH_3CN]^{+}$ (25%). IR (KBr/cm^{-1}) ν = 3372br, 3085m, 2932w, 2863w, 2251m, 2022w, 1622m, 1597s, 1510s, 1484s, 1432s, 1383s, 1346m, 1286m, 1215m, 1109br+s, 1008s, 960s, 874m, 825s, 808s, 781s, 754s, 701w, 625s, 571m, 475m. [λ_{max}, nm, (εM, M^{-1}cm^{-1})] in CH_3CN: 244(32843), 316(22927), 787(79). Magnetic moment (Evans method, 293K, Acetonitrile): μ_{eff} = 1.61μ_B. Found: C 42.85; H 2.38; N 4.06 (%) $C_{25}H_{16}N_2OBrCu(2ClO_4)$. Requires: C 42.71; H 2.30; N 3.99 (%).

Zn(II) bis(2-quinoline)(4-bromo-phenyl)menthanol $[ZnC_{25}H_{16}N_2OBr][ClO_4]_2$ (**5.4**):

A solution of Zn(II) perchlorate hexahydrate $[Zn(ClO_4)_2.6H_2O]$ (14.7mg, 0.0396mmol) in acetonitrile (0.5ml) was added in portions to a stirring solution of H**L5** (17.5mg, 0.0396mmol) in hot acetonitrile (2.5ml). The resulting pale yellow solution was stirred overnight and filtered through celite. Addition of diethyl ether to the filtered solution yielded an off-white precipitate that was filtered and dried in air. The solid was of good purity suitable for analysis (14.5mg, 45%). ^{1}H-NMR (CD_3CN; 250MHz): δ_H 8.78(2H, d, J=8.5Hz, CH), 8.39(2H, d, J=8.2Hz, CH), 8.19(2H, d, J=7.8Hz, CH), 8.08(4H, d, J=7.5Hz, CH), 7.85(2H, t, J=7.3Hz, CH), 7.60(2H, d, J=8.0Hz, CH), 7.4(2H, t, J=8.1Hz, CH). ^{13}C-NMR (CD_3CN; 125MHz): 160.1(C), 142.87(CH), 136.6(C), 133.1(CH), 132.01(CH), 131.0(C), 129.94(CH), 129.2(CH), 128.64(CH), 128.12(C), 125.21(CH), 123.12(C), 120.87(CH), 40.53(C). HRMS (ES-MS) *m/z* calcd. 505.9790 ; exp. 505.9714 $[2(ZnC_{25}H_{16}N_2OBr)]^{2+}$ (20%); calcd. 604.9278 ; exp. 604.9307 $[(ZnC_{25}H_{16}N_2OBr)(ClO_4)]^{+}$ (20%); calcd. 645.9546 ; exp. 645.9580 $[(ZnC_{25}H_{16}N_2OBr)(ClO_4)]^{+}$ (10%). IR (KBr/cm^{-1}) ν = 3475br+s, 3100m, 2926w, 1621s, 1597s, 1533m, 1508s, 1485m, 1432m, 1384m, 1345w, 1307w, 1218w, 1143s, 1108br+s, 1009s,

928m, 824s, 806s, 783m, 755m, 636s, 626s, 571w. Found: C 42.41; H 2.47; N 3.84 (%) $C_{25}H_{16}N_2OBrZn(2ClO_4)$. Requires: C 42.60; H 2.29; N 3.98 (%).

Rhenium-*fac*-tricarbonyl-bis(2-quinoline)(4-bromo-phenyl)menthanol bromide [$Re(CO)_3$(C25H17N2OBr)Br] (**5.5**):

L5 (85mg, 0.19mmol) and $Re(CO)_5Br$ (78mg, 0.19mmol) were both added to a flask along with dried and degassed toluene (60ml). The mixture was then refluxed under nitrogen for 14h producing a dark solution. The solution was then allowed to cool slightly before filtering warm (50°C) to remove any dark solid. The filtrate was then left to further cool yielding the product as a yellow precipitate in high purity. The product was filtered and dried using a minimum of diethyl ether (97mg, 64%). ^{1}H-NMR (DMSO; 300MHz): δ_H 8.68(d, 2H, J=9Hz, CH), 8.61(d, 2H, J=9Hz, CH), 8.31(s, 1H, OH), 8.08(m, 6H, J=9Hz, CH), 7.73(m, 4H, J=9Hz, CH), 7.56(d, 2H, J=9Hz, CH). ^{13}C-NMR (DMSO; 125MHz): 200.63(CO), 199.61(CO), 168.89(C), 147.02(C), 142.68(C), 140.68(CH), 137.80(C), 133.15(CH), 132.12(CH), 129.95(CH), 129.35(CH), 128.65(CH), 127.62(CH), 125.76(C), 121.55(CH), 97.25(C). HRMS (ES-MS) *m/z* calcd. 710.9913; exp. 710.9915 $[C_{28}H_{17}N_2O_4BrRe]^+$ (100%). FT-IR (KBr/cm^{-1}) ν = 3072w, 2359m, 2341m, 2216w, 2009s, 1980s, 1868.s, 1619m, 1593m, 1508m, 1490m, 1072m, 1011m, 997m, 872m, 824m, 809m, 779m, 759m, 732m, 644m. [λ_{max}, nm, (εM, M^{-1}cm^{-1})] in CH_3CN: 255(36857), 310(20126), 338(8810), 416(440). Found: C 47.33; H 2.45; N 3.86 (%) $C_{25}H_{16}N_2OBrRe(CO)_3$. Requires: C 47.31; H 2.27; N 3.94 (%).

Rhenium-*fac*-tricarbonyl-bis(2-quinoline)(4-bromo-phenyl)menthanol,

[$C_{25}H_{16}N_2OBrRe(CO)_3$] (**5.5a**):

A sample of **5.5** (10mg, 0.013mmol) was dissolved in d6-DMSO (1ml) and triethyl amine (0.1ml) was added. The mixture was stirred for 15 minutes and the resulting solution was directly analysed by ^{1}H-NMR giving the deprotonated product (100%). ^{1}H-NMR (DMSO; 300MHz): δ_H 8.68(d, 2H, J=9Hz, CH), 8.61(d, 2H, J=9Hz, CH), 8.08(m, 6H, J=9Hz, CH), 7.75(t, 2H, J=9Hz, CH), 7.70(d, 2H, J=9Hz, CH), 7.56(d, 2H, J=9Hz, CH). ^{13}C-NMR (DMSO; 125MHz): 168.95(C), 147.25(C), 142.85(C), 140.70(CH), 138.02(C), 133.15(CH), 132.12(CH), 130.20(CH), 129.0(CH), 127.40(CH), 126.00(CH), 125.91(C), 121.55(CH), 97.31(C).

5.4 References

1. D. H. Brown, R. H. Nuttall, J. McAvoy, D. W. A. Sharp,. *J. Chem. Soc A.*, **1966**, (7), 892-6.
2. R. D. Patel, H. S. Patel, S. R. Patel,. *Euro. Polym. J.*, **1987**, 23(3), 229-32.
3. P. Jiang, Z. Guo., *Coord. Chem. Revs.*, **2004**, 248, 205-229.
4. L. Xue, H-H. Wang, X-J. Wang, H. Jiang, *Inorg. Chem*. **2008**, 47(10), 4310-4318.
5. Y. Zhang, X. Guo,; W. Si, Jia, X. Qian, *Org. Letts.*, **2008**, 10(3), 473-476.
6. G. Scheibe, Rossne, *Bur. Dtsch. Chem. Ges B: Abhandlungen*, **1921**, 54B, 786-795.
7. G. Scheibe, H. J. Friedrich, *Z. Elktrochem. Angew. P.,* **1960,** 64*,* 720-726.
8. H. J. Friedrich, W. Gueckel, G. Scheibe,. *Chem. Ber.*, **1962**, 95, 1378-1387.
9. L. He, X. Wang, X. Gan, N. Tang, M. Tan,. *Wuji Huaxue Xuebao.*, **1990**, 6(3), 303-8.
10. D. S. C. Black, R. C. Srivastava,. *Aust. J. Chem.*, **1969**, 22, 1439-1447.
11. C. Deraeve, C. Boldron, A. Maraval, H. Mazarguil, H. Gornitzka, L. Vendier, M. Piti, B. Meunier, *Chem. Eur. J.* **2008,** 14, 682-696.

12) a) M. Mattson, *Nature.*, **2004,** 430, 631 – 639

b) M. Citron, *Nat. Rev. Neurosci*. **2004**, 5, 677 – 685

c) E. Gaggelli, H. Kozlowski, D. Valensin, G. Valensin, *Chem. Rev*. **2006**, 106, 1995–2044.

13. R. Cherny, J. Legg, C. McLean, D. Fairlie, X. Huang, C. Atwood, K. Beyreuther, R. Tanzi, C. Masters, A. Bush, *J. Biol. Chem*. **1999**, 274, 23223–23228.
14. R. Cherny, K. Barnham, T. Lynch, I. Volitakis, Q. Li, C. McLean, G. Multhaup, K. Beyreuther, R. Tanzi, C. Masters, A. Bush, *J. Struct. Biol*. **2000**, 130, 209–216.

15. a) K. A. Stephenson, S. R. Banerjee,T. Besanger, O. O. Sogbein, M. K. Levadala, N. McFarlane, J. A. Lemon, D. R. Boreham, K. P. Maresca,J. D. Brennan,. *J. Am. Chem. Soc.*, **2004**, 126, 8598-8599.

b) L. Wei, J. W. Babich, W. Ouellette, J. Zubieta,. *Inorg, Chem*, **2006**, 45(7), 3057-3066.

c) M. D. Bartholoma, A. R. Vortherms, S. Hillier, J. Joyal, J. Babich, R. P. Doyle, J. Zubieta***,*** *Dalton. Trans.*, **2011**, 40(23), 6216-25.

16. G. Gasser, A. Pinto, S. Neumann, A. M. Sosniak, M. Seitz, K. Merz, R. Heumann, N. Metzler-Nolte,. *Dalton Trans.*, **2012**, 41, 2304-2313.
17. N. Violas-Villegas, A. E. Rabideau, M. Bartholoma, J. Zubieta, R. Doyle,. *J. Med. Chem.*, **2009**, 52, 5253-5261.
18. S. Kunze, F. Zobi, P. Kurz, B. Spingler, R. Alberto,. *Angew. Chem. Int. Ed.*, **2004**, 43(38), 5025-5029.
19. G. R. Morais, A. Paulo, I. Santos, *Organometallics*, **2012**, 31, 5692-5714.

20. C. T Burns, R. F. Jordan, *Organometallics.,* **2007**, 26(27), 6737-6749.
21. L. Pazderski, J. Tousek, J. Sitkowski, L. Kozerski, E. Szłyk, *Magn. Reson. Chem*., **2007**, 45, 1059–1071.
22. A. B. P. Lever., *Inorg. Chem.,* **1965**, 4(7), 1042-1046.
23. D. F. Shriver and P. W. Atkins, 3rd Edition, Inorganic Chemistry, Oxford press, 1999.
24. P. L. Meredith, R. A. Palmer,. *Inorg. Chem*., **1971**, 10(7), 1546-1549.
25. B. K. Andzyulene, F. G. Anisimov, *J. Appl. Spectrosc*., **1980**, 33, 6, 1352-1354.
26. P. Tian-Tian, X. Duan-Jun,. *Acta. Crystallogr. E*., **2004**, 60(1), m56-m58.
27. B. Ji, D. Deng, Z. Wang, X. Liu, S. Miao,. *Struct. Chem*., **2008**, 19, 619-623.
28. J. Kang, J. K. Yeo, P-G. Kim, C. Kima, Y. Kimd., *Acta Cryst*. **2011**. E67, m1511
29. M. Balamurugan, R. Mayilmurugan, E. Sureshb, M. Palaniandavar*,. Dalton Trans*., **2011**, 40, 9413–9424.
30. C. Biswas, M. G. B. Drew, A. Figuerola, S. Gomez-Coca, E. Ruiz, V. Tangoulis, A. Ghosh, *Inorganica. Chimica. Acta*., 363, **2010**, 846-854.
31. X. Zhang, B. Li, J. Tang, J. Tian, G. Huang, J. Zhang, *Dalton. Trans*., 42, **2013**, 3308.
32. C-I. Yang, K-H. Cheng, S-P. Hung, M. Nakano, H-L. Tsai,. *Polyhedron*, **2011**, 30, 3272–3278.
33. Q-T. He, X-P. Li, Y. Liu, Z-Q. Yu, W. Wang, C-Y. Su,. *Angew. Chem. Int. Ed*., **2009**, 48, 6156.
34. J. Ankermann, F. Meyer, H. Pritzkow., *Z. Anorg. Allg. Chem*., **2004**, 630, 2627.
35. D. Maity, P. Mukherjee, A. Ghosh, M. G. B. Drew, C. Diaz, G. Mukhopadhyay,. *Eur. J. Inorg. Chem*, **2010**, 807.
36. Y. Agnus, R. Louis, B. Metz, C. Boudon, J. P. Gisselbrecht, M. Gross,. *Inorg. Chem*., **1991**, 30, 16, 3155.
37. N. Murakami Iha, G. Ferraudi, *J. Chem. Soc. Dalton. Trans.,* **1994**, 2565-2571.

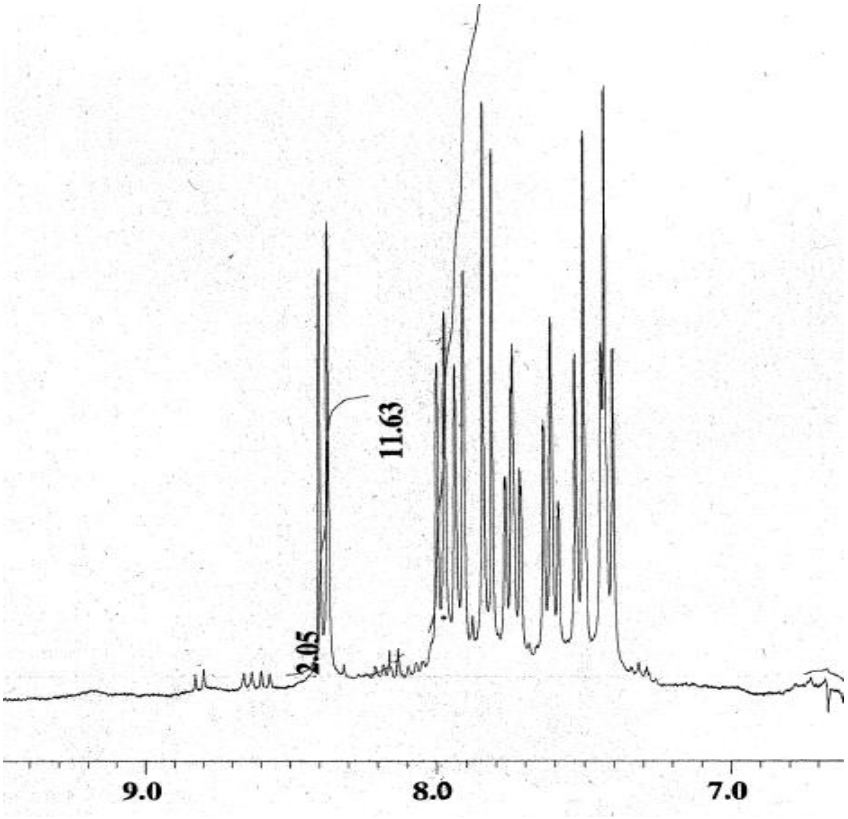

Fig. 1: aromatic region of H-NMR for compound H**L5** in DMSO**.**

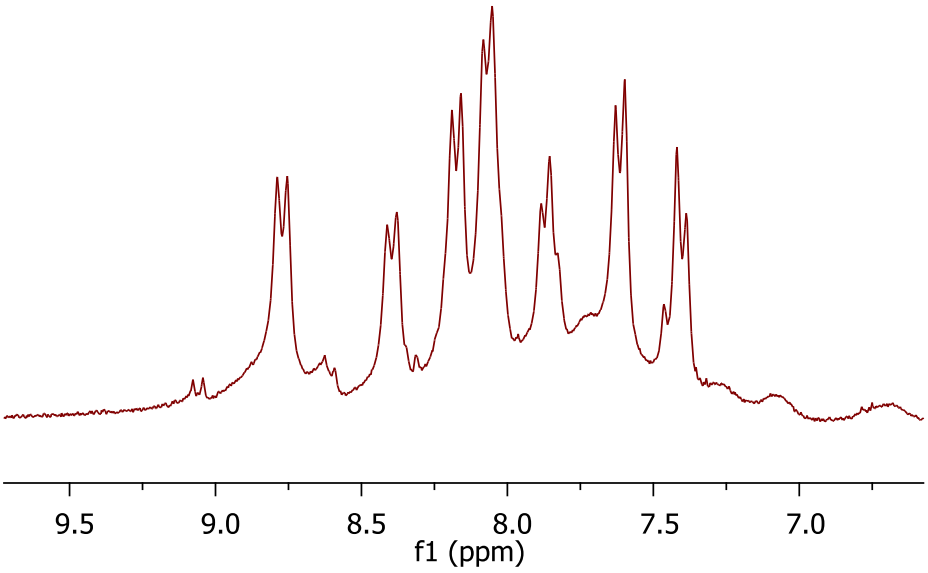

Fig 2: aromatic region of H-NMR for compound **5.4** in CH_3CN.

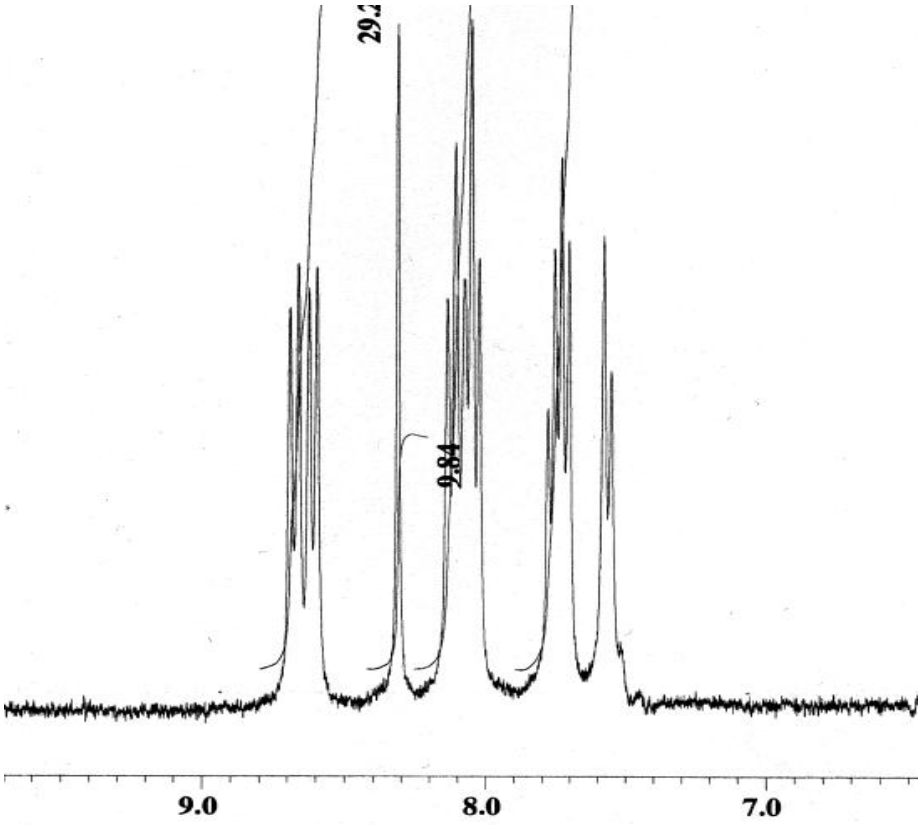

Fig 3: aromatic region of H-NMR for compound **5.5** in DMSO**.** With OH peak at 8.3ppm.

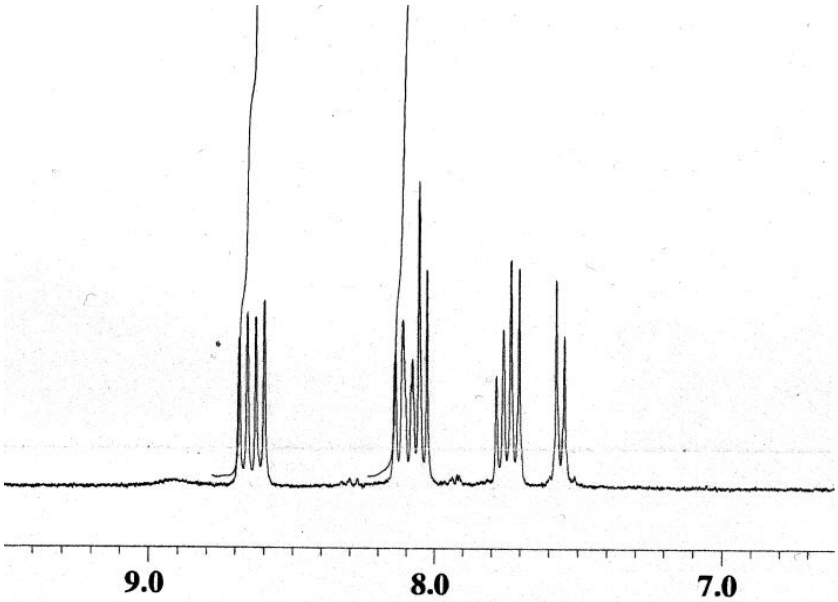

Fig 4: aromatic region of H-NMR for compound **5.5a** in DMSO**.** Noting the missing OH peak from 8.3ppm.

Table 1A: Crystallographic data for complexes of bis(2-quinoline)(4-bromo-phenyl)menthanol (**HL5**)					
Compound	**HL5**	**5.1**	**5.2**	**5.3**	**5.5**
Chemical formula	$C_{25}H_{17}N_2OBr.ClO_4.C_4H_{10}O$	$[Co(C_{25}H_{16}N_2OBr)_2].ClO_4.CH_3CN$	$2[Ni(C_{25}H_{16}N_2OBr)(CH_3CN)_3][5ClO_4]$	$2[3(CuC_{25}H_{16}N_2OBr)(ClO_4)].4ClO_4.5CH_3CN.H_2O$	$2[Re(CO)_3(C_{25}H_{16}N_2OBr)].CH_3CN$
Mr, g/mol	614.88	1080.05	1741.61	3843.12	1462.15
Crystal system	Orthorhombic	Triclinic	Triclinic	Monoclinic	Triclinic
Space Group	Pbcm	P-1	P-1	$P2_1/c$	P-1
T (k)	293 (2)	293 (2)	240 (2)	293 (2)	150 (2)
a, Å	11.4352 (16)	10.9328 (11)	13.2691 (6)	17.7289 (9)	13.8774 (5)
b, Å	14.1996 (19)	13.5827 (13)	16.8166 (10)	24.7641 (13)	14.5550 (3)
c, Å	16.3996 (17)	17.4172 (14)	18.6752 (12)	35.8048 (16)	14.6523 (4)
α, deg	90.00	99.429 (6)	78.288 (2)	90.00	84.347 (2)
β, deg	90.00	100.921 (5)	78.851 (4)	90.969 (3)	68.9950 (10)
γ, deg	90.00	108.764 (4)	89.625 (4)	90.00	66.230 (2)
V, $Å^3$	2662.9 (6)	2333.3 (4)	4001.1 (4)	15717.5 (13)	2524.85 (13)
Z	4	2	2	4	2
D_c g/cm^3	1.531	1.537	1.446	1.624	1.926
μ(Mo K α), mm^{-1}	1.692	2.194	1.709	2.504	6.436
Observed Reflections	2010	10431	13616	12196	11497
Reflections collected	7629	14692	20609	22779	16732
R_{int}	0.0955	0.0525	0.0553	0.1338	0.0287
R_I [I>2σ(I)]	0.1588	0.1174	0.1567	0.0955	0.0399
wR_2 (all data)	0.3673	0.2834	0.4377	0.2664	0.0892

Chapter 6:

Tripodal Bis-quinoline Butyl Framework Investigating Cu(II) and Re(I) Co-ordination and Luminescence Properties

6.0 Abstract

Herein is a continuation of the previous chapter, however, it now discusses the synthesis and co-ordination chemistry of the novel bis-quinoline ligand **HL6** (bis(2-quinoline)(butyl)methanol). This ligand has the addition of an aliphatic butane group which is proposed to aid compound transfer across cell membranes by increasing lipophilicity. Complexes of this ligand with Re(I) and Cu(II) were isolated for their uses in biomedical imaging, and have been fully characterised. X-ray crystallography revealed **L6** to form a monomeric structure with $[Re(CO)_3]^+$ and a trimeric cluster with Cu(II), similar to those observed with **L5**. In addition luminescence and lifetime data of the Re(I) complex (**6.2**) were measured showing a higher intensity and longer life time, with the addition of acid.

6.1 Introduction

Currently, research in imaging can be found in a range of techniques and disciplines which take advantage of different chemical or physical properties, to allow accurate detection of the imaging probes. The most common techniques in use to date include CT (Computer Tomography), PET (Positron Emission Tomography), MRI (Magnetic Resonance Imaging), SPECT (Single-Photon Emission Computed Tomography) and Fluorescence microscopy.[1-3] PET and SPECT are radioimaging techniques which are used in whole body imaging, due to their ease of detection through deep tissue mass, and at extremely low concentrations (pico-molar).[4] A disadvantage of this particular technique is lack of resolution (only mms), and relatively long acquisition times. In contrast, fluorescent imaging agents have the opposite advantages and disadvantages, where they have excellent resolution (nms) however poor tissue penetration and are therefore not ideal for whole body techniques.[5] If it was possible to incorporate both of these techniques into one imaging probe, all of the associated advantages could be exploited, and the disadvantages would be overcome.[6] ^{64}Cu and ^{99m}Tc are used as PET-active radioisotopes, but their stable complexes with quinoline-based ligands are underexplored. As discussed previously in chapter 5, technetium is an analogue of rhenium so it may be possible to investigate both its luminescent and radioactive properties, to give a truly bimodal imaging probe which contains only one metal centre. This is important as heavy metals are known to be highly cytotoxic in their free ion forms, so reduction of the quantity of metal probe or probes needed to be administered should reduce potential problems associated with metabolic

excretion of these complexes. For example, intravenous internalisation of a ^{64}Cu PET probe and injection of a Re fluorescent agent would not be necessary in this case.

In general heavy metal complexes with conjugated ligand systems, such as those utilising d^6 and d^8 transition metals or lanthanides, have several beneficial features. These include long luminescence life times, allowing techniques such as time-resolved fluorescence imaging[7] to be employed, as well as large Stokes shifts, which lower the energy of the emitted phosphorescence, decreasing tissue damage and allowing better tissue penetration. As well as easy differentiation of the excitation wavelength from the emission wavelength, they can also be differentiated from biological fluorophores such as NADP and flavones (also known as autofluorescence). They also show resistance to photo-bleaching, as is commonly observed with organic fluorophores.[8] These useful properties are attributed to the generation of triplet states and a metal-to-ligand-charge-transfer (MLCT) mechanism, and can be represented through the Jablonski diagram (see Fig. 1).

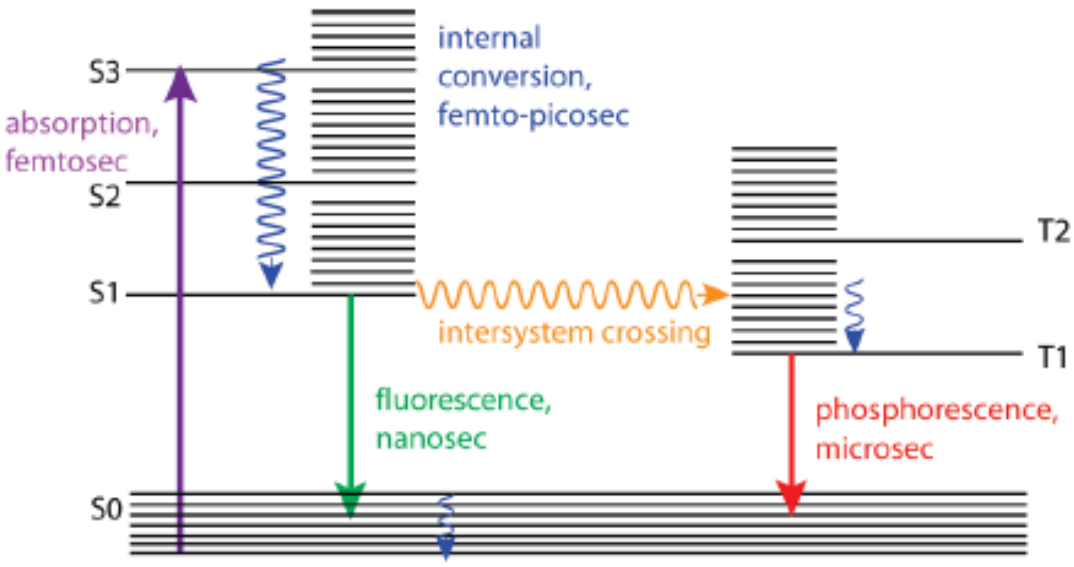

Figure 1: Jablonski diagram for metal-to-ligand-charge-transfer mechanisms for transition metal complexes.[9]

Initially, electrons are excited from metal-based orbitals by low energy UV, and sometimes high energy visible irradiation, which promotes them to a excited singlet state (^{1}MLCT) of the empty, antibonding orbitals of the conjugated π-system of the ligand (quinoline in the case of this

chapter), represented by the purple arrow in Figure 1. The electrons then relax via internal conversion to the lowest energy ground state, before rapid conversion to a triplet state through intersystem crossing (orange arrow, Fig. 1), due to the spin-orbit coupling of the heavy metal atom. Once again the electrons relax (internal conversion) to the lowest energy triplet state before relaxation to the ground state (red arrow, Fig. 1), where emission of photons with lower energy (longer wavelength) than the excitation wavelength can be observed. This relaxation to the ground state again occurs by intersystem crossing which involves a change in electron spin (triplet to singlet). These transitions are formally forbidden and give rise to the relatively long luminescence life times observed compared to organic fluorophores (ns). The difference between the excitation and emission wavelengths is known as the Stokes shift. Neutral Re complexes, such as $[Re(CO)_3(Bipy)X]$ where X represents Cl/Br (Sch. 1), generally have absorption and emission wavelengths of 350nm and 570nm respectively, with lifetimes up to hundreds of ns.[10] On the other hand, cationic species such as $[Re(CO)_3(Bipy)(py)]^+$ (Sch. 1), have more suitable photophysical properties for imaging, with significantly longer lifetimes, sometimes up to microseconds.[11]

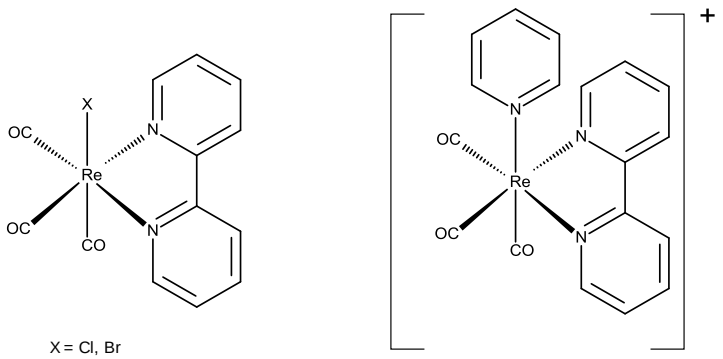

Scheme 1: Structures of neutral $Re(CO)_3(bipy)X$ and cationic $[Re(CO)_3(bipy)(Py)]^+$.

In light of the successful Cu(II) and Re(I) complexes with bis(2-quinoline)(4-bromo-phenyl)methanol (**L5**) in the previous chapter, it is of great interest to further pursue novel bis-quinoline type chelates with these metal ions, investigating their co-ordination chemistry and luminescence properties, discussing their potential as PET imaging agents, or in the case of Re (analogue of ^{99m}Tc) bimodal PET/fluorescent probes.

6.2 Results and Discussion

6.21 Ligand synthesis

The starting material Bis(2-quinoline)methanone (**S1**) as described previously (Chapter 5, Page. 197) was prepared and used to syntheses the new ligand bis(2-quinoline)(butyl)methanol (**HL6**). A stock of Butylmagnesium bromide Grignard was first made by the standard literature method of stirring magnesium metal in dried-degassed diethyl ether followed by the slow addition of 1-bromo-butane.[12] The compound bis(2-quinoline)(butyl)menthanol (Sch. 2) was synthesised by cooling a solution of the butyl-grignard (0.7M) and THF to -10°C followed by the slow addition of 1.2eq of **S1** also in THF. The resulting deep blue solution was kept at -10C for a minimum of 2h before quenching the reaction with acid. The purple mixture was then adjusted to pH8 using K_2CO_3 and chloroform added to scavenge the organic tripod. The organic layers were combined and reduced giving the crude product as a sticky brown solid in reasonable purity (~80%). The pure compound was isolated by silica column chromatography (DCM/hexane 70/30).

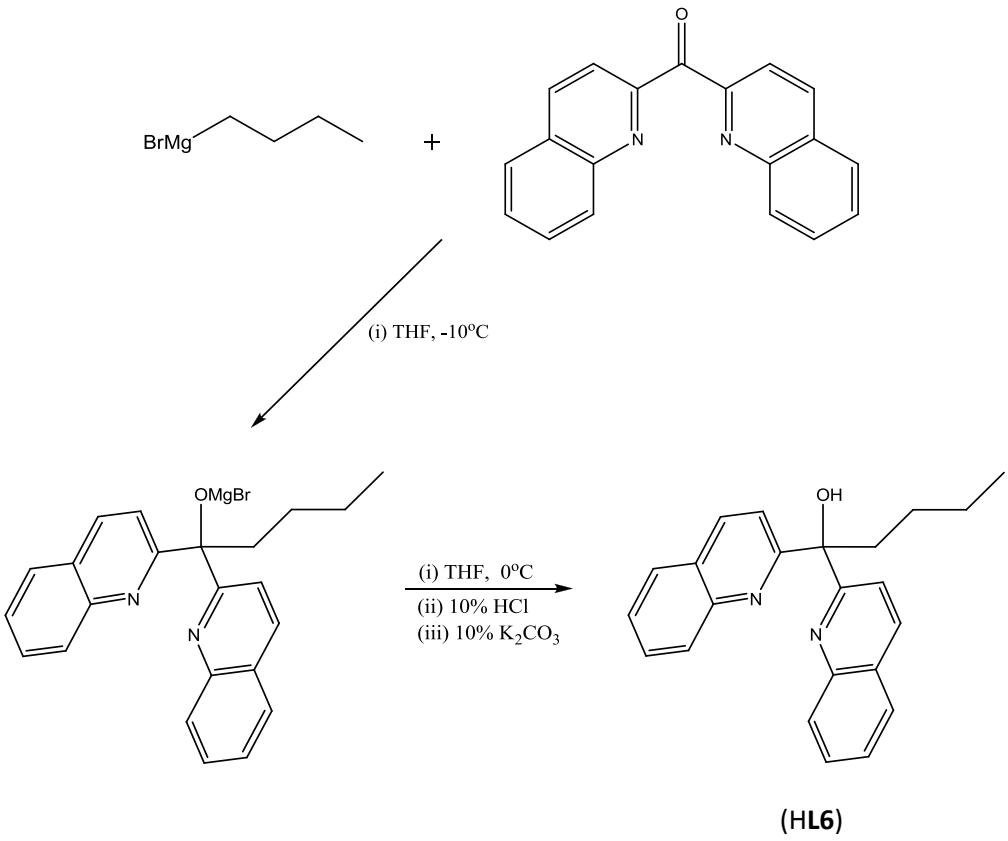

Scheme 2: Synthesis of bis(2-quinoline)(butyl)menthanol (H**L6**).

6.22 Synthesis of complexes

The ligand H**L6** is readily soluble in organic solvents and can be complexed with copper(II) and rhenium(I) giving complexes **6.1** and **6.2** respectively. The complexes were prepared in a 1:1 ligand:metal ratios. The synthesis of **6.1** involves the addition of a copper(II) perchlorate acetonitrile solution to a stirred solution of the ligand producing a vivid colour change from blue to emerald green. Complex **6.2** was achieved differently by refluxing H**L6** and rhenium penta-carbonyl bromide in toluene overnight which formed a yellow precipitate upon cooling. For the complex **6.2a**, a simple wash with excess trifluoroacetic acid (TFA) was carried out with a sample of **6.2**, which protonates the co-ordinating hydroxyl function, as discussed in the ^{1}H-NMR data.

6.23 Vibrational spectroscopy

The Infrared spectra of the following compounds were collected using KBr discs with their key absorption peaks listed in Table 1. All compounds show characteristics of the parent ligand such as, aromatic and saturated C-H stretches as well as broad OH stretching. The quinoline functions of the ligand contain C=C and C=N bonds which produce several stretches typically seen between 1640cm^{-1} and 1380cm^{-1}. In this region slight peak shifting to higher energy, can been seen for complex **6.1** when compared to the free ligand (**L6**), and is indicative of the co-ordination to the Cu(II) centre. Also for **6.1,** there are two strong Cl-O stretches present which, as discussed in Chapter 2, shows the perchlorate counter ions to be non co-ordinating, however there is evidence from weak absorptions at 961cm^{-1} (single peak) and 476cm^{-1} (doubley split), along with the splitting of the peak at 624.8cm^{-1}, that some co-ordinated perchlorate could be present. This correlates well with the crystallographic data where one of the three counter ions is shown to be involved in co-ordination. Due to the strength and broadness of the 1086cm^{-1} band it was not possible to observe any splitting of this stretch and therefore could not reinforce the presence of a co-ordinating perchlorate. The rhenium complex **6.2** is more easily identified by the very strong C=O absorptions observed at 2032cm^{-1}, 1944cm^{-1} and 1907cm^{-1} (Table 1). Upon co-ordination to the π-basic ligand the M-CO bonds strengthen through backbonding and hence weaken the C=O bond, which explains their shift to lower energy compared with the starting material ($Re(CO)_5Br$) and is indicative of co-ordination.

The closely spaced stretches 1944cm and 1907cm come from the symmetric and asymmetric stretches of the equatorial CO groups whilst the third stretch relates to the carbonyl trans to the oxygen donor. Another noted trend is the increased energy of the C-O stretch within the complexes. This increase in energy maybe related to the alcohol function also becoming involved in co-ordination to the metal centre, which would again correlate well with X-ray data.

Table 1: Showing characteristic vibrational modes of H**L6** and complexes.

compound	Aromatic v(C-H)	alkyl v(C-H)	v (O-H)	v (C=N) and (C=C)	v (C-O)	v (Cl-O) or (C≡O)
HL6	3062.9 (m)	2955.6 (s), 2924.3 (s), 2856.9 (s)	3350.7 (m)	1619.8 (m), 1588.0 (m), 1566.3 (m) and 1502.7 (m), 1461.8 (m), 1425.5 (m), 1393.7 (m)	1302.9 (m)	n/a
6.1	3118.8 (m), 3061.4 (m)	2960.7 (m), 2925.5 (m), 2868.6 (m)	3447.6 (m)	1638.0 (m), 1623.3 (m), 1600.2 (m) and 1510.5 (m), 1452.1(w), 1434.3 (w), 1383.2 (m)	1320.5 (m)	1085.7 (br+s), 960.9(w), 624.8 (s), 476.3 (w)
6.2	3070.6 (w)	2962.1 (m), 2927.4 (m), 2872.5 (w)	3447.6 (w)	1618.0 (w), 1594.8 (m) and 1512.9 (m), 1459.4 (m), 1432.9 (m)	1357.6 (m)	2032.1 (s), 1944.4 (s), 1906.8 (s)

6.24 NMR spectroscopy

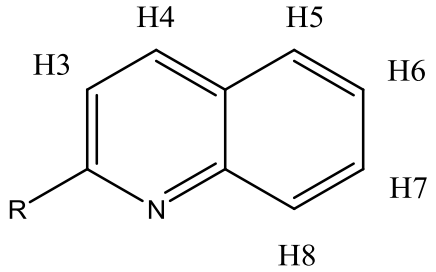

Scheme 3: 2-substituted quinoline and numbering system.

The diamagnetic arrangement (low spin d^6) of Re(I) complexes with high-field ligands such as CO allows the use of NMR for analysis. Compound **6.2** gave a yellow solution in $CDCl_3$ and the aromatic region of the ^{1}H-NMR is shown in Figure 2. The two most low-field doublets are attributed to the proton positions H4 and H8 on the quinoline group (Sch. 3) as they are likely to be the most influenced through electronic resonance effects (Sch. 4), but as they often occur at similar positions it is impossible to distinguish them purely by chemical shift.[13] It is expected that the mutual coupling between H4 and H3 means that the observed coupling constants associated with the peaks for H4 and H3 must be identical in value (both J= 8.3Hz) and allows the doublets 8.23ppm and 7.78ppm to be assigned H4 and H3 respectively. Therefore, the low-field peak at 8.92ppm can be assigned to H8. The high value of H8 could be attributed to resonance effects as wells as environmental influences resulting from H8 pointing directly towards the carbonyl ligands. The last remaining doublet at 7.81ppm can then be labelled H5. Finally there are two triplets to consider for H6 and H7, unfortunately these peaks are observed as apparent triplets at 400MHz and not the predicted doublet of doublets, thus precluding the matching of coupling constants for aiding peak labelling. Instead the simple observation of H7 having better conjugation and less distance to the aromatic N leads to the conclusion that H7 appears at 7.93ppm and hence H6 must be 7.59ppm, which fits with literature showing H6 to be the most downfield of the aromatic protons in quinolines.[14]

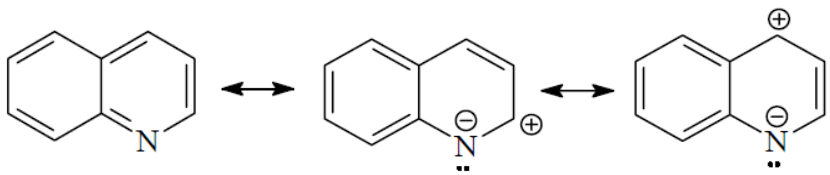

Scheme 4: Resonance forms of quinoline.

Complex **6.2** was then compared to the ^{1}H-NMR of **6.2a,** which had been exposed to excess TFA. The most dramatic changes occur from peaks of H4 and H8 which shift towards each other in the spectrum (H4 +0.22ppm and H8 -0.14ppm), along with the 4 remaining peaks which all move slightly downfield. This is most likely to occur from protonation of the apical oxygen, changing the electron density around the bonding modes and eventually altering the environment of the quinoline protons (Sch. 5). Although no ligand OH peak was observed in the spectra it was considered that possibly the proton could be exchanging with the TFA faster than the NMR time scale or even that the TFA peak is obscuring it. Also no NH peaks were observed reducing the possibility of a protonated quinoline function. Although oxygen protonation seems most likely, the fluxional argument breaks down when considering the observed increase in luminescence, as this would normally decrease in fluxional systems. Interestingly some shifting and broadening of the aliphatic proton peaks in the NMR of **6.2a,** suggests a change in the chemical environment of the butyl chain upon acidification. Another possible explanation could be a chain wrapping scenario where an increase in solvent polarity, due to adding acid, causes the less polar chain to wrap over part of the complex in order to reduce interactions with the solvent (Sch. 5). This argument could explain the observed shifting and broadening of the butyl chain peaks and some shifting of aromatic peaks, also to note is that chain wrapping is likely to cause an increase in luminescence which was observed for compound **6.2a**.

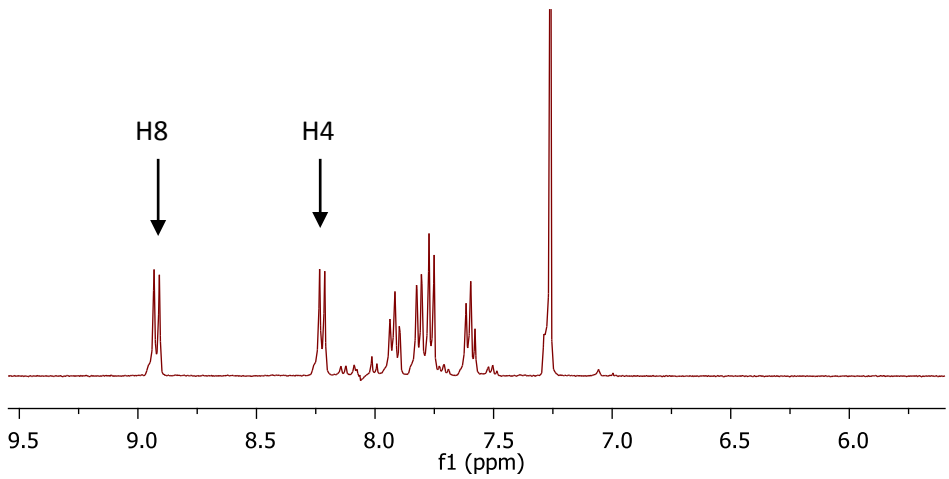

Figure 2: ^{1}H-NMR spectrum for **6.2** in $CDCl_3$.

Interestingly, the spectrum for **6.2a** (Fig. 3) has only 6 proton environments between 7-9ppm which suggests a symmetrical quinoline system. If N-protonation was occurring then the symmetrical ^{1}H-NMR would naturally suggest that both quinoline functions are becoming protonated, and not one, however this cannot be the case. It would be expected if both quinolines are affected by acid then the Re centre would no longer be bound to the π-system and consequently should no longer be able to fluoresce. If only one quinoline was protonated then an increased number of aromatic peaks would be expected. Since the complex does emit in acidic conditions it is unlikely that one or both quinolines are being protonated. Finally, the conclusion that agrees most with the evidence is a rapidly fluxional system between the ligand OH and TFA, the protonation of oxygen is thought reduce conjugation within the system and hence the observed blue shifting upon acidification.

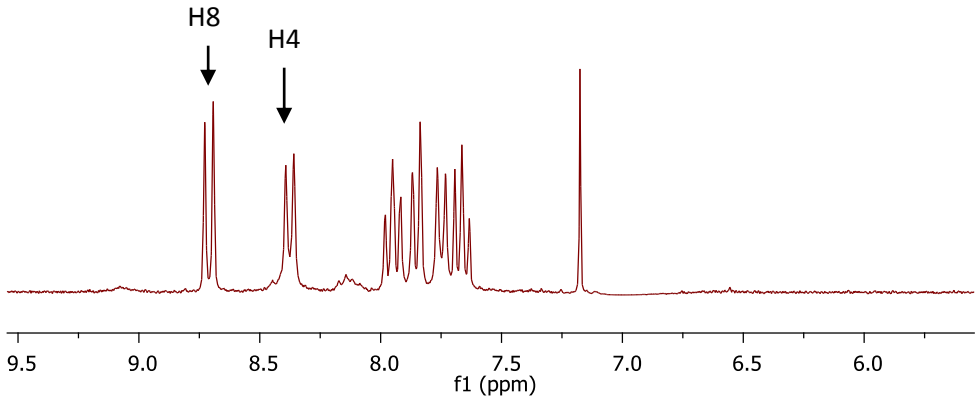

Figure 3: ^{1}H-NMR spectrum for **6.2**+TFA (**6.2a**) in $CDCl_3$.

Additionally oxygen protonation may possibly lead to dissociation of the OH from rhenium and thus giving the butyl chain more freedom (Sch. 5). This is suspected of allowing the butyl chain to 'wrap' around part of the complex to reduce interactions with the increasingly polar solvent and is one possibility for the observed increased in luminescence. Although a fluxional system with chain wrapping best describes the observed results further experiments would be required to confirm or disprove the mechanism within the system. Such as; comparing with a Lewis acid rather than a protic acid and using variable temperature NMR, to observe if the chain moves more freely at high temperatures.

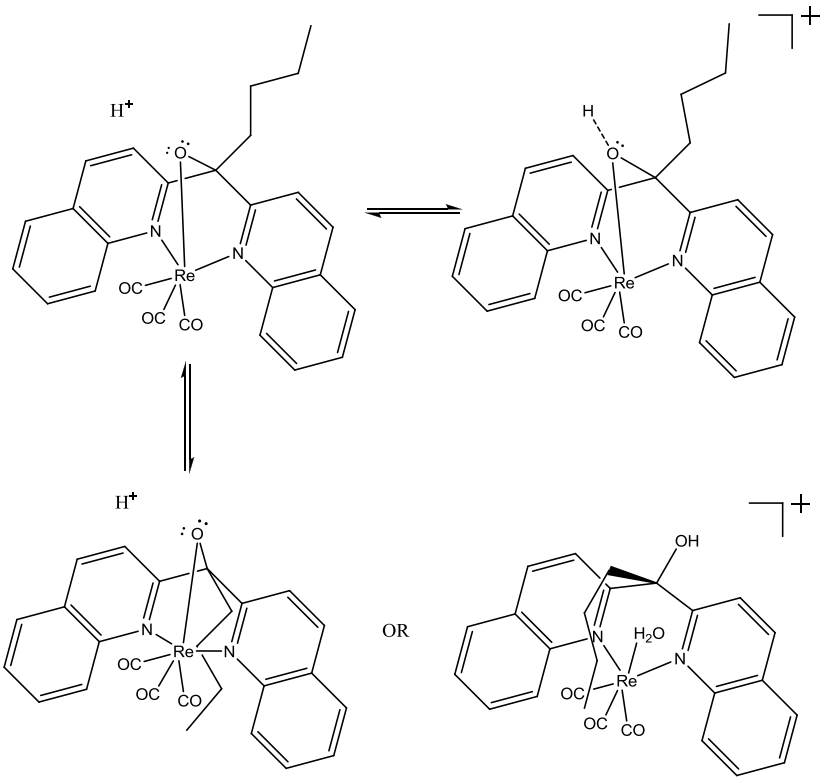

Scheme 5: Hypothetical scenarios that could cause ^{1}H-NMR differences upon acidification of **6.2** with TFA giving **6.2a** (bottom right).

6.25 Electronic absorption spectra

The UV/Vis absorption spectra for complexes **6.1** and **6.2** were run in acetonitrile solutions at concentrations around $1.5x10^{-5}moldm^{-3}$ using a 1cm path length, with their data displayed in Table 2.

Table 2: Electronic absorption spectral assignments						
compound	π-π* transitions / λ (nm)	MLCT λ (nm)	d-d transitions / λ (nm)	Dq	B (cm^{-1})	B^b
L6	255(22670), 294(14136), 316(13175)	-	-	-	-	-
6.1(Cu2+)	247(22293), 309(14019)	343(3902)	806(54)	1240	-	-
6.2(Re1+)	252(14771), 319(8260)	332(3776)	-	-	-	-

The copper complex **6.1**, presents a broad asymmetric band in the visible region reaching an absorbance maximum of $12407cm^{-1}$ (806nm), with a slight shoulder visible at lower energy. The band is considered a combination of two spin allowed transitions; $^2E' \leftarrow {}^2E''$ and $^2A_1' \leftarrow {}^2E''$ presuming the Cu(II)'s were octahedral in geometry, which would lead to a Dq value of $1240cm^{-1}$. However, this value should be treated tentatively as crystallographic data suggests the geometry of the three coppers in **6.1** are five co-ordinate and show to be very similar to each other. Their geometry is intermediate between square pyramidal and trigonal bipyramidal with some distortion owed to the formation of a trimeric species. If this solid-state geometry is maintained in solution, it is expected that both the ^2E_g and $^2T_{2g}$ terms would split into ($^2B_{1g}$ and $^2A_{1g}$) and ($^2B_{2g}$ and ^2E_g) respectively. Resulting in three absorptions labelled $v_1 = {}^2A_{1g} \leftarrow {}^2B_{1g}$, $v_2 = {}^2B_{2g} \leftarrow {}^2B_{1g}$ and $v_3 = {}^2E_g \leftarrow {}^2B_{1g}$. Generally these bands are close in energy and are seen to contribute to one asymmetric band like that observed in figure 4.[15] Another feature is that 5 co-ordinate absorptions are usually observed at lower energies (c.a cm^{-1}) compared to that of octahedral species. For example the square pyramidal complexes $[Cu(bipy)_2(OH_2)][S_2O_2]$ and $[Cu(bipy)_2(Cl)][ClO_4]$ produce broad asymmetric bands with shoulders, giving values of $14,120cm^{-1}$ and $10,075cm^{-1}$ and $13,240cm^{-1}$ and $10,470cm^{-1}$ respectively,[16] and compare well with the observed spectra for **6.1**. Overall these results are encouraging and suggest that maybe the three five co-ordinate Cu(II) species are retained in solution.

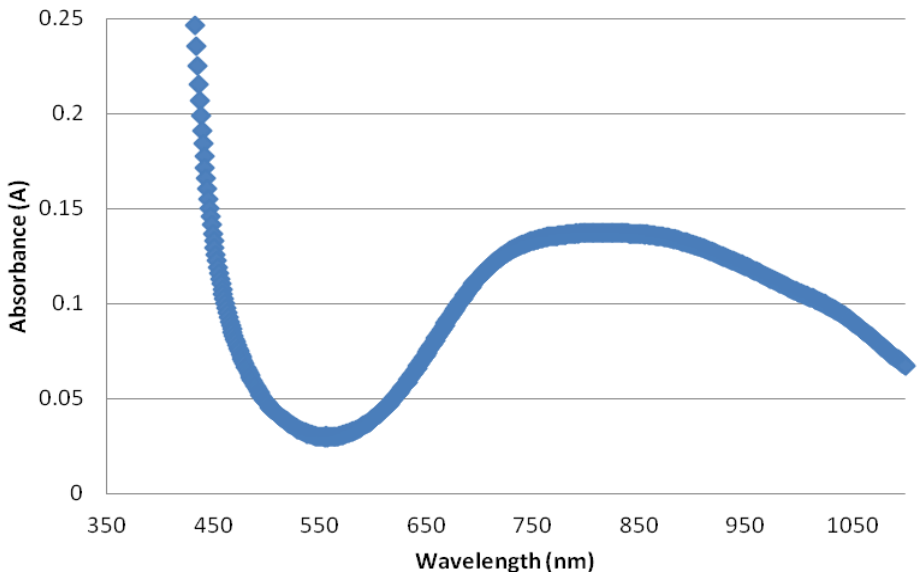

Figure 4: Visible region of the electronic absorption spectrum for **6.1**.

For complex **6.2**, two strong bands at 39,683 cm^{-1} and 31,348 cm^{-1} are observed and can be assigned to the intra-ligand π→π* transitions on the quinoline moieties. In addition a respectively weak transition at 30,120 cm^{-1} (332nm), appearing as a shoulder, is also seen. This transition is attributed to the ^{1}MLCT excitation mechanism occurring within the system. Due to low spin d^6 nature of Re(I) no readily observable d-d transitions are present in this spectra.

6.26 Luminescence

Rhenium fac-tricarbonyl complexes are extensively studied with reference to imaging, due to their often intense luminescence *via* an MLCT mechanism. The fluorophore rhenium(I) tricarbonyl core coordinated to a N,N-bis(quinolinoyl), when linked with vitamin B_{12} has shown great potential in cancer diagnostics and/or treatments.[17] In addition rhenium is an analogue to the PET active ^{99m}Tc isotope giving compound **6.2** potential as a bimodal probe (facilitating PET and fluoresecence).[6,18-20] The two conditions (protonated and unprotonated) of complex **6.2** show typical absorption and emission profiles when compared to other bis-quinoline type complexes with absorption maxima around 360nm and emission maxima around 595nm (or 535nm for **6.2a**).[18,21] The excitation spectrum of **6.2** shows several bands around 300nm (Fig. 6). The higher energy bands are associated with π-π* ligand transitions. The lower energy absorptions of this spectra (~350nm) are assigned, with reference to literature,[22,23] as d π-π*

^{1}MLCT in character which is in accordance with its electronic spectra where a band is observed around 325nm with a extinction coefficients in the region of 4300 $M^{-1}cm^{-1}$(the electronic spectra was recorded in acetonitrile not DCM giving a slightly different peak maximum). The emission spectrum of **6.2** was measured by exciting at 360nm, see Fig. 6, and contains one broad band around 595nm due to the ^{3}MLCT, shown in Figure 5, revealing a large Stokes shift of 235nm, which is a good characteristic for a potential imaging probe.

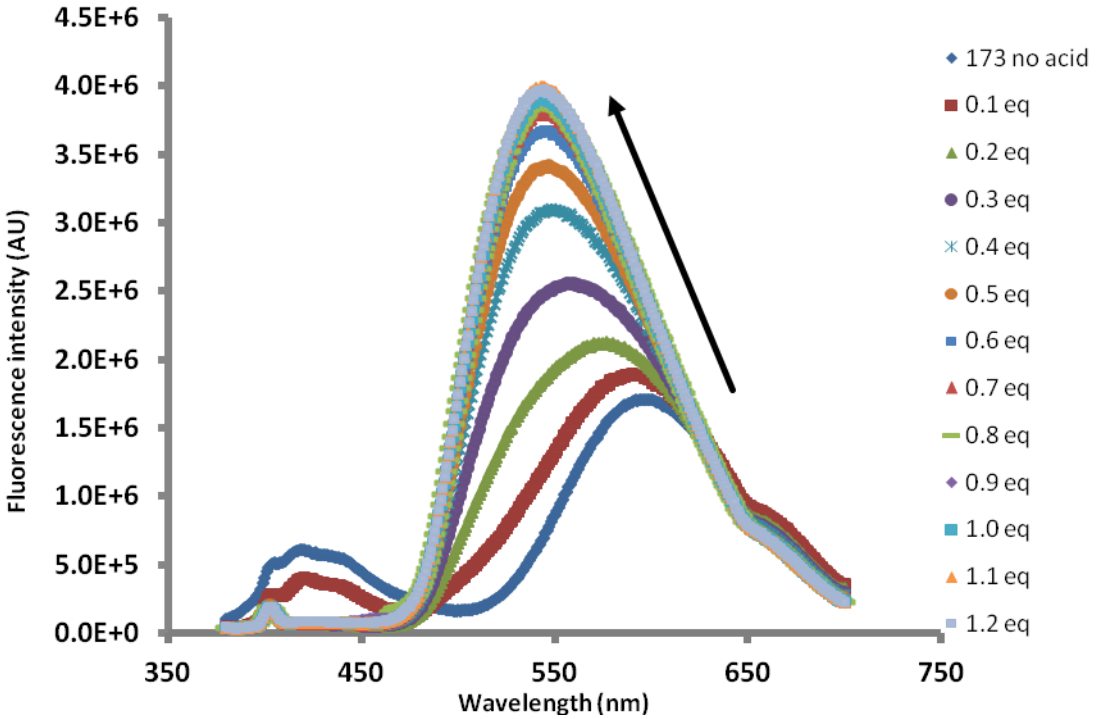

Figure 5: Overlaid luminescence emission spectra for complex **6.2** from no equivalents to 1.2 equivalents of trifluoroacetic acid (TFA) in a DCM solution.

It was first noted that a change in fluorescence wavelength was induced from **6.2** in acidic conditions, using TFA (fluorescing orange at pH 7 and changing to green at lower pH). Consequently a fluorescence acid titration experiment was carried out in DCM giving the overlaid graph shown in Figure 5. It can be seen that the emission maxima for the acidified complex has shifted 60nm higher in energy (blue shift) as well as an increase in fluorescence intensity when compared to **6.2** giving a smaller, but still suitable, Stokes shift of 175nm (Fig. 6). It is most likely that protonation of the oxygen is occurring within the complex, which reduces conjugation within the system resulting in higher energy levels and hence a blue shift. The energy gap rule could be used to explain the observed properties between **6.2** and **6.2a**.

The rule states that an increase in energy gap (blue shift) results in a slower rate of non-radiative decay (less non-emissive energy loss) and would therefore increase the amount of energy lost via emission increasing peak intensity and life times. However, another possibility where emission intensity is also expected to increase is if 'wrapping' of the butyl chain around part of the complex is occurring, which could be suspected from the broadening of alkyl peaks seen in the ^{1}H NMR data. It is possible that shielding from the chain over the Re(I) centre reduces non-radiative decay, through solvent interactions, and hence an increased emission intensity.

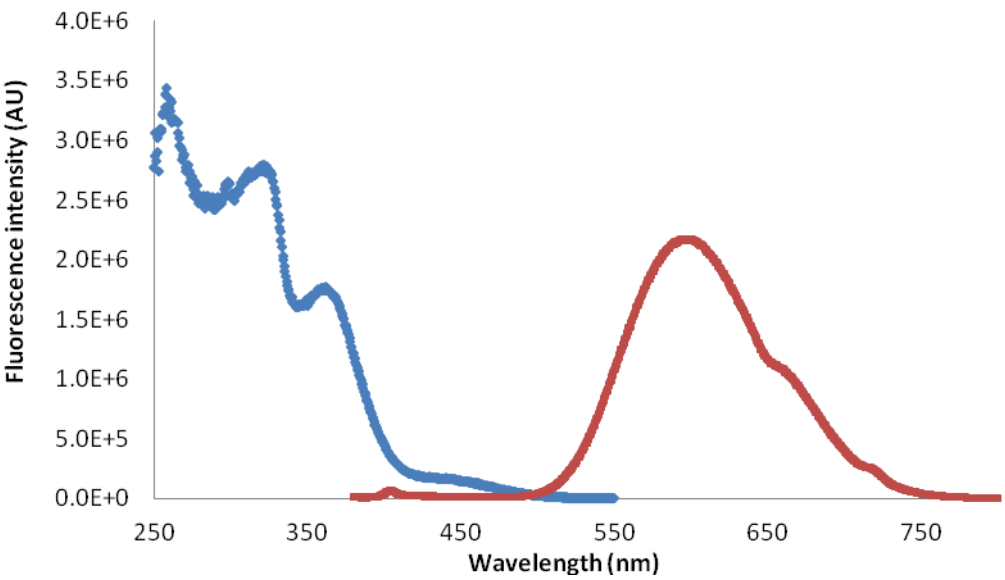

Figure 6: Excitation (blue line) and emission (red line) overlay for **6.2** in DCM. Showing the large stokes shift. λ_{excit} = 360nm and λ_{emis} = 595nm

The octahedral geometry of Re(I) is considered to be maintained even after acidification, because a lowering of the T_2g levels would occur, and would consequently produce the blue shift observed in Figure 7. In contrast, if O_h geometry was not maintained then a red shift would be expected. If oxygen protonation is occurring co-ordination of a solvent or anion in place of the oxygen is possible, especially in order to retain octahedral geometry, however the effects on the spectra are hard to determine as they would depend on what was actually replacing the oxygen and the overall Re environment. Protonating both the quinoline functions, as mentioned in the NMR data, would lead to a loss in MLCT (no luminescence) and therefore considered unlikely to be occurring in this example. In addition to this, if free ligand did exist in

solution, excitation would lead to emission wavelengths beyond the visible region (<400nm) and therefore is ruled out as a possible cause for the peak at 535nm (Table 3). Another interesting property of these compounds is the life time of 70ns (**6.2**) which increases dramatically to 539ns in 1eq of TFA (**6.2a**), where both samples show a mono exponential decay (χ^2 = 1.0096 and χ^2 = 1.0064 respectively). This large difference shows the potential of **6.2** in other types of analysis such as time gated luminescence experiments. As mentioned earlier the large change in lifetime is owed to the energy gap law or possibly chain wrapping.

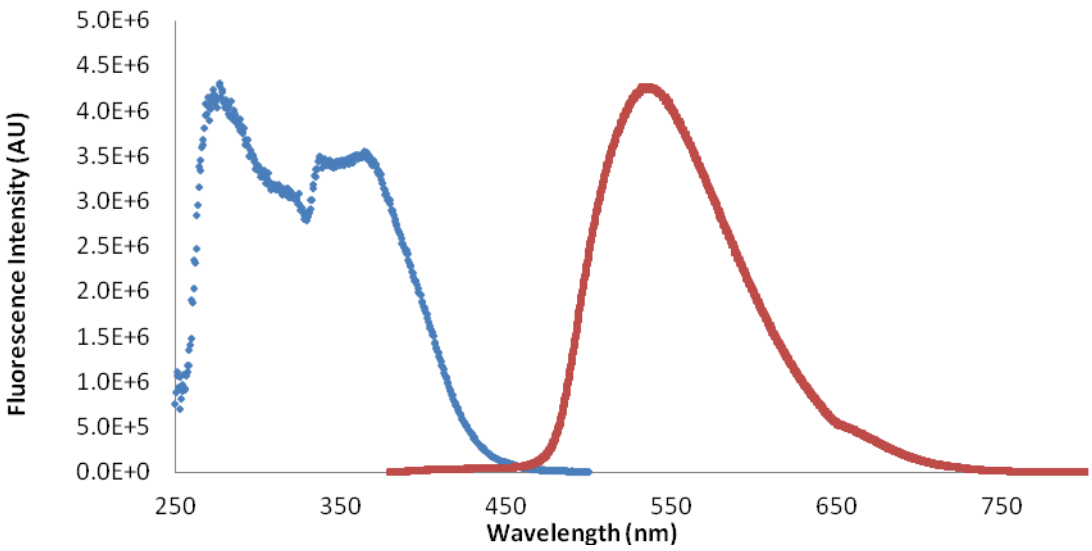

Figure 7: Excitation (blue line) and emission (red line) overlay for **6.2a** (6.2+TFA) in DCM. Showing the large stokes shift. λ_{excit} = 360nm and λ_{emis} = 535nm

In conclusion, the NMR and luminescence evidence suggests that oxygen protonation is most likely occuring and that the octahedral geometry of the Re centre is also maintained. From these results it is difficult to say whether geometry is maintained through the existence of a trivalent oxygen species, as shown in Scheme 5, or through the addition of a new axial donor (such as H_2O, trifluoroacetate or halide), due to the dissociation of the alcohol moiety from the rhenium. The increased emission seen upon addition of TFA could possibly be owed to the energy gap rule or butyl chain wrapping. Also to note is that the longer lifetime (539ns, Table 3) of **6.2a**, compared to **6.2**, may be attributed to the formation of a cationic Re(I) species however, lifetimes in the order of microseconds would be more typical. While there may be some error in these measurements, the data (Fig. 8) clearly shows the curve leading to a maximum when approximately 1eq of H^+ is binding to the molecule. This implies that either the

oxygen is being protonated or maybe one of the two N-quinoline's. Given the relative binding strengths and the symmetry observed in the ^{1}H-NMR spectrum, the protonation of the oxygen would seem most likely.

Table 3: Excitation, Emission and lifetime values for the Re(I) complex **6.2** before and after addition of 1 eq of TFA. All measurements were run from solutions in DCM.

compound	Excitation λ_{max} (nm)	Emission λ_{max} (nm)	Life-time (ns)[a]
6.2	361	595	70[b]
6.2a	360	535	539[c]

[a] excitation wavelength 372nm. Life-time values measured at [b] 595nm and [c] 535nm.

The titration experiment (represented in Fig. 5 and 8) also demonstrates the possibility for using **6.2** in a crude ratiometric type of analysis, where the amount of acid present could be approximately determined by the wavelength shift and intensity of the peaks observed. However, above 0.5eq of acid the curve begins to lose gradient, see Figure 8, and so shortening the range of detection possible in a ratiometric scenario. Other systems using Ru(II) tris bipy,[24] Pt(II) terpyridyl alkynyl[25] and lanthanide macrocycle (crown ethers) complexes[26] have already shown their potential as pH sensors. In addition, the tethering of a lanthanide tag, which contains a non-variable reference peak, onto **6.2** would allow more accurate measurement for the change in intensity and thus improving the system as a ratiometric analyte.

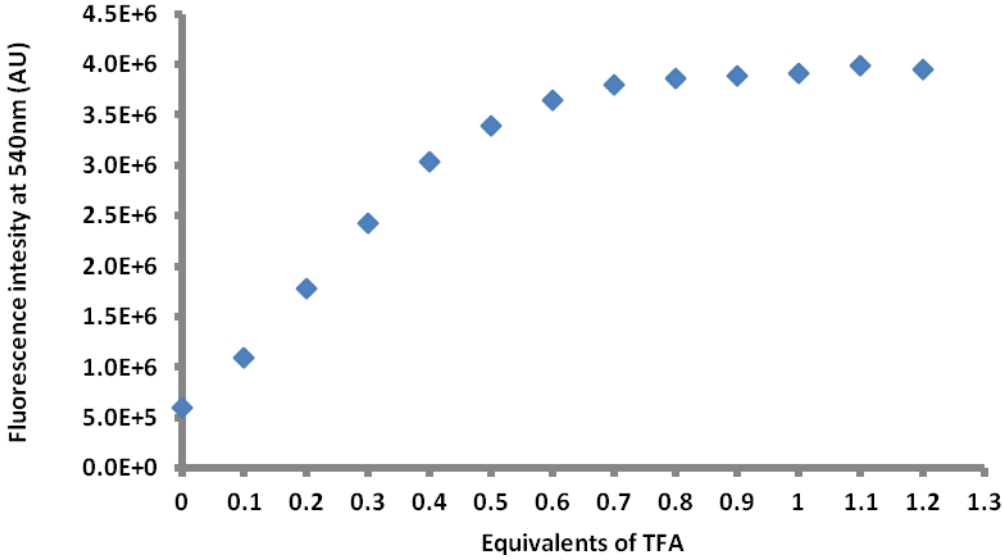

Figure 8: Graph representing the fluorescence intensity at the peak maxima (540nm) as TFA equivalents are increased. Showing the maxima intensity levelling off after 0.7 equivalents.

6.27 X-ray Crystallography

The crystallographic data collected for complexes **6.1** and **6.2** have been described below, with details of their crystal parameters and data collection listed in Table 4.

Table 4: Crystallographic data for complexes **6.1** and **6.2**

Compound	**6.1**	**6.2**
Chemical formula	$[3(CuC_{23}H_{22}N_2O).3ClO_4]$	$[Re(CO)_3(C_{23}H_{22}N_2O].2CHCl_3$
Mr, g/mol	1515.83	852.43
Crystal system	Triclinic	Triclinic
Space Group	P-1	P-1
T (k)	150 (2)	150 (2)
a, Å	13.8496 (4)	9.20250 (10)
b, Å	14.9354 (5)	12.8755 (3)
c, Å	21.3220 (5)	14.2968 (3)
α, deg	74.544 (2)	68.1820 (10)
β, deg	87.440 (2)	83.7910 (10)
γ, deg	66.0890 (10)	79.8050 (10)
V, $Å^3$	3876.05 (19)	1546.15 (5)
Z	6	2
D_c g/cm^3	1.472	1.827
μ(Mo K α), mm^{-1}	0.992	4.485
Observed Reflections	11087	7532
Reflections collected	19093	11089
R_{int}	0.0666	0.0364
R_I [I>2σ(I)]	0.0739	0.0413
wR_2 (all data)	0.1791	0.1058

Crystal Structure of $[(CuL6)_3(ClO_4)][ClO_4]_2$ (6.1)

X-ray diffraction of **6.1** revealed a solid state structure very similar to that of **5.3,** discussed in chapter 5, Page 215. The complex formula $[(Cu\mathbf{L6})_3(ClO_4)][ClO_4]_2$ was obtained through vapour diffusion of diethyl ether again from an acetonitrile solution, yielding green crystals. In this example the compound crystallised in the triclinic space group P-1 with the asymmetric unit containing only one trimeric species, as well as the three perchlorate counter ions. As discussed for **5.3**, compound **6.1** again has a central six-membered Cu-O ring, from the linking of three Cu(II) and three ligand groups, *via* bridging of the apical oxygens (Fig. 9). **6.1** also shows very

similar 5 co-ordinate copper geometries, which are best described as between trigonal bipyramidal and square pyramidal. Each Cu(II) is also bound with two quinoline donors which originate from separate ligands, with all the copper axial donor sites occupied by a capping perchlorate molecule. Figure 10 clearly displays how the ligands are arranged so that all three pendent butyl groups point in the same direction out of the cluster, effectively creating a lipophilic face.

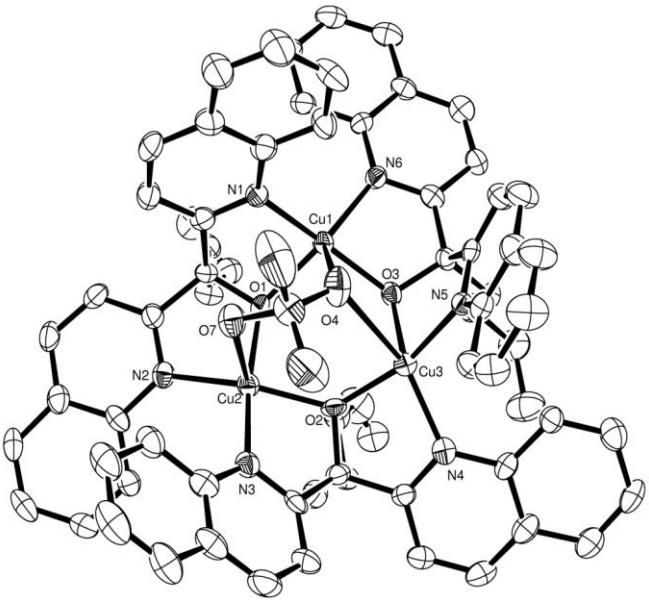

Figure 9: ORTEP Perspective view of the asymmetric unit for [Cu^{II}(**L6**)[ClO_4]]showing the trimer species from above, only showing the co-ordinated perchlorate molecule. Displacement ellipsoids are shown at 50% probability with H atoms, solvent and two non co-ordinating perchlorate counter ions excluded for clarity.

A Previous trinuclear oxygen bridged complex developed by Biswas *et al.* using the ligand 2-[(2-amino-ethylimino)-methyl]-phenol, gave an average Cu-µO bond length of 1.985(4) Å[27] which is very similar to the observed Cu-µO average bond length, 1.929(4) Å. Unsurprisingly these lengths also compare well to compound **5.3** which gave an average Cu-µO bond length of 1.943(14) Å. Another example is that of a Cu(II) tetramer $[(py)_2Cu(\mu OH)]_4$, which gave an average Cu-µO bond length of 1.967(5) Å.[28]

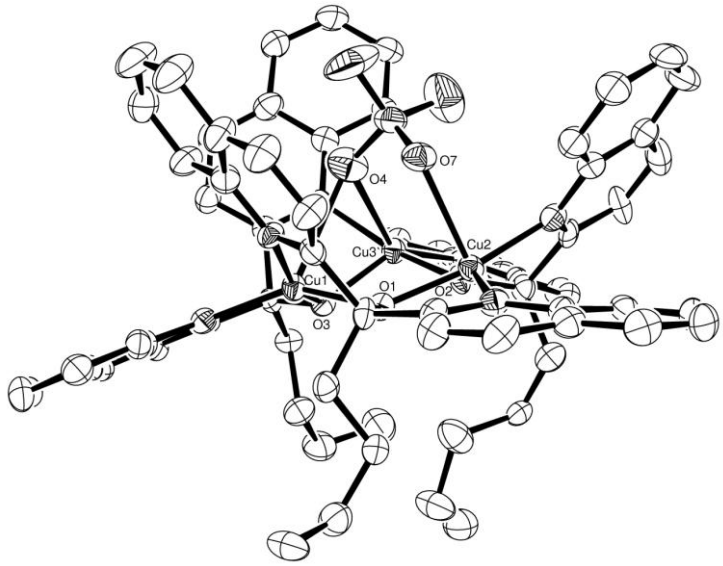

Figure 10: ORTEP Perspective side on view of the asymmetric unit for [Cu^{II}(**L6**)[ClO_4]]showing the trimer species side on. This also demonstrates how the ligands arrange so that the pendant butyl chains protrude in the same direction. Displacement ellipsoids are shown at 50% probability with H atoms and solvent excluded for clarity.

The Cu-N bond lengths average at 1.999(6) Å which is again comparable to **5.3,** which gave an average Cu-N distance of 2.006(18) Å. These co-ordination distances also match well with analogous bonds found in the Cu(II) tetramer [$(py)_2Cu(\mu OH)]_4$, mentioned earlier, where each copper centre similarly co-ordinates through two bridging oxygens and two pyridyl functions, giving an average Cu-N length of 2.013(6) Å.[28]

A slight difference to that seen in **5.3**, is in the capping perchlorate molecule which is now co-ordinating through only two of its oxygens rather than three, see Figure 10. Interestingly O4 is bridging between Cu1 and Cu3 (Fig. 11). This is unlike **5.3** where each Cu(II) centre is co-ordinating to its own perchlorate oxygen. As a result the bridging Cu-O4 bonds are approximately 0.3 Å longer than the equivalent unbridged Cu-O7 bond (Tab. 5). However, on average the Cu-perchlorate bonds measured for this complex (2.618(4) Å) are almost identical to those for **5.3** (2.611(14) Å).

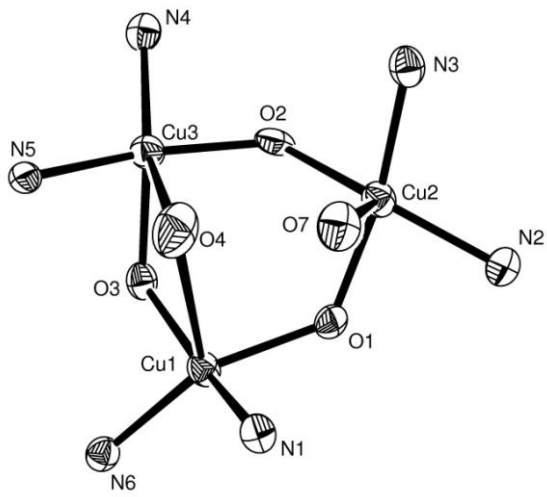

Figure 11: A view of the copper trimer centre for **6.1** showing only the co-ordinating atoms., where O4 and O7 are part of the same perchlorate molecule effectively capping the system. Displacement ellipsoids are shown at 50% probability with H atoms excluded for clarity.

Table 5: Selected bond Distances (Å) and Angles (°) for **6.1**

Bond	Length (Å)	Bond	Length (Å)	Bond	Length (Å)
Cu1-N1	1.963 (5)	Cu2-N2	2.027 (5)	Cu3-N4	2.008 (6)
Cu1-N6	2.042 (6)	Cu2-N3	1.988 (6)	Cu3-N5	1.965 (5)
Cu1-O1	1.969 (4)	Cu2-O1	1.923 (4)	Cu3-O2	1.882 (4)
Cu1-O3	1.894 (4)	Cu2-O2	1.949 (4)	Cu3-O3	1.954 (5)
Cu1-O4	2.726 (4)	Cu2-O7	2.438 (5)	Cu3-O4	2.690 (4)
Bonds	**Angle (°)**	**Bonds**	**Angle (°)**	**Bonds**	**Angle (°)**
N1- Cu1 –N6	105.2 (2)	N2- Cu2 –N3	106.1 (2)	N4- Cu3 –N5	109.6 (2)
N1- Cu1 –O1	82.64 (19)	N2- Cu2 –O1	82.8 (2)	N4- Cu3 –O2	84.4 (2)
N1- Cu1 –O3	160.0 (2)	N2- Cu2–O2	154.1 (2)	N4- Cu3 –O3	138.6 (2)
N1- Cu1 –O4	80.38 (17)	N2- Cu2 –O7	96.07 (19)	N4- Cu3 –O4	141.52 (17)
N6- Cu1 –O1	148.8 (2)	N3- Cu2 –O1	169.7 (2)	N5- Cu3 –O2	160.7 (2)
N6- Cu1 –O3	83.5 (2)	N3- Cu2–O2	81.0 (2)	N5- Cu3 –O3	83.1 (2)
N6- Cu1 –O4	123.74 (19)	N3- Cu2 –O7	88.9 (2)	N5- Cu3 –O4	71.21 (17)
O1- Cu1 –O3	99.27 (17)	O1- Cu2–O2	93.17 (18)	O2- Cu3 –O3	95.24 (18)
O1- Cu1 –O4	87.15 (17)	O1- Cu2 –O7	85.04 (17)	O2- Cu3 –O4	89.5 (2)
O3- Cu1 –O4	79.79 (18)	O2- Cu2 –O7	109.13 (17)	O3- Cu3 –O4	79.76 (18)

Crystal Structure of [Re(CO)$_3$(L6)] (6.2)

Crystals suitable for X-ray crystallographic studies of the complex [Re(CO)$_3$(**L6**)] were obtained through slow evaporation of a concentrated chloroform solution of the complex, yielding bright yellow crystals. The complex crystallised in the triclinic space group P-1 with the asymmetric unit containing only one mononuclear complex and two solvent molecules (Fig. 12). The overall molecular symmetry is crudely assigned C_S as the freely moving butyl chain can affect the only plane of symmetry, in which the compound would be more correctly labelled as C_1. This complex is very similar to that of **5.5** where the two quinolines and oxygen donate in a *fac* arrangement (Fig. 13), giving an octahedral geometry and resulting in an overall neutral complex charge. The average bond lengths to the Rhenium centre are Re-N 2.221(4) Å, Re-O 2.087(4) Å and Re-CO 1.919(6) Å (Tab. 6). These distances, as expected, are virtually identical to that seen in complex **5.5** and also compare with the complex *fac*-[Re(CO)$_3$(quinoline)$_2$Cl], (Re-N 2.206(3) Å and Re-CO 1.925(4) Å).[29]

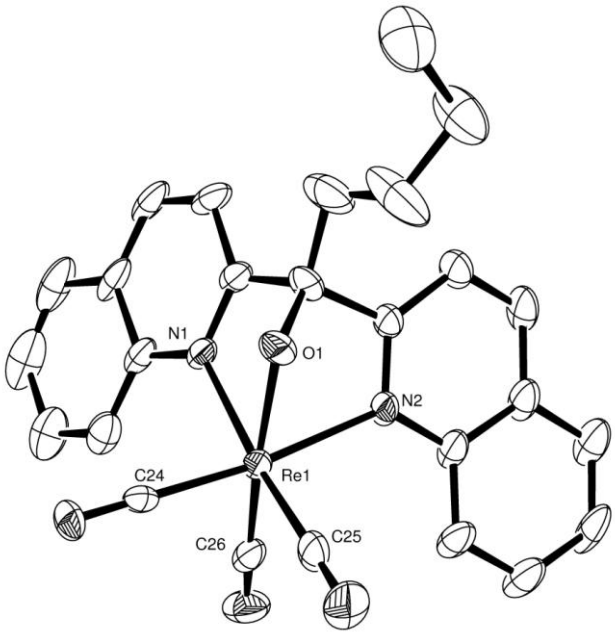

Figure 12: ORTEP Perspective view of the asymmetric unit for octahedral [Re(CO)$_3$(**L6**)] complex. Displacement ellipsoids are shown at 50% probability with H atoms and chloroform solvent excluded for clarity

In the data the butyl chain shows some disorder, this is not unusual as the linear chain is not rigid and within the lattice can orientate several ways creating the disorder. The availability of this butyl function is encouraging for increasing the complexes lipophilcity, giving it potential for biological applications that involve crossing the cell membrane.

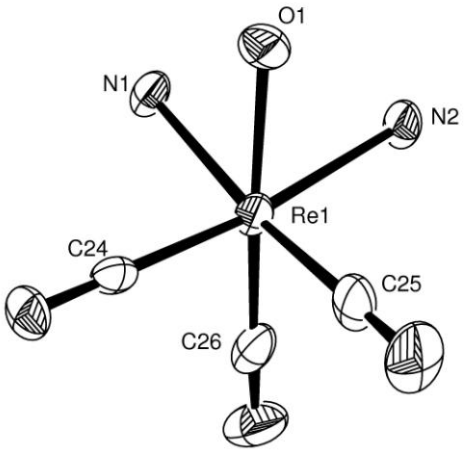

Figure 13: ORTEP Perspective view of the octahedral centre for [Re(CO)$_3$(**L6**)]. Displacement ellipsoids are shown at 50% probability with H atoms and chloroform solvent excluded for clarity

Table 6: Selected bond Distances (Å) and Angles (°) for complex **6.2**			
Bond	Length (Å)	Bond	Length (Å)
Re1-N1	2.227 (4)	Re1-C24	1.914 (5)
Re1-N2	2.214 (4)	Re1-C25	1.923 (6)
Re1-O1	2.087 (4)	Re1-C26	1.921 (6)
Bonds	Angle (°)	Bonds	Angle (°)
N1- Re1 –N2	83.22 (15)	N2- Re1 -C26	97.2 (2)
N1- Re1 –O1	74.31 (16)	O1- Re1 –C24	98.25 (17)
N1- Re1 –C24	92.58 (17)	O1- Re1-C25	97.0 (2)
N1- Re1 –C25	171.3 (2)	O1- Re1 –C26	170.69 (17)
N1- Re1 –C26	100.0 (2)	C24- Re1-C25	89.1 (2)
N2- Re1 –O1	75.01 (16)	C24- Re1 –C26	89.3 (2)
N2- Re1 –C24	172.80 (18)	C25- Re1 –C26	88.5 (3)
N2- Re1-C25	94.21 (19)		

6.28 Conclusion

The novel tridentate ligand bis(2-quinoline)-1-butyl-menthanol (H**L6**) has been isolated and complexes with Cu(II) and Re(I) were successfully isolated. Both complexes were reacted in a 1:1 stoichiometry in acetonitrile and have been fully characterised, where the ligand was seen to act as an anionic donor facilitated through binding of the apical OH group. The Cu(II) complex was found to form a trimeric structure, similar to that of **5.3**, where three ligands and three copper centres bind together resulting in the formation of a central Cu-O six membered ring, with the aid of μO moieties. All three copper centres were found to be 5 co-ordinate, giving near square pyramidal geometries. Additionally, the co-ordination of one perchlorate molecule capping over the three copper centres was also observed, where two of the coppers (Cu1 and Cu3) share donation from one of the perchlorate oxygens. This is unlike the analogous complex **5.3** in which each copper centre binds with a separate oxygen moiety of the capping perchlorate counterion. The absorption spectra of complex **6.1** suggest that the three Cu(II) centres retain their 5 co-ordinate geometries, presumably as the trimeric species, even in solution.

The Re(I) complex was found to be monomeric, with the ligand chelating in a *fac* arrangement, and is isostructural to complex **5.5** in the previous chapter. Discussion of the ^{1}H-NMR of this complex before and after the addition of TFA (H^{+}) was carried out. These results showed that protonation of the sample caused a general downfield shift of the aromatic peaks, attributed to the protonation of the anionic oxygen donor. Also, some broadening and slight shifting of the butyl chain proton peaks lead to the suggestion that some possible chain wrapping scenario may be occurring, due to the increased solvent polarity. Luminescence studies of the Re(I) complex reveal a blue shift (595nm→535nm) and intensity enhancement of the emission maximum upon gradual addition of H^{+}(Fig. 5). It is not possible to conclude whether the energy gap rule, due to oxygen protonation, or chain wrapping is the cause of these observations. In addition to this, lifetime measurements of **6.2** were also obtained, showing that addition of 1 equivalent of H^{+} to the sample, dramatically altered the lifetime from 70 ns to 539 ns (Tab. 3), suggesting that either a cationic, or more shielded complex is present in acidic conditions. Finally these results show that the Re complex has great stability in both solution and solid state. Furthermore the luminescent sensitivity of **6.1** in acidic conditions, plus the potential as a

PET active ^{99m}Tc analogue, grants much enthusiasm for this system in the future and presents great potential for assays in biological media. However, boundaries such as solubility and targeting may still need to be overcome.

6.3 Experimental

Bis(2-quinoline)-1-butyl-menthanol [$C_{23}H_{22}N_2O$] (H**L6**):

Butylmagnesium bromide solution (0.74ml, 0.7M, 0.52mmol) was added to dried and degassed THF (20ml) with continuous stirring under N_2. The mixture was then cooled to -10°C using a salted ice bath. Next Bis(2-quinoline)methanone **S1** (123mg, 0.43mmol) was dissolved in THF (20ml) and added dropwise to the grignard reagent over 30 minutes. The resulting deep blue mixture was stirred and kept at -10°C for 2h. The solution was then allowed to reach 0°C before quenching with HCl (10%) until pH2-3 followed by neutralization with K_2CO_3 (10%) until pH8. The crude product was then extracted into chloroform (3x20ml). The combined organic layerwas then dried over $MgSO_4$, filtered and reduced giving a crude sticky brown solid. The crude product was purified by column chromatography using a 20/80 hexane/dichloromethane solvent system producing an off white solid of high purity. (65mg, 44%).

^{1}H-NMR ($CDCl_3$; 400MHz): δ_H 8.10(2H, d, J=8.3Hz, CH), 8.02(2H, d, J=8.7Hz, CH), 7.96(2H, d, J=8.7Hz, CH), 7.69(2H, d, J=8.1Hz, CH), 7.62(2H, t, J=7.7Hz, CH), 7.42(2H, t, J=7.5Hz, CH), 2.57(2H, t, J=8.0Hz, CH_2), 1.26(2H, m, CH_2), 1.20(2H, m, CH_2), 0.75(3H, t, J=7.1Hz, CH_3), ^{13}C-NMR ($CDCl_3$; 100MHz): δ_C 163.63(C), 146.38(C), 136.59(CH), 129.35(CH), 129.14(CH), 127.49(CH), 127.21(C), 126.29(CH), 119.29(CH), 79.27(C), 41.08(CH_2), 25.87(CH_2), 23.10(CH_2), 14.13(CH_3). HRMS (ES-MS) *m/z* calcd. 343.1810; exp. 343.1821, $[C_{23}H_{23}N_2O]^+$, (100%), calcd. 365.1630: exp. 365.1620, $[C_{23}H_{22}N_2ONa]^+$, (30%), calcd. 381.1369; exp. 381.1416, $[C_{23}H_{23}N_2OK]^+$, (50%), calcd. 406.1895; exp. 406.1910, $[C_{23}H_{23}N_2O.CH_3CN.Na]^+$, (50%). FT-IR (KBr/cm^{-1}) ν = 3351br+m, 3062m, 2956s, 2924s, 2857s, 1620m, 1588m, 1566w, 1503m, 1462w, 1425w, 1394m, 1303m, 1257w, 1217w, 1139m, 1089m, 1017w, 837m, 808w, 782w, 760m. UV-Vis [λ_{max}, nm, (εM, M^{-1}cm^{-1})] in CH_3CN: 255(22670), 294(14136), 315(13175), 324(4295).

Cu(II) bis(2-quinoline)-1-butyl-menthanol [$(CuC_{23}H_{22}N_2O)_3(ClO_4)][ClO_4]_2$ (**6.1**):

HRMS (ES-MS) *m/z* calcd. 808.1900; exp. 808.3124, $[2(CuC_{23}H_{21}N_2O)]^+$, (75%), calcd. 956.2576; exp. 956.3755, $[2(CuC_{23}H_{21}N_2O).3CH_3CN.Na]^+$, (20%), calcd. 1066.0427; exp. 1066.4736, $[2(CuC_{23}H_{21}N_2O).Na.Cl][2ClO_4]^+$, (20%). FT-IR (KBr/cm^{-1}) ν = 3448br+m, 3119m, 3061m, 2961m, 2925m, 2869m, 2005w, 1692s, 1623m, 1600s, 1538w, 1510s, 1452m, 1434m, 1383s, 1321s, 1268w, 1215m, 1158br+s, 1086br+s, 961m, 856m, 821m, 795m, 771s, 625s, 578w, 476w. UV-Vis [λ_{max}, nm, (εM, M^{-1}cm^{-1})] in CH_3CN: 247(22293), 309(14019), 343(3902), 806(54). Magnetic moment (Evans method, 293K, Acetonitrile): μ_{eff} = 1.80μ_B. Found: C 45.56; H 3.58; N 4.45 (%) $CuC_{23}H_{22}N_2O(ClO_4)_2$ Requires: C 45.65; H 3.67; N 4.63 (%).

Re(I) bis(2-quinoline)-1-butyl-menthanol [$Re(CO)_3C_{23}H_{22}N_2O$] (**6.2**):

^{1}H-NMR ($CDCl_3$; 400MHz): δ_H 8.92(2H, d, J=8.9Hz, CH), 8.23(2H, d, J=8.5Hz, CH), 7.93(2H, t, J=7.9Hz, CH), 7.81(2H, d, J=8.1Hz, CH), 7.78(2H, d, J=8.5Hz, CH), 7.59(2H, t, J=7.5Hz, CH), 2.71(2H, br.t, J=8.1Hz, CH_2), 1.66(2H, m, J=5.1Hz, CH_2), 1.55(2H, m, J=7.3Hz, CH_2), 0.97(3H, t, J=7.2Hz, CH_3). ^{13}C-NMR ($CDCl_3$; 100MHz): δ_C 169.45(C), 147.84(C), 139.31(CH), 132.46(CH), 128.99(CH), 128.48(CH), 127.77(CH), 127.38(C), 118.17(CH), 92.72(C), 37.47(CH_2), 25.55(CH_2), 23.67(CH_2), 14.28(CH_3). HRMS (ES-MS) *m/z* calcd. 611.1109; exp. 611.1096, $[Re(CO)_3C_{23}H_{22}N_2O]^+$, (100%), calcd. 654.1403; exp. 654.1375, $[C_{23}H_{22}N_2ORe(CO)_3.CH_3CN]^+$, (45%), calcd. 676.1222; exp. 676.1042, $[C_{23}H_{21}N_2ONa.Re(CO)_3.CH_3CN]^+$, (40%). FT-IR (KBr/cm^{-1}) ν = 3448br+w, 2962m, 2927m, 2873w, 2032s, 1944s, 1907br+s, 1669w, 1618w, 1595m, 1513m, 1459w, 1433w, 1358br+s, 1297w, 1261s, 1217w, 1176s, 1147m, 1096br+s, 1025br+s, 959m, 910m, 869m, 801br+s, 760m, 733m, 647w, 541w, 528m. UV-Vis [λ_{max}, nm, (εM, M^{-1}cm^{-1})] in CH_3CN: 252(14771), 319(8260), 332(3776).

Re(I) bis(2-quinoline)-1-butyl-menthanol+TFA [$Re(CO)_3C_{23}H_{22}N_2O$+TFA] (**6.2a**):

^{1}H-NMR ($CDCl_3$; 400MHz): δ_H 8.78(2H, d, J=8.9Hz, CH), 8.45(2H, d, J=8.3Hz, CH), 8.02(2H, t, J=7.9Hz, CH), 7.93(2H, d, J=8.0Hz, CH), 7.81(2H, d, J=8.3Hz, CH), 7.73(2H, t, J=7.6Hz, CH), 7.27(1H, s, OH), 3.03(2H, br.s, CH_2), 1.62(4H, m, J=5.9Hz, 2xCH_2), 0.99(3H, t, J=6.9Hz, CH_3).

6.4 References

1. A. R. Kherlopian, T. Song, Q. Duan, M. A. Neimark, M. J. Po, J. K. Gohagan, A. F. Laine,. *BMC Syst. Biol*., **2008**, 2, 74.
2. M. A. Pysz, S. S. Gambhir, J. K. Willmann., *Clin. Radiol*., **2010**, 65, 500.
3. M. Baker., *Nature*, **2010**, 463, 997.
4. T. Kihlberg, F. Karimi, B. Långström, *J. Org. Chem.*, **2002**, 67, 3687.
5. V. Fernandez-Moreira, F. L. Thorp-Greenwood, M. P. Coogan, *Chem. Commun.*, **2010**, 46, 186.
6. F. L. Thorp-Greenwood and M. P. Coogan, *Dalton Trans.*, **2011**, 40, 6129.
7. S. W. Botchway, M. Charnley, J. W. Haycock, A. W. Parker, D. L. Rochester, J. A. Weinstein, and J. A. G. Williams, *PNAS*, **2008**, 105, 16071.
8. V. Saxena, M. Sadoqi, J. Shao, *J. Pharm. Sci.*, **2003**, 92, 2090.
9. M. Y. Berezin, S. Achilefu, *Chem. Rev.*, **2010**, 110, 2641.
10. L. A. Worl, R. Duesing, P. Chen, L. Della Ciana, T. J. Meyer, *J. Chem. Soc. Dalton Trans.*, **1991**, 849.
11. F. N. Castellano, X.-Q. Guo, L. Li, H. Szmacinski, J. Sipior, J. R. Lakowicz, *Proc. SPIE-Int. Soc. Opt. Eng.*, **1998**, 3256, 223.
12. P. Borgstrom, F. C. Wagner, H. C. Griffin, *J. Am. Chem. Soc*., **1929**, 51, 1861.
13. L. Pazderski, J. Tousek, J. Sitkowski, L. Kozerski, E. Szłyk, *Magn. Reson. Chem*., **2007**, 45, 1059.
14. I.W. Elliot, P. Yates, *J. Org. Chem.*, **1961**, 26, 1287.
15. A.B.P. Lever, Inorganic Electronic Spectroscopy (second edition), *Elsevier Science B.V.*, 565-569.
16. S. Tyagi, B. J. Hathaway, *J. Chem. Soc. Dalton*, **1983**, 199.
17. N. Viola-Villegas, A. E. Rabideau, M. Bartholoma, J. Zubieta, R. P. Doyle, *J. Med. Chem*., **2009**, 52, 5253.
18. 2- L. Wei, J. W. Babich, W. Ouellette, J. Zubieta*, Inorg. Chem*., **2006**, 45, 7, 3057

19. 3- K. A. Stephenson, S. R. Banerjee, T. Besanger, O. O. Sogbein, M. K. Levadala, N. McFarlane, J. A. Lemon, D. R. Boreham, K. P. Mareca, J. D. Brennan, J. W. Babich, J. Zubieta and J. F. Valliant., *J. Am. Chem. Soc*., **2004**, 126, 8598-8599.

20. 4- G. Ribeiro Morais, A. Paulo, I. Santos, *Organometallics*, **2012**, 31, 5693-5714

21. G. Gasser, A. Pinto, S. Neumann, A. M. Sosniak, M. Seitz, K. Merz, R. Heumann, N. Metzler-Nolte, *Dalton. Trans*., **2012**, 41, 2304-2313.

22. D. J. Stufkens and A. Vlcek, *Coord. Chem. Rev.,* **1998**, 177, 127.

23. A. J. Hallet, S. J. A. Pope, *Inorg. Chem. Commun.*, **2011**, 14, 1606.

24. R. Grigg and W. D. J. Amilaprasadh Norbert,*. J. Chem. Soc., Chem. Commun*., **1992**, 1330-1302.

25. K. Man-Chung Wong, W-S. Tang, X-X. Lu, N. Zhu, V. Wing-Wah Yam., *Inorg. Chem*., **2005**, 44, 1492−1498.

26. D. Parker, *Coord. Chem. Revs*., **2000**, 205, 109–130.

27. C. Biswas, M. G. B. Drew, A. Figuerola, S. Gomez-Coca, E. Ruiz, V. Tangoulis, A. Ghosh, *Inorganica. Chimica. Acta*., 363, **2010**, 846-854.

28. G. A. Bowmaker, C. Di Nicola, F. Marchetti , C. Pettinari, B. W. Skeltonc, N. Somers, A. H. Whitec., *Inorg. Chim. Acta.,* **2011**, 375, 31–40.

29. N. Murakami, G. Ferraudi. *J. Chem. Soc. Dalton. Trans*., **1994**, 2565-2571.

7.0 Final Conclusion

The research presented in this thesis reveals the synthesis of five novel ligand frameworks (**L2-L6**), all involving and incorporating multiple imine donors, with the exception of **L1** which has previously been synthesised and involves neutral amine donors. All the ligands presented have shown a high affinity for transition metals, generally giving stable compounds suitable for analysis. **L1** is unique from the other ligands in that it utilises two small macrocyclic functionalities (tacn), each containing three nitrogen donors. Complexation of **L1** with several metals produced five new monomeric complexes (Ga^{III}, Fe^{II}, Co^{II}, Cd^{II} and Hg^{II}) with the Gallium and Iron compounds being potentially PET active. These structures were found to form in a sandwich conformation (page 12) where the two rings coordinate to a single metal centre, confirmed by X-ray diffraction. This produced complexes with distorted hexadentate coordination of geometries between octahedral and trigonal prismatic. The geometry of the Fe^{II} and Cd^{II} complexes were analysed and it was found that the xylyl linker group has to buckle in order to allow close enough coordination of both ring systems around a single metal ion. The Fe^{II} complex showed the most amount of octahedral character, most likely driven by it's electronic preference for O_h geometry. Additionally, ionic size is thought to influence the distance between the macrocycles, with Fe^{II} being smaller in diameter than Cd^{II}. This would increase non-bonding interactions, which are expected to reduce upon twisting the macrocycles away from the trigonal prismatic arrangement set by the ligand. In both cases the two macrocycles do not coordinate in perfect parallel, suggesting that the linker group is larger than ideal.

Ligands **L2**-**L3** are both constructed from three pyridyl-pyrazolyl donor units tethered by a tertiary methanol group. **L2** and **L3** are analogous in their donor set with the only difference coming from appended phenyls (**L3**) in place of methyls (**L2**) on the pyrazole backbone. These two structures are tripodal type ligands with each arm containing two imine donors, where the ligand has a natural preposition for trigonal prismatic geometry. Both of these ligands were found to readily complex with a variety of transition metals, some of which are known to be PET active. Complexes of **L2** and **L3** gave stable crystalline products of high purity. **L2** proved to be the most successful of the ligands studied, yielding twelve novel complexes. Nine of these compounds (all using 2+ metals except Fe^{III}) were found to form descrete hexa-coordinated

structures where the metal ion is encapsulated within the ligand cavity, and from electronic absorption studies, are also stable in acetonitrile solution. All of these complexes were found to have a geometry between trigonal prismatic and octahedral with only the Ni^{II} complex showing more O_h than TP character. A trend can be seen between these complexes, revealing that smaller metal ions produce the largest amount of Bailar twist (Table 21, page 85). Analysis of the crystal data shows that clashing of the three lowest methyl groups on **L2** are the main cause of geometric distortion, revealing that the electronic preferences of individual metal ions is only having a small effect on the resultant geometry. This is highlighted when only considering the d^{10} metals, where Zn^{II} possessed a relatively large Bailar angle whilst Hg^{II} did not. The larger ions have to push the three donor arms out and apart in order to fit within the ligand cavity, creating a truncated coordination sphere, resulting in the lowest pyrazole methyl groups interacting far less. This was also confirmed when comparing these compounds to analogous complexes of TBM (page 34) which showed much lower Bailar twisting from the same series of metals, largely due to the absence of any methyl interactions. Interestingly, although **L3** is isostructural to **L2,** the presence of large phenyl groups instead of methyls dramatically alters its coordinating ability. **L3** was found to coordinate readily with 2+ transition metals forming stable solids. However, crystal data revealed that this ligand only binds through four of its potential six donors, with a fifth donor to the metal coming from a acetonitrile molecule. This generally gives these complexes a geometry between square pyramidal and trigonal bipyramidal, with UV-Vis data supporting this theory even in the solution state. Appending these aromatic groups was considered for their potential in DNA chelation, altered solubility and cell membrane prefusion, however, these large groups evidently interact significantly with each other causing highly disordered coordination spheres. The conformation of these five coordinate complexes could lead to potential catalytic reagents, as the metal centres could provide an alternative or lower energy pathway for a reaction, opening an avenue for exploration. Interestingly, complexes of **L3** with large metal ions such as Cd^{II} and Hg^{II} were also isolated. No crystal data could be collected for these structures however, ^{1}H-NMR and mass spectroscopy data revealed that both were symmetrical monomeric species, unlike the complexes of smaller metal ions (Cu^{II} Co^{II} and Ni^{II}). This may suggest that larger ions have a similar effect on **L3** to that seen in **L2**, where the ligand arms become pushed outward allowing Cd^{II} and Hg^{II} to fit within the ligand cavity, thus producing a symmetrical six coordinate species.

The ligand **L4** is built from two pyridyl-pyrazolyl units creating a planar tetradentate molecule. This ligand was found to complex with many different 2+ metal ions all producing distorted octahedral complexes where the two extra donors come from either counter ions or solvent. All complexes of **L4** produced discrete monomeric structures where the smaller metal ions produced geometries with more O_h character, due to the increased bite angle with each bis-imine unit creating a more ideal geometry. The Ni^{II} complex in this series is the only structure to form differently in that it facilitates the binding of two ligands around one metal rather than the intended 1:1 ratio. This structure type is most likely to have occurred due to the different solvent system used to obtain crystals, where conventional arguments of sterics, electronic and cation size could not explain why the 2:1 conformation is preferred. This does mean that each ligand of the Ni^{II} complex contains a pendent pyrazole moiety which may be utilized in further investigations for the formation of multinuclear or heteronuclear species.

Two new bis-quinoline functionalised ligands, H**L5** and H**L6**, were also investigated in this thesis, where both are found to coordinate readily with first row transition metals as well as Re^{I}, giving strongly octahedral structures with potential PET activity. These two ligands differ from previous ones in that they are now only tridentate with a *fac* donor arrangement. As a result these ligands utilize the apical alcohol moiety upon coordination, giving **L5** and **L6** a negative charge. **L5** was functionalised with a para-substituted phenyl bromide which in the solid state orientates away from the metal centre. This brings great potential for **L5** to be further functionalised, such as adding hypdrophilic/phobic or biologically active groups, possibly through coupling reactions, to the pendant phenyl bromide, increasing specificity of a complex in medical applications. This, along with the incredible ability of the ligand to complex with an array of transition metals, presents **HL5** as an appealing ligand for medical investigation. **HL6** is very similar to **HL5**, however, the pendent phenyl bromide is replaced with a linear butyl chain. **L6** was found to strongly bind with Cu^{II} and Re^{I}, where the copper species was found to form a trimer consisting of three ligands and three metals, creating a central Cu-O six membered ring. This results in each copper being only five coordinate with near square pyramidal geometry. Another notable feature is the presence of a capping perchlorate molecule over the three copper ions which is an unusual trait seen in metal complexes. This species of trimer is also observed in the copper complex of **L5** forming an almost identical scaffold, again with a capping perchlorate. This demonstrates that the trimer species was not a random result and that this

structure may be a favourable system for further investigation into Cu^{II} imaging or catalysis. In addition, the orientation of the pendent groups in both trimer compounds reside on the same side of the complex, effectively creating a reactive or hydrophobic face, which may be advantageous for biological assays. The Rhenium complex of **L6** formed a neutral strongly octahedral structure with *fac* arrangement. Due to the properties of heavy d^6 metals, such as rhenium, luminescence studies were carried out. Interestingly, upon addition of acid (TFA) to the complex a noticeable blue shift was observed in the resulting emission wavelength, as well as an intensity enhancement. This was concluded to be either a result of protonation of the coordinating oxygen (energy gap rule) or chain wrapping of the pendent butyl group due to the change in solvent polarity. In addition fluorescence lifetime measurements were also collected which again increased dramatically in the presence of acid and supports the presence of a cationic species or a more shielded complex. The apparent stability, great luminescent properties and long lifetime of this complex gives it great potential for biomedical investigations, especially those involving variable pH levels. Moreover the aliphatic pendent chain is also thought to enhance the mobility of the complex through a cell membrane, allowing delivery of the compound in tissues. The possibilities of this particular complex are further increased by the modern application of PET imaging where Re is an analogue of the active ^{99m}Tc isotope making this complex a potentially bimodal imaging agent.

Overall this series of novel ligands and complexes have shown the strong and varied coordinating ability of hexa and tri-imine frameworks in solid and solution state. It also reveals how sterics can play a vital role on the observed geometry, where increasing steric bulk decreases the co-ordination number of the metal ions. Furthermore, by applying more aromatic quinolines to the ligand along with active metals, this opens up opportunites for luminescent applications with further investigation.